

Analysis and Optimization of Copper-Catalyzed Azide–Alkyne Cycloaddition for Bioconjugation**

Vu Hong, Stanislav I. Presolski, Celia Ma, and M. G. Finn*

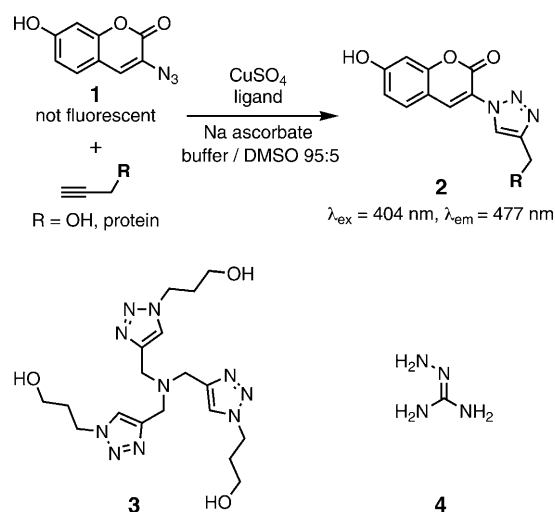
Since its discovery in 2002, the copper-catalyzed azide–alkyne cycloaddition (CuAAC)^[1] reaction—the most widely recognized example of click chemistry^[2]—has been rapidly embraced for applications in myriad fields.^[3] The attractiveness of this procedure (and its copper-free strained-alkyne variant^[4]) stems from the selective reactivity of azides and alkynes only with each other. Because of the fragile nature and low concentrations at which biomolecules are often manipulated, bioconjugation presents significant challenges for any ligation methodology. Several different CuAAC procedures have been reported to address specific cases involving peptides, proteins, polynucleotides, and fixed cells, often with excellent results,^[5] but also occasionally with somewhat less satisfying outcomes.^[6] We describe here a generally applicable procedure that solves the most vexing click bioconjugation problems in our laboratory, and therefore should be of use in many other situations.

The CuAAC reaction requires the copper catalyst, usually prepared with an appropriate chelating ligand,^[7] to be maintained in the Cu^I oxidation state. Several years ago we developed a system featuring a sulfonated bathophenanthroline ligand,^[8] which was optimized into a useful bioconjugation protocol.^[9] A significant drawback was the catalyst's acute oxygen sensitivity, requiring air-free techniques which can be difficult to execute when an inert-atmosphere glove box is unavailable or when sensitive biomolecules are used in small volumes of aqueous solution. We also introduced an electrochemical method to generate and protect catalytically active Cu^I-ligand species for CuAAC bioconjugation and synthetic coupling reactions with minimal effort to exclude air.^[10] Under these conditions, no hydrogen peroxide was produced in the oxygen-scrubbing process, resulting in protein conjugates that were uncontaminated with oxidative byproducts. However, this solution is also practical only for the specialist with access to the proper equipment. Other protocols have employed copper(I) sources such as CuBr for labeling fixed cells^[11] and synthesizing glycoproteins.^[12] In these cases, the instability of Cu^I in air imposes a requirement

for large excesses of Cu (greater than 4 mM) and ligand for efficient reactions, which raises concerns about protein damage or precipitation, plus the presence of residual metal after purification.

The most convenient CuAAC procedure involves the use of an in situ reducing agent. Sodium ascorbate is the reductant of choice for CuAAC reactions in organic and materials synthesis, but is avoided in bioconjugation with a few exceptions.^[13] Copper and sodium ascorbate have been shown to be detrimental to biological^[14] and synthetic^[15] polymers due to copper-mediated generation of reactive oxygen species.^[16] Moreover, dehydroascorbate and other ascorbate byproducts can react with lysine amine and arginine guanidine groups, leading to covalent modification and potential aggregation of proteins.^[6a,17] We hoped that solutions to these problems would allow ascorbate to be used in fast and efficient CuAAC reactions using micromolar concentration of copper in the presence of atmospheric oxygen. This has now been achieved, allowing demanding reactions to be performed with biomolecules of all types by the non-specialist.

For purposes of catalyst optimization and reaction screening, the fluorogenic coumarin azide **1** developed by Wang et al. has proven to be invaluable (Scheme 1).^[18] The progress of cycloaddition reactions between mid-micromolar concentrations of azide and alkyne in aqueous buffers was followed by the increase in fluorescence at 477 nm upon formation of the triazole **2**.



Scheme 1. Top: Reaction used for screening CuAAC catalysts and conditions. Below: Accelerating ligand **3** and additive **4** used in these studies. DMSO = dimethylsulfoxide.

[*] V. Hong, S. I. Presolski, C. Ma, Prof. M. G. Finn
Department of Chemistry and The Skaggs Institute for Chemical Biology, The Scripps Research Institute
10550 North Torrey Pines Road, La Jolla, CA 92037 (USA)
Fax: (+1) 858-784-8850
E-mail: mgfinn@scripps.edu

[**] This work was supported by The Skaggs Institute for Chemical Biology, Pfizer, Inc., and the NIH (RR021886). We are grateful to Matthias Park for assistance with the synthesis of **3**.

Supporting information for this article is available on the WWW under <http://dx.doi.org/10.1002/anie.200905087>.

Ligand/Cu ratio: The results of a survey of known and new tris(heterocycle)methylamine accelerating ligands under conditions appropriate for bioconjugation will appear elsewhere.^[19] For the reasons discussed below, we focused on the catalyst incorporating varying amounts of ligand **3** [tris(3-hydroxypropyltriazolylmethyl)amine, THPTA], a water-soluble member of the tris(triazolylmethyl)amine family.^[7a] The performance of this system was found to be sensitive to the nature of the solvent and the overall copper concentration. At less than 50 μM in metal, the number of turnovers was poor and depended on the concentration of ligand, but initial reaction rates were similar (see Supporting Information). A copper concentration of 50 μM marked a transition point at which the use of ligand in any ratio greater than 1:1 with respect to metal gave rise to complete reaction in less than 10 min (Figure 1 A). At 100 μM Cu, the reaction was very fast

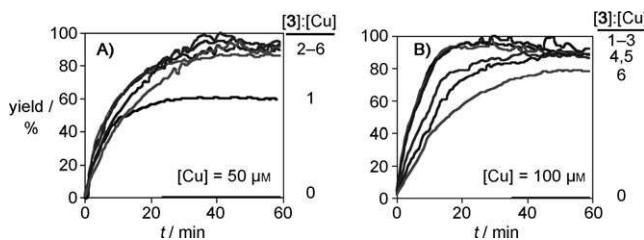


Figure 1. Conversion–time profiles as a function of ligand/Cu ratio. Conditions: propargyl alcohol (100 μM), **1** (50 μM), CuSO_4 , and ligand **3** (indicated concentrations), 0.1 M potassium phosphate buffer (pH 7.0)/DMSO 95:5, sodium ascorbate (5.0 mM), room temperature.

(Figure 1 B), and the rate decreased modestly as more than 1 equivalent of ligand was used. At a ligand/Cu ratio of 5:1, the overall reaction rate was only reduced by half. This striking tolerance of excess ligand such as **3** has been previously noted,^[19,20] and is crucial to the practical bioconjugation protocol described below.

Ascorbate concentration: The amount of ascorbate required to keep the active copper(I) catalyst available was similarly determined (Supporting Information). Reactions involving 100 μM Cu and 500 μM **3** in air, initiated by the addition of different concentrations of sodium ascorbate, were found to stop before completion in the presence of 1 mM or less reducing agent. The next highest concentration tested, 2.5 mM, proved to be sufficient; further increases did not enhance the rate. This is consistent with the need to remove oxygen from the aqueous solution (approximately 0.27 mM at room temperature, plus whatever diffuses in during the reaction) in order to maintain copper in the active +1 oxidation state.

Substrate oxidation: Copper ions mediate the catalytic oxidation of sodium ascorbate by molecular oxygen, producing hydrogen peroxide in a two-step process involving the superoxide radical anion as an intermediate.^[14b,21] If this reaction occurs in the presence of polypeptides, oxidation (such as of cysteine, methionine, and histidine imidazole groups)^[22] or cleavage of the biomolecule can occur. We tested the ability of CuAAC-accelerating ligands to affect this type of process in a model reaction with *N*-benzoylhistidine

(**5**). The compound was stable in the presence of CuSO_4 or ascorbate alone in pH 7 buffer, but the combination of the two induced the oxidation of approximately 16 % of **5** to **6** in 90 min, increasing to 65 % after 20 h (Figure 2 A).

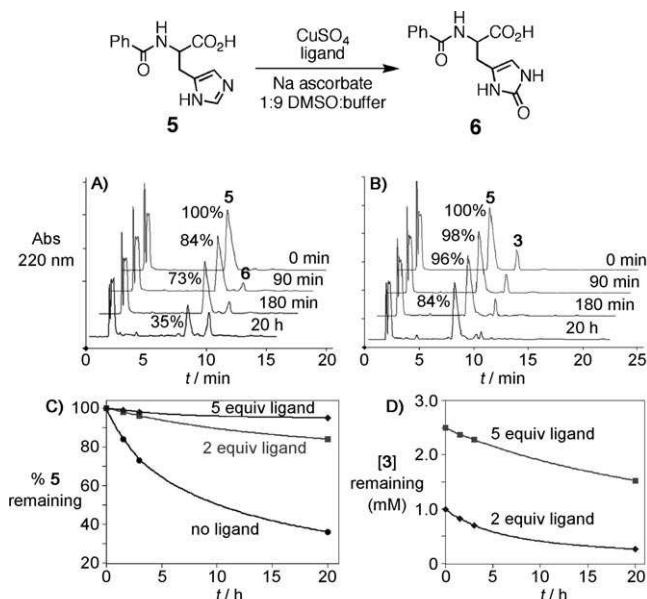


Figure 2. A) HPLC profiles for the oxidation of **5** (2 mM) in the presence of CuSO_4 (0.5 mM) and ascorbate (5 mM) in 10% DMSO/0.1 M phosphate buffer pH 7. B) The same analysis as in (A) in the presence of ligand **3** (1 mM). C,D) Summary of data showing oxidative loss of **5** and **3** in the presence of different amounts of **3**.

Ligand **3** protected the histidine moiety in a manner proportional to the ligand concentration. At a ligand/Cu ratio of 2:1, no histidine oxidation was observed after 90 min, and only approximately 15 % of **5** was lost after 20 h (Figure 2 B). At 5:1, less than 5 % of histidine was oxidized after 20 h (Figure 2 C). Ligand **3** was also found to be consumed over the same period, with approximately the same amount lost (0.7–1 mM) when two or five equivalents was used relative to Cu (Figure 2 D). We therefore suggest that the ligand protects against histidine oxidation as a sacrificial reductant, intercepting reactive oxygen species in the coordination sphere of the metal as they are generated.^[23] Thus, an excess of ligand is required, and the unusual nature of this class of ligand, outlined in Figure 1 and explored more fully elsewhere,^[19,20] allows such an excess to be used without sacrificing much in the way of CuAAC rate.

We also measured H_2O_2 concentrations under various CuAAC conditions by the standard amplex red–horseradish peroxidase assay, with the results shown in Figure 3. The initial production of peroxide took place in a Cu-ascorbate dependent manner, with slightly greater activity at lower ascorbate concentrations in the presence of 5 equivalents of ligand **3** per metal (Figure 3 A,C). However, after 60 min, the highest levels of hydrogen peroxide were accumulated in the presence of the lowest concentration of copper (Figure 3 B), showing that the metal mediates the decomposition of H_2O_2 as well as its formation. The presence of ligand **3** strongly

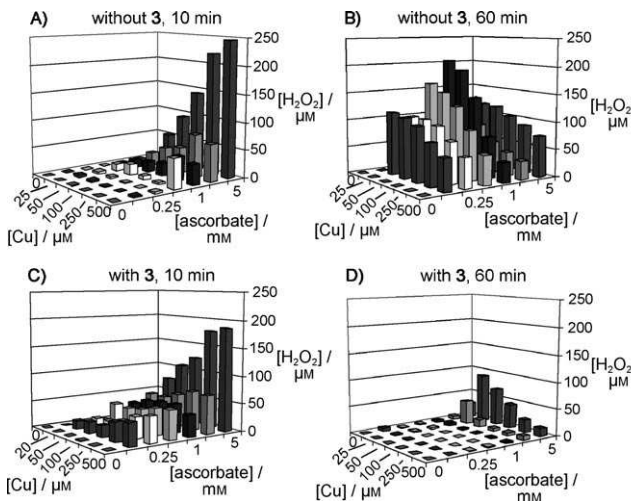


Figure 3. Hydrogen peroxide formation in the presence of various concentrations of CuSO_4 (0–500 μM) and sodium ascorbate (0–5 mM), monitored by fluorescence of amplex red ($\lambda_{\text{ex}} = 570 \text{ nm}$, $\lambda_{\text{em}} = 590 \text{ nm}$) in the presence of horseradish peroxidase at 10 and 60 min after addition of ascorbate: A,B) In the absence of ligand 3; C,D) in the presence of 5 equivalents of ligand 3 with respect to Cu.

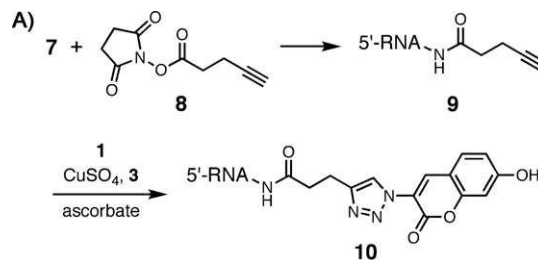
accelerated the peroxide decomposition reaction (Figure 3D). For these reasons, we recommend that five equivalents of tris(triazolyl)methylamine ligands such as **3** be used in most cases, and especially when substrate oxidation is a danger.

Ascorbate byproducts: Early applications of CuAAC to bioconjugation using sodium ascorbate led to protein adduct formation, crosslinking, and precipitation.^[6a] The initial oxidation product, dehydroascorbate, is a potent electrophile, and can also hydrolyze to form reactive aldehydes such as 2,3-diketogulonate and presumably glyoxal.^[24] These species can make connections with arginine, N-terminal cysteine, and lysine side-chains.^[25] To avoid such unwanted side-reactions, we require an additive to efficiently capture reactive carbonyl compounds while not inhibiting the CuAAC reaction. Aminoguanidine (**4**) and pyridoxamine are known to alleviate glyoxal toxicity in mammalian cells,^[24] so we investigated the properties of the former molecule. The rate of the CuAAC reaction mediated by 100 μM Cu was unaffected by **4** at 1 mM, but was noticeably lowered when **4** was present at 5 mM and higher (Supporting Information). At a higher Cu concentration (0.5 mM), additive **4** had very little inhibitory effect even up to 20 mM. These results show that aminoguanidine is only a modest inhibitor with fairly weak binding affinity for Cu¹.

The ability of **4** to prevent protein crosslinking was assayed using cowpea mosaic virus (CPMV), which we have found previously to be unstable in the presence of CuSO_4 and sodium ascorbate due to aggregation-dependent decomposition.^[14a] As shown in the Supporting Information, ligand **3** and aminoguanidine (**4**) were both helpful in protecting the protein while allowing for rapid CuAAC coupling.

Tests of the refined bioconjugation protocol: The use of excess amounts of ligand **3** in CuAAC bioconjugation was tested on a 21-mer siRNA strand, as a chemically sensitive biomolecule used in low concentration. Oligonucleotide **7**,

obtained from a commercial supplier as a 3'-amine derivative, was condensed with an excess of NHS ester **8** to give the alkyne **9** after ethanol precipitation. A click reaction of **9** (10 μM) was then performed with coumarin azide **1** (50 μM) mediated by CuSO_4 (100 μM) and **3** (500 μM) in 0.1 M phosphate buffer at pH 7, to give **10**. Fluorescence measurements showed the reaction to be complete within 1 h, and HPLC analysis showed the single peak of the starting material **7** to be converted to a single product (Supporting Information). Gel electrophoresis revealed only one fluorescent band (Figure 4, lane 3), which shifted after binding to its complementary strand (lane 7), suggesting that no strand breaks occurred. In addition, MALDI-TOF mass spectrometry showed the expected molecular weight for the corresponding cycloadduct.



7 = 5'-[21-mer RNA]-n-hexylamine
11 = 23-mer RNA complementary sequence to **7**

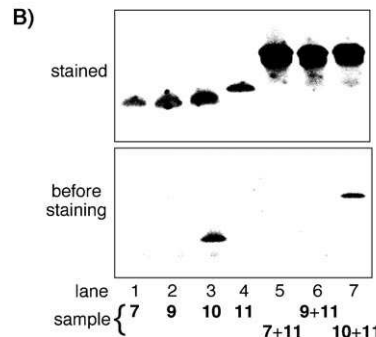


Figure 4. Demonstration of RNA modification by the CuAAC reaction: A) Reaction scheme. B) RNA gel visualized under long-wavelength UV light before (bottom) or after (top) staining with SYBR Green. The duplexes analyzed in lanes 5–7 were formed by annealing equimolar amounts of the two strands at room temperature for 30 min.

The bioconjugation method described here was further verified in reactions involving the capsid derived from bacteriophage Q β , an icosahedral particle comprised of 180 copies of a 14 kDa coat protein. We have previously attached gadolinium complexes, carbohydrates, and other species to this particle using $[\text{Cu}(\text{MeCN})_4](\text{OTf})$ and sulfonated bathophenanthroline ligand under oxygen-free conditions in a glovebox.^[26] The polyvalent azide-decorated capsid **12** was prepared by acylation of surface lysine and N-terminal amine groups (4 per subunit; 720 per particle) with a large excess of 5-(3-azidopropylamino)-5-oxopentanoic acid NHS ester (Figure 5). Subsequent click reaction of **12** (1 mg mL⁻¹

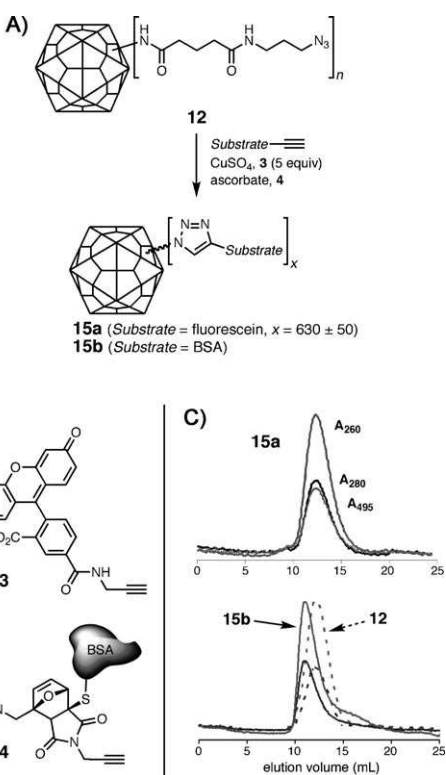


Figure 5. CuAAC reactions on the Q β virus-like particle using an excess of **3** as a ligand. A) Reaction scheme. B) Substrate alkynes. **14** was prepared by reaction of highly purified BSA (10 mg mL^{-1}) with two equivalents of an oxanorbornadiene electrophile, followed by size-exclusion purification. C) Size-exclusion chromatography of the products.

protein, $0.4\text{ }\mu\text{M}$ in particles, approximately $280\text{ }\mu\text{M}$ in azide) with only 2 equivalents of fluorescein alkyne **13** per azide ($250\text{ }\mu\text{M}$ CuSO₄, 1.25 mM **3**, 5 mM aminoguanidine **4**, 5 mM sodium ascorbate, pH 7 phosphate buffer) for 1 h gave an excellent yield of particles (**15a**) bearing an average of 630 dyes per capsid, determined by MALDI-TOF. No effort was made to exclude air other than to cap the Eppendorf tube containing the reaction mixture after initiation of the CuAAC reaction by addition of sodium ascorbate.

The coupling of a protein to the outer surface of the Q β virus-like particle served as a final example of the ability of the new CuAAC conditions to accomplish efficient bioconjugation. Bovine serum albumin (BSA), which contains one free cysteine residue (C34) was labeled first with a thiol-reactive linker^[27] to afford the alkyne-derivatized protein **14**. Ligation of **14** (1 equiv per capsid subunit) to the polyvalent azide **12** provided a high yield of BSA-coated particle **13b** within 1 h. Densitometry analysis after denaturing gel electrophoresis on the purified product allowed us to estimate that an average of 50 BSA molecules were attached to each capsid. This is consistent with size-exclusion chromatography (Figure 5B) and dynamic light scattering (hydrodynamic radius increase from 14 to 22 nm) analyses of the product (Supporting Information).

The CuAAC ligation chemistry illustrated here for connecting RNA and protein to small and large molecules was

performed with the same convenient protocol in all cases, a far cry from the testing of varying methods that has often been required to achieve maximal rates in demanding settings. However, in our experience problems can still arise in two general circumstances. First, one of the substrates may contain groups that strongly bind copper ions. In the case of proteins, this is potentially problematic because the bound metal may be unavailable for CuAAC catalysis, and because the Cu ions may induce protein precipitation.^[28] For example, we tested catalase to decompose hydrogen peroxide in the studies described by Figure 2 and 3. However, copper is a noncompetitive inhibitor of catalase, and the enzyme reciprocally inhibited the CuAAC reaction by sequestering the metal. We have also found that hexahistidine-tagged proteins can have the same effect. In such cases, three adjustments are suggested. 1) The concentration of the metal–ligand complex can be increased to a maximum of 0.5 mM , or 2–3 equivalents with respect to the His₆ sequence. 2) An accelerating ligand with greater affinity for Cu ions can be employed in place of THPTA.^[19] 3) Other metal ions such as Ni^{II} or Zn^{II} can be added to occupy the metal-binding protein motif in competition with Cu (see the Supporting Information for a brief discussion of these options).

Second, the azide or alkyne group on the biomolecule may be sterically hindered or somehow inaccessible to the catalyst and the coupling partner. Such cases are more difficult to both diagnose and remedy, but increasing the reaction temperature or adding solubilizing agents such as DMSO can have a beneficial effect. We presume this is because even modest increases in temperature or in the ability of the medium to solvate hydrophobic domains can boost the conformational dynamics of large molecules so as to expose hindered sites to a potent catalyst. We therefore recommend testing difficult cases at as high a temperature (and/or in the presence of as much DMSO) as the substrates can withstand, taking care to cap the reaction vessel while heating so as to minimize exposure to oxygen.

In summary, the key elements for the use of the optimized bioconjugation procedure are the following.

- Sodium ascorbate is the preferred reducing agent for most applications, due to its convenience and effectiveness at generating the catalytically active Cu^I oxidation state.
- Cu concentrations should generally be between 50 and $100\text{ }\mu\text{M}$. The lower limit is necessary to achieve a sufficient concentration of the proper catalytic complex which incorporates more than one metal center, and more than $100\text{ }\mu\text{M}$ Cu is usually not necessary to achieve high rates. A fluorogenic or colorimetric assay, such as that enabled by coumarin **1**,^[18] is strongly recommended for optimization of specific cases.
- At least five equivalents of THPTA (**3**, or other water-soluble variants) relative to Cu should be employed. The purpose is to intercept and quickly reduce reactive oxygen species generated by the ascorbate-driven reduction of dissolved O₂ without compromising the CuAAC reaction rate very much.
- Aminoguanidine is a useful additive to intercept byproducts of ascorbate oxidation that can covalently modify or crosslink proteins.

- e) Compatible buffers include phosphate, carbonate, or HEPES in the pH 6.5–8.0 range. Tris buffer should be avoided as the tris(hydroxymethyl)aminomethane molecule is a competitive and inhibitory ligand for Cu; sodium chloride (as in phosphate-buffered saline) up to 0.5 M can be used.
- f) Ascorbate should not be added to copper-containing solutions in the absence of the ligand. As a matter of routine, we first mix CuSO₄ with the ligand, add this mixture to a solution of the azide and alkyne substrates, and then initiate the CuAAC reaction by the addition of sodium ascorbate to the desired concentration.
- g) The Cu–THPTA catalyst in water is inhibited by excess alkyne, and so the procedure described here is useful for alkyne concentrations less than approximately 5 mM. When more concentrated solutions are used, a different ligand is suggested (Supporting Information).
- h) Free thiols such as glutathione at more than two equivalents with respect to copper are strong inhibitors of the CuAAC reaction in the form described here.

Experimental Section

A sample experimental protocol that takes into account the above factors is provided in the Supporting Information.

Received: September 10, 2009

Published online: November 26, 2009

Keywords: alkynes · azides · bioconjugation · cycloaddition · copper

- [1] a) C. W. Tornøe, C. Christensen, M. Meldal, *J. Org. Chem.* **2002**, *67*, 3057; b) V. V. Rostovtsev, L. G. Green, V. V. Fokin, K. B. Sharpless, *Angew. Chem.* **2002**, *114*, 2708; *Angew. Chem. Int. Ed.* **2002**, *41*, 2596.
- [2] H. C. Kolb, M. G. Finn, K. B. Sharpless, *Angew. Chem.* **2001**, *113*, 2056; *Angew. Chem. Int. Ed.* **2001**, *40*, 2004.
- [3] a) M. D. Best, *Biochemistry* **2009**, *48*, 6571; b) W. H. Binder, R. Sachsenhofer, *Macromol. Rapid Commun.* **2008**, *29*, 952; c) A. D. Moorhouse, J. E. Moses, *ChemMedChem* **2008**, *3*, 715; d) H. Nandivada, X. Jiang, J. Lahann, *Adv. Mater.* **2007**, *19*, 2197; e) H. C. Kolb, K. B. Sharpless, *Drug Discovery Today* **2003**, *8*, 1128.
- [4] a) N. J. Agard, J. A. Prescher, C. R. Bertozzi, *J. Am. Chem. Soc.* **2004**, *126*, 15046; b) J. M. Baskin, J. A. Prescher, S. T. Laughlin, N. J. Agard, P. V. Chang, I. A. Miller, A. Lo, J. A. Codelli, C. R. Bertozzi, *Proc. Natl. Acad. Sci. USA* **2007**, *104*, 16793; c) J. A. Codelli, J. M. Baskin, N. J. Agard, C. R. Bertozzi, *J. Am. Chem. Soc.* **2008**, *130*, 11486.
- [5] a) A. E. Speers, B. F. Cravatt, *Chem. Biol.* **2004**, *11*, 535; b) K. E. Beatty, F. Xie, Q. Wang, D. A. Tirrell, *J. Am. Chem. Soc.* **2005**, *127*, 14150; c) J. Gierlich, K. Gutsmiedl, P. M. E. Gramlich, A. Schmidt, G. A. Burley, T. Carell, *Chem. Eur. J.* **2007**, *13*, 9486; d) T.-L. Hsu, S. R. Hanson, K. Kishikawa, S.-K. Wang, M. Sawaya, C.-H. Wong, *Proc. Natl. Acad. Sci. USA* **2007**, *104*, 2614.
- [6] a) M. R. Levingood, C. C. Kerwood, C. Chatterjee, W. A. van der Donk, *ChemBioChem* **2009**, *10*, 911; b) M. Galibert, P. Dumy, D. Boturyn, *Angew. Chem.* **2009**, *121*, 2614; *Angew. Chem. Int. Ed.* **2009**, *48*, 2576.
- [7] a) T. R. Chan, R. Hilgraf, K. B. Sharpless, V. V. Fokin, *Org. Lett.* **2004**, *6*, 2853; b) V. O. Rodionov, S. I. Presolski, S. Gardiner, Y. H. Lim, M. G. Finn, *J. Am. Chem. Soc.* **2007**, *129*, 12696.
- [8] W. G. Lewis, F. G. Magallon, V. V. Fokin, M. G. Finn, *J. Am. Chem. Soc.* **2004**, *126*, 9152.
- [9] S. Sen Gupta, J. Kuzelka, P. Singh, W. G. Lewis, M. Manchester, M. G. Finn, *Bioconjugate Chem.* **2005**, *16*, 1572.
- [10] V. Hong, A. K. Udit, R. A. Evans, M. G. Finn, *ChemBioChem* **2008**, *9*, 1481.
- [11] a) A. J. Link, D. A. Tirrell, *J. Am. Chem. Soc.* **2003**, *125*, 11164; b) D. C. Dieterich, J. J. Lee, A. J. Link, J. Graumann, D. A. Tirrell, E. M. Schuman, *Nat. Protoc.* **2007**, *2*, 532.
- [12] a) S. I. van Kasteren, H. B. Kramer, H. H. Jensen, S. J. Campbell, J. Kirkpatrick, N. J. Oldham, D. C. Anthony, B. G. Davis, *Nature* **2007**, *446*, 1105; b) S. I. Van Kasteren, H. B. Kramer, D. P. Gamblin, B. G. Davis, *Nat. Protoc.* **2007**, *2*, 3185.
- [13] a) M. A. Bruckman, G. Kaur, L. A. Lee, F. Xie, J. Sepulvecla, R. Breitenkamp, X. Zhang, M. Joralemon, T. P. Russell, T. Emrick, Q. Wang, *ChemBioChem* **2008**, *9*, 519; b) R. Kumar, A. El-Sagheer, J. Tumpane, P. Lincoln, L. M. Wilhelmsson, T. Brown, *J. Am. Chem. Soc.* **2007**, *129*, 6859; c) P. Kocalka, A. H. El-Sagheer, T. Brown, *ChemBioChem* **2008**, *9*, 1280; d) A. H. El-Sagheer, T. Brown, *J. Am. Chem. Soc.* **2009**, *131*, 3958; e) A. J. Dirks, J. J. L. M. Cornelissen, R. J. M. Nolte, *Bioconjugate Chem.* **2009**, *20*, 1129.
- [14] a) Q. Wang, T. R. Chan, R. Hilgraf, V. V. Fokin, K. B. Sharpless, M. G. Finn, *J. Am. Chem. Soc.* **2003**, *125*, 3192; b) S. C. Fry, *Biochem. J.* **1998**, *332*, 507.
- [15] E. Lallana, E. Fernandez-Megia, R. Riguera, *J. Am. Chem. Soc.* **2009**, *131*, 5748.
- [16] P. Y. Liu, N. Jiang, J. Zhang, X. Wei, H. H. Lin, X. Q. Yu, *Chem. Biodiversity* **2006**, *3*, 958.
- [17] R. H. Nagaraj, D. R. Sell, M. Prabhakaram, B. J. Ortwerth, V. M. Monnier, *Proc. Natl. Acad. Sci. USA* **1991**, *88*, 10257.
- [18] K. Sivakumar, F. Xie, B. M. Cash, S. Long, H. N. Barnhill, Q. Wang, *Org. Lett.* **2004**, *6*, 4603.
- [19] S. I. Presolski, V. Hong, M. G. Finn, **2009**, unpublished results.
- [20] V. O. Rodionov, S. I. Presolski, D. D. Diaz, V. V. Fokin, M. G. Finn, *J. Am. Chem. Soc.* **2007**, *129*, 12705.
- [21] W. L. Baker, J. Goode, L. Cooper, *Mikrochim. Acta* **1992**, *106*, 143.
- [22] a) Y. Liu, G. Sun, A. David, L. M. Sayre, *Chem. Res. Toxicol.* **2004**, *17*, 110; b) K. Uchida, S. Kawakishi, *Biochem. Biophys. Res. Commun.* **1986**, *138*, 659.
- [23] A more polar compound derived from the ligand was observed but not characterized during these experiments. This material is presumably produced by oxidation at one of the C–H sites adjacent to the triazole ring, or at the central nitrogen atom.
- [24] N. Shangari, T. S. Chan, K. Chan, S. H. Wu, P. J. O'Brien, *Mol. Nutr. Food Res.* **2007**, *51*, 445.
- [25] P. J. Thornalley, *Chem. Biol. Interact.* **1998**, *111–112*, 137.
- [26] a) E. Strable, D. E. Prasuhn, A. K. Udit, S. Brown, A. J. Link, J. T. Ngo, G. Lander, J. Quispe, C. S. Potter, B. Carragher, D. A. Tirrell, M. G. Finn, *Bioconjugate Chem.* **2008**, *19*, 866; b) E. Kaltgrad, M. K. O'Reilly, L. Liao, S. Han, J. Paulson, M. G. Finn, *J. Am. Chem. Soc.* **2008**, *130*, 4578; c) D. E. Prasuhn, P. Singh, E. Strable, S. Brown, M. Manchester, M. G. Finn, *J. Am. Chem. Soc.* **2008**, *130*, 1328.
- [27] V. Hong, A. A. Kislyukhin, M. G. Finn, *J. Am. Chem. Soc.* **2009**, *131*, 9986.
- [28] a) R. Agarwal, M. N. Gupta, *Biotechnol. Tech.* **1994**, *8*, 655; b) T. B. Osborne, C. S. Leavenworth, *J. Biol. Chem.* **1916**, *28*, 109.



NIH Public Access

Author Manuscript

Chembiochem. Author manuscript; available in PMC 2014 September 30.

Published in final edited form as:
Chembiochem. 2010 June 14; 11(9): 1273–1279. doi:10.1002/cbic.201000125.

Multivalent Display and Receptor-Mediated Endocytosis of Transferrin on Virus-Like Particles

Deboshri Banerjee^a, Allen P. Liu^b, Neil Voss^b, Sandra L. Schmid^{*b}, and M.G. Finn^{*a}

^a Department of Chemistry The Scripps Research Institute 10550 N. Torrey Pines Rd., La Jolla, CA, USA

^b Department of Cell Biology The Scripps Research Institute 10550 N. Torrey Pines Rd., La Jolla, CA, USA

Abstract

The structurally regular and stable self-assembled capsids derived from viruses can be used as scaffolds for the display of multiple copies of cell- and tissue-targeting molecules and therapeutic agents in a convenient and well-defined manner. The human iron-transfer protein transferrin, a high affinity ligand for receptors upregulated in a variety of cancers, has been arrayed on the exterior surface of the protein capsid of bacteriophage Q β . Selective oxidation of the sialic acid residues on the glycan chains of transferrin was followed by introduction of a terminal alkyne functionality via an oxime linkage. Attachment of the protein to azide-functionalized Q β capsid particles in an orientation allowing access to the receptor binding site was accomplished by the Cu^I-catalyzed azide-alkyne cycloaddition (CuAAC) click reaction. Transferrin conjugation to Q β particles allowed specific recognition by transferrin receptors and cellular internalization via clathrin-mediated endocytosis, as determined by fluorescence microscopy on cells expressing GFP-labeled clathrin light chains. By testing Q β particles bearing different numbers of transferrin molecules, it was demonstrated that cellular uptake was proportional to ligand density, but that internalization was inhibited by equivalent concentrations of free transferrin. These results suggest that cell targeting with transferrin can be improved by local concentration (avidity) effects.

Keywords

virus-like particles; transferrin; receptor-mediated endocytosis; polyvalency; click chemistry

Introduction

Human holo-transferrin (Tfn) is an 80 kDa bi-lobed iron-carrier glycoprotein in vertebrates,^[1] which is essential for iron homeostasis.^[2] Transferrin is specifically recognized by Tfn receptors (TfnR) overexpressed on the surface of a variety of tumor cells^[3] and efficiently taken up by cells in a well-characterized process of clathrin-mediated endocytosis.^[4] The Tfn-TfnR interaction has been exploited as a potential pathway for

* Fax: (+1)-858-784-8850 mgfinn@scripps.edu Fax: (+1)-858-784-9126 sandys@scripps.edu.

Supporting information for this article is available on the WWW under <http://www.chembiochem.org> or from the author.

uptake of Tfn-conjugated drugs by targeted cells.^[4-5] For example, polyvalent assembly of transferrin on liposomes^[6] and gold nanoparticles^[7] has been reported previously. In the current study, we wished to explore the mechanisms of interactions of TfnR-bearing cells with Tfn displayed on a uniform protein nanoparticle scaffold on which different densities of Tfn could be displayed.

We have previously described the conjugation of transferrin to cowpea mosaic virus (CPMV) by modification of both proteins with complementary azide and alkyne residues, and their subsequent ligation by the efficient Cu^I-catalyzed azide-alkyne cycloaddition (CuAAC) “click” reaction.^[8] In this study, we used the capsid of bacteriophage Q β , a virus-like particle (VLP) of 30 nm diameter and icosahedral symmetry, as the scaffold. Q β consists of 180 copies of a single coat-protein subunit, and, like CPMV,^[9] may be chemically addressed by acylation of surface lysine groups.^[10] It differs from CPMV in having a higher density of such amine attachment points and an overall smoother structure.

In addition to amine acylation, site-specific modification of proteins such as transferrin is often achieved by selective derivatization of cysteine thiols with maleimide or related electrophilic reagents, or oxidation of N-terminal serine or threonine to corresponding aldehydes and subsequent coupling with alkoxyamines or hydrazine derivatives.^[11] A disadvantage of these strategies is the possibility of irreversibly altering the structure or blocking the action of a key region of the protein, such as a catalytic site or binding motif, which may lead to a loss of activity. We describe here the alternative manipulation of transferrin by the derivatization of its sialic acid moieties, thus preserving the protein in its functional form, allowing us to efficiently and controllably graft it to the surface of the VLP scaffold.

Results and Discussion

Preparation and characterization of Q β -Tfn conjugates

Use of CuAAC chemistry for the attachment of transferrin to Q β requires the introduction of an azide or alkyne group to each partner. In a previous study, a maleimide-alkyne linker was used to derivatize transferrin at one or more accessible cysteine residues.^[8] While the target cysteines are not supposed to be near the site bound by the transferrin receptor, their derivatization introduces uncertainty in the position of the attachment site, and therefore in the orientation of the displayed protein. We turned here to the mild periodate oxidation of the sialic acid residues on transferrin. The main form of the human transferrin displays up to four terminal sialic acids per molecule.^[12] De-sialylated transferrin is reported to be internalized by both asialoglycoprotein and transferrin receptors,^[12b, 13] and the structure of the Tfn-TfnR interaction shows the glycosylation sites to be on a face of the protein far removed from the receptor-binding site.^[14] We therefore anticipated that connections made to derivatized sialic acid should not interfere with receptor-mediated endocytosis.

Oxidation of sialic acids on transferrin was followed by attachment of the aminoether linker 2 via the rapid formation of a physiologically-stable oxime linkage,^[15] giving the alkynefunctionalized transferrin 3 (Scheme 1). In order to determine the extent of this modification on the transferrin structure, a sample was condensed with azide-derivatized

fluorescein by CuAAC reaction using acceleratory ligand **4** under recently-reported optimized conditions.^[16] The product was analyzed by SDS-PAGE, verifying covalent attachment of the dye, and by UV-vis spectroscopy and determination of protein concentration by Bradford assay, showing that an average of 3.4 fluorescein molecules were attached per transferrin (Supporting Information). Thus, each transferrin molecule displayed 3-4 oxidized and derivatized sialic acid residues.

The surface-exposed lysine residues of the Q β capsid were simultaneously derivatized with an alkylazide^[8] and AlexaFluor® 568 by reaction with a 35:1 mixture of their corresponding N-hydroxysuccinimide esters (Scheme 1). The resulting particles **1** were thereby labeled with a small amount of dye to allow visualization by fluorescence microscopy in cell-binding studies while providing for multiple sites for subsequent transferrin attachment. The yield of **1** after purification of the protein from excess reagent was 80-85%, composed exclusively of intact particles as determined by size-exclusion chromatography (SEC).

Q β -Tfn conjugates (**5**) were prepared by CuAAC reaction of **1** with **3** in the presence of Cu^I and ligand **4**. The conjugates were purified by size-exclusion chromatography (SEC) and characterized by analytical SEC, UV-Vis spectroscopy, dynamic light scattering (DLS), transmission electron microscopy (TEM), SDS-PAGE and Western immunoblotting (Figure 1). The A₂₆₀/A₂₈₀ ratios confirmed the presence of intact, RNA-containing capsids, and SEC analysis showed **5** to elute more quickly than the underderivatized particle, indicating that the Tfn-decorated particles are larger (Figure 1A). Indeed, TEM showed intact and monodispersed particles of 26±2 nm diameter for the wild-type particles and 29±3 nm for the protein-conjugated particles, determined by automated image analysis. The same trend was observed by DLS, showing hydrodynamic diameters of 28.4 and 38.4 nm, for underderivatized and Tfn-labeled particle **5b**, respectively.

Western analysis further confirmed the attachment of Tfn molecules to the exterior surface of the virus-like particle (Figure 1D). The loading of Tfn molecules on the particle surface was determined by densitometry analysis after Coomassie staining of the SDS-PAGE gel (Figure 1C). Correcting for the relative molecular masses of the components, approximately 45 and 55 transferrin molecules were attached to Q β VLPs after reaction times of 2 h and 5 h, respectively. The CuAAC reaction was therefore revealed to be highly efficient at the micromolar concentrations of azide and alkyne components used, and little improvement was exhibited by longer reaction times.

In an early attempt to make fluorescently labeled particles for cell-binding studies, the red fluorescent protein mCherry was genetically encoded into approximately 15 copies of the Q β coat protein using a previously published method.^[17] While the resulting particles were insufficiently bright for the desired purpose, they were readily addressed with transferrin in analogous fashion to **5b**, resulting in the attachment of approximately 55 Tfn molecules per VLP as before. Cryo-electron microscopy analysis and image reconstruction revealed no difference between the mCherry-containing particles and the wild-type because of the sparse and presumably random distribution of mCherry fusions on the particle surface. In contrast, the cryo-EM image reconstruction of the conjugate of Tfn-alkyne with Q β (mCherry)-azide (see Supporting Information) showed clear density attributable to the added transferrin

protein (Figure 2). The bulk of the new density was found approximately 26 Å from the particle surface (shown most clearly in cutaway Figure 2D), consistent with the expected length of the linker connecting the VLP to Tfn.

Specific Binding and Internalization of Q β -Tfn conjugates

Tfn-TfnR complexes are known to enter the cell through clathrin-mediated endocytosis.^[18] To monitor clathrin-mediated endocytosis and to study the interaction between Tfn-VLPs and surface-exposed TfnRs, we used African Green Monkey kidney epithelial cells (BSC1) expressing a fusion between clathrin light chain (Clc) and enhanced green fluorescence protein (EGFP). Similar concentrations of dye-labeled Q β (**1**) and Q β -Tfn (**5**) were prebound at 4°C for 30 min to determine surface binding, and followed by an incubation at 37 °C for 1 hr to measure internalization. Surface binding and cellular internalization were analyzed by epi-fluorescence microscopy of fixed cells (Figure 3). No binding (Figure 3Ai) or uptake (Figure 3Aii) were observed with **1** even after 60 min at 37°C, indicating that Q β particles neither bind to cell surface receptors nor are internalized by these cells in a non-specific manner. In contrast, Q β -Tfn bound to the cell surface at 4°C (Figures 3Bi) as detected by the red fluorescence of the dye on **5**. Furthermore, substantial internalization was observed after 1 h at 37 °C. The red particles were observed to accumulate in intracellular structures at the cell periphery and in the peri-nuclear regions indicative of localization in endosomal structures (Figure 3Bii). VLP binding and internalization were abolished when excess unlabeled free transferrin was included in the incubations (Figure 3Aiii, 3Biii), demonstrating that binding and internalization occur through a Tfn-TfnR mediated pathway.

The involvement of TfnRs during virus uptake was further supported by overexpressing TfnR in BSC1 cells using adenovirus infection,^[19] resulting in significantly greater binding and uptake of Q β -Tfn conjugates by the infected cells (and not by the cells in the same sample that escaped adenovirus infection; Figures 3Ci, 3Cii). Binding and internalization of Q β -Tfn to TfnR overexpressing cells were again abolished in the presence of excess free Tfn (Figure 3Ciii). We also examined the localization of surface bound Q β -Tfn relative to clathrin-coated pits (CCPs) after 30 min incubation at 4°C (Figure 3D) and after pre-incubation followed by 5 min at 37°C (Supporting Information). Under both conditions, we could identify multiple CCPs containing VLPs, suggesting CCPs are the transport carrier of VLPs into the cell (Figure 3D, circled spots).

To examine the endocytic mechanism, we performed live cell imaging by total internal reflection fluorescence (TIRF) microscopy, which selectively illuminates the bottom surface of the plasma membrane (approx. 100 nm penetration depth). Dye-labeled Q β -Tfn conjugates were added to live cells at 37°C, and imaged for green fluorescence followed by red at 2 second intervals. Two main dynamic behaviors were observed: the recruitment of surface bound VLP to pre-formed clathrin-coated pits (CCPs), as shown in Figure 4A and B, and the apparent nucleation of CCPs by VLP binding to the TfnRs (Figure 4C). In both cases, endocytosis was often the result as evidenced by the disappearance or reduced intensity of the red (VLP) and green (clathrin) signals (Figure 4B). These results are reminiscent of those observed for the entry of dengue virus into BSC1 cells by clathrin-mediated endocytosis.^[20]

To explore the dependence of internalization on the surface density of transferrin molecules attached to the VLP surface, three versions of AlexaFluor-labeled Q β -Tfn conjugates were prepared with varying loadings of transferrin per particle, as shown in Figure 5. Azide-functionalized VLP **1** was addressed in three different CuAAC reactions, each containing the same total concentration of alkyne but differing in the ratio of transferrin-alkyne and propargyl alcohol. This provides for approximately the same density of triazoles on the particle surface, but differing amounts of the desired protein ligand. Reactions **a** and **b** differed by a factor of six in Tfnalkyne concentration, and resulted in a similar (five-fold) difference in attachment density (5 vs. 25 Tfn molecules per capsid). A further six-fold increase in Tfn-alkyne concentration (to 70 μ M, reaction **c**) increased the loading of Tfn by only 60 percent (to 40 \pm 5 per VLP), presumably because of steric crowding or occlusion of azide sites with increasing density of Tfn molecules on the particle surface. Until such steric limitations were reached at the highest loading, the CuAAC reactivity of the two alkynes were approximately the same, in spite of their great difference in size (Supporting Information).

The particles **6a-c** were found to be clean, monodisperse structures in the same manner as for conjugates **5**. Dynamic light scattering (DLS) measurements indicated the hydrodynamic diameters of the conjugates to be 32.4, 34.2, and 36.2 nm, respectively, compared to that of 28.4 nm for the wild-type particles and 38.4 nm for particle **5b** bearing the greatest number of Tfn molecules in this study (55 per particle). Mixtures of normal (rather than TfnR-upregulated) BSC1 cells with identical concentrations of dye-labeled Q β **1** or the three dye-Q β -Tfn conjugates were analyzed by flow cytometry to allow for more quantitative characterization of the internalization process. Figure 6A and B show results for the negative control **1** lacking transferrin and the particle bearing the greatest density of transferrin ligands, **6c**, respectively. Similar analyses for each of the particles as a function of incubation time with the cells showed maximum internalization to occur within 30-60 minutes.

The cellular uptake of Tfn-labeled particles and the inhibition of uptake by free Tfn were found to be consistent with single-point Tfn-TfnR interactions. Thus, while no uptake was observed with dye-labeled Q β **1** (Figure 6A), significant uptake was seen in a time-dependent manner when cells were incubated with Tfn-labeled VLP (Figure 6B). The extent of uptake was dependent on the number of Tfn units/particle (Figure 6C): only a low amount of specific uptake was observed with **6a**, bearing an average of 5 Tfn units per particle, uptake was moderate with **6b** (25 Tfn per particle) and quite efficient with **6c** (40 Tfn per particle). Considering the concentrations of Tfn involved (overall approximately 4, 15, and 24 nM for **6a**, **6b**, and **6c**, respectively), these data correspond roughly to what one would expect for a single-point binding interaction of about 5-10 nM, consistent with the reported low-nanomolar affinity of Tfn for the Tfn receptor.^[21] The efficient internalization of **6b** and **6c** was inhibited with free transferrin in a dose-dependent fashion (Figure 6D), with IC₅₀ values of approximately 1 μ g/mL (13 nM) for **6c** and 0.5 μ g/mL (6 nM) for **6b**. For both particles, 10 μ g/mL (125 nM) or more of free transferrin was completely inhibitory, while less than 0.01 μ g/mL (125 pM) had no effect. Since Q β -Tfn uptake was effectively inhibited by approximately equivalent concentrations of free Tfn as were presented by the particles, the

Tfn-conjugated VLP ligands did not appear to benefit from their polyvalency with respect to affinity or avidity.

Conclusion

The oxidation and derivatization of the sialic acid residues of transferrin is a convenient and effective method for introducing a connecting linkage that can provide a consistent display geometry while retaining binding affinity to transferrin receptors. Conjugation of transferrin-alkyne thus prepared to the azide-functional groups on the Q β virus capsid was accomplished using the powerful CuAAC click reaction in a recently-reported optimized protocol.^[16] These conjugates were specifically internalized by cells expressing transferrin receptors via clathrin-mediated endocytosis.

Our studies represent the first test of transferrin polyvalency on receptor-mediated cell entry in which the protein ligands are arranged in a well-defined platform-based manner. On a per-unit basis, the Q β -Tfn conjugates have greater affinities for TfnR-bearing cells than free Tfn, and the rates of uptake of Tfn-bearing particles were strongly improved by the attachment of greater numbers of Tfn ligands to each particle (Figure 6C). These findings suggest that polyvalent transferrin conjugates can enhance the targeting of specific cell populations in complex mixtures. However, on a per-Tfn basis, the VLPs did not exhibit significantly increased affinity relative to the free ligand. This interesting disconnection of affinity (or avidity)^[22] and internalization efficiency remains unexplained at present, but changes in recycling^[23] and intracellular trafficking pathways exhibited by multivalent constructs may be at least partially responsible. These findings make transferrin assemblies potentially useful in the delivery of drugs for therapeutic purposes.^[24]

Experimental Section

Details of instrumentation and the purchase or preparation of all reagents, including the Q β VLPs, are given in Supporting Information.

Preparation of Alexa Fluor® 568 labeled Q β -azide (1)

A solution of wild-type Q β VLPs (5 mg/mL in 0.1 M phosphate buffer, pH 7) was treated with a pre-mixed DMSO solution of NHS-linker-azide (final concentration 12 mM, 35-fold excess per Q β subunit) and the NHS ester of the dye (final concentration 0.35 mM), such that the final reaction mixture contained 20% DMSO. The solution was allowed to stand for 12 h at room temperature, and the derivatized VLP was purified away from excess reagents on a 10-40% sucrose gradient and concentrated by ultrapelleting. The virus pellet was resuspended in HEPES buffer (0.1 M, pH 7.3). FPLC analysis of **1** indicated that >95% of the virus consisted of intact particles. Protein concentration was analyzed by using the Coomassie Plus (Bradford) Protein Assay (Pierce).

Synthesis of O-(prop-2-ynyl)hydroxylamine (2)

Phthalimide-protected O-(prop-2-ynyl)hydroxylamine (5.0 g, 24.9 mmol) was stirred with hydrazine monohydrate (1.4 g, 27.8 mmol) for a few minutes before the addition of diethyl ether (25 mL). This mixture was stirred at room temperature for 45 min. The white

precipitate was filtered off and 18 mL of 2 N ethereal HCl was added to the filtrate with continuous stirring. The yellow-white precipitate was filtered and dried under vacuum to give **2** (2.1 g, 78%), which was characterized by ¹H NMR spectroscopy, matching the data previously reported.^[25]

Preparation of Transferrin-Alkyne Conjugate (3)

Transferrin (2 mg/mL) was incubated with sodium *meta*-periodate (1 mM) in sodium acetate buffer (0.1 M, pH 5.5; 30 mL) on ice in the dark for 30 min. The mixture was concentrated to less than 1 mL using centrifugal filter tubes (Millipore), and then dialyzed against HEPES buffer (0.1 M, pH 7.2) using Slide-A-Lyzer® Dialysis Cassette Kit (Pierce). The resulting oxidized transferrin was incubated with **5** (8.2 mM, 350-fold excess) in HEPES buffer with 20% DMSO (total volume 25 mL) for 5 h at room temperature by gentle tumbling. Concentration and dialysis as above provided **3** as a pink-colored solution in HEPES buffer; the protein concentration was estimated using the Bradford protein assay.

Preparation of Q β -Transferrin Conjugate (5) by CuAAC Reaction

Two identical reaction mixtures were prepared, each containing Q β -azide **1** (1.7 mg/mL, 0.11 mM in protein subunits) and transferrin-alkyne **3** (10.2 mg/mL, 0.12 mM) in HEPES buffer (0.1 M, pH 7.3, 1 mL), containing sodium ascorbate (5 mM), copper sulfate (0.25 mM) and the ligand **4** (1.25 mM). CuSO₄ was mixed with **4** in a separate microtube prior to addition to each reaction mixture. The reaction mixtures were allowed to stand at room temperature for 2 h and 5 h, respectively. The resulting conjugates (**5a**, **5b**) were purified by size-exclusion FPLC on a Superose 6 column.

For all of the above steps, we used diferric Tfn under conditions designed to minimize the loss of iron. After conjugation, the protein absorbance ratio (A₄₆₅/A₂₈₀) was found to be 0.043, within the range (0.042-0.046) indicating the presence of Fe in the protein.^[26] If Fe is lost, the ability of the attached Tfn to bind its receptor would be somewhat diminished, as the affinity for TfnR for apo-Tfn is approximately 10-fold less than for Fe₂Tfn.^[21, 27]

SDS-PAGE and Western Blot Analysis of Q β -Tfn Conjugates

Q β VLP samples **1** and **5a,b** were analyzed on denaturing 4–12% NuPage protein gels using 1x MES buffer (Invitrogen). The gel was observed under UV illumination to detect fluorescent dye-labeled bands before staining with Coomassie SimplyBlue™ SafeStain (Invitrogen). For Western blot analysis, after electrophoretic separation on the gel, the proteins were transferred to a nitrocellulose membrane (Millipore) by electrophoretic blotting. After blocking with 5% (w/v) dry milk in TBS-T for 1 h, transferrin conjugation to Q β was detected with HRP-conjugated mouse monoclonal anti-transferrin antibody (Abcam), diluted 1:5000 in TBS-T buffer. HRP detection of peroxide was performed with SuperSignal chemiluminescence substrate (Pierce) and exposure to X-ray film.

Cell Culture and Uptake Studies

BSC1 monkey kidney epithelial cells stably expressing rat brain EGFP-clathrin light chain (EGFPLCa) were provided by Dr. T. Kirchhausen, Harvard Medical School and cultured in DMEM supplemented with 10% fetal bovine serum (FBS) and 500 µg/mL G418. For

microscopy studies, cells were plated on glass coverslip at a density of 8.3×10^3 cells/cm² overnight. Cells were washed twice in PBS, and VLPs diluted in PBS⁴⁺ (1 mM CaCl₂, 1 mM MgCl₂, 0.2% BSA (w/v), and 5 mM glucose) at a concentration of 0.6 µg/ml. The cells were either kept at 0°C for binding or shifted to 37°C for the desired amount of time. The cells were washed again twice in PBS, and then fixed in 4% paraformaldehyde for 30 minutes at room temperature. The cells were visualized at 60× magnifications using an Olympus X71 epifluorescence microscope equipped with the appropriate filter sets and a CCD camera.

Measurement of Virus Binding by Flow Cytometry

BSC1 cells were cultured on 15 cm dishes to confluence, and then lifted from surface by treating the cells with PBS/5mM EDTA for 15 minutes at room temperature. The cells were pelleted at 1,000 rpm for 10 minutes and resuspended in 500 µL of PBS⁴⁺. VLPs were added to the cells suspensions at 1:200 or 1:500 dilution and aliquoted to different tubes for incubation at 37°C water bath for various amount of time. Cells were washed twice in PBS supplemented with 1% FBS, 25mM HEPES, and 1mM EDTA. The pelleted cells were finally resuspended in 200 µL of PBS and then fixed by adding 200 µL 4% paraformaldehyde in PBS. Fixed cells were typically analyzed within 1 hr on Vantage Diva cell sorter.

Electron micrographs were acquired using a Tecnai F20 Twin transmission electron microscope operating at 120 kV, a nominal magnification of 80,000X, a pixel size of 0.105 nm at the specimen level, and a dose of ~20 e⁻/Å². 348 images were automatically collected by the Leginon system^[28] and recorded using a Tietz F415 4k × 4k pixel CCD camera. Experimental data were processed using the Appion software package.^[29] 3,554 particles were manually selected and then filtered down to 2,239 particles for the reconstruction. The 3D reconstruction was carried out using the EMAN reconstruction package.^[30] A resolution of 17.4 Å was determined by even-odd Fourier Shell Correlation (FSC) at a cutoff of 0.5.

Supplementary Material

Refer to Web version on PubMed Central for supplementary material.

Acknowledgments

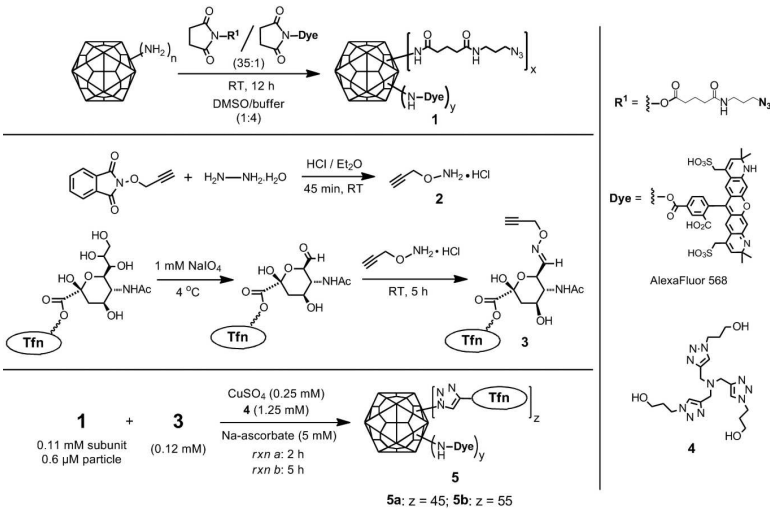
This work was supported by the NIH (CA112075), The Skaggs Institute for Chemical Biology, and Pfizer Global Research and Development. The authors would like to thank Dr. Malcolm R. Wood for guidance in acquiring TEM images, Mr. Cody Fine for assistance with flow cytometry data collection, and Mr. Steven Brown for the mCherry-bearing particles used for Tf_n attachment and cryo-EM analysis.

References

1. Huebers HA, Finch CA. *Physiol. Rev.* 1987; 67:520. [PubMed: 3550839]
2. Anderson GJ, Vulpe CD. *Cell. Mol. Life Sci.* 2009; 66:3241. [PubMed: 19484405]
3. Ryschich E, Huszty G, Knaebel HP, Hartel M, Buechler MW, Schmidt J. *Eur. J. Cancer.* 2004; 40:1418. [PubMed: 15177502]
4. a Daniels TR, Delgado T, Helguera G, Penichet ML. *Clinical Immunology.* 2006; 121:159. [PubMed: 16920030] b Daniels TR, Delgado T, Rodriguez JA, Helguera G, Penichet ML. *Clinical Immunology.* 2006; 121:144. [PubMed: 16904380]

5. a Li H, Qian ZM. *Med. Res. Rev.* 2002; 22:225. [PubMed: 11933019] b Li H, Sun H, Qian ZM. *Trends Pharmacol. Sci.* 2002; 23:206. [PubMed: 12007993] c Qian ZM, Li H, Sun H, Ho K. *Pharmacol. Rev.* 2002; 54:561. [PubMed: 12429868] d Widera A, Norouziyan F, Shen WC. *Adv. Drug Delivery Rev.* 2003; 55:1439.
6. Derycke ASL, Kamuhabwa A, Gijsens A, Roskams T, de Vos D, Kasran A, Huwyler J, Missiaen L, de Witte PAM, Natl J. Cancer Inst. 2004; 96:1620.
7. Yang P-H, Sun X, Chiu J-F, Sun H, He Q-Y. *Bioconjugate Chem.* 2005; 16:494.
8. Sen Gupta S, Kuzelka J, Singh P, Lewis WG, Manchester M, Finn MG. *Bioconjugate Chem.* 2005; 16:1572.
9. Wang Q, Kaltgrad E, Lin T, Johnson JE, Finn MG. *Chem. Biol.* 2002; 9:805. [PubMed: 12144924]
10. a Strable E, Finn MG. *Curr. Top. Microbiol. Immun.* 2008; 327:1.b Prasuhn DE Jr. Singh P, Strable E, Brown S, Manchester M, Finn MG. *J. Am. Chem. Soc.* 2008; 130:1328. [PubMed: 18177041]
11. a Hermanson, GT. *Bioconjugate Techniques*. Second Edition. Academic Press; San Diego: 2008. b Geoghegan KF, Stroh JG. *Bioconjugate Chem.* 1992; 3:138.c Goodson RJ, Katre NV. *Biotechnology*. 1990; 8:343. [PubMed: 1366535]
12. Petren S, Vesterberg O. *Biochim. Biophys. Acta, Protein Struct. Mol. Enzymol.* 1989; 994:161. Welch S. *Transferrin: The Iron Carrier*. 1992:253.CRC PressBoca Raton The number of sialic acid groups on transferrin, as well as the total serum sialic acid level, is used as a diagnostic marker of alcoholism. See: Chrostek L, Cylwik B, Krawiec A, Korcz W, Szmitkowski M. *Alcohol Alcohol*. 2007; 42:588–592. [PubMed: 17573378]
13. Beguin Y, Bergamaschi G, Huebers HA, Finch CA. *Am. J. Hematol.* 1988; 29:204. [PubMed: 3189316]
14. a Cheng Y, Zak O, Aisen P, Harrison SC, Walz T. *J. Struct. Biol.* 2005; 152:204. [PubMed: 16343946] b Cheng Y, Zak O, Aisen P, Harrison SC, Walz T. *Cell.* 2004; 116:565. [PubMed: 14980223]
15. a Dawson PE, Kent SBH. *Annu. Rev. Biochem.* 2000; 69:923. [PubMed: 10966479] b Dirksen A, Hackeng TM, Dawson PE. *Angew. Chem., Int. Ed.* 2006; 45:7581.
16. Hong V, Presolski SI, Ma C, Finn MG. *Angew. Chem., Int. Ed.* 2009; 48:9879.
17. Brown SD, Fiedler JD, Finn MG. *Biochemistry*. 2009; 48:11155. [PubMed: 19848414]
18. Warren RA, Green FA, Enns CA. *J. Biol. Chem.* 1997; 272:2116. [PubMed: 8999911]
19. Loerke D, Mettlen M, Yarar D, Jaqaman D, Jaqaman H, Danuser G, Schmid SL. *PLoS Biol.* 2009; 7:e57. [PubMed: 19296720]
20. Van der Schaaf HM, Rust MJ, Chen C, Van der Ende-Metselaar H, Wilschut J, Zhuang X. *PLoS Pathogens.* 2008; 4:e1000244. [PubMed: 19096510]
21. Ciechanover A, Schwartz AL, Dautryvarsat A, Lodish HF. *J. Biol. Chem.* 1983; 258:9681. [PubMed: 6309781]
22. For definitions and discussion of affinity and avidity in the context of polyvalent interactions, see: Mammen M, Choi S-K, Whitesides GM. *Angew. Chem. Int. Ed.* 1998; 37:2754–2794. We also recommend the following paper for an excellent example of their application: Arranz-Plaza E, Tracy AS, Siriwardena A, Pierce JM, Boons G-J. *J. Am. Chem. Soc.* 2002; 124:13035–13046. [PubMed: 12405830]
23. Marsh EW, Leopold PL, Jones NL, Maxfield FR. *J. Cell Biol.* 1995; 129:1509. [PubMed: 7790351]
24. Lim CJ, Shen WC. *Pharm. Res.* 2004; 21:1985. [PubMed: 15587919]
25. Goldberg MW, Lehr HH, Muller M. Hoffmann-La Roche, Inc., US. 1968
26. Zak O, Ikuta K, Aisen P. *Biochemistry*. 2002; 41:7416. [PubMed: 12044175]
27. a Dautry-Varsat A, Ciechanover A, Lodish HF. *Proc. Natl. Acad. Sci. U.S.A.* 1983; 80:2258. [PubMed: 6300903] b Hasegawa T, Ozawa E. *Develop. Growth Differ.* 1982; 24:581.
28. Suloway C, Pulokas J, Fellmann D, Cheng A, Guerra F, Quispe J, Stagg S, Potter CS, Carragher B. *J. Struct. Biol.* 2005; 151:41. [PubMed: 15890530]
29. a Lander GC, Stagg SM, Voss NR, Cheng A, Fellmann D, Pulokas J, Yoshioka C, Irving C, Mulder A, Lau P-W, Lyumkis D, Potter CS, Carragher B. *J. Struct. Biol.* 2009; 166:95. [PubMed:

- 19263523] b Voss NR, Lyumkis D, Cheng A, Lau P-W, Mulder A, Lander GC, Brignole EJ, Fellmann D, Irving C, Jacovetty EL, Leung A, Pulokas J, Quispe JD, Winkler H, Yoshioka C, Carragher B, Potter CS. *J. Struct. Biol.* 2010 in press (PMID: 20018246).
30. Ludtke SJ, Baldwin PR, Chiu W. *J. Struct. Biol.* 1999; 128:82. [PubMed: 10600563]



Scheme 1.
Synthesis of Q β -Tfn conjugates.

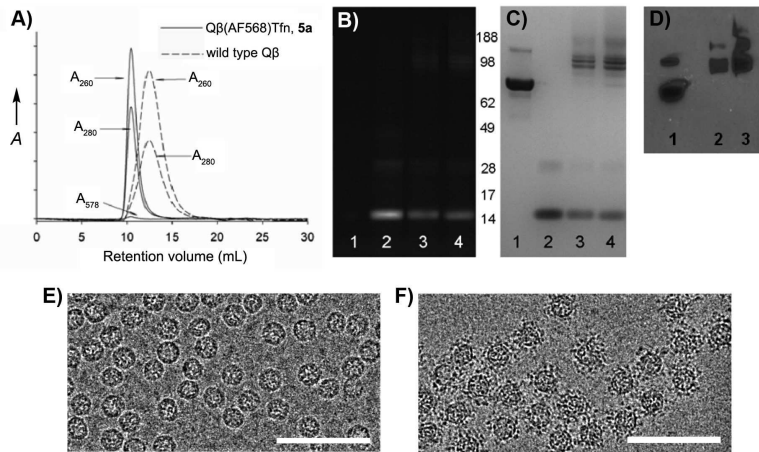


Figure 1.
Characterization of Q β -Tfn conjugates. (A) Size-exclusion FPLC (Superose-6 column). (B) SDS-PAGE analysis of the protein gel under UV illumination and (C) after SimplyBlue staining. For (B) and (C), lanes: (1) transferrin, (2) Q β -azide/dye conjugate **1**, (3) Q β -Tfn conjugate **5a** (45 Tfn/particle), (4) Q β -Tfn conjugate **5b** (55 Tfn/particle). (D) Western blot analysis, probing with anti-transferrin antibody; lanes: (1) transferrin, (2) **5a**, (3) **5b**. (E) TEM of underivatized Q β . (F) TEM of Q β -Tfn conjugate **5b**. Scale bar = 100 nm.

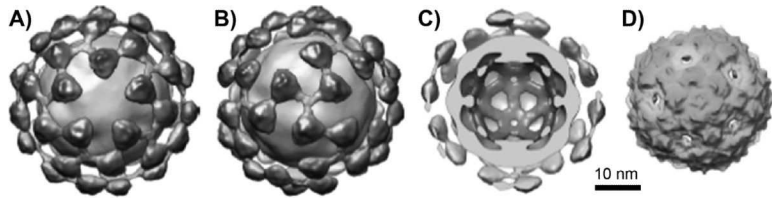
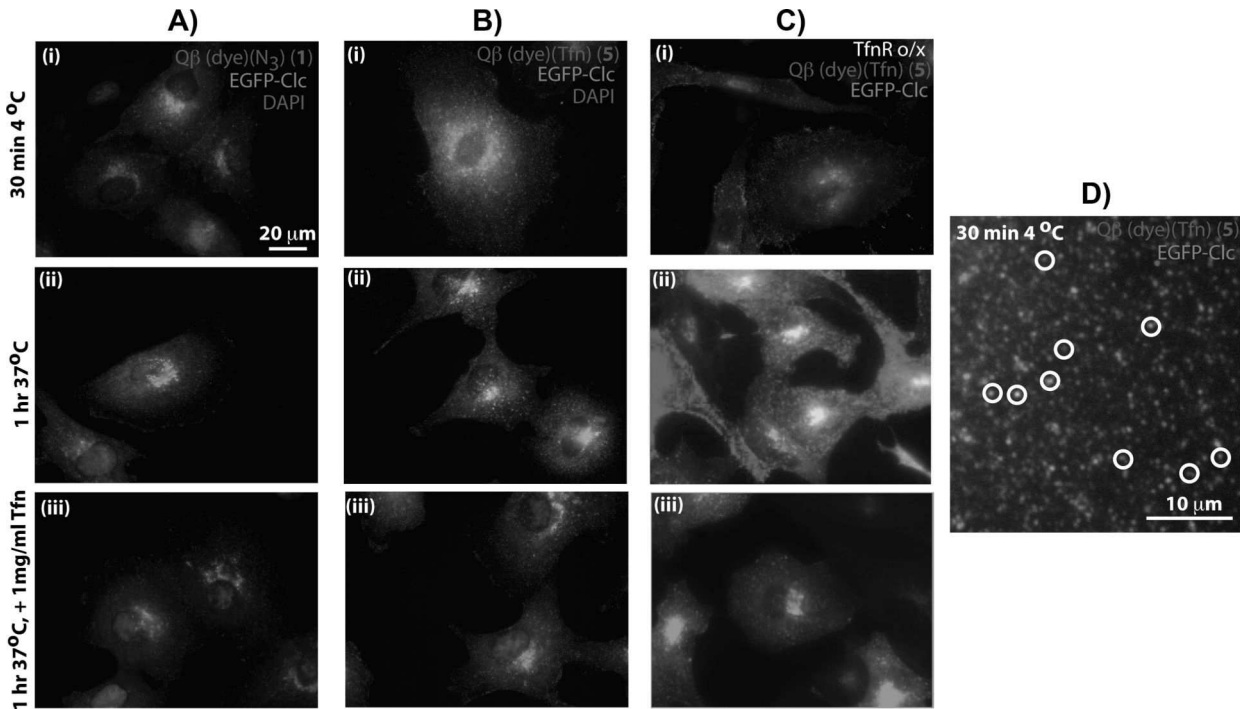
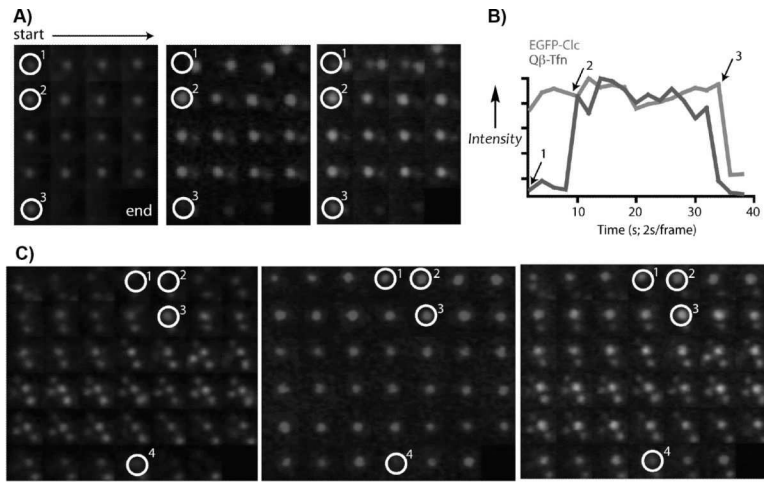


Figure 2.

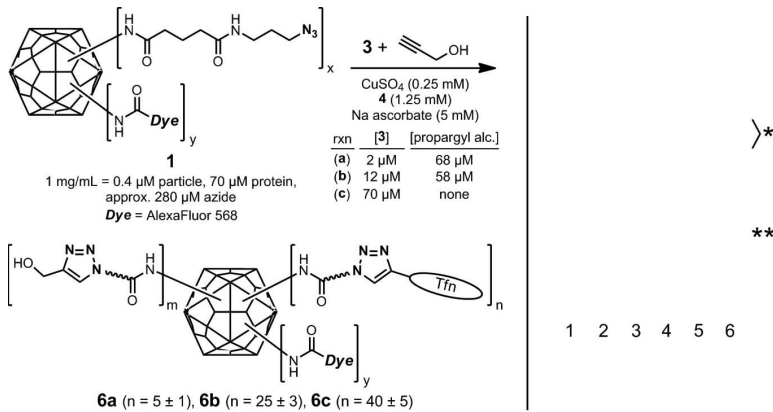
Cryo-electron microscopy image reconstructions at 17.4 Å resolution. (A,B) Q β (mCherry) (Tfn)₅₅ conjugate; views down the 5- and 3-fold symmetry axes, respectively. (C) Cross-sectional view showing added density other than that of the VLP in light blue. (D) Wild-type Q β and Q β (mCherry).

**Figure 3.**

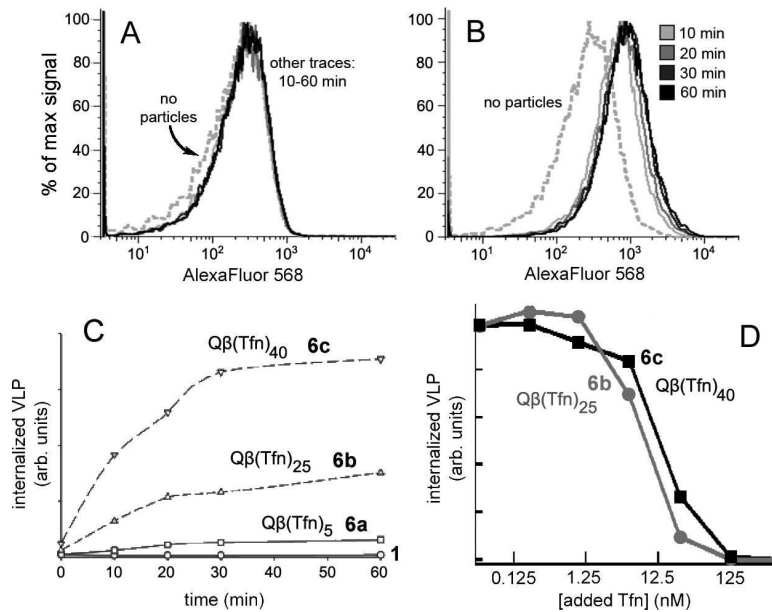
Representative epi-fluorescence microscopy images showing binding and internalization of VLP particles in EGFP-Clc BSC1 cells. (Column A) Q β particle **1** with EGFP-Clc BSC1 cells. (Column B) Q β -Tfn conjugate **5b** with EGFP-Clc BSC1 cells. (Column C) **5b** and EGFP-Clc BSC1 cells overexpressing transferrin receptors. (Row *i*) After incubation at 4°C for 30 min. (Row *ii*) Preincubated at 4°C followed by shift to 37°C for 60 min. (Row *iii*) As in Row *ii*, except in the presence of excess free Tfn (1 mg/mL). (D) High-magnification image showing punctate red (**5b**), green (EGFP-Clc), and colocalized (circled) VLPs with CCPs on the surface of a BSC1 cell after 30 minutes at 4°C. Very similar images were observed with cells incubated at 37°C for 5 min (Supporting Information). In all experiments, VLP concentration was 1.2 μ g/mL (0.47 nM in particles).

**Figure 4.**

Live cell TIRF images showing green (EGFP-Clc), red (Q β -Tfn particle **5b**), and merged channels of an approximately $2 \mu\text{m}^2$ area of the bottom surface of a BSC1 cell. Images go left-to-right across each row, and from top to bottom, taken at 2-second intervals with the green channel preceding the red channel. (A) VLPs associating with a pre-existing coated pit (circled white), followed by internalization of the complex as a whole. Position 1 shows the pre-existing coated pit. Position 2 marks the initial recruitment of the VLP. Position 3 is the time point at which internalization occurs between the acquisition of the green and red channels; note that both are gone at the next time point. (B) Plot of intensity profiles of the CCP (green) and VLP (red) at the indicated spot in (A), normalized each to their respective maximum intensity. (C) VLP nucleating a CCP. Position 1 shows a bound VLP but no clathrin signal. At positions marked 2, the CCP is beginning to assemble at the VLP. By position 3, the pit is fully formed, and it is internalized at position 4. In this case the internalized VLP remains close to the plasma membrane, while the clathrin coat disassembles.

**Figure 5.**

(Left) Synthesis of particles with varying loadings of attached transferrin. (Right) Coomassie stained protein gel of transferrin (lane 2), Q β -azide **1** (lane 3), Q β -Tfn conjugates **6a** (lane 4), **6b** (lane 5), and **6c** (lane 6). (Standard protein molecular weight markers appear in lane 1). The bands labeled with a single asterisk denote linked transferrin-Q β linkages with differing numbers of Q β coat protein attached to each transferrin molecule. Bands marked with a double asterisk are due to Q β capsid protein dimers that remain noncovalently associated even under the denaturing conditions of the analysis.

**Figure 6.**

FACS analysis following incubation of Q β -Tfn conjugates with BSC1 cells at 37°C for the specified time, followed by washing and chemical fixation. (A) Underderivatized Q β VLP 1 (3 μ g/mL, 1.2 nM in particles), showing no evidence of binding. (B) Q β -Tfn VLP 6c (1.6 μ g/mL (0.6 nM in particle), showing significant and rapid virus uptake. (C) Summary of data for 1 and 6a-c, showing that higher Tfn load leads to increased uptake by cells. (D) Effect of increasing concentrations of free unlabeled Tfn on cellular uptake of 1.6 μ g/mL 6b (i.e. 0.6 nM particle, 15 nM Tfn) or 6c (24 nM Tfn) as detected by FACS.

RNA-Directed Packaging of Enzymes within Virus-like Particles**

Jason D. Fiedler, Steven D. Brown, Jolene L. Lau, and M. G. Finn*

Dedicated to Professor John E. Johnson on the occasion of his 65th birthday

The sequestration of functional units from the environment is a hallmark of biological organization. In addition to encapsulation within lipid membrane-bound organelles, proteinaceous cages serve this purpose for many prokaryotes.^[1] From a chemical perspective, the outstanding advantages of such packages are their capabilities for high selectivity and activity, both achieved by encapsulating only those catalysts required for the desired task in confined space, and the potential for the container to control its position in a complex environment. Artificial encapsulation or immobilization on solid supports has been shown to confer stability as well as facilitate purification and re-use.^[2] While chemists have sequestered enzymes in or on a wide variety of nonbiological compartments, nature remains the undisputed master of the art.

Protein nanoparticles represent a uniquely useful bridge between chemistry, materials science, and biology because they combine robust self-assembly properties with genetically enabled atomic control of chemical reactivity. The synthetic biomimetic packaging of functional proteins has been accomplished with different types of protein nanoparticles. Two general strategies have been employed: 1) genetic fusion of the cargo to a component that directs localization to the particle interior,^[3] and 2) nonspecific packaging by in vitro assembly.^[4] However, yields of the encapsulated protein products have been low, and, while examples of increased stability towards a variety of treatments have been noted,^[3b,c,4b] no quantitative kinetic comparisons of enzymes in free versus protein-encapsulated forms have been described. We report here the use of a virus-like particle for this purpose, providing a general and robust method for the encapsulation of highly active enzymes.

Bacteriophage Q β form icosahedral virus-like particles (VLPs) from 180 copies of a 14.3 kDa coat protein (CP).^[5] These VLPs are highly stable under a variety of conditions and have been used to display functional small molecules,^[6] immunogenic ligands,^[7] and peptides and proteins on their

exterior surface.^[8] The infectious phage particle packages its single-stranded RNA genome by virtue of a high-affinity interaction between a hairpin structure and interior-facing residues of the CP.^[9] This interaction is preserved when the CP is expressed recombinantly to form VLPs^[10] and we used this to direct the packaging of cargo materials (Figure 1). A related approach has been reported by Franzen and co-workers to entrain gold nanoparticles inside red clover necrotic mosaic virus.^[11]

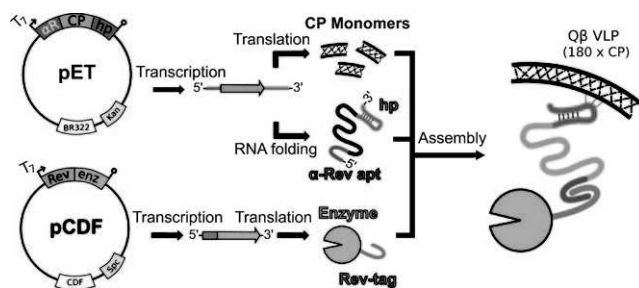


Figure 1. The technique used to package protein inside Q β VLPs. Dual-plasmid transformation of *E. coli* with compatible T7 expression vectors is the only input into the system. IPTG induction results in the expression of coat protein (CP), Rev-tagged cargo enzyme, and bifunctional mRNA. The Rev-tag binds to the α -Rev aptamer (apt) and Q β genome packaging hairpin (hp) binds to the interior of the CP monomers, thus tethering the enzyme to the interior of the VLP with the coat protein RNA sequence (cp) acting as the linker.

To facilitate RNA-directed encapsidation, two binding domains were introduced to the CP mRNA, carried on a ColE1-group plasmid. An RNA aptamer developed by in vitro selection to bind an arginine-rich peptide (Rev) derived from HIV-1^[12] was inserted just upstream of the ribosome binding site. The sequence of the Q β packaging hairpin was positioned immediately downstream of the stop codon. The cargo enzyme was N-terminally tagged with the Rev peptide and inserted into a compatible CloDF13-group plasmid. Transformation with both plasmids and expression in BL21-(DE3) *E. coli* yielded VLPs encapsidating the Rev-tagged protein. Such species are designated Q β @(protein) $_n$, where n = the average number of proteins packaged per particle, determined by electrophoretic analysis as in Figure 2a and Figure S1a in the Supporting Information. We report here the packaging of the 25-kDa N-terminal aspartate dipeptidase peptidase E (PepE),^[13] 62-kDa firefly luciferase (Luc), and a thermostable mutant of Luc (tsLuc)^[14] inside VLPs.

The enzyme-filled VLPs were indistinguishable from standard VLPs by techniques that report on the exterior dimensions of the particles (transmission electron micro-

[*] J. D. Fiedler, S. D. Brown, J. L. Lau, Prof. M. G. Finn
Department of Chemistry and The Skaggs Institute for Chemical Biology, The Scripps Research Institute
10550 North Torrey Pines Road, La Jolla, CA 92037 (USA)
Fax: (+1) 858-784-8850
E-mail: mgfinn@scripps.edu

[**] We are grateful to Dr. So-Hye Cho for assistance in acquiring TEM images, and to Dr. Joshua Price for analytical ultracentrifugation. The pRevTRE-Luc vector was a kind gift from Ashley Pratt. This project was supported by the National Institutes of Health (CA112075 and RR021886), the Skaggs Institute for Chemical Biology, and the W.M. Keck Foundation.

Supporting information for this article is available on the WWW under <http://dx.doi.org/10.1002/anie.201005243>.

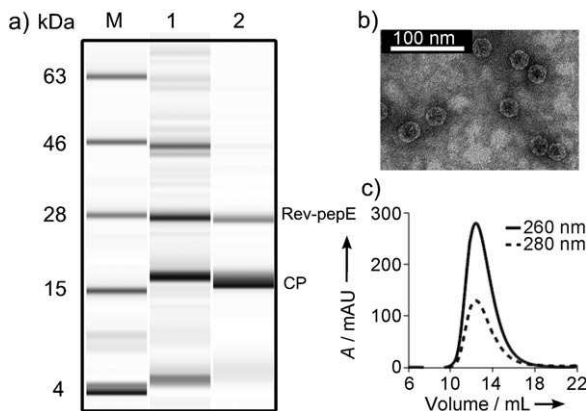


Figure 2. Characterization of $\text{Q}\beta@(\text{RevPepE})_{18}$. a) Electrophoretic analysis: lane M = protein ladder marker, 1 = *E. coli* cell lysate 4 h after induction, 2 = purified particles showing CP and Rev-pepE bands. b) Transmission electron micrograph; images are indistinguishable from those of WT $\text{Q}\beta$ VLPs. c) Size-exclusion fast protein liquid chromatography (FPLC; Superose 6) showing the intact nature of the particles.

py, size-exclusion chromatography, and dynamic light scattering; Figure 2b,c, Figure S2b,c and Table S3). However, the particles exhibited different densities by analytical ultracentrifugation: nonpacked $\text{Q}\beta$ VLPs, 76S; $\text{Q}\beta@(\text{RevLuc})_4$, 79S; and $\text{Q}\beta@(\text{RevPepE})_{18}$, 86S (Figure S2). These values agree with variations expected in overall molecular weights calculated from estimates of the RNA and protein content of each particle (Supporting Information).

The average number of encapsidated cargo proteins was controlled by changing expression conditions or by removing interaction elements from the plasmids (Table S2). In this way, PepE incorporation could be reproducibly varied between 2 and 18 per particle. Fewer copies of Luc proteins were packaged: 4–8 copies per particle were found for most conditions, whereas the number of packaged tsLuc molecules varied between 2 and 11 per VLP. In addition to its larger size, Luc is less stable than PepE and its gene was not optimized for expression in *E. coli* (Supporting Figure S1a, lane 1)—all factors that could contribute to the lower numbers of packaged enzyme in this case. Yields of purified particles ranged from approximately 50–75 mg per liter of culture for the typical particles encapsidating PepE, and 75–140 mg per liter for the Luc or tsLuc particles (Table S2).

To test the functional capabilities of the packaged enzymes, the activities of encapsidated Rev-PepE and free PepE were compared using the fluorogenic substrate Asp-AMC^[15] (Figure 3). The kinetic parameters, obtained by standard Michaelis–Menten analysis, were found to be quite similar for the two forms of the enzyme, with k_{cat}/K_m for free PepE exceeding that of $\text{Q}\beta@(\text{RevPepE})_9$ by a factor of only three ($1.8 \pm 0.2 \times 10^{-2}$ vs. $6.3 \pm 0.9 \times 10^{-3}$). The observed K_m values are comparable to those reported for cleavage of Asp-Leu (0.3 mM).^[13] For this analysis, all copies of encapsidated RevPepE in $\text{Q}\beta@(\text{RevPepE})_9$ were assumed to be independently and equivalently active, and the substrate and product were assumed to diffuse freely in and out of the capsid. The

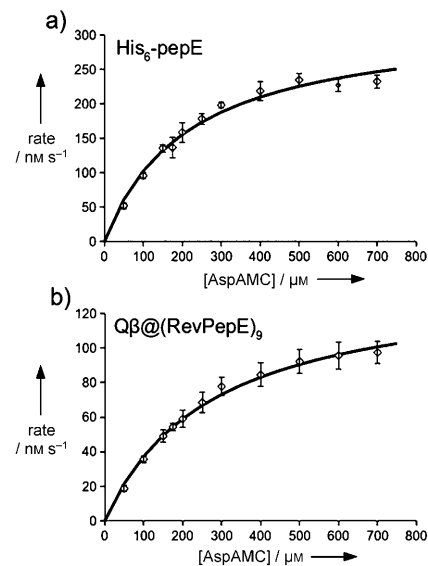


Figure 3. Kinetics of PepE-catalyzed hydrolysis of fluorogenic Asp-AMC. Squares show the average of three independent initial rate measurements (< 4 min) with standard deviation as the error bars. Solid curves show the best fit using the Michaelis–Menten equation, giving the parameters: a) $v_{\text{max}} = 322 \pm 4 \text{ nm s}^{-1}$, $k_{\text{cat}} = 3.8 \pm 0.1 \text{ s}^{-1}$, $K_{m,\text{app}} = 210 \pm 20 \mu\text{M}$; b) $v_{\text{max}} = 140 \pm 2 \text{ nm s}^{-1}$, $k_{\text{cat}} = 1.7 \pm 0.1 \text{ s}^{-1}$, $K_{m,\text{app}} = 270 \pm 20 \mu\text{M}$.

close correspondence between the reactions of free and encapsidated enzyme appear to support these assumptions.

Peptidase E was also significantly stabilized by encapsidation. Free PepE retained only half of its initial activity after incubation for 30 min at 45 °C and 20% of its activity at 50 °C (Figure 4a). In contrast, $\text{Q}\beta@(\text{RevPepE})_9$ showed no loss of activity at temperatures up to 50 °C for 30 min. Extended incubation at these temperatures showed the packaged enzyme was about 60 times more resistant than the free enzyme to thermal deactivation (Figure S3). Heating did not disrupt the particle structure (Figure S4), suggesting that at least partial denaturation of the packaged protein can occur inside the capsid shell. Packaged RevPepE was also protected from protease digestion, maintaining more than 80% activity under conditions in which the activity of the free enzyme was entirely degraded by proteinase K (Figure 4b).

The activity of $\text{Q}\beta@(\text{RevLuc})$ was similarly compared to free recombinant firefly luciferase. In this case, packaging of the enzyme did not substantially change k_{cat} , but K_m in both luciferin and ATP substrates was significantly higher for the packaged enzyme (Table 1, Figure S5). Luciferase is quite unstable toward thermal denaturation in both free and immobilized forms,^[16] the free tsLuc variant having a half-life at 37 °C of only 16 min.^[14] No improvement in thermal sensitivity was observed for $\text{Q}\beta@(\text{Rev-tsLuc})_9$, but both packaged enzymes were protected from inactivation (presumably from adsorption) to unblocked polystyrene plates, to which the free enzyme was highly susceptible (Figure S6).

The increase in apparent K_m for packaged Luc and tsLuc, but not PepE, may reflect a variety of factors. The encapsidated enzymes are apparently able to easily access small-molecule substrates and release products, presumably

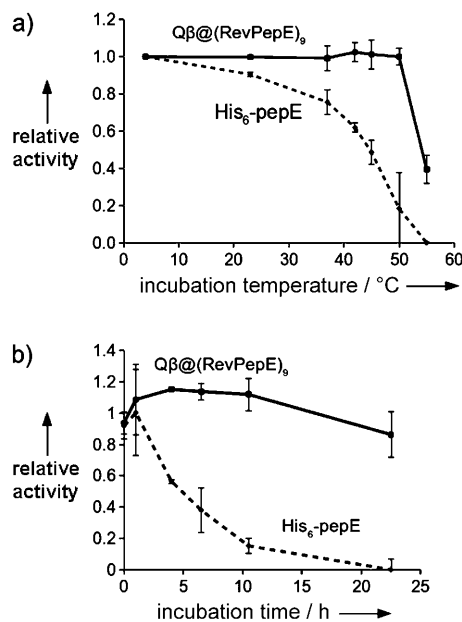


Figure 4. Protection from thermal and protease inactivation of peptidase E by encapsidation. a) Relative initial (< 10 min) rates of substrate hydrolysis after incubation of the enzyme for 30 min at the indicated temperature followed by cooling to room temperature before assay. The rate exhibited by enzyme incubated at 4°C was set at 100%. b) Relative initial rates of substrate hydrolysis after incubation at specified time with proteinase K. Data is represented as a percentage of a buffer control at each time point. Points are averages of independent measurements in triplicate and error bars are the standard deviation.

Table 1: Kinetic constants for free and packaged luciferase enzymes.^[a]

	K _{m,app} [μM] luciferin	K _{m,app} [μM] ATP	k _{cat} [s ⁻¹]
free luciferase	7.9 ± 0.1	60 ± 10	38 ± 1.9
Qβ@(RevLuc) ₄	140 ± 7	460 ± 30	22 ± 0.4
Qβ@(RevtsLuc) ₂	77 ± 3	360 ± 20	35 ± 8
Qβ@(RevtsLuc) ₉	171 ± 8	550 ± 30	20 ± 2

[a] Calculated from specific activity of luciferase (4.89×10^{10} light units mg⁻¹) and conversion to moles of pyrophosphate released.

through the 20 large pores that exist at the quasi-six fold axes of the icosahedral capsid.^[17] However, since it requires a ternary complex for catalysis (enzyme, luciferin, and ATP), luciferase may have a greater sensitivity to lower diffusion rates of the VLP–enzyme capsule. (The diffusion coefficient of icosahedral nanoparticles of this type and size is approximately 2×10^{-7} cm²s⁻¹,^[18] ten-fold lower than that of the free enzymes.) Alternatively, the packaged enzyme may have less dynamic flexibility in a manner that affects its kinetic performance. Consistent with the latter hypothesis, we found superior kinetic parameters for particles containing two copies of RevtsLuc compared to particles containing nine copies (Table 1). Similar observations and issues have been described for luciferase immobilized to a variety of heterogeneous supports.^[19]

These results represent the first examples of polynucleotide-mediated packaging of functional enzymes inside a protein shell, and the first kinetic comparisons between free and protein-encapsulated catalysts. While some differences were noted in kinetic parameters, the free and encapsidated enzymes exhibited very similar activities at saturation on a per-enzyme basis, showing that the enzyme-filled capsids can be highly potent catalytic engines.

The RNA-mediated packaging method combines the binding functions of two linked RNA aptamers, the first a natural hairpin sequence that engages in a strong association with the inside of the VLP, and the second an artificial aptamer selected by in vitro methods to bind to an oligopeptide tag fused to the desired cargo. The fact that the second of these aptamers works is especially significant, since it shows that the active conformation of the aptamer is accessible even when the sequence is coded into a larger piece of expressed and packaged messenger RNA.

This method of packaging enzymes inside protective protein shells has several attributes that distinguish it from existing technologies. First, since the entire packaging scheme is present within the host bacteria, the complete structure is assembled by the end of the expression. There is no need to purify separate elements and bring them together in vitro as in other systems.^[3e,4] These time-consuming steps are often low-yielding, requiring large amounts of starting material. Secondly, purification is largely independent of the packaged material, allowing the same efficient procedures to be used for a large range of packaged proteins. Thirdly, in contrast to most other co-expression systems,^[3a–e] we use a scaffold that was evolved in *E. coli*, and expression in the native host provides high yields of pure VLP in a short amount of time. Finally, other systems have packaged functional enzymes^[3a,b,d,4b] and showed activity, but none have supplied kinetic analyses compared to the free enzyme. Such testing is critical for further development of therapeutically relevant targets.

The active nature of the encapsulated enzymes, and the ability of the capsid shell to stabilize them against thermal degradation, protease attack, and hydrophobic adsorption, shows that this method may be generally applicable to the production of fragile or difficult-to-purify enzymes. All production and assembly steps occur within the bacterial cell, with indirect control of amount of packaged cargo possible by simply changing the expression media or the nature of the components of the packaging system. VLPs are produced in high yields and are purified by a convenient standard procedure, independent of the protein packaged inside. This system therefore represents a unique method for the harnessing of enzymatic activity in a process-friendly fashion.

Received: August 21, 2010

Published online: November 9, 2010

Publication delayed at authors' request

Keywords: encapsulation · enzymes · Qβ bacteriophage · RNA–protein interactions · virus-like particles

-
- [1] C. A. Kerfeld, M. R. Sawaya, S. Tanaka, C. V. Nguyen, M. Phillips, M. Beeby, T. O. Yeates, *Science* **2005**, *309*, 936.
- [2] a) W. Tischer, F. Wedekind, *Top. Curr. Chem.* **1999**, *200*, 95; b) U. Hanefeld, L. Gardossi, E. Magner, *Chem. Soc. Rev.* **2009**, *38*, 453.
- [3] a) G. Beterams, B. Bottcher, M. Nassal, *FEBS Lett.* **2000**, *481*, 169; b) V. A. Kickhoefer, Y. Garcia, Y. Mikyas, E. Johansson, J. C. Zhou, S. Raval-Fernandes, P. Minoofar, J. I. Zink, B. Dunn, P. L. Stewart, L. H. Rome, *Proc. Natl. Acad. Sci. USA* **2005**, *102*, 4348; c) F. P. Seebeck, K. J. Woycechowsky, W. Zhuang, J. P. Rabe, D. Hilvert, *J. Am. Chem. Soc.* **2006**, *128*, 4516; d) T. Inoue, M. A. Kawano, R. U. Takahashi, H. Tsukamoto, T. Enomoto, T. Imai, K. Kataoka, H. Handa, *J. Biotechnol.* **2008**, *134*, 181; e) L. E. Goldsmith, M. Pupols, V. A. Kickhoefer, L. H. Rome, H. G. Monbouquette, *ACS Nano* **2009**, *3*, 3175; f) I. J. Minten, L. J. A. Hendriks, R. J. M. Nolte, J. J. L. M. Cornelissen, *J. Am. Chem. Soc.* **2009**, *131*, 17771.
- [4] a) K. W. Lee, W. S. Tan, *J. Virol. Methods* **2008**, *151*, 172; b) M. Comellas-Aragonès, H. Engelkamp, V. I. Claessen, N. A. J. M. Sommerdijk, A. E. Rowan, P. C. M. Christianen, J. C. Maan, B. J. M. Verduin, J. J. L. M. Cornelissen, R. J. M. Nolte, *Nat. Nanotechnol.* **2007**, *2*, 635.
- [5] a) T. M. Kozlovska, I. Cielens, D. Dreilin  a, A. Dislers, V. Baumanis, V. Ose, P. Pumpens, *Gene* **1993**, *137*, 133; b) R. Golmohammadi, K. Fridborg, M. Bundule, K. Valeg  rd, L. Liljas, *Structure* **1996**, *4*, 543.
- [6] E. Strable, M. G. Finn, *Curr. Top. Microbiol. Immunol.* **2009**, *327*, 1.
- [7] a) E. Kaltgrad, S. Sen Gupta, S. Punna, C.-Y. Huang, A. Chang, C.-H. Wong, M. G. Finn, O. Blixt, *ChemBioChem* **2007**, *8*, 1455; b) J. Cornuz, S. Zwahlen, W. F. Jungi, J. Osterwalder, K. Klingler, G. van Melle, Y. Bangala, I. Guessous, P. M  ller, J. Willers, P. Maurer, M. F. Bachmann, T. Cerny, *PLoS ONE* **2008**, *3*, e2547.
- [8] a) I. Vasiljeva, T. Kozlovska, I. Cielens, A. Strelnikova, A. Kazaks, V. Ose, P. Pumpens, *FEBS Lett.* **1998**, *431*, 7; b) S. D. Brown, J. D. Fiedler, M. G. Finn, *Biochemistry* **2009**, *48*, 11155; c) D. Banerjee, A. P. Liu, N. R. Voss, S. L. Schmid, M. G. Finn, *ChemBioChem* **2010**, *11*, 1273.
- [9] G. W. Witherell, O. C. Uhlenbeck, *Biochemistry* **1989**, *28*, 71.
- [10] H. Weber, *Biochim. Biophys. Acta* **1976**, *418*, 175.
- [11] L. Loo, R. H. Guenther, S. A. Lommel, S. Franzen, *J. Am. Chem. Soc.* **2007**, *129*, 11111.
- [12] W. Xu, A. D. Ellington, *Proc. Natl. Acad. Sci. USA* **1996**, *93*, 7475.
- [13] R. A. Lassy, C. G. Miller, *J. Bacteriol.* **2000**, *182*, 2536.
- [14] P. J. White, D. J. Squirrell, P. Arnaud, C. R. Lowe, J. A. Murray, *Biochem. J.* **1996**, *319*, 343.
- [15] a) R. A. Larsen, T. M. Knox, C. G. Miller, *J. Bacteriol.* **2001**, *183*, 3089; b) I. T. Mononen, V. M. Kaartinen, J. C. Williams, *Anal. Biochem.* **1993**, *208*, 372.
- [16] C. Y. Wang, S. Hitz, J. D. Andrade, R. J. Stewart, *Anal. Biochem.* **1997**, *246*, 133.
- [17] For an example in which the protein shell provides some barrier to the interactions of small-molecule substrates with a packaged catalyst, see: T. Ueno, M. Suzuki, T. Goto, T. Matsumoto, K. Nagayama, Y. Watanabe, *Angew. Chem.* **2004**, *116*, 2581–2584; *Angew. Chem. Int. Ed.* **2004**, *43*, 2527–2530.
- [18] a) H. Neurath, G. R. Cooper, *J. Biol. Chem.* **1940**, *135*, 455; b) M. E. Bayer, R. W. Deblois, *J. Virol.* **1974**, *14*, 975.
- [19] a) Y. Lee, I. Jablonski, M. DeLuca, *Anal. Biochem.* **1977**, *80*, 496; b) L. J. Blum, P. R. Coulet, *Biotechnol. Bioeng.* **1986**, *28*, 1154; c) J. Eu, J. Andrade, *Luminescence* **2001**, *16*, 57.

Chapter 8

α -Galactosyl-Bearing Epitopes as Potent Immunogens in Chagas' Disease and Leishmaniasis

José Luis Avila

1. INTRODUCTION

Anti- α -galactosyl (anti-Gal) is a human natural antibody which constitutes as much as 1% of circulating IgG and which interacts specifically with the carbohydrate epitope Gal α 1-3Gal β 1-4GlcNac-R (termed the α -gal epitope). This natural antibody is unique among known human natural antibodies because of its unusually high concentration in the serum (30–100 μ g/ml) (Avila *et al.*, 1989; Davin *et al.*, 1987; Galili *et al.*, 1984), and is present in all humans (Galili *et al.*, 1984). The only other mammals producing anti-Gal are Old World monkeys and apes (Galili *et al.*, 1987b).

Anti-Gal is a natural antibody which may be of physiologic significance since it is continuously produced in large amounts by a high proportion of B lymphocytes in all humans.

The ubiquitous presence of anti-Gal in high concentrations in human serum throughout life (Galili *et al.*, 1984) raised the question of the source for such a

José Luis Avila Instituto de Biomedicina, Caracas 1010A, Venezuela.

chronic immunogenic stimulus. Studies on other natural carbohydrates antibodies, i.e., anti-blood group A and anti-blood B antibodies suggested that bacteria within the normal intestinal flora provide the constant antigenic stimulation for the production of these antibodies (Springer and Horton, 1969).

This review discusses the possible role of anti-Gal against *Trypanosoma* and *Leishmania* infection.

2. AMERICAN TRYPANOSOMIASIS OR CHAGAS' DISEASE

Chagas' disease is the most common form of chronic myocarditis in the world (Lancet, 1965). On the basis of published data from various parts of Latin America, it is estimated that at least 20 million individuals are infected with *Trypanosoma cruzi*, and that over 65 million live in endemic areas where the risk of this infection exists (WHO, 1995).

2.1. Acute Chagas' Disease

The acute stage is characterized by general malaise with a variety of clinical manifestations. The symptoms can be very mild and atypical. Consequently the disease is often not recognized at this stage, indeed, and diagnosed in only 1% to 2% of all patients, whereas in the remaining cases pass unnoticed. General symptoms are fever, enlarged liver and spleen, generalized oedema, and swollen lymph-nodes. Up to 30% of cases show electrocardiographic or radiological abnormalities due to acute myocarditis of different degrees.

2.2. Indeterminate Stage

The indeterminate stage begins 8–10 weeks after the acute stage, whether there have been clinical manifestations or not. This stage may last several years or persist indefinitely. It is characterized by the absence of clinical symptoms, the subjects being fully capable of normal physical activity and showing normal electrocardiograms and chest X-rays. However, serological tests for Chagas disease remain positive, and parasitemia can be recognized in 20–60% of cases by xenodiagnosis (this technique is performed by feeding third-instar nymphs of *Triatoma infestans* or *Rhodnius prolixus* with patient's blood. Thirty and 60 days after the blood-meal, their faeces and intestines are examined under the microscope for trypomastigotes or epimastigotes of *T. cruzi*).

2.3. Chronic Chagas' Disease

It is estimated that up to 30% of persons with the indeterminate form of the infection will suffer from cardiac, digestive, or neurological damage, 10–20 years after having contracted the disease. The cardiac form is the most studied, the best

known, and the easiest to diagnose. The clinical manifestations depend on the degree of myocardial damage, the presence of arrhythmias and the degree of heart failure. Carrasco *et al* (1982) according to the clinical and electrocardiographic characteristics and the results of the left cineventriculogram proposed to include chagasic patients in three groups with the following characteristics: group I was subdivided into groups Ia and Ib (group Ia= normal electrocardiogram (EKG) and normal cineventriculogram; group Ib = normal EKG and abnormal left cineventriculogram); group II = abnormal EKG, but not signs of congestive failure; group III = abnormal EKG and congestive failure.

In the digestive form any portion of the digestive tract can be involved but the most commonly affected segments are the oesophagus and the colon.

Mild to profound involvement of the central, peripheral or autonomic nervous system have been reported in chronic stage.

2.4. Pathogenesis

In spite of the importance of the disease, little is known of its pathogenesis. The myocardial fibrosis develops in association with a chronic inflammatory reaction (Andrade *et al.*, 1989; Andrade and Grimaud, 1986; Andrade, 1985). Sequential studies of mice with experimentally induced chagasic myocarditis have shown that the inflammatory reaction is initially associated with interstitial deposits of fibronectin and subsequently with increased amounts of interstitial connective tissue proteins, including type III and IV collagen and laminin (Andrade *et al.*, 1989). These observations are important because "anti-laminin" antibodies (latter demonstrated to be exclusively directed against the α -gal epitope abundantly present in murine laminin [Towbin *et al*, 1987]) were found to increase in the sera of patients, monkeys and mice infected with *T. cruzi* (Sanchez *et al.*, 1993; Unterkircher *et al.*, 1993; Avila, 1992; Laguens *et al.*, 1991; Gazzinelli *et al.*, 1991a; Towbin *et al.*, 1987; Milei and Storino, 1987; Avila *et al.*, 1984; Szarfman *et al.*, 1982). Ultrastructural studies of endomyocardial biopsy specimens from patients with the chronic form of the disease have revealed severe thickening of the basement membranes of the myocytes, endothelial cells and vascular smooth muscle cells (Milei *et al.*, 1992; Palacios-Prü *et al.*, 1989; Ferrans *et al.* 1988). More recently, Sanchez *et al.*(1993) have found in 10 patients with chagasic cardiomyopathy, marked thickening of the basement membranes on staining with the periodic acid silver-methenamine (PAM) method, specific for glycoconjugates.

3. HUMAN LEISHMANIASIS

The true incidence and prevalence of leishmaniasis is uncertain because many cases are undiagnosed or unreported in areas where the infection is endemic. In 1993, the World Health Organization estimated that 350 million people world-

Table I
Correlation of *Leishmania* Species, Geographical Distribution and Disease

Agent	Geographical distribution	Clinical presentations
<i>L. braziliensis</i>	Argentina, Belize, Bolivia, Brazil, Colombia, Costa Rica, Guatemala, Honduras, Panama, Paraguay, Perú, Venezuela	CL, MCL
<i>L. mexicana</i>	Belize, Colombia, Costa Rica, Dominican Republic, Guatemala, Mexico, Panama, Venezuela, USA	CL, VL, DCL
<i>L. amazonensis</i>	Bolivia, Brazil, Colombia, Costa Rica, Ecuador, Guyana, Panama, Perú, Venezuela	CL, MCL, VL, DCL
<i>L. tropica</i>	Israel, Jordan, Iran, Iraq, Libya, Azerbaijan, Turkmen, Uzbek, Syria, Afghanistan, India, Greece	CL
<i>L. major</i>	NW China, Pakistan, Kazakhstan, Afghanistan, India, Saudi Arabia, Iran, Iraq, Kuwait, Jordan, Libya, Israel, Algeria, Tunisia, Ethiopia, United Arab Republic, Senegal, Sudan, Kenya, Mali,	CL, VL
<i>L. aethiopica</i>	Ethiopia, Kenya	CL, DCL, MCL
<i>L. donovani</i>	Africa, Asia	VL
<i>L. infantum</i>	Mediterranean basin	VL
<i>L. chagasi</i>	Central and South America	VL

CL: cutaneous leishmaniasis; DCL: diffuse cutaneous leishmaniasis; MCL: mucocutaneous leishmaniasis; VL: visceral leishmaniasis.

wide were at risk for infection. The incidence of cutaneous leishmaniasis has been estimated to be 1.0–1.5 million cases per year, and the incidence of visceral disease has been estimated to be 500,000 cases per year (PAHO, 1994).

Leishmaniasis are caused by protozoa of the genus *Leishmania* (Table I), family Trypanosomatidae, order Kinetoplastida. Histologically the lesions are characterized by a diffuse inflammatory infiltrate composed of macrophages, plasma cells and lymphocytes, which may or may not exhibit amastigotes. A wide spectrum of clinical manifestations can be observed in tegumentary leishmaniasis, varying from the localized cutaneous and mucocutaneous leishmaniasis (CL and MCL), representing the responsive pole, to diffuse cutaneous leishmaniasis (DCL), the unresponsive pole. Between these polar forms a borderline or intermediate disease has been characterized.

Leishmania are generally divided into parasites which cause tegumentary disease (*L. braziliensis*, *L. amazonensis* and *L. mexicana* in the New World and *L. tropica* and *L. aethiopica* in the Old World) (Table 1) and those agents of visceral disease (*L. donovani* and *L. chagasi*).

3.1. New World Cutaneous Leishmaniasis

The cutaneous lesions begin at the site of parasite entrance as a small papule which develops into a nodule that ulcerates in the center. Lesions can take aspects

of papules, nodules, ulcers, tubercles or infiltrated plaques. Less frequently, vegetation and verrucous lesions may be observed. The most frequent aspect observed in CL cases is an ulcer with elevated borders and a sharp crater. *L. braziliensis* is responsible for the more severe forms of CL, lesions develop rapidly and show a tendency to heal slowly without treatment. Rarely (approximately 1% of cases), disseminated CL can be observed with several lesions in a patient. The lesions appear as acneiform elements, papules and small ulcers. Disseminated CL is completely different from diffuse CL, an entity in which many lesions are also observed but they are nodular and non-ulcerated.

3.2. Mucocutaneous Leishmaniasis

Mucosal involvement, probably due to hematogenous spread from the primary lesion, occurs in approximately 3% of patients infected by *L. braziliensis*, and is related to multiple or extensive skin lesions above the belt and inadequate therapy of the primary lesion. Initial involvement of the nasal mucosa can spread to the hard and soft palate, uvula, pharynx, gums and upper lip. Septal perforation is observed in up to 42% of the MCL patients. A great enlargement of the upper lip and nose can result from infiltration and confer a tumoral aspect.

3.3. Diffuse and Borderline Cutaneous Leishmaniasis

The initial lesion of DCL resemble those of CL without ulceration. The lesions are erythematous and appear as papules, nodules, tuberous lesions, infiltrated plaques and diffuse infiltration of a part of the body. Even in the DCL pole there are subtle differences in presentation, with patients exhibiting the classical aspects and other exhibiting small ulcerations in a few lesions, despite the great predominance of nodular non-ulcerated lesions.

3.4. Human Visceral Leishmaniasis

Visceral leishmaniasis (Kala azar) is typically caused by *L. donovani* in India and Africa and by two closely related species, *L. infantum* in the Mediterranean littoral and *L. chagasi* in Latin America. Cases tend to occur sporadically in rural areas where the organisms are endemic. The majority of cases occur in children < 10 years of age. It is now known that only in a minority of cases of infections with *Leishmania* progress to classic visceral leishmaniasis. The remainder of these infections are asymptomatic or are associated with mild symptoms that eventually resolve spontaneously when protective immune responses develop. The clinical manifestations of visceral leishmaniasis seem to be similar throughout the world.

Kala azar is characterized by fever, malaise, weight loss, hepatomegaly and splenomegaly. Severe cachexia develops over time. Measles, diarrhea, bacterial pneumonia, tuberculosis, and other secondary infections are common late in the

course of visceral leishmaniasis and frequently contribute to death (Pearson and Queiroz-Sousa, 1996).

4. α -GAL EPITOPE ON SEVERAL *TRYPANOSOMA CRUZI* MACROMOLECULES

Almeida *et al.* (1994, 1993) using McConville technique for extraction of glycoinositolphospholipids (GIPLs) (McConville and Bacic, 1989) and lipophosphoglycan (LPG) from *Leishmania* (reviewed in Avila 1993; McConville and Ferguson, 1993) extracted GIPL and LPGs from *T. cruzi* trypomastigotes and obtained three different fractions called F1-F3. The more hydrophobic fraction F1 was separated by thin layer chromatography and immunostained with chagasic sera. Reactive components migrated slowly in this system, in a region corresponding to the migration of *L. major* GIPLs, which also react with chagasic sera (Avila, 1993; Avila *et al.*, 1991). Although a strong reaction with F1 components was obtained with a serum from a patient with a positive hemoculture the reaction was rather poor with purified chagasic anti-Gal. In contrast, fractions F2 and F3 contained most of the components reacting with chagasic anti-Gal present in lysates of trypomastigotes. When separated by SDS-PAGE, fraction F2 formed two bands at Mr 74 kD and 95.6 kD that could be distinguished by their reactivity with anti-Gal. Fraction F3 formed a broad band at Mr 120–200 kD (main peak at 150 kD) that reacted with both chagasic anti-Gal and the 3C9 monoclonal antibody (recognizing sialyl epitopes of the Ssp-3 glycoconjugate from trypomastigotes). Interestingly, adsorption of chagasic serum *T. cruzi* lytic antibodies by F2 and F3 fractions fixed on polyvinylidene difluoride (PVDF) paper removed 70% of the initial lytic activity. These adsorbed antibodies could be eluted from the paper with citric acid, and were shown to promote *T. cruzi* lysis.

Using ELISA technique, reactions of the F1 fraction with chagasic sera showed low affinity and cross-reactivity with cutaneous leishmaniasis was detected, as has previously been demonstrated (Avila *et al.*, 1991). Fractions F2 and F3 contained antigens that displayed better sensitivity and specificity. Fractions F2 and F3 demonstrated positive reactions with chagasic and treated not-cured chagasic sera and did not react with treated-cured chagasic, visceral and mucocutaneous leishmaniasis and normal human sera (Almeida *et al.*, 1994; 1993).

An Octyl Sepharose sample of purified F2/F3 fractions was found to be rich in carbohydrate (Gal, Man, GlcNac, sialic acid, Glc and Xyl) and certain amino acids (Thr, Glx, Ser, Pro, Asx, Gly and Ala). In addition it contained myo-inositol and ethanolamine in a molar ratio of approximately 1:1. The finding of the latter components, together with lipid in the form of monoalkylglycerol (1-O-hexadecylglycerol) suggested the presence of glycosylphosphatidylinositol(GPI)-anchored glycoconjugates. Labelling with galactose oxidase/NaB₃H₄

and reductive β -elimination showed that the F2/F3 material contained: 1) a small (4.5 glucose units [GU]) chagasic anti-Gal-positive oligosaccharide that was not found in a sialylated form; 2) a group of oligosaccharitols in the 5–12 GU size range, some of which terminated in α -Gal and were chagasic anti-Gal positive, and some of which (mostly from the chagasic anti-Gal negative fraction) were found in a sialylated form; 3) a group of chagasic anti-Gal positive and chagasic anti-Gal negative acidic structures that were neuraminidase-resistant, which was not further characterized.

The 4.5 GU oligosaccharide, obtained by hydrazinolysis followed by NaB_3H_4 reduction and Bio-Gel P-4 purification, was subjected to strong acid hydrolysis and re-N-acetylation, plus coffee-bean α -galactosidase treatment. The oligosaccharide was identified as $\text{Gal}\alpha 1\text{-}3\text{Gal}\beta 1\text{-}4\text{GlcNAc}(N\text{-acetylglucosaminitol})$.

Binding studies with immobilized purified F2/F3 fractions in chemiluminiscence ELISA showed that the affinity of chagasic anti-Gal for these glycoconjugates was about 100-fold that of normal human serum anti-Gal (Figure 1). As expected, treatment of the F2/F3 glycoconjugates with α -galactosidase abolished almost all of the immunoreactivity. Similarly, only chagasic anti-Gal bound significantly on several α Gal-containing structures from the GPI anchor of *T. brucei* VSG (Zamse *et al.*, 1991) and the glycoinositol phospholipids (GIPL) of *Leishmania major* (Avila, 1993; Avila *et al.*, 1991). These data are summarized in Table 2. Previous results suggest that chagasic anti-Gal can bind to structures terminating in $\text{Gal}\alpha 1\text{-}2\text{Gal}$, $\text{Gal}\alpha 1\text{-}3\text{Gal}$, $\text{Gal}\alpha 1\text{-}6\text{Gal}$ and $\text{Gal}\alpha 1\text{-}3\text{Galf}$ (where Galf is galactofuranose) (Almeida *et al.*, 1994, 1993; Avila, 1992; Avila *et al.*, 1992, 1991, 1989) because it has little specificity for the penultimate units or longer oligo-saccharides linked to the terminal non-reducing α -Gal residues.

In other experiments, Almeida *et al* (1994) found that most cell-derived trypomastigotes react strongly with chagasic anti-Gal, but not with normal human serum anti-Gal. Treatment with phosphatidylinositol-specific phospholipase C (PI-PLC) almost completely abolished binding of chagasic anti-Gal to the parasites. These results show that most of the antigens recognized by chagasic anti-Gal on the trypomastigote cell surface are PI-PLC-sensitive and are therefore probably GPI-anchored. Consistent with the above result, partially purified F2/F3 glycoconjugates digested with PI-PLC were rendered hydrophilic and could no longer bind to the PVDF membrane. Taken together, these data demonstrate that the majority of the chagasic anti-Gal reactive molecules were GPI-anchored glycoconjugates. A GPI-anchored trypomastigote-specific glycoprotein named Tc-85 also have been described in *T. cruzi* (Couto *et al.*, 1993) and its N-linked carbohydrate chain has the α -gal epitope (Couto *et al.*, 1990).

Avila *et al.* (1991) reported the presence of several GIPLs in *T. cruzi*. Some of them comigrated with purified *L. major* GIPL-1, GIPL-2 and GIPL-3 in high-performance thin layer chromatography. Several other GIPLs have been described

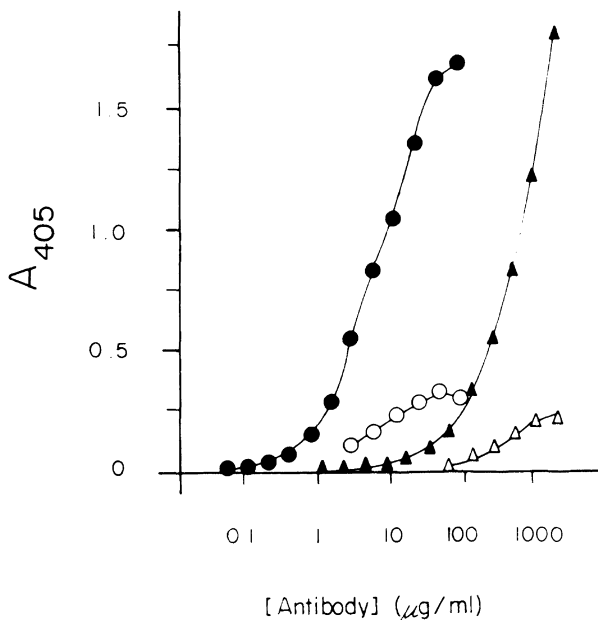


Figure 1. Microtitre plates coated with F2/3 were probed with a range of chagasic anti-Gal (●) and normal human serum (▲) antibody concentrations. The intensity of the reactions was determined by chemiluminescent ELISA. The open symbols represent the same experiment following prior treatment of the coated plates with coffee-bean α -galactosidase. From Almeida *et al.* (1994), with permission.

in *T. cruzi*, series 1 oligosaccharides having only terminal $\text{Gal}_\beta(1\rightarrow3)\text{Man}$ units (Carreira *et al.*, 1996). These may correspond to GIPLs reported by Avila *et al.* (1991), that show high chromatographic mobility. According to Carreira *et al.* (1996) these GIPLs have 2–3 phosphate groups whereas *L. major* GIPLs have one phosphate.

5. α -GAL EPITOPE ON SEVERAL *LEISHMANIA* MACROMOLECULES

The glycoinositolphospholipids (GIPLs) are the major glycolipids synthesized by *Leishmania* parasites. Three distinct types of GIPLs have been identified, which are expressed in markedly different levels in different species or developmental stages (McConville and Ferguson (1993)(for a chemical description see Table II). The α -gal epitope is present in GIPL-2 from *L. major* (McConville *et al.*, 1990; McConville and Bacic, 1989) and from *L. mexicana* (McConville *et al.*, 1993). The several GIPLs may coat a significant proportion of the plasma membrane, thus acting as a shield against lysosomal hydrolases and as receptors for the interaction with host cells (Winter *et al.*, 1994).

Table II
Binding of Chagasic and Normal Human Serum Anti-Gal to Different
 α -Gal-Containing Epitopes

Epitope	Origin	Anti-Gal binding	
		ChHS	NHS
Gal α 1,3Gal β 1,4GlcNAc β 1-0-R	Synsorb 115	+	-
Gal α 1,3Gal β 1,4GlcNAc β 1-0-R	CPH	+	-
Gal α 1,3Gal β 1,4GlcNAcol	F2/F3 <i>T. cruzi</i>	+	-
Gal α 1,2Gal α 1,6Gal α 1,3[Man ₃ AHM]	VSG 117	+	-
Gal α 1,2Gal α 1,6(Gal α 1,2)Gal α 1,3[Man ₃ AHM] VSG 117		+	-
Gal α 1,6(Gal α 1,2)Gal α 1,3[Man ₃ AHM]	VSG 117	+	-
Gal α 1,3Galf β 1,3ManGlcNH ₂ -PI	GIPL-2	+	-
Gal α 1,6Gal α 1,3Gal β 1,3ManGlcNH ₂ -PI	GIPL-3	+	-

ChHS: chagasic human serum; NHS: normal human serum; CPH: ceramide pentahexoside from rabbit erythrocytes; VSG, variant surface glycoprotein from *Trypanosoma brucei*; GIPL-2 and GIPL-3, glycoinositolphospholipid from *L. major*; AHM, anhydromannitol; PI, phosphatidylinositol.

Taken from Almeida *et al* (1994) with permission.

6. MECHANISMS OF PRODUCTION OF ELEVATED ANTI-GAL IN KINETOPLASTIDAE INFECTIONS

Towbin *et al.* (1987) proposed that members of the *Leishmania* and *Trypanosoma* possess highly immunogenic α -gal epitopes, which induced elevated anti-Gal antibody production.

This hypothesis was studied using three different approaches:

6.1. Biochemical Isolation and Characterization of α -Gal Epitope-Bearing Molecules

See above Sections 4 and 5.

6.2. Ligand Analysis of α -Gal Epitope Expression on *Trypanosoma* and *Leishmania*

This was assessed by the use of two antibodies and two lectins, all of which interact specifically with this epitope: a) the natural human anti-Gal, b) the monoclonal antibody Gal-13. This mouse IgG mab was found to be highly specific for glycolipids with terminal Gal(α 1-3)Gal β 1-4GlcNac-R residues (Galili *et al*, 1987a). Gal-13 does not bind, however, to these residues on N-glycosylated glycoproteins such as the Gal α 1-3Gal β 1-4GlcNac residues on mouse laminin or bovine thyroglobulin (Galili, 1987a), c) The specific lectin *Bandeiraea simplicifolia* IB₄ (BS). This lectin was found to bind to the α -gal epitope of

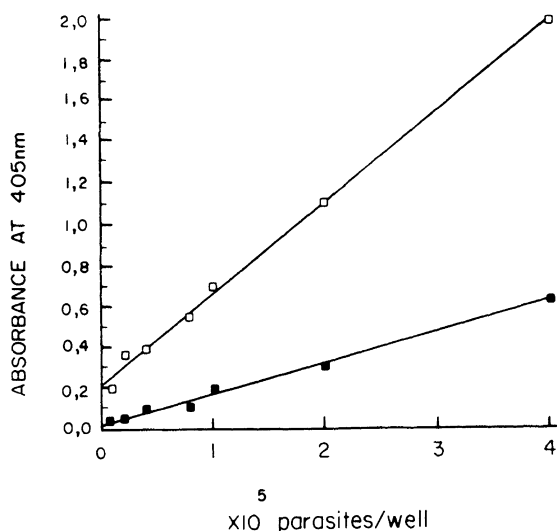


Figure 2. Binding of purified human anti-Gal to *T. cruzi* epimastigotes. Several parasite concentrations (0 to 4×10^5 parasites/well) were exposed to freshly purified human anti-Gal antibody (10 µg/ml) for 1 h at 37°C. □, anti-Gal binding to *T. cruzi* epimastigotes; ■, anti-Gal binding to 10 mM periodate-treated *T. cruzi* epimastigotes. From Avila *et al.* (1989), with permission.

glycoconjugates and with less affinity to the Gal(α1-3(Fucα1-2)Gal residues which represent the blood group B antigen (Egge *et al.*, 1985; Wood *et al.*, 1979). Figure 2 shows the dose-dependent binding of anti-Gal to *T. cruzi* epimastigotes. Periodate treatment of the parasites greatly decreased the binding of anti-Gal, further demonstrating the carbohydrate nature of the anti-Gal binding sites on the parasite. Figure 3 shows the binding of Gal-13 to fixed *T. cruzi* epimastigotes and American *Leishmania* promastigotes. The strong binding of Gal-13 to the parasite surface suggested that a substantial proportion of the α-gal epitope on these parasites is expressed as epitopes on glycolipids.

To further corroborate the presence of terminal α-gal-bearing glycoconjugates in *T. cruzi* and American *Leishmania*, Avila *et al.* (1989) used BS lectin. Table III and Figure 4 shows BS lectin binding to *T. cruzi* epimastigotes and American *Leishmania* promastigotes. Periodate treatment of fixed parasites strongly blocked lectin binding, confirming the carbohydrate nature of the lectin binding sites on *T. cruzi* epimastigotes and *Leishmania* promastigotes.

To study the occurrence of glycolipids with α-gal epitope in the parasites' membrane, crude total lipids fraction was assessed for interaction with the three α-gal binding molecules. Figure 5 shows the dose-dependent binding of purified human anti-Gal, of mouse mAb Gal-13 and of BS lectin to increasing amounts of *Leishmania* crude lipids. These data confirm that at least part of the α-gal epitopes on the parasite are on glycolipid molecules.

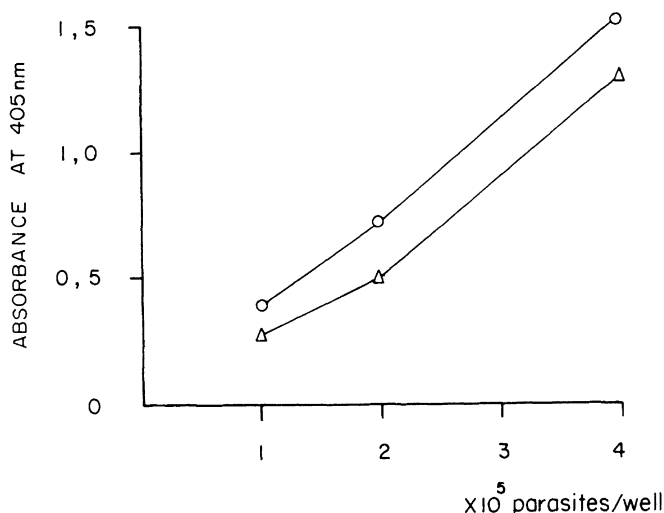


Figure 3. Binding of the mAb Gal-13 to fixed *T. cruzi* epimastigotes and American *Leishmania* promastigotes as a function of parasite concentration. (○), *T. cruzi* epimastigotes; (Δ), *Leishmania* promastigotes. From Avila *et al* (1989), with permission.

Table III
Binding of *Bandeiraea simplicifolia* IB₄ Lectin to American *Leishmania* and *T. cruzi* Epimastigotes and Trypomastigotes under Different Experimental Conditions

Experimental conditions	<i>Leishmania</i> ^b	% of control ^a	
		Epimastigotes	Trypomastigotes
20 mM PMSF-10 mM EDTA	100	100	100
1 % formaldehyde	94 ± 4	90 ± 2	93 ± 6
1 % glutaraldehyde	65 ± 6	60 ± 9	74 ± 8
0.01 % sodium azide	83 ± 5	78 ± 7	69 ± 6
0.5 M galactose ^c	18 ± 3	21 ± 4	19 ± 4
0.5 M glucose ^c	94 ± 5	91 ± 7	87 ± 6
10 mM periodate ^c	23 ± 3	20 ± 6	16 ± 3

^aMean ± standard deviation of six different experiments.

^bData obtained with MP, HM, LR, JAP, MHOM/4147 and MHOM/ M2903 strains of American *Leishmania* and Marin-1, Bertoldo, FL, Ma, Ya and Y strains of *T. cruzi*.

^cExperiments were carried out in PMSF-EDTA fixed parasites.

Taken from Avila *et al* (1989) with permission.

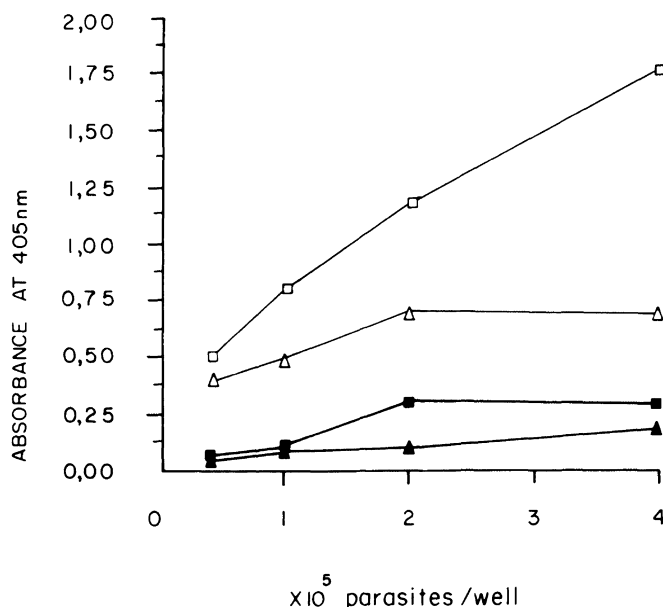


Figure 4. Binding of *Bandeiraea simplicifolia* IB₄ (BS) lectin to fixed *T. cruzi* epimastigotes and American *Leishmania* promastigotes as a function of parasite concentration. □, *T. cruzi*; Δ, American *Leishmania*; (■, ▲), binding in the presence of 0.5 M Galactose. From Avila *et al* (1989), with permission.

6.3. Immunolocalization of the α -Gal Epitope by Electron and Immunofluorescence Microscopy

Bretaña *et al* (1986) using immunogold technique studied the immunocytochemical localization of a "laminin-like protein" in the plasma membrane of *T. cruzi* and American *Leishmania*. They reported the immunoreactivity as located in *T. cruzi* trypomastigotes on the external surface of the plasma membrane, close to the sites where the flagellar veil attaches to the plasma membrane. Laminin immunoreactivity was rapidly lost when trypomastigotes were cultured in liquid medium and no reactivity was found in fresh epimastigotes. Promastigotes and amastigotes of American *Leishmania* spp. also showed a specific localization of laminin immunoreactivity, this being limited to the lips of the flagellar pocket and to the parasitic side exactly opposite to the flagellar exit. These results confirmed the presence of a "laminin-like molecule(s)" in both trypanosomatids. Once established that human anti-laminin antibodies are indeed reacting with α -gal epitopes (as demonstrated using mouse laminin by Towbin *et al.*, 1987) we used more specific methods to detect the presence of the α -gal epitope on Trypanosomatidae. Thus, Bretaña *et al* (1992) using three colloidal

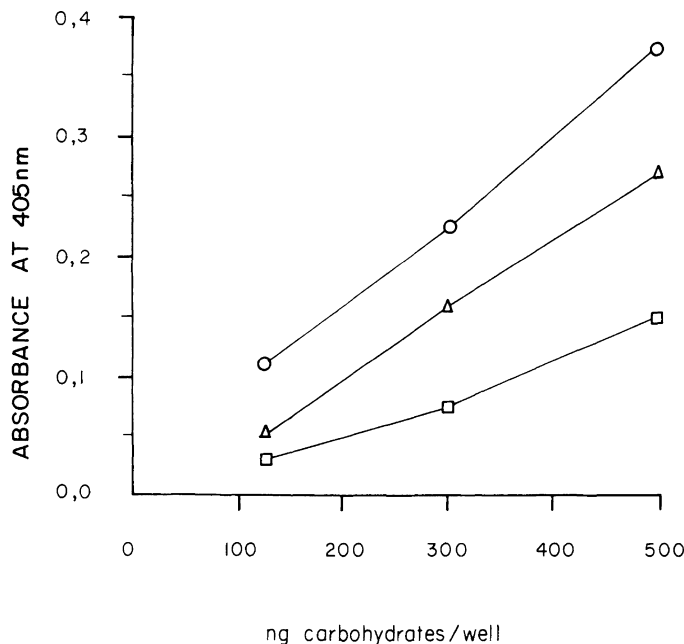


Figure 5. Binding of (□), BS lectin; (Δ), Gal-13; and (○) human anti-Gal to American *Leishmania* lipid fraction, as a function of carbohydrate concentration. From Avila *et al* (1989), with permission.

gold-linked specific markers: mAb Gal-13, rabbit anti-nidogen antibodies and a lectin (*B. simplicifolia* IB₄) found terminal α -gal epitopes on the *T. cruzi* external surface of trypomastigotes but not in intact epimastigotes (although disrupted epimastigotes strongly stained), in the lips of the flagellar pocket, and on the parasitic side exactly opposite to the flagellar pocket in amastigote and promastigote forms of American *Leishmania*. These results resemble those obtained before using anti-laminin antibodies in both trypanosomatids (Bretaña *et al*, 1986).

In other studies, Gazzinelli *et al* (1991b) using the fluorescent-labeled lectin *Euonymus europaeus* (EE)(specific for the α -gal epitope) and acute chagasic serum studied the distribution of α -gal epitope in mono- and heteroxenic trypanosomatids. They found that this epitope is present in all trypanosomatids. Although more EE receptors seem to be present in some monoxenic trypanosomatids and *Phytomonas* than in *Trypanosoma* species, the differences are not as evident. EE recognizes a wide range of glycoconjugates in all trypanosomatids. In *T. cruzi* this lectin recognizes a major glycoprotein of apparent Mr of 60 to 90 kDa. In contrast, acute chagasic serum recognizes many glycoconjugates of the several trypanosomatids tested. Most of these cross-reacting antigens are absorbed when acute chagasic serum is treated with mouse laminin or melibiose.

Using antibody-mediated agglutination and immunofluorescence, Almeida *et al.* (1991) demonstrated anti-Gal binding on live liver infusion-tryptose-cultured metacyclics and Hela cell-derived trypomastigotes of two different *T. cruzi* strains. In both cases the minimum antibody concentration needed for parasite agglutination was higher for normal human serum anti-Gal than for chagasic anti-Gal. The observed anti-Gal binding to living trypomastigotes was followed by lysis of the parasites when complement was added.

Finally, more recently Souto-Padron *et al.* (1994), using *T. cruzi* epimastigotes, trypomastigotes and amastigotes, an immunogold labeling method and human chagasic anti-Gal, have confirmed Bretaña *et al.* (1992) in that epimastigotes were poorly labeled, whereas extracellular trypomastigotes and amastigotes bound heterogeneously the antibody with many cells being intensely labeled at the cell surface. Generally, a strong surface reaction was accompanied by a weak cytoplasmic labeling. Conversely, a more intense intracellular or vacuolar labeling was observed in parasites with low surface labeling, suggesting different stages of processing of the carbohydrate epitope in different parasites. The Golgi complex of trypomastigotes was strongly labeled. Intracellular parasites were labeled at the parasite cell surface or within vacuolar structures.

6.4. The α -Gal Epitope in Other Protozoa

The presence of terminal α -gal epitope has been demonstrated in other protozoa. In the asexual blood stages of *Plasmodium falciparum* by: a) the α -galactosidase sensitivity of particular parasite antigens; b) by the ability of *B. simplicifolia* lectin to bind to the parasite (Ramasamy and Reese, 1986) and c) because anti-Gal inhibit *P. falciparum* growth in culture (Ramasamy and Rajakaruna, 1997).

The α -gal epitope was also reported on the type II and type III variant surface glycoproteins of *Trypanosoma brucei* (Zamse *et al.*, 1991).

7. ANTI-GAL RESPONSE IN *T. CRUZI*-INFECTED HUMAN SUBJECTS

7.1. In Acute Infection

Szarfman *et al.* (1982) were the first in demonstrating, using mouse laminin as antigen, that the sera from both acute and chronic chagasic patients contained antibodies to laminin and that the highest titers were present in the acute phase. Patients with acute *T. cruzi* infection had high titers of IgM and IgG antibodies, which react with laminin. Similar findings have been later demonstrated by Gazzinelli and Brener (1988). They found about 6- and 12-fold more immunoreactivity in

acute chagasic than in chronic chagasic patients and in controls respectively. Grauert *et al.* (1993) have studied the kinetics of anti-laminin antibody response in an acute case of human Chagas' disease. Anti-laminin IgG and IgM antibodies peaked on day 30, antibody reaching levels higher than 200% of basal values. Acute chagasic sera presented high quantities of anti-Gal but low levels of antibodies against total *T. cruzi* antigens, suggesting that the α -gal epitope is a major *T. cruzi* antigen occurring in this stage of the disease.

7.2. In Chronic Patients

As mentioned above, Szarfman *et al.* (1982) using mouse laminin as antigen, were the first to demonstrate that the sera from nine chronic chagasic patients contained elevated levels of antibodies to laminin. Subsequently, Avila *et al.* (1984) studying a larger group (37 patients) found 84% of chronic chagasic patients had anti-laminin antibody levels higher than normal. These antibodies were mainly of the IgG class. Similar results were later reported by Unterkircher *et al.*, (1993) (80% of 80 patients with confirmed Chagas' disease), Milei *et al.* (1993) (58% of 47 patients), Gazzinelli *et al.* (1988) and Avila *et al.* (1987) (73% of 92 chronic chagasic patients).

That anti-murine laminin antibodies are similar to anti-Gal was reported by Towbin *et al.* (1987), after the report of Avila *et al.* (1986) that chagasic patients also have increased anti-mouse nidogen antibody levels, nidogen being a structurally different protein that laminin (Paulsson *et al.*, 1987).

Avila *et al.* (1989) have reported that when measured by hemagglutination assay with rabbit red cells, anti-Gal in healthy individuals usually yields a titer of 1/640 to 1/1280 (Figure 6A). In sera passed through a Gal α 1-3Gal β 1-4GlcNac-R adsorbent (Synsorb 115), most (>85%) of the anti-Gal reactivity is retained on the column, as can be seen by a more than 10-fold decrease in the hemagglutinating reactivity in the effluent serum (Figure 6C). The antibodies eluted from the adsorbent column by low pH displayed a titer of 1/320 to 1/640 in healthy individuals (Figure 6B).

A similar pattern of anti-Gal reactivity was observed in sera of five patients with various bacterial infections. Eighty per cent of these patients displayed normal anti-Gal activity. However, in the serum of patients with Chagas' disease and *Leishmania* infection, the mean anti-Gal titer was 10-fold and 16-fold higher than that of healthy individuals or infection controls respectively (Figure 6A). This marked elevation in hemagglutinating reactivity was due to an increase in anti-Gal reactivity because, as observed with sera from healthy individuals, passage on Gal α 1-3Gal β 1-4GlcNac-R adsorbent removed more than 90% of the hemagglutinating reactivity in the sera of the chagasic and leishmanic patients (Figure 6C). The adsorbed anti-Gal of these patients, when eluted, displayed a 6- to 20-fold higher titers, respectively, as compared to that in normal individuals

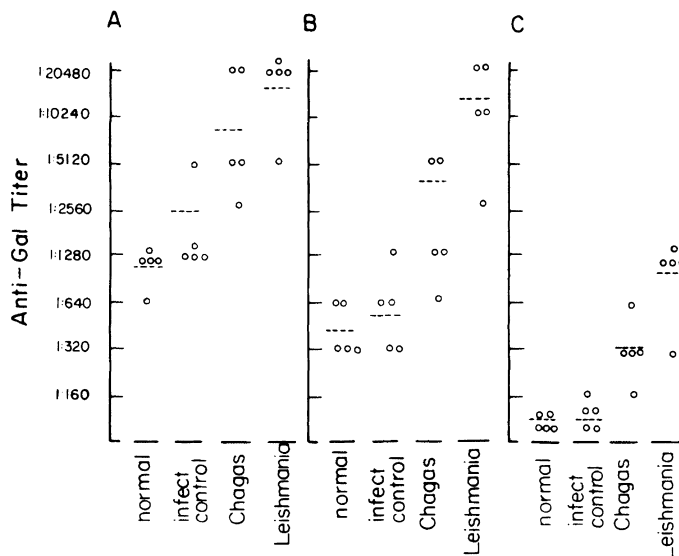


Figure 6. Anti-Gal titers in sera of patients with Kinetoplastida infections. Normal, healthy individuals; Infect. controls, patients with bacterial infections. Each circle represent one patient. A, Anti-Gal in serum. B, Anti-Gal eluted from Gal α 1-3Gal β 1-4GlcNac-R adsorbent. C, anti-Gal in the serum effluent passed on the Gal α 1-3Gal β 1-4GlcNac-R adsorbent. Dashed line represent the mean titer. From Avila *et al.* (1989), with permission.

(Figure 6B). When IgG concentration was measured in the sera of healthy individuals, infection controls and chagasic or leishmaniasic patients, all the patient groups exhibited only a 2–3-fold increase in total IgG concentration when compared with that in healthy individuals (Table IV). This suggested that the severalfold increase in anti-Gal reactivity in chagasic patients exceeded the increase in IgG concentration and thus may have resulted from a specific immune response against the α -gal epitope in these patients. These data confirm previous observations on elevation in antibody reactivity to α -gal epitopes in chagasic patients (Avila *et al.*, 1988a,b; Towbin *et al.*, 1987).

In order to study the association between anti-Gal levels and the clinical stage, Avila (1992) measured this antibody activity in patients at different clinical stages of chagasic and non-chagasic dilatatory cardiomyopathies. No differences were found in anti-Gal activity or in the proportion of anti-Gal positive patients. However anti-Gal in the two groups was significantly elevated compared with control subjects suggesting that : a) there is no relationship between anti-Gal levels and clinical stage and b) the existence in tropical areas of another anti-Gal antibody-elevated cardiomyopathy (nutritional, toxic, viral, rickettsial ?) (Table V). Similar results, were also reported by Milei *et al.* (1993). These authors divided

Table IV
IgG and Anti-Gal Concentrations in Sera of Various Patients

Antibody concentrations in subjects	IgG concentration (mg/ml)	Anti-Gal concentration (μg/ml)
Healthy individuals (n= 9)		
Range	7–11.0	48–91
Mean ^a	8.7 ± 1.0	74 ± 28
Infection controls (n= 23)		
Range	10–40	56–96
Mean ^a	26 ± 1.2	71 ± 2.6
Leishmanic patients (n= 31)		
Range	12–40	302–490
Mean ^a	24 ± 1.1	380 ± 9.2
Chagasic patients (n= 31)		
Range	14–40	72–419
Mean ^a	28 ± 1.6	213 ± 16.6

^a± standard error.

Taken from Avila *et al* (1989) with permission.

Table V
Anti-*Trypanosoma cruzi* and Anti-Gal Levels in Control Subjects and in Chagasic and Non-Chagasic Cardiomyopathy Patients Classified According to Their Degree of Myocardial Damage

Groups	Anti- <i>T. cruzi</i> antibodies ^{a,b}	Anti-Gal antibodies ^{b,c}	% of anti-Gal positive
Control (106)	343 ± 94	235 ± 151	8
Chagasic Ia (21)	1106 ± 359 ^d	549 ± 388 ^e	29
Chagasic Ib (12)	1170 ± 353 ^d	420 ± 236 ^f	30
Chagasic II (56)	1134 ± 355 ^d	825 ± 928 ^e	45
Chagasic III (13)	1244 ± 327 ^d	631 ± 535 ^e	36
Non-chagasic I (12)	247 ± 43	422 ± 202 ^f	25
Non-chagasic II (12)	285 ± 128	697 ± 658 ^e	38
Non-chagasic III (16)	268 ± 151	482 ± 386	5 ^g

^aExpressed as OD₄₀₅ at a serum dilution of 1:800. A value of > 437 is considered as positive.

^bMean ± standard deviation (10⁻³).

^cExpressed as OD₄₀₅ at a serum dilution of 1:50. A value of > 613 is considered positive. Antigen used: purified rabbit erythrocyte ceramide pentasaccharide.

^dP < 0.001 compared with control group.

^eP < 0.005 compared with control group.

^fP < 0.010 compared with control group.

^gP < 0.010 compared with chagasic type III group.

Taken from Avila *et al* (1992) with permission.

their chronic chagasic patients into three groups: group I: asymptomatic patients, normal thorax X-ray and ECG; Group II: conduction disturbances and/or arrhythmia and Group III: cardiomegaly with heart failure and abnormal ECG. Abnormal levels of anti-laminin antibodies were detected in 46% of the patients from group I, in 58% from group II and in 50% from group III. Percentages of the three groups were statistically similar. Nevertheless, very high titers of antibodies were detected in 10% of the patients from group II and 37% from group III.

Studies in chronic chagasic patients, have indicated that the levels of anti-Gal do not differ within the different clinical forms of Chagas' disease (indeterminate, cardiac and digestive patients) (Gazzinelli, 1992).

Interestingly, in chronic Chagas' disease patients, anti-Gal antibodies are significantly elevated mainly in the IgG class and there is lesser immunoreactivity in IgA and IgM classes (Unterkircher *et al.*, 1993; Avila *et al.*, 1992, 1988a, 1986, 1984).

Based on the affinity of chagasic antibodies to laminin and *T. cruzi* antigens fixed to immunoadsorbents, Unterkircher *et al.* (1993) have reported that there are two populations of anti-laminin antibodies in chronic chagasic patients: one that seems to be specific for the α -gal epitope on murine laminin and on the parasite and the other cross-reacting with other antigens on the parasite as well as with other antigens, both populations having a dissociation constant of 7×10^{-8} – 10^{-7} .

Of note, Milei *et al.* (1993) have reported higher titres of these antibodies in some chagasic patients who progressed in the severity of their disease (worsening of its clinical conditions). However, as emphasized by Kierszembbaum (1986), it remains to be shown whether such antibodies develop subsequently to the production of tissues damage or are elicited by the parasite prior to the occurrence of tissue lesions.

Interesting, Goin *et al.* (1990) have reported that anti-Gal can mimic the negative inotropic action of cholinergic agonists. On the other hand, Milei and Storino (1987) could not reproduce myocardial lesions resembling chronic Chagas' cardiomyopathy in rabbits immunized with murine laminin. However we must point out that it is hard to compare the immunogenicity of α -gal epitope present in murine laminin with that elicited by α -gal epitopes present in *T. cruzi* trypomastigotes, which are mostly linked to glycolipid structures where other membranous components can possibly act as powerful adjuvants (Bretaña *et al.*, 1992; Avila *et al.*, 1989; Avila, Harner and Barrios (unpublished results)[see also Section 15.1]).

It has been suggested that the findings of anti-laminin antibodies are in accord with the observation that the surfaces of cardiac myocytes of patients with chagasic cardiomyopathy are the sites of deposition of immunoglobulins and complement (Molina *et al.*, 1984). It is possible that infected cardiac muscle cells may change their surface structure by inserting parasite-derived α -gal epitopes, or changing host carbohydrate components by new posttranslational modifications

due to the intracellular residence of parasites. The autoimmunity observed in Chagas disease may therefore not be the result of cross-reacting structures present *per se*, but due to a modified structure arising in the *T. cruzi*-infected cells (Avila, 1994). Another alternative explanations, proposed by Avila *et al.* (1987), is that injury to cardiac basement membranes occurs in Chagas' disease, and leads to the release of basement membrane components (including laminin) which become antigenic, or that released *T. cruzi* metabolites may induce an inflammatory response. This interaction (analogous to xenograft rejection) may explain part of the extensive inflammatory response in the infected tissues in humans. These three explanations are not mutually exclusive.

It is worth mentioning that Wolff *et al.* (1989) have reported alterations in laminin distribution and antibodies to "laminin" (measured using mouse laminin and therefore clearly representing anti-Gal) in myocarditis (73% of the cases) and dilated cardiomyopathy (78% of the cases).

7.3. Anti-Gal(α 1-2)Gal Antibodies in Chronic Chagas' Disease Patients

Since Gal(α 1-2)Gal residues have been recently shown to be a structural unit of a phosphatidylinositol anchor for inserting variable surface glycoproteins of *T. brucei* (Ferguson *et al.*, 1988) and certain proteins of *T. cruzi* (Ledekremer *et al.*, 1990) into their cell surface, it was hypothesized that specific Gal(α 1-2)Gal antibodies could arise in *T. cruzi*-infected human subjects (Avila *et al.*, 1992).

Significantly elevated Gal(α 1-2)Gal antibody levels were indeed found in 66% of chronic chagasic cardiomyopathy patients (Table VI). In contrast, other acute or chronic Kinetoplastidae infections such as *T. rangeli*-infection, localized, mucocutaneous, diffuse cutaneous or visceral leishmaniasis did not induce significantly elevated Gal(α 1-2)Gal antibody levels.

To investigate whether results in chronic Chagas' disease patients were associated with degree of myocardial damage, patients were subdivided into several groups (Carrasco *et al.*, 1982). Among chagasic groups there was no significant difference in anti-Gal(α 1-2)Gal antibody levels or in percentage of patients that have elevated antibody levels. Nevertheless, Gal(α 1-2)Gal antibody levels were significantly higher in all chagasic groups when compared with healthy individuals or with patients having other non-chagasic cardiomyopathies.

Analysis of previous results has suggested that in human healthy individuals, as well as in *T. cruzi*-infected subjects, there are at least three types or clones of terminal α -galactosyl-reactive antibodies: One is detected by ELISA with rabbit neutral glycosphingolipids-enriched for ceramide pentasaccharide (Avila *et al.*, 1988a), murine laminin (Unterkircher *et al.*, 1993; Avila *et al.*, 1984; Szarfman *et al.*, 1982) or murine nidogen (Avila *et al.*, 1986) as solid phase antigens. These antibodies are mainly IgG and highly specific for the α -gal epitope as they are almost completely adsorbed by rat, rabbit, and guinea pig red blood cells as well as for

Table VI
Anti-Gal(α 1-2)Gal Antibody Levels in Healthy Controls, in
Patients with Localized Cutaneous (LCL), Mucocutaneous
(MCL), and Diffuse Leishmaniasis (DCL), Kala azar, *T. rangeli*-
Infection, Chronic Chagasic Cardiomyopathy, and Different
Inflammatory Diseases

Study group (No. patients)	OD ₄₀₅ (10 ⁻³) ^a	% Positive ^b	P ^c
Healthy controls (83)	1,000 ± 535	0	
LCL (47)	2,379 ± 1,063	28	> 0.050
MCL (30)	1,762 ± 1,224	20	> 0.050
DCL (22)	2,011 ± 1,266	32	> 0.050
Kala azar (20)	1,854 ± 951	10	> 0.050
<i>T. rangeli</i> -infected (28)	2,422 ± 1,266	39	> 0.050
Chronic chagas' disease (81)	3,656 ± 2,333	66	< 0.005
Inflammatory diseases (69)	932 ± 370	0	> 0.050

^aMean ± standard deviation in ELISA (serum dilution of 1:800).

^bAn OD of 2.338 represents the upper limit of normality, defined as the mean plus 2.5 standard deviations, of the healthy control group. The percentage of patients with levels higher than this is presented.

^cDifferences between OD₄₀₅ values determined in comparison with the control group.
Taken from Avila *et al.* (1992) with permission.

murine laminin or nidogen. All these red cells and glycoproteins have many Gal(α 1-3)Gal-bearing residues (Towbin *et al.*, 1987). These antibodies are likely correspond to those described by Unterkircher *et al.* (1993) as exhibiting high affinity for the α -gal epitope.

The second type of antibodies is detected in ELISA using an American *Leishmania* glycoinositolphospholipid preparation bearing terminal Gal(α 1-3)Man or Gal(α 1-3)Man disaccharide as solid phase antigen (Avila and Rojas, 1990). These antibodies are mainly IgM, and also bound to Gal(α 1-3)Gal-linked synthetic antigens, but did not interact with the same residues present on rabbit, rat and guinea-pig erythrocytes or in murine laminin or nidogen. These antibodies are equally blocked by low concentrations of Gal(α 1-3)Man and Gal(β 1-4)Man. They are strongly elevated in 89% and 84% of diffuse and localized cutaneous leishmaniasis patients (Avila and Rojas 1990).

The third type of terminal α -galactosyl-reactive antibodies are Gal(α 1-2)Gal antibodies, which are not blocked by > 200 mM Gal(α 1-3)Man or Gal(β 1-4)Man and are elevated only in 38% and 28% of diffuse and localized cutaneous leishmaniasis patients. The fact that they are unadsorbed neither by rabbit, rat or guinea-pig red blood cells or murine laminin and nidogen or by pronase-treated human O erythrocytes, nor is their binding affected by methyl- α -Galactopyranoside, melibiose and stachyose, adds further evidence for the fact that these

latter antibodies are indeed different from anti-Gal. They may correspond to the second type of α -gal epitope-reactive antibodies reported by Unterkircher *et al.* (1993). Given the polyclonal nature of anti-Gal (Towbin *et al.*, 1987), our results suggest that among the three different antibody types we found to increase in chronic chagasic cardiomyopathy sera, a considerable proportion of antibody clones might have a different affinity for the protein-(Couto *et al.*, 1990) or lipid-linked α -gal epitopes (Avila *et al.*, 1991; 1989) present on *T. cruzi* membrane. Furthermore, individual differences in the overall affinity to α -gal epitopes on *T. cruzi* may determine the capacity of this family of antibodies to prevent infection and destroy the invading parasite. In supporting of this view, Almeida *et al.* (1991) reported that chagasic anti-Gal had a lower affinity for Gal(α 1-6)Glc bound to agarose than for the α -gal epitope, and was several times more effective in lysis of trypomastigotes than corresponding anti-Gal from normal human serum. This demonstrates a considerable diversity in the recognition of the α -gal epitope by natural antibodies.

Anti-Gal(α 1-2)Gal antibodies also may have a biological significance since they may cross-react with α -gal epitope on the parasite, thus they may contribute to the protection against invading protozoa (Gazzinelli *et al.*, 1991a; Avila *et al.*, 1988b).

7.4. Lysis of *T. cruzi* Trypomastigotes by Human Anti-Gal Antibodies

Participation of antibodies in the resistance against *Trypanosoma cruzi* has been demonstrated at the chronic phase by protection subsequent to passive transfer of immune serum (Krettli and Brener, 1976) or immunoglobulins fractions to infected mice (Takehara *et al.*, 1981). Specific anti-*T. cruzi* antibodies are involved in resistance through alternative and classical complement mediated lysis (Krettli and Brener, 1982; Krettli *et al.*, 1979) and antibody cell-mediated cytotoxicity (Lima-Martins *et al.*, 1985). A lytic activity against *T. cruzi* induced by antibody binding and which is complement independent has recently been detected, in acute chagasic sera, but not in chronic chagasic sera or normal human sera (Stefani *et al.*, 1987). Araújo (1989) found that 17 out of 27 patients at the acute phase of Chagas disease displayed lytic activity.

7.4.1. Direct Lysis in Acute Chagas' Disease

The fact that:

- a. In acute Chagas disease there are high levels of anti-Gal antibodies (IgM and IgG) in contrast to low titres of specific anti-*T. cruzi* antibodies (Gazzinelli *et al.*, 1988),
- b. that lytic activity in acute Chagas disease has been associated with Ig fraction (Stefani *et al.*, 1987), and

- c. that highly purified anti-Gal antibodies from chronic chagasic sera induced infectivity inactivation (Milani and Travassos, 1988; Milani *et al.*, 1988), made Gazzinelli *et al.* (1991a) to propose that lytic activity of anti-Gal antibodies is responsible in the decline of the parasitemia from the acute to the chronic chagasic phase in Chagas' disease.

Thus pre-absorption of acute Chagas serum with mouse laminin, that contains α -gal epitopes (Towbin *et al.*, 1987), or with melibiose (Galactosyl(α 1-6)Glucopyranoside), or α -D-Galactopyranoside, completely abolished the direct lytic activity. Furthermore, the lytic effect of acute chagasic serum was also inhibited by the presence in the incubation medium of melibiose or α -D-Galactopyranoside with Gal(α 1-3)Gal being 5-fold more active than Gal(α 1-4)Gal (Gazzinelli *et al.* (1991a).

Investigation of the characteristics of the cell lysis reaction showed that the lysis of *T. cruzi* by chagasic human sera occurred a few minutes after the samples of the parasite and anti-Gal antibodies are mixed and that this interaction is temperature-dependent (optimal temperature being 37°C). In contrast, chronic chagasic sera and normal sera were unable to carry out direct lysis of parasites.

7.4.2. Complement-Mediated Lysis in Chronic Chagas' Disease

Anti-Gal from chronic chagasic patients lysed *T. cruzi* trypomastigotes in a complement-dependent reaction (Figure 7a). At the concentration of 300 µg/ml, (a concentration frequently found in chagasic sera [Avila *et al.*, 1989]) this antibody caused the lysis of more than 80% of the parasites. Pooled anti-Gal from chagasic sera and complement readily lysed the CL strain trypomastigotes, even at 1 µg/ml (Figure 7b). The complement-mediated lysis seemed to occur via the alternative pathway, inasmuch as the addition of EGTA did not prevent lysis. The specificity for α -gal-containing epitopes in the lysis reaction was confirmed by inhibition with α - but not β -galactopyranosides (Table VII).

To assess the importance of anti-Gal from chagasic serum in the total serum lytic power, these antibodies were adsorbed by Synsorb 115 (i.e. synthetic α -gal epitopes linked to silica beads) followed by rabbit erythrocyte adsorption. Purified chagasic anti-Gal at 300 µg/ml, whole chagasic serum, and normal human serum were tested for residual lytic activity. With ligand-free Synsorb (silica beads) as the adsorbent control, no significant decrease in the lytic activity was obtained. Following adsorption on Synsorb 115 and rabbit erythrocyte, the lytic activity of both the chagasic anti-Gal and the chagasic whole serum was reduced to 25 to 30% of its initial value (Gazzinelli *et al.*, 1991a). Almeida *et al.* (1991) concluded that most of the chagasic serum lytic activity is a result of the presence of antibodies recognizing α -gal epitope-containing structures (Figure 8). They further proposed that in individuals contracting Chagas' disease, the affinity of natural anti-Gal

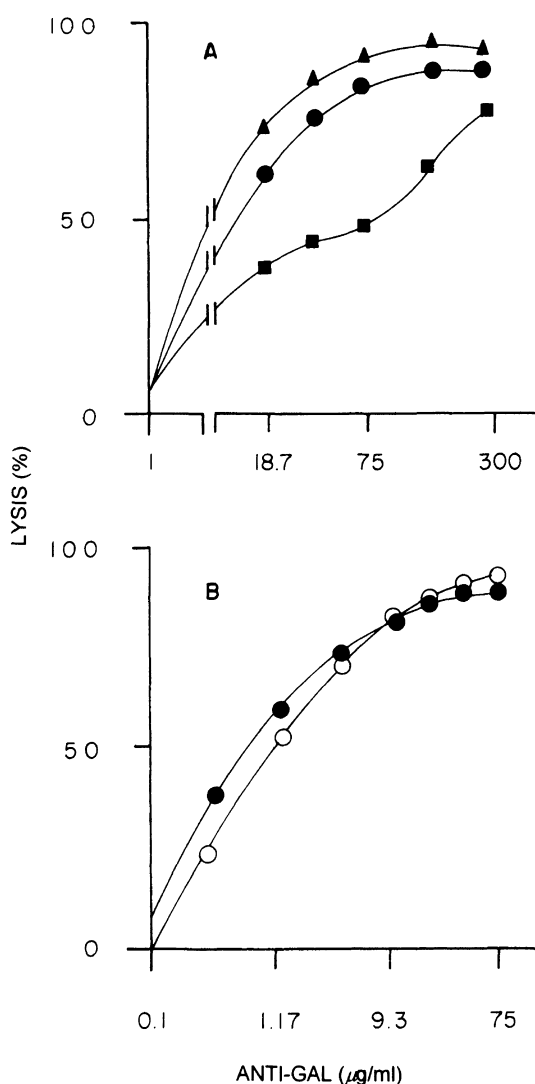


Figure 7. Complement-mediated lysis of metacyclic trypomastigotes by anti-Gal. A, Y strain trypomastigotes; black triangles, circles, and squares, three different anti-Gal preparations from pools pCh7, pCh-5 and pCh-6, respectively, of chagasic sera. B, C1 strain trypomastigotes; lytic response to chagasic anti-Gal in presence of EGTA (alternative complement pathway), black circles; without EGTA, open circles. From Almeida *et al* (1991), with permission.

Table VII
Effect of Carbohydrates on the Immunolysis of Metacyclic Trypomastigotes of *Trypanosoma cruzi*

Carbohydrate ^a	% lysis of parasites ^b		
	Anti-Gal ^c	Chagasic serum ^d	Normal serum ^d
None	96 (90) ^e	92 (91)	14 (12)
O-Methyl- α -D-Galp ^f	18 (25)	21 (20)	6 (5)
O-Methyl- β -D-Galp	87 (85)	86 (89)	12 (13)
Galactose	24 (23)	25 (22)	8 (8)
N-Acetylgalactosamine	32 (31)	36 (32)	11 (9)
Glucose	91 (87)	86 (87)	15 (17)
Melibiose	19 (26)	18 (22)	8 (10)
Lactose	91 (86)	88 (24)	15 (11)

^aAt final concentration of 100 mM.

^bValues \pm 5 % average the results of three experiments.

^cAt final concentration of 300 μ g/ml. from chagasic serum.

^dChagasic serum and normal human serum at a final dilution of 1:2.5.

^eNumbers in parentheses: complement-mediated lysis (%), alternative pathway (in presence of 10 mM EGTA).

^fGalactopyranoside.

Taken from Almeida *et al* (1991) with permission.

clones may be too low to mount an effective complement-mediated lysis, thus, some of the parasites succeed in invading cells and thereby evade destruction by the immune system.

We mentioned above, that Gazzinelli *et al* (1991b) have demonstrated that monoxenic trypanosomatids are very rich in α -gal epitopes, and indeed Souza *et al* (1974) have demonstrated a partial protection of *T. cruzi* infection induced by immunization with monoxenic trypanosomatids. This increased resistance may be mediated by elevated anti-Gal induced by monoxenic parasites α -gal residues.

8. ANTI-GAL RESPONSE IN *T. RANGELI*-CHRONICALLY INFECTED HUMAN SUBJECTS

Avila *et al* (1987) detected elevated levels of anti-Gal in 82% of 38 *T. rangeli*-infected patients, who are free of any *T. cruzi* infection. This strong immune response is due probably to the presence of α -gal residues on *T. rangeli* as latter demonstrated by Gazzinelli *et al* (1991b). It is noteworthy that 33% of apparently hemoflagellate-free subjects living in a *T. rangeli*-endemic area and who have normal levels of antibody against *T. cruzi* and *T. rangeli* antigens were found to have elevated anti-Gal levels. This may be the result either of a cryptic or a very low parasitemia *T. rangeli* infection, undetected even after three consecutive separate hemocultures.

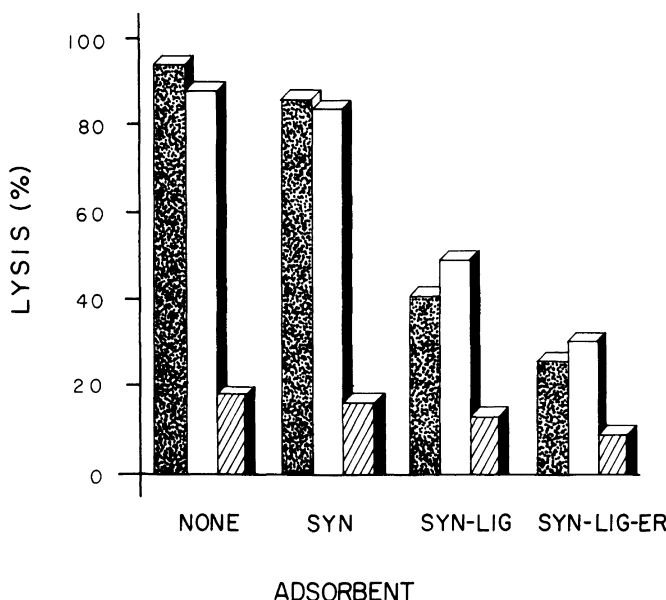


Figure 8. Removal of lytic antibodies by Synsorb 115 followed by rabbit erythrocyte absorption. Chagasic anti-Gal at 300 μ g/ml (▨), whole chagasic serum (□) and normal human serum (▨), were mixed with 2 vol dry ligand-free Synsorb (SYN) as well as with Synsorb 115 (SYN-LIG) for 2 h at 37°C. Supernatants were assayed for their lytic activity with metacyclic trypomastigotes (Y strain). They were then further absorbed with 2 vol of a washed pellet of rabbit erythrocytes (SYN-LIG + ER) and tested for lytic activity. From Almeida *et al* (1991), with permission.

9. ANTI-GAL IN CUTANEOUS AND VISCERAL LEISHMANIASIS PATIENTS

Anti-Gal response to *Leishmania* infection have been studied in cutaneous, mucocutaneous and visceral leishmaniasis (Towbin *et al.*, 1987; Avila *et al.*, 1984; 1988b). Eighty-one percent of American cutaneous leishmaniasis patients (i.e., patients having ulcers or recently closed ulcers) and 34% of the patients with treated and healed ulcers had high "anti-laminin" antibody levels. Further studies of our group revealed that anti-Gal accounted for most of the anti-laminin antibody reactivity in these patients, because these antibodies interact with the α -gal epitope on the N-glycosylated carbohydrate chains of mouse laminin (Towbin *et al.*, 1987). Additional studies showed no correlation between the time course of the leishmaniasis and the anti-Gal antibody levels. We found that mucocutaneous leishmaniasis patients had the highest anti-Gal levels whereas patients with active localized cutaneous leishmaniasis and those with a recently closed cutaneous

Table VIII
Anti-Gal Antibody Levels in Healthy Controls and in
Study Group of Patients

Study group (no. of patients)	A ₄₀₅ ^a	Positivity (%)	P value ^b
Controls (169)	235 ± 151	8	
Cutaneous ACL (91)	1.594 ± 1.208	67	< 0.01
MCL (6)	1.975 ± 657	87	< 0.01
Recently closed ACL ulcer ^c (54)	1.493 ± 993	80	< 0.01
Chronic Chagas' disease (26)	972 ± 812	50	< 0.05
<i>T. rangeli</i> infection (31)	946 ± 582	74	< 0.05
Inflammatory diseases (69)	293 ± 126	4	> 0.1

^aMean ± standard deviation (10^{-3}).

^bDetermined in comparison with anti-Gal values found in control subjects.

^cThese patients were studied after ACL ulcer had been clinically cured for 2 to 3 months.

ACL = American cutaneous leishmaniasis; MCL = Mucocutaneous leishmaniasis.

Taken from Avila *et al* (1988a) with permission.

leishmaniasis ulcer have significantly elevated levels when compared with control patients (Table VIII).

Both IgG and IgM classes of anti-Gal were elevated in acute leishmaniasis patients whereas anti-Gal IgA levels was low (Avila *et al.*, 1984). In a subsequent study, Avila *et al* (1988b) detected elevated anti-Gal levels in 76% of children with active visceral leishmaniasis and in 42% of clinically cured patients with this disease who had been treated about 5 years previously with meglumine antimonate. In that studies rabbit erythrocyte ceramide pentasaccharide-rich neutral glycolipids were used as solid phase antigen in ELISA.

Table IX
Anti-Gal Antibody Levels in Healthy Control Children and in Patients with
Active, Cured or Treated Presumptive Leishmaniasis Visceral

Study group (no. of patients)	A (10^{-3}) ^a	Positivity (%) ^b	Value ^c
Control (62)	235 ± 151		
Active Kala Azar (10)	956 ± 262	76	< 0.001
Treated Kala Azar (38) ^d	603 ± 311	42	< 0.050
Treated presumptive Kala azar (25) ^d	547 ± 293	56	< 0.050

^aMean ± standard deviation.

^bAn A₄₀₅ of 0.613 represents the upper limits of normal values, defined as the mean ± 2.5 standard deviation units of the control group. A reading of 0.613 or greater was therefore considered positive.

^cDetermined in comparison with anti-Gal levels found in control subjects.

^dThe posttreatment period varied between 0.1 and 13 years, being 5.2 ± 3.3 years for patients with Kala Azar and 4.7 ± 3.0 years for patients with presumptive Kala azar.

Taken from Avila *et al* (1988b) with permission.

The long-term persistence of elevated anti-Gal was also found in 56% of children living in the same geographic zone who, at the time of the initial clinical examination, had fever and evident splenomegaly with hyperglobulinemia but had a negative bone marrow aspirate for leishmanial bodies. Five years after antimonate treatment, these clinically cured children with presumptive Kala azar were studied serologically. Their mean anti-Gal values were slightly lower than those in patients with active Kala azar but were still abnormal (Table IX). Anti-Gal was primarily of the IgG and IgM classes in patients with active Kala azar and in antimonate-treated patients with clinically cured Kala azar. The possibility of the remnant living parasites or the persistence of inserted α -gal epitopes in parasitized macrophages was proposed as a mechanism to explain the long-term persistence of abnormal anti-Gal in patients apparently cured of Kala azar (Avila *et al.*, 1988b).

10. IS THERE AUTOIMMUNITY MEDIATED BY ANTI-GAL IN HUMAN CHAGAS' DISEASE ?

It has long been speculated that many autoimmune diseases are the result of infectious agents. Examples of autoimmune diseases believed to have an infectious "trigger" include rheumatic heart disease (group A streptococcus)(Van der Rijn *et al.*, 1977), ankylosing spondylitis and Reiter's syndrome (*Klebsiella pneumoniae*)(Schwimmbeck *et al.*, 1987), celiac disease (adenovirus), non-rheumatoid arthritides (Oldstone, 1987) and myasthenia gravis (herpes simplex virus)(Schwimmbeck *et al.*, 1989). For example, six consecutive amino acids (QTDRED) are identical between the hypervariable domain of HLA-B27 and *K. pneumoniae* nitrogenase. Sera from a significant proportion of HLA-B27 individuals with Reiter's syndrome (53%) or ankylosing spondylitis (29%), but not from appropriate controls, reacted with a synthetic peptide containing the homologous region of HLA-B27 and *K. pneumoniae* nitrogenase. These observations suggest that Reiter's syndrome and ankylosing spondylitis are autoimmune diseases, with HLA-B27 serving as the autoantigen. Induction would be caused by a microbe(s) encoding a protein with sequence homology to HLA-B27 (variable region) and the disease would presumably be related to an unusual concentration of HLA antigen in certain tissues-like joints. In fact, joint tissue from 92% ankylosing spondylitis patients studied heavily expressed HLA-B27 sequences (QTDRED). In contrast, these sequences were not observed either in synovial tissue of individuals with non-arthropathies or in skin biopsy from non-ankylosing spondylitis but HLA-B27 positive individuals.

Another possibility is that a pathogen with the capacity to persist in its host may continuously or cyclically express its antigens. Although expression of a pathogen genome may be restricted so that no infectious multiplication exists, pro-

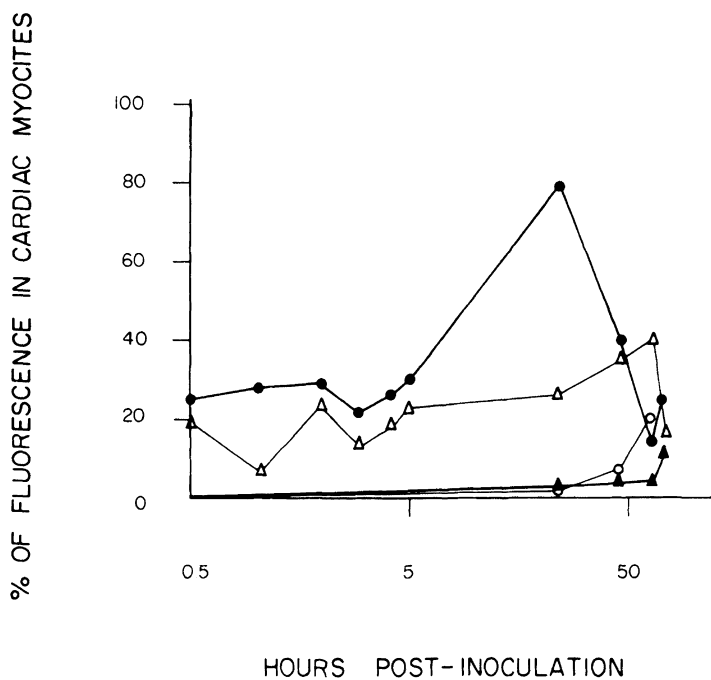


Figure 9. Indirect immunofluorescence staining of fetal murine cardiac myocytes infected with *T. cruzi* trypomastigotes. Kinetics of expression of parasitic antigens on the plasma membrane (Δ). cytoplasm (●) and contractile fibers (▲). (○) Indicates percent of *T. cruzi*-infected cells.

duction of a pathogen antigen in common with that of the host might continue. This would allow initiation of an immune response and/or autoimmunity, either one leading to cyclic, chronic, or progressive disease. Moreover, some viruses and other microbes contain chemical structural components that mimic normal host "self" proteins or terminal oligosaccharide (molecular mimicry).

Trypanosoma cruzi is implicated in autoimmunity on the basis of three findings. First, autoimmune responses are *de novo* concomitant with infection. This point is strengthened by the second finding that, in experimental animals, both acute and persistent *T. cruzi* infection can induce autoimmune responses and cause autoimmune disease (Cunha-Neto *et al.*, 1995; Avila, 1994; Petry and Eisen, 1989; Schmuñis, 1987). Third, by evaluating molecular mimicry in human Chagas' disease, several cross-reacting antigens have been found including: Fl-160 antigen (Van Voorhis *et al.*, 1991), cardiac myosin (Cunha-Neto *et al.*, 1995), cholesterol sulphate-like structure (Avila *et al.*, 1996) and asialoganglioside and monosialoganglioside (Avila *et al.*, 1998). This may be related to Chagas' disease pathogenesis where in the chronic stage, parasite numbers decline to virtual insignificance whereas the disease symptoms become most apparent. This paradox

may be explained by the parasite-triggered autoimmunity, as originally proposed by Körberle (1968).

Autoimmunity in Chagas' disease may be associated with the α -gal epitope. Salma and Avila (1991) have recently shown that *T. cruzi*-infected murine myocytes and nervous tissue cells abundantly express the α -gal epitope. This was demonstrated using polyvalent goat anti-human Ig-FITC conjugate and purified human chagasic anti-Gal. Figure 9 shows the percentage of *T. cruzi*-infected murine myocytes positive by immunofluorescence. The reaction, located on plasma membrane, increased steadily reaching maximal value at 72 hours after infection, thereafter decreasing. Cytoplasmic staining reached maximum value at 24 hours after infection. Fluorescence in contractile fibers steadily increased up to 60 hours after infection. Under our working conditions, no immunofluorescence was found in non-infected (control) murine myocytes or nervous tissue cells as chagasic human serum had been previously absorbed with respective uninfected murine cells.

Figure 10 shows the percentage of *T. cruzi*-infected murine nervous tissue cells positive by immunofluorescence. This localized in plasma membrane reaching a maximum at 24–48 hours after infection. Cytoplasm showed maximal fluorescence 48 hours post-infection, thereafter steadily decreasing. In contrast, immunofluorescence on neurofilaments slowly increased reaching maximal value at 60 hours post-infection.

A clear expression of α -gal epitopes have been reported, using immunogold labeling for electron microscopy, for Vero cells infected with *T. cruzi* trypomastigotes (Souto-Padron *et al.*, 1994). Thus, it is possible that infected cells (macrophages, muscle cells, nervous cells) may change their surface structure by inserting parasite-derived α -gal epitopes, or changing host carbohydrate components by new posttranslational modifications due to the intracellular residence of parasites. The autoimmunity observed in Chagas disease may therefore not be the result of cross-reacting structures present *per se*, but due to a modified structure arising in the *T. cruzi*-infected cells (Avila, 1994). Antibodies involved in the initiation of this process might be the high affinity anti-Gal from chronic chagasic patients, rather than the natural anti-Gal from healthy individuals.

Whereas the epitope recognized by anti-Gal may be a simple disaccharide, the conditions allowing antibodies to bind to that epitope are complex. Platt (1996) have proposed that expression of the α -gal epitope by itself may not be sufficient to allow substantial binding of complement fixing in xenoreactive antibodies. Rather, natural antibodies seem to bind preferentially to certain glycoproteins bearing that epitope.

One important factor in antibody binding appears to be the clustering of epitopes allowing multivalent interactions between antibody molecules and the cell surface. The clustering of α -gal epitope have been clearly demonstrated on *T. cruzi* and *Leishmania* plasma membrane outer face (Souto-Padron *et al.*, 1994;

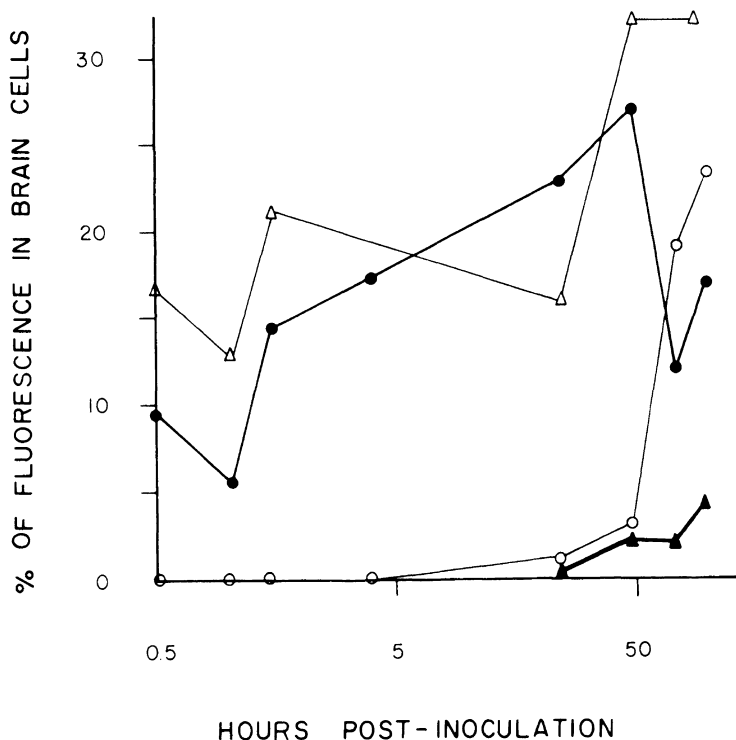


Figure 10. Indirect immunofluorescence staining of fetal murine brain cells infected with *T. cruzi* trypomastigotes. Kinetics of expression of parasitic antigens on the plasma membrane (Δ), cytoplasm (\bullet) and neurofilaments (\blacktriangle). (\circ) Indicates percent of *T. cruzi*-infected cells.

Bretaña *et al.*, 1992). It remains to be determined whether this α -gal epitope clustering occurs in *T. cruzi*-infected cells.

The optimal clustering of epitopes is not random, however, as the binding of xenoreactive anti-Gal to purified proteins containing similar numbers of α -gal epitope varies over approximately 1000-fold (Platt and Holzknecht, 1994). Further evidence that the manner in which α -gal epitope is expressed, rather than the total number of epitopes, determine the extent of antibody binding, emerged from studies on variation in antigen expression by the population of potential organ donors (Geller *et al.*, 1994). Analysis of the binding level of xenoreactive antibodies to cells from populations of pigs suggests that there is an up to 10-fold range of antibody binding suggesting variation in antigen expression (Alvarado *et al.*, 1995; Geller *et al.*, 1994). The nature of the core structures bearing the α -gal epitope modifications recognized by xenoreactive natural anti-Gal has several significant implications for the development of xenograft reaction. Thus, the core structures

determine to a certain extent the three-dimensional array of the epitopes and may thus determine the amount of antibody binding to a target cell (Cotterell *et al.*, 1995). Accordingly, interaction of *T. cruzi*-infected cells with high affinity chagasic anti-Gal will lead to cell death only if the α -gal epitope express optimal conditions for a successful antigen-antibody interaction. If so, this would lead to a local inflammatory reaction mediated by granulocytes, macrophages, and killer lymphoid cells interacting with the Fc portion of the bound anti-Gal. These cytotoxic cells would subsequently exert their lytic activity toward the cells having the α -gal epitope in an antibody-dependent, cell mediated cytolysis (ADCC) process, as demonstrated recently by Takeuchi *et al.* (1996) in human cells transfected with a porcine cDNA encoding α 1-3Galactosyltransferase. Mononuclear cellular infiltrates (consisting of macrophages, lymphocytes and plasma cells) are the usual morphological findings in acute (Palacios-Prü *et al.*, 1989) as well as in chronic chagasic cardiomyopathy (consisting of macrophages and lymphocytes) (Milei *et al.*, 1992).

11. THE UDP-GAL: β -GAL- α 1-3GAL-GALACTOSYLTTRANSFERASE KNOCKOUT MICE

In 1995, Thall *et al* generated mice deficient in a gene (α 1,3GT) encoding the UDP-Gal: β -Gal- α 1-3galgalactosyl-transferase enzyme responsible for α -gal synthesis and expression. These mice develop normally and exhibit no gross phenotypic abnormalities. The α -gal epitope is absent from the vascular endothelium and other tissues in α 1,3GT(–/–) adult mice. By contrast, α 1,3GT(–/–) mice, like humans, develop naturally occurring anti-Gal normally absent in wild type mice. We hypothesized that these mice could be a good experimental model for testing not only the importance of the anti-Gal in experimental acute Chagas' disease and in cutaneous leishmaniasis but also the humoral immune response to the α -gal epitope. Thus, we have compared the parasitemia curve, and anti-Gal levels of adult α 1,3GT(–/–) and of wild type mice that were experimentally infected with *T. cruzi*. We also monitored the development of *Leishmania* infection in rear foot-pads.

11.1. Acute *T. cruzi* Infection

Adult female α 1,3GT(–/–) and wild type control mice were used in these experiments. Non-infected α 1,3GT(–/–) mice have about 1.5-fold higher anti-Gal levels compared with wild type mice. Both groups were infected with *T. cruzi* trypomastigotes and the parasitemia curve and serum anti-Gal levels followed by about 30 days. In α 1,3GT(–/–) mice parasitemia began to be detected at about eight days post-inoculation and was paralleled by an increase in anti-Gal levels. Interestingly, about day 13 post-inoculation there was a small fall in both para-

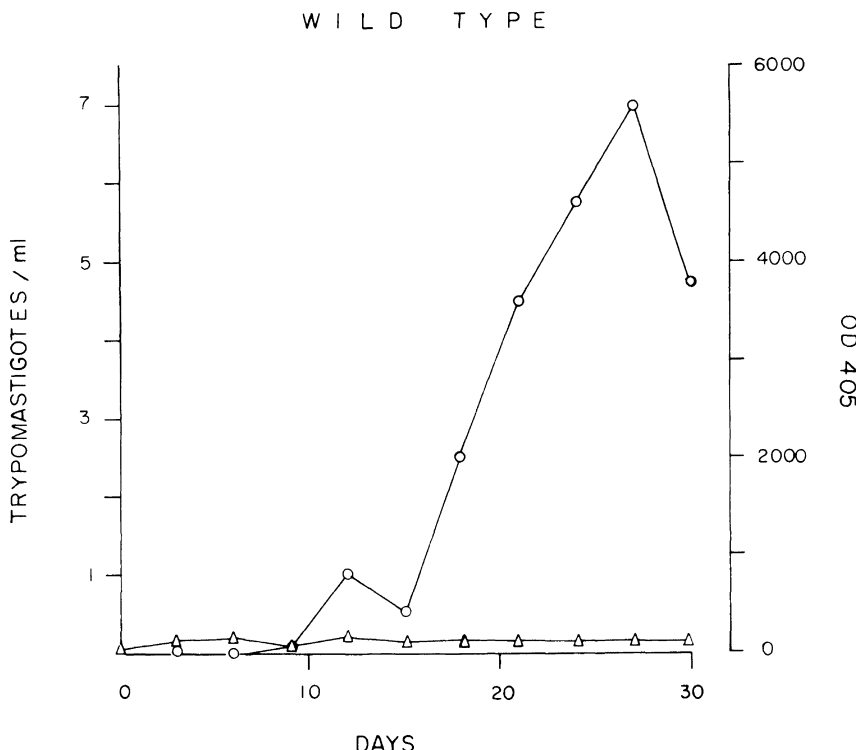


Figure 11. Kinetics of parasitemia (O) and anti-Gal response (Δ) of α 1,3GT ($-/-$) and wild type mice intraperitoneally inoculated with 1×10^7 or 5×10^7 *T. cruzi* trypomastigotes of the Be strain.

sitemia and anti-Gal levels, thereafter parasitemia increased about 6-fold while anti-Gal levels maintained in a plateau (Figure 11). This represented an increase of 54-fold for α 1,3GT($-/-$) mice when compared with same uninfected mice. Anti-Gal levels were not modified in wild type mice. Noteworthy, parasitemia curve was similar to that found for α 1,3GT($-/-$) mice. However, parasitemia levels in α 1,3GT($-/-$) mice was significantly lower ($P < 0.01$) than in wild type mice suggesting that anti-Gal is capable of partially controlling *T. cruzi* infection. The rapid response in α 1,3GT($-/-$) mice in anti-Gal levels to *T. cruzi* inoculation suggest that indeed parasitic α -gal epitopes are highly immunogenic. Wild type mice were immunotolerant to α -gal epitope.

11.2. Cutaneous Leishmaniasis Infection

No difference in the time course of *Leishmania* nodule growth nor in the appearance of anti-Gal levels was found between α 1,3GT($-/-$) and wild type control

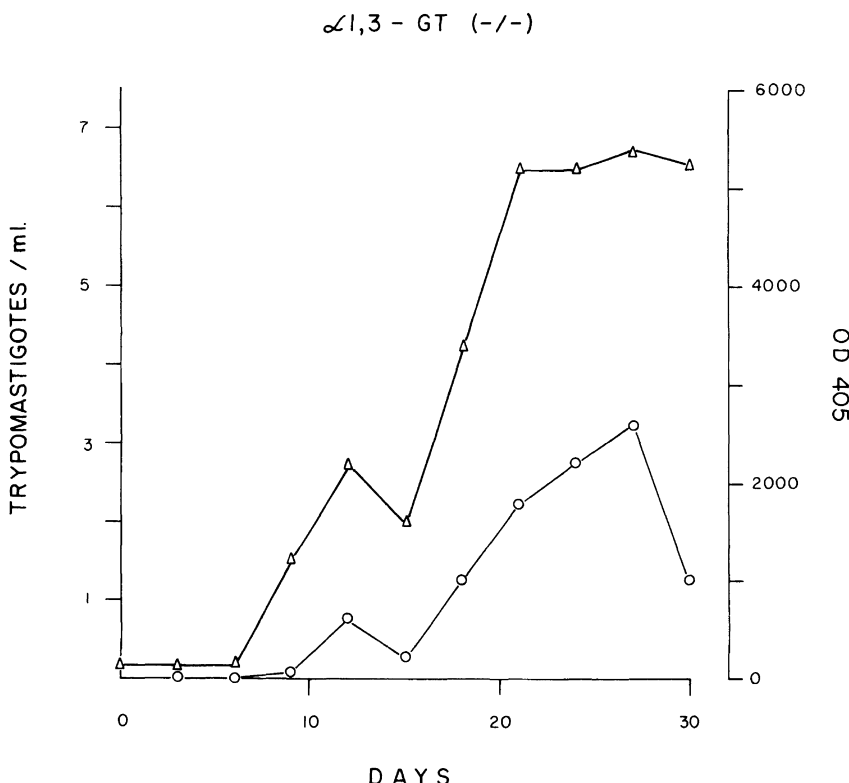


Figure 11. (Continued)

mice (Figure 12). It should be noted however that *Leishmania* acted as a powerful immunogen as in $\alpha 1,3GT(-/-)$ mice anti-Gal levels began to increase only at day 12 post- inoculation with 100 or 500 amastigotes, remaining in a plateau thereafter. This delayed response may be due to the initial slow development of the disease. The sharp increase in nodule size observed 120 days post-inoculation was not followed by a significant ($P > 0.05$) modification in anti-Gal levels.

Leishmania-infected wild type animals did not modified its anti-Gal values. Similar to the observations with *T. cruzi* it is evident that anti-Gal response by itself is not capable of controlling cutaneous *Leishmania* infection.

12. CONCLUSIONS

Anti-Gal is a human natural antibody which interacts specifically with the mammalian carbohydrate structure $Gal\alpha 1-3Gal\beta 1-4GlcNac-R$, termed, the α -gal

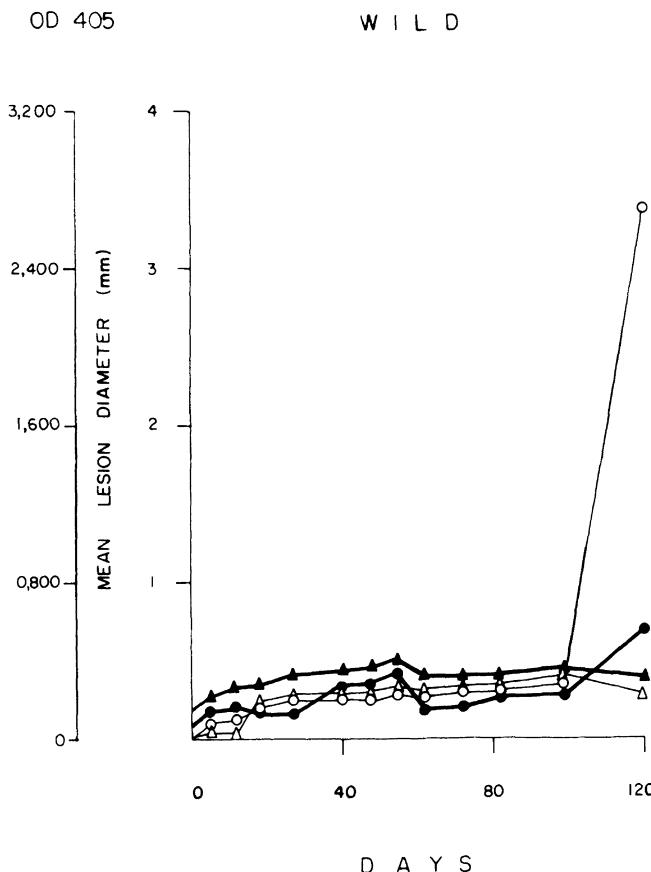


Figure 12. Development of leishmanial lesions in foot-pads (○,●) and anti-Gal response (Δ , \blacktriangle) of α 1,3GT (-/-) mouse and wild type control mice. Mice were inoculated with 1×10^2 (○) or 5×10^2 (●) of GML473 isolate of *Leishmania mexicana mexicana*.

epitope. This antibody constitutes approximately 1% of circulating IgG in human serum and is produced, upon stimulation, by 1% of circulating B lymphocytes. The antigenic source for the constant production of anti-Gal seems to be the α -gal-like epitopes found on many bacteria of the gastrointestinal flora. The physiological role of this antibody is not clear as yet.

Several biochemical and morphological reports have given clear evidence of the presence in *Trypanosoma* and in *Leishmania* of α -gal-rich structures on glycolipids and glycoproteins.

Patients with acute Chagas disease have about nine-fold higher anti-Gal levels compared with chronic chagasic patients. In this latter condition no relationship was found between clinical evolution and anti-Gal levels. Anti-Gal readily

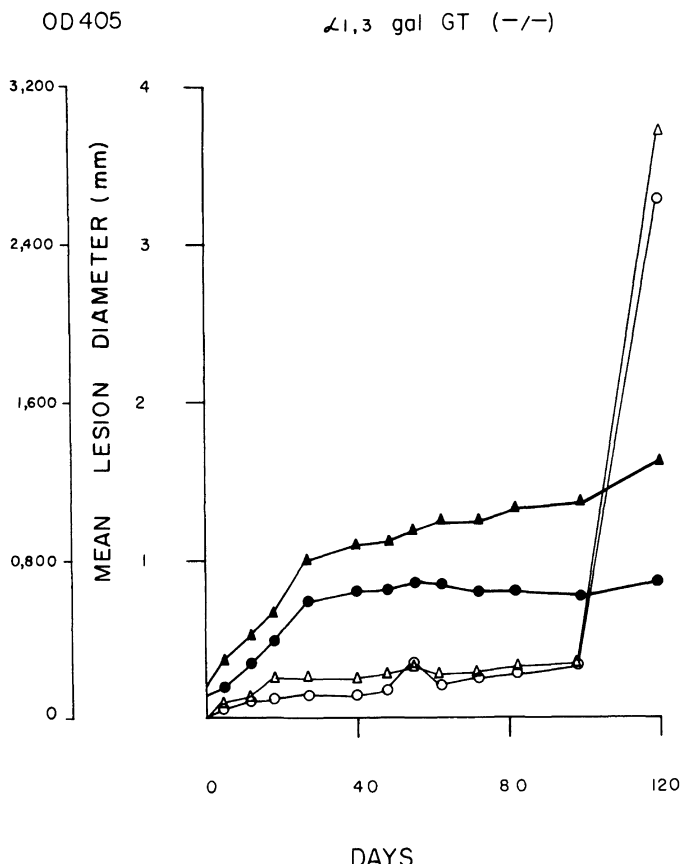


Figure 12. (Continued)

binds to *T. cruzi* and can induce either direct lysis or complement-mediated lysis of the parasite. Thus, anti-Gal may contribute to natural immunity against *T. cruzi*.

Eighty-two percent of *T. rangeli*-infected patients displayed significantly elevated anti-Gal levels. Noteworthy, 33% of apparently hemoflagellate-free subjects living in a *T. rangeli*-endemic area and having control antibody levels against *T. cruzi* and *T. rangeli* antigens showed elevated anti-Gal levels. This suggests the possibility either of a cryptic or a very low parasitemia *T. rangeli* infection, undetected even after three consecutive separate hemocultures.

Cutaneous and visceral leishmaniasis patients also have elevated anti-Gal levels. In Kala azar antigenic stimulation persists even years after apparent clinical cure suggesting that given the strong immunogenic capacity of α -gal epitopes present on *Leishmania* parasites, even a few remaining parasites are able to main-

tain a longstanding immunological stimulation. No information is still available on the importance of anti-Gal on *Leishmania* promastigote or amastigote lysis or in the development of lesions.

Using adult female mice deficient in a gene encoding the UDP-Gal:β-Gal-α1-3galgalactosyltransferase (enzyme responsible for α-gal synthesis and expression)(α1,3GT) [α1,3GT(−/−)] and wild type mice experimentally infected with *T. cruzi* trypomastigotes, we found a significant difference in the parasitemia levels: α1,3GT(−/−) mice having significantly lower parasitemia than wild type mice. The contrary was true for anti-Gal levels, thus while α1,3GT(−/−) mice have a 54-fold increase in anti-Gal levels, wild type mice maintained basal levels. These results suggests that anti-Gal has an important role in the control of parasitemia and that *T. cruzi* is a highly immunogenic parasite. This was not the case in *Leishmania*-infected mice, whose foot-pad lesion diameter (*Leishmania*) between both groups of mice was close suggesting a minor role for anti-Gal in the control of experimental cutaneous *Leishmania* infection. *Leishmania*-infected α1,3GT(−/−) mice showed a significant increase in anti-Gal levels, but very discrete compared with *T. cruzi*-infected mice, due perhaps to the fact that this infection was limited only to one rear foot-pad. Again wild type mice did not increase anti-Gal levels. Finally, the eventual role of anti-Gal in the autoimmunity existing in Chagas' disease is discussed. Thus, the possibility exist that *T. cruzi*-infected cells (macrophages, muscle cells, nervous cells) due to the intracellular residence of parasites, may change their surface structure by inserting parasite-derived α-gal epitopes or changing host components by new posttranslational modifications. The autoimmunity observed in Chagas disease may therefore not be due to cross-reacting structures present *per se*, but to a modified structure arising in the *T. cruzi*-infected cells.

ACKNOWLEDGMENTS. This work is a product of fruitful collaborations with many colleagues. In particular, I thank Miguel Rojas, Antonio Bretaña, Nunciada Salma, Alvaro Acosta-Serrano, María Argelia Polegre, Angela Avila, Gladys Velazquez-Avila, Rando García, Ivo Tremont-Lukats, Jaime Wilder, Esther Arbona, Leonardo García, Marisol Zambrano, Olga L. Wittig, Egidio Romano, Manuel Rieber, Rupert Timpl, H. Von der Mark, Harry Towbin, Uri Galili, Michael A.J. Ferguson, Malcom McConville, Hugo Carrasco, Jacinto Convit, G.A Maekelt and Felipa Merecuana. I thank María Leboso for graphic art assistance. This work was supported by Consejo Nacional de Investigaciones Científicas y Tecnológicas (CONICIT) and World Bank.

REFERENCES

- Almeida, I.C., Milani, S.R., Gorin, P.A.J., and Travassos, L.R., 1991, Complement mediated lysis of *Trypanosoma cruzi* trypomastigotes by human anti-α-galactosyl antibodies. *J. Immunol.* **146**: 2394–2400.

- Almeida, I.C., Krautz, G.M., Krettli, A.U., and Travassos, L.R., 1993, Glycoconjugates of *Trypanosoma cruzi*: A 74 Kd antigen of trypomastigotes specifically reacts with lytic anti- α -galactosyl antibodies from patients with chronic Chagas disease. *J. Clin. Laborat. Anal.* **7**: 307–316.
- Almeida, I.C., Ferguson M.A., Schenkman, S., and Travassos, L., 1994, Lytic anti- α -galactosyl antibodies from patients with chronic Chagas' disease recognize novel O-linked oligosaccharides on mucin-like glycosylphosphatidylinositol-anchored glycoproteins of *Trypanosoma cruzi*. *Biochem. J.* **304**: 793–802.
- Alvarado, C.G., Cotterell, A.H., McCurry, K.R., Collins, B.H., Magee, J.C., Berthold, J., Logan, J.S., and Platt, J.L., 1995, Variation in the level of xenoantigen expression in porcine organs. *Transplantation* **59**: 1589–1594.
- Andrade, Z., 1985, A patologia da doença de Chagas no homem. *Ann. Soc. Belg. Med. Trop.* **65** (Suppl 1): 15–30.
- Andrade, S.G., and Grimaud, J.A., 1986, Chronic murine myocarditis due to *Trypanosoma cruzi*: an structural study and immunochemical characterization of cardiac interstitial matrix. *Mem. Inst. Oswaldo Cruz* **81**: 29–41.
- Andrade, S.G., Grimaud, J.A., and Stocker-Guerret, S., 1989, Sequential changes of the connective matrix components of the myocardium (fibronectin and laminin) and evaluation of cardiac fibrosis in mice infected with *Trypanosoma cruzi*. *Am. J. Trop. Med. Hyg.* **40**: 151–60.
- Araujo, M.A., 1989, Lise de *Trypanosoma cruzi* por soros de pacientes na fase aguda da doença de Chagas. Ph.D. Thesis, University of São Paulo.
- Avila, J.L., 1992, Molecular mimicry between *Trypanosoma cruzi* and host nervous tissues. *Acta Cient. Venez.* **43**: 330–340.
- Avila, J.L., 1993, Glycosyl phosphatidylinositols in *Leishmania* and *Trypanosoma*. *Trends in Comparat. Biochem. Physiol.* **1**: 881–906.
- Avila, J.L., 1994, Molecular mimicry between *Trypanosoma cruzi* and host nervous tissues. In: *Chagas' disease and the nervous system*. Pan American Health Organization. Sci. Publ. N° 547, Washington, pp. 268–292.
- Avila, J.L., and Rojas, M., 1990, A galactosyl(α 1–3)mannose epitope on phospholipids of *Leishmania mexicana* and *L. braziliensis* is recognized by trypanosomatid-infected human sera. *J. Clin. Microbiol.* **28**: 1530–1537.
- Avila, J.L., Rojas, M., and Reiber, M., 1984, Antibodies to laminin in American cutaneous leishmaniasis. *Infect. Immun.* **43**: 402–406.
- Avila, J.L., Rojas, M., and Towbin, H., 1988a, Serological activity against galactosyl- α (1-3)galactose in sera from patients with several kinetoplastida infections. *J. Clin. Microbiol.* **26**: 126–132.
- Avila, J.L., Rojas, M., and García, L., 1988b, Persistence of elevated levels of galactosyl- α (1–3)galactose antibodies in sera from patients cured of visceral leishmaniasis. *J. Clin. Microbiol.* **26**: 1842–1847.
- Avila, J.L., Rojas, M., and Galili, U., 1989, Immunogenic Gal α 1-3Gal carbohydrate epitopes are present on pathogenic American *Trypanosoma* and *Leishmania*. *J. Immunol.* **142**: 2828–2834.
- Avila, J.L., Rojas, M., and Acosta, A., 1991, Glycoinositol phospholipids from American *Leishmania* and *Trypanosoma spp.*: Partial characterization of the glycan cores and the human humoral immune response to them. *J. Clin. Microbiol.* **29**: 2305–2312.
- Avila, J.L., Rojas, M., and Velasquez-Avila, G., 1992, Characterization of a natural human antibody with anti-galactosyl(α 1–2)galactose specificity that is present at high titers in chronic *Trypanosoma cruzi* infection. *Am. J. Trop. Med. Hyg.* **47**: 413–421.
- Avila, J.L., Rojas, M., and Avila, A., 1996, Cholesterol sulphate-reactive autoantibodies are specifically increased in chronic chagasic human patients. *Clin. Exp. Immunol.* **103**: 40–46.
- Avila, J.L., Rojas, M., and Avila, A., 1998, Increase in asialoganglioside- and monosialoganglioside-reactive antibodies in chronic Chagas' disease patients. *Am J. Trop. Med. Hyg.* **58**: 338–342.

- Avila, J.L., Rojas, M., Velazquez-Avila, G., Von Der Mark, H., and Timpl, R., 1986. Antibodies to basement membrane protein nidogen in Chagas' disease and American cutaneous leishmaniasis. *J. Clin. Microbiol.* **24**: 775–778.
- Avila, J.L., Rojas, M., Velazquez-Avila, G., and Rieber, M., 1987. Antibodies to laminin in *Trypanosoma rangeli*-infected subjects. *Parasitol. Res.* **73**: 178–179.
- Bretaña, A., Avila, J.L., Arias-Flores, M., Contreras, M., and Tapia F.J., 1986. *Trypanosoma cruzi* and American *Leishmania* spp.: immunocytochemical localization of a laminin-like protein in the plasma membrane. *Exp. Parasitol.* **61**: 168–175.
- Bretaña, A., Avila, J.L., Contreras-Bretaña, M., and Tapia, F., 1992. American *Leishmania* spp. and *Trypanosoma cruzi*: Galactosyl(1–3)galactose epitope localization by colloidal gold immuno-cytochemistry and lectin cytochemistry. *Exp. Parasitol.* **74**: 27–37.
- Carrasco, H.A., Barboza, J.S., Inglessis, G., Fuenmayor, A., and Molina, C., 1982. Left ventricular cineangiography in Chagas' disease: detection of early myocardial damage. *Am. Heart J.* **104**: 595–602.
- Carreira, J.C., Jones, C., Wait, R., Previato, J.O., and Mendonca-Previato, L., 1996. Structural variation in the glycoinositol phospholipids of different strains of *Trypanosoma cruzi*. *Glyco-conjugate J.* **13**: 955–966.
- Cotterell, A.H., Collins, B.H., Parker, W., Harland, R.C., and Platt, J.L., 1995. The humoral immune response in humans following cross-perfusion of porcine organs. *Transplantation* **60**: 861–864.
- Couto, A.S., Goncalves, M.F., Colli, W., and Lederkremer, R.M., 1990. The N-linked carbohydrate chain of the 85 kilodalton glycoprotein from *Trypanosoma cruzi* trypomastigotes contains sialyl, fucosyl and galactosyl(α1–3)galactose units. *Mol. Biochem. Parasitol.* **39**: 101–108.
- Couto, A.S., Lederkremer, R.M., de, Colli, W., and Alves, M.J., 1993. The glycosylphosphatidylinositol anchor of the trypomastigote-specific Tc-85 glycoprotein from *Trypanosoma cruzi*. Metabolic-labeling and structural studies. *Eur. J. Biochem.* **217**: 597–602.
- Cunha-Neto, E., Duranti, M., Gruber, A., Zingales, B., De Messias, I., Stolfi, N., Bellotti, G., Patarroyo, M. E., Pilleggi, F., and Kalil, J., 1995. Autoimmunity in Chagas disease cardiopathy: Biological relevance of a cardiac myosin-specific epitope crossreactive to an immunodominant *Trypanosoma cruzi* antigen. *Proc. Natl. Acad. Sci. USA* **92**: 3541–3545.
- Davin, J.C., Malaise, M., Foidart, J.M., and Mahieu, P., 1987. Anti-α-galactosyl antibodies and immune complexes in children with Henoch-Schonlein purpura of IgA nephropathy. *Kidney Int.* **31**: 1132–1139.
- Editorial, 1965. New light on Chagas' disease. *Lancet*, **1**: 1150–1151.
- Egge, H., Kordowicz, M., Peter-Katalinic, J., and Hanfland, P., 1985. Immunochemistry of I/i-active oligo- and polyglycosylceramides from rabbit erythrocyte membranes. *J. Biol. Chem.* **260**: 4927–4935.
- Ferguson, M.A.J., Homans, S.W., Dwek, R.A., and Rademacher, T.W., 1988. Glycosylphosphatidylinositol moiety that anchors *Trypanosoma brucei* variant surface glycoprotein to the membrane. *Science* **239**: 753–759.
- Ferrans, V.J., Milei, J., Tomita, Y., and Storino, R., 1988. Basement membrane thickening in cardiac myocytes and capillaries in chronic Chagas' disease. *Am. J. Cardiol.* **61**: 1137–1140.
- Galili, U., Rachmilewitz, E.A., Peleg, A., and Flechner, I., 1984. A unique natural human IgG antibody with anti-α-galactosyl specificity. *J. Exp. Med.* **160**: 1519–1531.
- Galili, U., Basbaum, C.B., Shohet, S.B., Buehler, J., and Macher, B.A., 1987a. Identification of erythrocyte Gal α 1–3Gal glycosphingolipids with a mouse monoclonal antibody Gal-13. *J. Biol. Chem.* **262**: 4683–4688.
- Galili, U., Clark, M.R., Shohet, S.B., Buehler, J., and Macher, B.A., 1987b. Evolutionary relationship between the anti-Gal antibody and the Gal α 1–3Gal epitope in primates. *Proc. Natl. Acad. Sci. USA* **84**: 1369–1373.

- Gazzinelli, R.T., 1992, Natural anti-Gal antibodies prevent, rather than cause, autoimmunity in human Chagas' disease. *Res. Immunol.* (36th Forum in Immunology) **142**: 164–167.
- Gazzinelli, G., and Brener, Z., 1988, Anti-laminin and specific antibodies in acute Chagas disease. *Trans. R. Soc. Trop. Med. Hyg.* **82**: 574–576.
- Gazzinelli, R.T., Galvao, L.M.C., Cardoso, J.R., Cancado, J.R., Krettli, A.U., Brener, Z., and Gazzinelli, G., 1988, Anti-*Trypanosoma cruzi* and antilaminin antibodies in chagasic patients after specific treatment. *J. Clin. Microbiol.* **26**: 1795–1800.
- Gazzinelli, R.T., Pereira, M.E.S., Romanha, A., Gazzinelli, G., and Brener, Z., 1991a, Direct lysis of *Trypanosoma cruzi*: a novel effector mechanism of protection mediated by human anti-gal antibodies. *Parasite Immunol.* **13**: 345–356.
- Gazzinelli, R.T., Romanha, A.J., Fontes, R., Chiari, E., Gazzinelli, G., and Brener, Z., 1991b, Distribution of carbohydrates recognized by the lectins *Euonymus europaeus* and Concanavalin A in monoxenic and heteroxenic trypanosomatids. *J. Protozool.* **38**: 320–325.
- Geller, R.L., Rubinstein, P., and Platt, J.L., 1994, Variation in expression of porcine xenogeneic antigens. *Transplantation* **58**: 272–274.
- Grauert, M.R., Houdayer, M., and Hontebeyrie-Joskowicz, M., 1993, *Trypanosoma cruzi* infection enhances polyreactive antibody response in an acute case of human Chagas' disease. *Clin. Exp. Immunol.* **93**: 85–92.
- Goin, J.C., Borda, E., Denduchis, B., Milei, J., Storino, R., and Sterin-Borda, L., 1990, Anticuerpos circulantes en pacientes chagásicos con actividad colinérgica que regulan la función cardíaca. *Medicina (Bs.As)* **50**: 385–386.
- Kierszenbaum, F., 1986, Autoimmunity in Chagas' disease. The debate goes on. Reply. *Parasitol Today* **2**: 22–23.
- Koberle, F., 1968, Chagas' disease and Chagas' syndromes: The pathology of American trypanosomiasis. *Adv. Parasitol.* **6**: 63–116.
- Krettli, A.U., and Brener, Z., 1976, Protective effects of specific antibodies in *Trypanosoma cruzi* infection. *J. Immunol.* **116**: 755–760.
- Krettli, A.U., and Brener, Z., 1982, Resistance against *Trypanosoma cruzi* associated to anti-living trypomastigotes antibodies. *J. Immunol.* **128**: 2009–2012.
- Krettli, A.U., Weisz-Carrington, P., and Nussenzweig, R.S., 1979, Membrane-bound antibodies to bloodstream *Trypanosoma cruzi* in mice: strain differences in susceptibility to complement-mediated lysis. *Clin. Exp. Immunol.* **37**: 416–423.
- Laguens, R.P., Meckert, P.C., and Chambo, J., 1991, Origin and significance of anti-heart and anti-skeletal muscle autoanti-bodies in Chagas' disease. *Res. Immunol.* **142**: 160–163.
- Lederkremer, R.M., Lima, C., Ramírez, M.I., and Casal, O.L., 1990, Structural features of the lipopeptidophosphoglycan from *Trypanosoma cruzi* common with the glycoprophosphatidylinositol anchors. *Eur. J. Biochem.* **192**: 337–345.
- Lima-Martins, M.V.C., Sánchez, G., Krettli, A.U., and Brener, Z., 1985, Antibody-dependent cell cytotoxicity against *Trypanosoma cruzi* is only mediated by protective antibodies. *Parasite Immunol.* **7**: 367–370.
- McConville, M.J., and Bacic, A., 1989, A family of glycoinositol phospholipids from *Leishmania major*. Isolation, characterization and antigenicity. *J. Biol. Chem.* **24**: 757–766.
- McConville, M.J., Homans, S.W., Thomas-Oates, J.E., Dell, A., and Bacic, A., 1990, Structures of the glycoinositol phospholipids from *Leishmania major*. A family of novel galactofuranose-containing glycolipids. *J. Biol. Chem.* **265**: 7385–7394.
- McConville, M.J., Collidge, T.A.C., Ferguson, M.A.J., and Schneider, P., 1993, The glycoinositol phospholipids of *Leishmania mexicana* promastigotes. Evidence for the presence of three distinct pathways of glycolipid biosynthesis. *J. Biol. Chem.* **268**: 15595–15604.

- McConville, M.J., and Ferguson, M.A.J., 1993. The structure, biosynthesis and function of glycosylated phosphatidylinositol in the parasitic protozoa and higher eukaryotes. *Biochem. J.* **294**: 305–324.
- Milani, S.R., and Travassos, L.R., 1988. Anti- α -galactosyl antibodies in chagasic patients. Possible biological significance. *Brazil. J. Med. Biol. Res.* **21**: 1275–1286.
- Milani, S.R., Oliveira, T.G., and Travassos, L.R., 1988. Protective effect of lytic human antibodies binding to carbohydrate epitopes against trypomastigote infection in mice. *Memorias do Instituto Oswaldo Cruz* **82** (Suppl): 142.
- Milei, J., and Storino, R., 1987. Laminin in chagasic auto-immunity? (Letter to Editor). *Parasitol Today* **3**: 119.
- Milei, J., Storino, R., Fernández-Alonso, G., Beigelman, R., Vanzulli, S., and Ferrans, V.J., 1992. Endomyocardial biopsies in chronic chagasic cardiomyopathy. *Cardiology* **80**: 424–437.
- Milei, J., Sánchez, J., Storino, R., Yu, Z.X., Denduchis, B., and Ferrans, V.J., 1993. Antibodies to laminin and immunohistochemical localization of laminin in chronic chagasic cardiomyopathy: a review. *Mol. Cell. Biochem.* **129**: 161–170.
- Molina, H.A., Milei, J., and Storino, R., 1984. Chronic Chagas myocardopathy. Demonstration of in vivo immunoglobulins in heart structures by the immunoperoxidase technique. *Cardiology* **71**: 297–306.
- Oldstone, M.B.A., 1987. Molecular mimicry and autoimmune diseases. *Cell* **50**: 819–820.
- PAHO, Division of Communicable Disease Prevention and Control, Communicable Disease Program, HPC/HCT, 1994. *Leishmaniasis in the Americas. Epidemiol Bull.* **15**: 8–11.
- Palacios-Pru, E., Carrasco, H., Scorz, C., and Espinoza, R., 1989. Ultrastructural characteristics of different stages of human chagasic myocarditis. *Am. J. Trop. Med. Hyg.* **41**: 29–40.
- Paulsson, M., Aumailley, M., Deutzmann, R., Timpl, R., Beck, K., and Engel, J., 1987. Laminin-nidogen complex. Extraction with chelating agents and structural characterization. *Eur. J. Biochem.* **166**: 11–19.
- Pearson, R.D., and de Queiroz-Sousa, A., 1996. Clinical spectrum of leishmaniasis. *Clin. Infect. Dis.* **22**: 1–13.
- Petry, K., and Eisen, H., 1989. Chagas's disease: a model for the study of autoimmune diseases. *Parasitol Today* **5**: 111–116.
- Platt, J.L., 1996. The immunological barriers to xenotransplantation. *Crit. Rev. Immunol.* **16**: 331–358.
- Platt, J.L., and Holzknecht, Z.E., 1994. Porcine platelet antigens recognized by human xenoreactive natural antibodies. *Transplantation* **57**: 327–329.
- Ramasamy, R., and Reese, R.T., 1986. Terminal galactose residues and the antigenicity of *Plasmodium falciparum* glycoproteins. *Mol. Biochem. Parasitol.* **19**: 91–101.
- Ramasamy, R., and Rajakaruna, R., 1997. Association of malaria with inactivation of α -1,3-galactosyl transferase in catarrhines. *Biochim. Biophys. Acta* **1360**: 241–246.
- Salma, N., and Avila, J.L., 1991. Interaction between various strains of *T. cruzi* and cardiac primary cultures. *Acta Cient. Venez.* **42**: 185.
- Sánchez, J.A., Milei, J., Yu, Z.X., Storino, R., Wenthold, R. Jr., and Ferrans, V.J., 1993. Immunohistochemical localization of laminin in the heart of patients with chronic chagasic cardiomyopathy: Relationship to thickening of basement membranes. *Amer. Heart J.* **126**: 1392–1401.
- Schwimmbeck, P.L., Yu, D.T.Y., and Oldstone, M.B.A., 1987. Autoantibodies to HLA-B27 in the sera of HLA-27 patients with ankylosing spondylitis and Reiter's syndrome: Molecular mimicry with *Klebsiella pneumoniae* as potential mechanism of autoimmune disease. *J. Exp. Med.* **166**: 173–181.
- Schwimmbeck, P.L., Dyrberg, T., Drachman, D., and Oldstone, M.B. A., 1989. Molecular mimicry and myasthenia gravis: Uncovering a novel site of the acetylcholine receptor that has biologic

- activity and reacts immunochemically with herpes simplex virus. *J. Clin. Invest.* **84**: 1174–1180.
- Schmuñis, G.A., 1987, Autoimmunity in Chagas' disease. *Mem. Inst. Oswaldo Cruz* **82**: 288–310.
- Souto-Padrón, T., Almeida, I.C., De Souza, W., and Travassos, L.R., 1994, Distribution of α -galactosyl-containing epitopes on *Trypanosoma cruzi* trypomastigote and amastigote forms from infected Vero cells detected by chagasic antibodies. *J. Euk. Microbiol.* **41**: 47–54.
- Souza, M.C., Reis, A.P., Dias da Silva, W., and Brener, Z., 1974, Mechanism of acquired immunity induced by *Leptomonas pessoa*i against *Trypanosoma cruzi* in mice. *J. Protozool.* **21**: 579–584.
- Springer, G.F., and Horton, R.F., 1969, Blood group isoantibody stimulation in man by feeding blood group-active bacteria. *J. Clin. Invest.* **48**: 1280–1291.
- Stefani, M.M.A., Oliveira, E.B., Luquetti, A.O., and Dias Da Silva, W., 1987, Complement independent lysis of *Trypanosoma cruzi* Y strain by sera from acute phase chagasic patients. C-reactive protein and protein involvement. *Memorias do Instituto Oswaldo Cruz* **82** (Suppl): 140.
- Szarfman, A., Terranova, V.P., Rennard, S.I., Foidart, J.M., De Fatima Lima, M., Scheinman, J.I., and Martin, G.R., 1982, Antibodies to laminin in Chagas' disease. *J. Exp. Med.* **155**: 1161–1171.
- Takehara, H.A., Perini, A., Da Silva, M.H., and Mota, I., 1981, *Trypanosoma cruzi*: role of different antibody classes in protection against infection in the mouse. *Exp. Parasitol.* **52**: 137–146.
- Takeuchi, Y., Porter, C.D., Strahan, K.M., Preece, A.F., Gustafsson, K., Cosset, F-L., Weiss, R.A., and Collins, M.K.L., 1996, Sensitization of cells and retroviruses to human serum by (α -1-3)galactosyltransferase. *Nature* **379**: 85–88.
- Thall, A.D., Maly, P., and Lowe, J.B., 1995, Oocyte gal- α -1,3gal epitopes implicated in sperm adhesion to the zona pellucida glycoprotein ZP3 are not required for fertilization in the mouse. *J. Biol. Chem.* **270**: 21437–21440.
- Towbin, H., Rosenfelder, G., Wieslander, J., Avila, J.L., Rojas, M., Szarfman, K., Esser, K., Nowack, H., and Timpl, R., 1987, Circulating antibodies to mouse laminin in Chagas disease, American cutaneous leishmaniasis, and normal individuals recognize terminal galactosyl(α -1-3)galactose epitopes. *J. Exp. Med.* **166**: 419–432.
- Unterkircher, C., Avrameas, S., and Ternynck, T., 1993, Autoantibodies in the sera of *Trypanosoma cruzi*-infected individuals with or without clinical Chagas' disease. *J. Clin. Laborat. Anal.* **7**: 60–69.
- Van der Rijn, I., Zabriskie, J.B., and McCarty, M., 1977, Group A streptococcal antigens cross-reactive with myocardium: purification of heart-reactive antibody and isolation and characterization of the streptococcal antigen. *J. Exp. Med.* **146**: 579–599.
- Van Voorhis, W.C., Schleketwy, L., and Trong, H.L., 1991, Molecular mimicry by *Trypanosoma cruzi*: The Fl-160 epitope that mimics mammalian nerve can be mapped to a 12-amino acid peptide. *Proc. Natl. Acad. Sci. USA* **88**: 5993–5997.
- WHO, 1995, Twelfth Programme Report of the UNDP/World Bank/WHO Special Programme for research and training in tropical diseases. In WHO-Tropical Diseases Research, World Health Organization, Geneva, p. 125.
- Winter, G., Fuchs, M., McConville, M.J., Stierhof, Y-D., and Overath, P., 1994, Surface antigens of *Leishmania mexicana* amastigotes: characterization of glycoinositol phospholipids and a macrophage-derived glycosphingolipid. *J. Cell. Sci.* **107**: 2471–2482.
- Wolff, P.G., Kuhl, U., and Schultheiss, H-P., 1989, Laminin distribution and autoantibodies to laminin in dilated cardiomyopathy and myocarditis. *Am. Heart J.* **117**: 1303–1309.
- Wood, C., Kabat, E.A., Murphy, L.A., and Goldstein, I.J., 1979, Immunological studies on the combining sites of two isolectins A₄ and B₄ isolated from *Bandeiraea simplicifolia*. *Arch. Biochem. Biophys.* **198**: 1–8.
- Zamze, S.E., Ashford, D.A., Wooten, E.W., Rademacher, T.W., and Dwek, R.A., 1991, Structural characterization of the asparagine-linked oligosaccharides from *Trypanosoma brucei* type II and III variant surface glycoproteins. *J. Biol. Chem.* **266**: 20244–20261.

A new one-pot synthesis of α -Gal epitope derivatives involved in the hyperacute rejection response in xenotransplantation

Yuhang Wang, Qingyan Yan, Jingping Wu, Li-He Zhang and Xin-Shan Ye*

The State Key Laboratory of Natural and Biomimetic Drugs, School of Pharmaceutical Sciences, Peking University,
Xue Yuan Rd #38, Beijing 100083, China

Received 5 November 2004; revised 31 January 2005; accepted 3 February 2005

Available online 16 March 2005

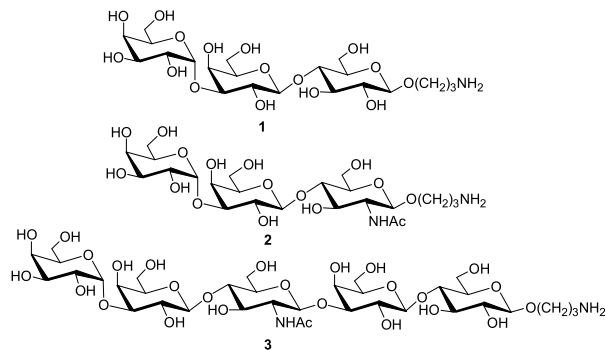
Abstract—Xenotransplantations from pig to human are rapidly rejected because of the interaction between α -Gal epitopes carried by the graft and natural antibodies (anti-Gal antibodies) present in the blood of the recipient. This paper describes a three-component one-pot synthesis of three α -Gal related oligosaccharides with minimal protecting group manipulations in a very short period of time.
© 2005 Elsevier Ltd. All rights reserved.

1. Introduction

Nowadays the major barrier to a successful pig-to-human xenotransplantation is antibody- and complement-dependent hyperacute rejection (HAR),¹ known to be due to the specific interaction of recipient xenoreactive antibodies with antigens present on the endothelium of the donor organ, followed by activation of the complement cascade.² It has been identified that trisaccharides Gal α 1-3Gal β 1-4Glc β -R and Gal α 1-3Gal β 1-4GlcNAc β -R and pentasaccharide Gal α 1-3Gal β 1-4GlcNAc β 1-3Gal β 1-4Glc β -R are the main α -Gal epitopes, which show high affinity with xenoreactive natural antibodies (XNAs) in human sera.³ In order to prevent the hyperacute rejection, elimination or reduction of the interaction between α -Gal and anti-Gal have been studied by various approaches including anti-Gal immunoabsorption and anti-Gal neutralization.⁴ Furthermore, α -Gal epitopes could be covalently attached to certain antiviral agents through appropriate linkers. The α -Gal-conjugated antiviral agents are envisaged to bind virus with α -Gal epitopes, resulting in the killing of the virus via antibody-mediated cytotoxicity and/or antibody-dependent, complement-mediated lysis of virus particles and virus-infected cells.⁵ Such approaches would require access to a substantial amount of α -Gal oligosaccharides and α -Gal analogues.

Several methods were reported for the synthesis of α -Gal epitope oligosaccharides. Wang et al. described a chemo-

enzymatic approach to synthesize various α -Gal derivatives including trisaccharide and pentasaccharide epitopes based on the use of recombinant α (1-3)-galactosyltransferase.⁶ Boons et al. reported a highly convergent synthesis of the methyl glycoside of the pentasaccharide.⁷ And a direct synthesis of ceramide pentasaccharide based on the trichloroacetimidate methodology was carried out by the Schmidt group.⁸ In the synthetic process of these oligosaccharides, the necessary regio- and stereocontrol often led to laborious synthetic transformations, tremendous protecting group manipulations, and tedious intermediate isolations which complicated the overall synthetic process and decreased synthetic efficiency. Herein we present a new method for the synthesis of two trisaccharides **1** and **2**, and a pentasaccharide **3** (Scheme 1) using a three-component one-pot strategy.⁹ The aminopropyl group was incorporated as a side chain for further derivation.¹⁰ We envisaged that the incorporation of the one-pot strategy with no intermediate work-up or purification may simplify this



Scheme 1. The structures of α -Gal oligosaccharide derivatives **1**, **2**, **3**.

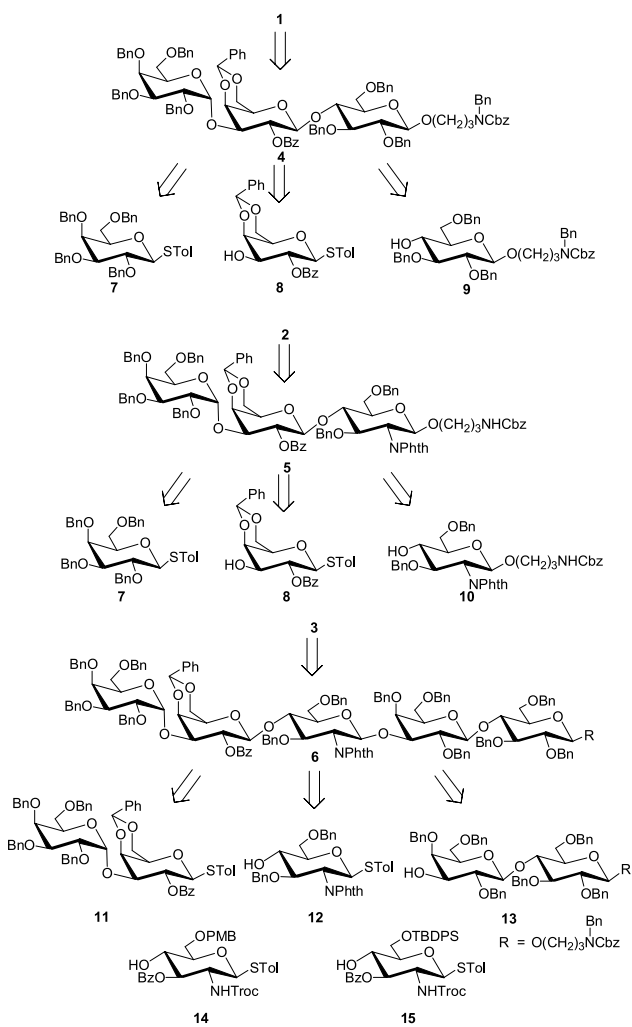
Keywords: α -Galactosyl epitopes; One-pot synthesis; Glycosylations; Oligosaccharides; Xenotransplantation.

* Corresponding author. Tel.: +86 108 2801570; fax: +86 10 62014949; e-mail: xinshan@bjmu.edu.cn

complicated synthetic operation and improve the synthetic efficiency.

2. Results and discussion

The initial design of building blocks and selection of protecting groups were the key step in our one-pot synthesis. The retrosynthetic analysis of α -Gal derivatives **1**, **2**, **3** is shown in Scheme 2. Fully protected trisaccharides **4** and **5** could both be divided into three units: a non-reducing end galactosyl, a hydroxy bridging galactosyl, and a side chain binding glucosyl or glucosaminyl unit. The fully protected pentasaccharide **6** was retrosynthetically disconnected into three saccharide building blocks: disaccharide building block **11**, glucosaminyl building block **12**, and lactosyl building block **13**. Implementation of one-pot oligosaccharide synthesis requires a descending order of reactivity for the three building blocks in each one-pot reaction. The non-reducing end unit should have the highest reactivity among the three components, and the reducing end component should have no reactivity due to its *O*-glycoside which cannot be activated by thioglycoside promoters. The selection of protecting groups was the main concern in



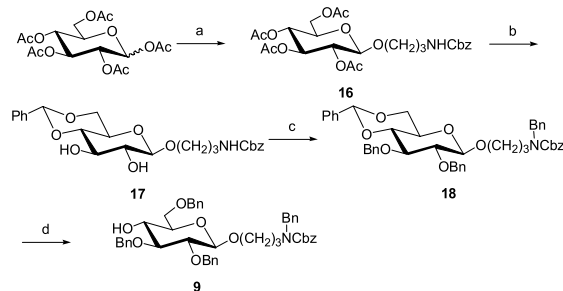
Scheme 2. The retrosynthetic analysis of one-pot synthesis of α -Gal derivative **1**, **2**, **3**.

the design of the in-between building blocks, because the presence of a free hydroxyl group and thiotoluene functionality would make it act as both a glycosyl acceptor and donor. Besides, their relative reactivities towards glycosylation should fall between non-reducing and reducing end component. To charge these building blocks with different reactivities, different protecting groups were used according to the reactivity order of thioglycosides based on the method which Wong group developed.^{9a,c} Thus four functional building blocks **7**, **8**, **9**, and **10** were designed and synthesized for one-pot glycosylation of the two trisaccharides **4** and **5**. As for the one-pot synthesis of pentasaccharide **6**, building blocks **11** and **13** were used as non-reducing and reducing end unit, respectively. We designed three building blocks **12**, **14** and **15** for the choice of the in-between component of **6**, and it was demonstrated that only **12** was suitable for the one-pot synthesis by experiments.

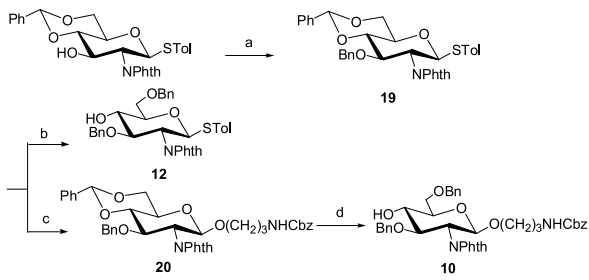
We chose thioglycosides as glycosyl donors due to the advantage that they are stable enough in most conditions and can be activated by a variety of promoters. In order to perform an efficient one-pot synthesis, we have tested several promoter systems, such as dimethyl(thiomethyl)sulfonium triflate (DMTST),¹¹ *N*-iodosuccinimide and triflic acid (NIS/TfOH),¹² phenylsulfonyl chloride and silver triflate (PhSCl/AgOTf),¹³ 1-benzenesulfonyl piperidine and triflic anhydride (BSP/Tf₂O).¹⁴ Eventually we found that NIS/TfOH was a suitable promoter for trisaccharide synthesis and BSP/Tf₂O was an efficient coupling agent for pentasaccharide synthesis.

2.1. Synthesis of building blocks

Building blocks **7** and **8** were prepared by literature procedures.^{9a} The synthesis of glucosyl acceptor **9** was performed as depicted in Scheme 3. The synthesis was started from glucose pentaacetate, which was converted to the β -glucoside **16** by the reaction with benzyl *N*-(3-hydroxypropyl)-carbamate in the presence of BF₃·Et₂O. Deacetylation of **16** followed by 4,6-*O*-benzylidene protection produced saccharide **17**. The benzylation of the two remaining hydroxyls of **17** was performed using sodium hydride and benzyl bromide in DMF to give compound **18**. Subsequent selectively reductive cleavage of 4,6-*O*-benzylidene acetal of **18** gave the 4-OH exposed saccharide **9** in 88% yield.



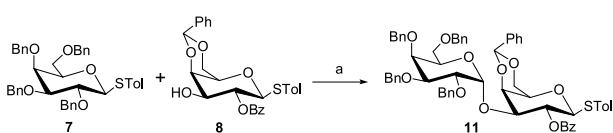
Scheme 3. (a) HO(CH₂)₃NHCbz, BF₃·Et₂O, CH₂Cl₂, rt, 41%; (b) (i) NaOMe/MeOH, rt; (ii) PhCH(OMe)₂, CSA, CH₃CN, rt, 66%; (c) BnBr/NaH/DMF, 0 °C to rt, 97%; (d) HCl-Et₂O/NaCNBH₃/THF, rt, 88%.



Scheme 4. (a) $\text{BnBr}/\text{NaH}/\text{DMF}$, 0°C to rt, 92%; (b) $\text{HCl}\cdot\text{Et}_2\text{O}/\text{NaCNBH}_3/\text{THF}$, rt, 90%. (c) $\text{HO}(\text{CH}_2)_3\text{NHCbz}/\text{NIS}/\text{TfOH}$, CH_2Cl_2 , 4 Å MS, 0°C , 49%; (d) $\text{HCl}\cdot\text{Et}_2\text{O}/\text{NaCNBH}_3/\text{THF}$, rt, 91%.

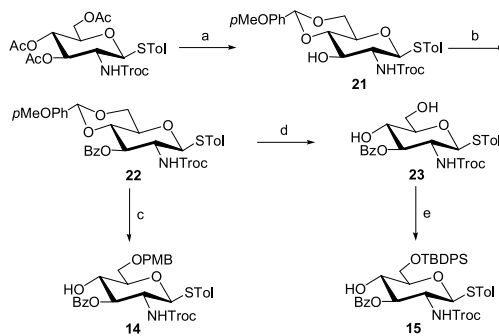
The synthesis of building blocks **10** and **12** was shown in Scheme 4. Benzylation of *p*-methylphenyl 4,6-*O*-benzylidene-2-deoxy-2-phthalimido-1-thio- β -D-glucopyranoside^{9a} gave saccharide **19** in 92% yield. Regioselective reductive ring-opening of 4,6-*O*-benzylidene acetal of **19** produced **12** in 90% isolated yield with the 4-hydroxyl group exposed.¹⁵ And the coupling reaction between compound **19** and benzyl *N*-(3-hydroxypropyl)-carbamate was promoted by NIS/TfOH, producing compound **20**, followed by the same regioselective ring-opening reaction to give building block **10** (91% yield).

Building block **11** was synthesized by glycosylation between perbenzylated galactosyl thioglycoside donor **7** and galactosyl acceptor **8** (Scheme 5). We chose the donor and acceptor according to their relative reactivity values (RRV) measured by the Wong group.^{9c} The large disparity of the reactivity between **7** and **8** (RRV of **7**= 5.2×10^4 , RRV of **8**=1791) enables the high sequence selectivity of glycosidic coupling reaction. Much attention was paid to the choice of the glycosylation conditions. At first, we used DMTST¹¹ and NIS/TfOH¹² as promoters, respectively. However, the use of DMTST required a harsh condition. The operation inconvenience limited its use in this glycosylation reaction. In the presence of NIS/TfOH (1.1 or 1.2 equiv), donor **7** was coupled with acceptor **8** to give the target disaccharide **11** in moderate yield (54%), attributed to the formation of byproducts. Two possible byproducts could have formed. One is the succinimide product,^{9a} the other is the hydrolyzed product due to the fact that the anomeric thiotoluene functionality of compound **11** could be further activated by the excessive NIS/TfOH and substituted by hydroxyl group after work-up with water. Finally, we turned our attention to BSP/Tf₂O,^{14b} developed by Crich and Smith,^{14a} in order to improve the efficiency of the glycosylation protocol. Utilizing BSP/Tf₂O as the promoter system, the coupling reaction of **7** and **8** proceeded smoothly, and the desired product was isolated in 90% yield.



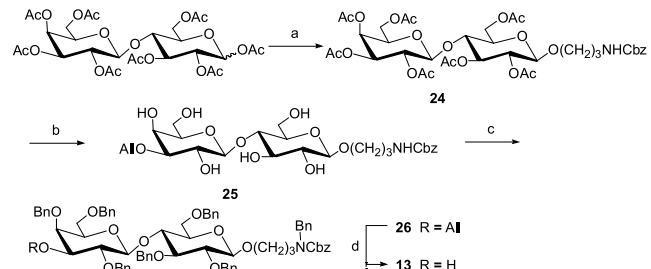
Scheme 5. (a) $\text{BSP}, \text{Tf}_2\text{O}, \text{CH}_2\text{Cl}_2$, 4 Å MS, -70°C to rt, 90% or $\text{NIS}, \text{TfOH}, \text{CH}_2\text{Cl}_2$, 4 Å MS, 0°C , 54%.

The preparation of building block **14** and **15** is summarized in Scheme 6. The synthesis was started from *p*-methylphenyl 3,4,6-tri-*O*-acetyl-2-(2,2,2-trichloroethoxylcarbonylamino)-1-thio- β -D-glucopyranoside,^{9a} which was deacetylated by using NaOMe/MeOH, followed by the *p*-methoxylbenzylidene formation between C₄/C₆ hydroxyls to produce compound **21**. The remaining C₃ hydroxyl of **21** was converted to a benzoyl ester, giving fully protected thioglycoside **22**. Subsequent selective cleavage of 4,6-*O*-methoxylbenzylidene acetal of **22** gave 6-*O*-methoxylbenzyl ether **14** in 80% yield. Compound **23** was produced by removal of the *p*-methoxylbenzylidene protecting group, followed by the selective protection of C₆ hydroxyl by *tert*-butyldiphenylsilyl (TBDPS) group, yielding building block **15** in 86% yield.



Scheme 6. (a) (i) NaOMe/MeOH , rt; (ii) $p\text{-CH}_3\text{OPhCH}(\text{OMe})_2$, CSA, CH_3CN , rt, 90%; (b) BzCl , pyridine, 0°C , 83%; (c) $\text{CF}_3\text{COOH}/\text{NaCNBH}_3/\text{DMF}$, 4 Å MS, rt to 40°C , 80%; (d) HOAc , rt, 91%; (e) TBDPSCI , imidazole, DMF, rt, 86%.

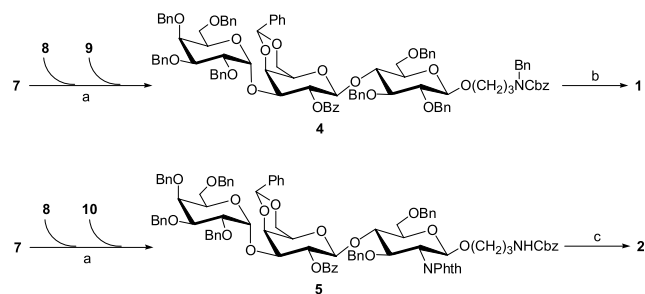
The synthesis of building block **13** began with lactose peracetate, which was converted to the β -lactoside **24** by reaction with benzyl *N*-(3-hydroxypropyl)-carbamate in the presence of $\text{BF}_3\cdot\text{Et}_2\text{O}$. Compound **24** was deacetylated by using NaOMe/MeOH, then treated with dibutyltin oxide, followed by the reaction with allyl bromide to provide selective 3'-*O*-allyl protected lactoside **25**. The following benzylation of the remaining hydroxyls of **25** was performed using sodium hydride and benzyl bromide in DMF to give compound **26**. And building block **13** was prepared by removal of the allyl protecting group of **26** using palladium (II) chloride (Scheme 7).¹⁵



Scheme 7. (a) $\text{HO}(\text{CH}_2)_3\text{NHCbz}$, $\text{BF}_3\cdot\text{Et}_2\text{O}$, CH_2Cl_2 , rt, 43%; (b) (i) NaOMe/MeOH , rt; (ii) $\text{MeOH}/\text{Bu}_2\text{SnO}$, 110°C ; then $\text{CH}_2=\text{CH}-\text{CH}_2\text{Br}$, Bu_4NI , C_6H_6 , 120°C , 4 Å MS; (c) $\text{BnBr}/\text{NaH}/\text{DMF}$, 0 °C, 70% from **24** to **26**; (d) PdCl_2 , MeOH , rt, 98%.

2.2. The one-pot synthesis of fully protected α -Gal derivatives 4, 5, 6 and the preparation of their deprotected products 1, 2, 3

With all building blocks in hand, we began to assemble the three target oligosaccharides using a two-step three-component one-pot coupling protocol. The synthesis of the two trisaccharides was depicted in Scheme 8. The more reactive building block **7** was first activated in the presence of NIS/TfOH at 0 °C to couple with the less reactive building block **8** and the reaction was monitored by TLC. After complete consumption of donor **7** the third building block **9** along with another molar equivalent of NIS was then added. The resulting trisaccharide **4** was obtained in 55% isolated yield. The synthesis of **5** was identical with that of **4** except that the final acceptor used was building block **10**. Trisaccharide **5** was obtained also in 55% isolated yield. The yield of the two trisaccharides is higher than that of the disaccharide **11** (54%). This is presumably because that the *O*-functionality in the reducing end of the trisaccharides is innate to the thioglycoside promoters, which cannot undergo the byproduct formation process as disaccharide **11** (*vide supra*). Complete deprotection of **4** was involved in two steps: the benzoyl group was removed by NaOMe/MeOH, and the benzyl, benzylidene, and benzyl carbamate protecting groups were cleaved by catalytic hydrogenolysis over 10% Pd-C to give trisaccharide **1** (in the form of acetate) in 70% isolated yield. Full deprotection of **5** was accomplished as follows:⁷ the phthalimido group was converted into an NHAc moiety by treatment with NH₂NH₂·H₂O followed by reacetylation with acetic anhydride in pyridine, the benzoyl group was removed by NaOMe/MeOH, the benzyl, benzylidene and benzyl carbamate protecting groups were removed with Pd-C catalyzed hydrogenolysis to afford trisaccharide **2** (in the form of acetate) in 70% isolated yield. The α , β anomeric configurations of the two trisaccharides were conformed by their ¹H and ¹³C NMR spectra referred to the structure of the pentasaccharide we reported recently.¹⁵

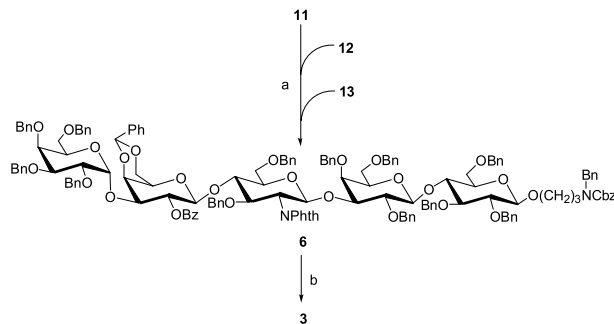


Scheme 8. (a) NIS, TfOH, CH₂Cl₂, 4 Å MS, 0 °C, 55% for **4**, 55% for **5**; (b) (i) NaOMe, MeOH; (ii) H₂, Pd-C, HOAc/THF/H₂O, 70%; (c) (i) NH₂NH₂·H₂O, EtOH, reflux; (ii) Ac₂O, pyridine; (iii) NaOMe, MeOH; (iv) H₂, Pd-C, HOAc/THF/H₂O, 70%.

For the one-pot synthesis of the pentasaccharide **3**, we have tried different building blocks and promoter systems, and finally we found most suitable ones. To carry out the glycosylation reaction, a variety of promoters (DMTST, NIS/TfOH, PhSCl/AgOTf, BSP/Tf₂O) were used. Nevertheless, when compound **14** or **15** was used as the second building block, we found that even the first glycosylation between **11** and **14** or **15** did not occur in the presence of any

of the promoter systems. This is possibly because of the steric hindrance of the bulky group TBDPS and the electron-withdrawing effect of Bz group which decreased the activity of the 4-OH, and also because the PMB ether is sensitive to acid while the coupling condition we used are all slightly acidic.

In view of the failure of glycosylation using *N*-Troc building blocks, we turned to *N*-Phth building block **12**. We protected the 3-OH and 6-OH with benzyl group, which we expected to improve the activity of the 4-OH. The promoters mentioned above were also tried in this one-pot synthesis and BSP/Tf₂O promoted the glycosylation most efficiently. For the BSP/Tf₂O promoted one-pot operation,^{14b} the donors must be activated at -70 °C and the reaction temperature was increased gradually to room temperature. The equivalent of BSP ranged from 0.5 to 1.0, and 0.5 equiv acted best. The first glycosylation between the disaccharide donor **11** and the glucosaminyl unit **12** was accomplished in 3 h to provide the trisaccharide which subsequently reacted with the lactose acceptor **13** in the second glycosylation, giving the fully protected pentasaccharide glycoside **6** (Scheme 9). The isolated yield of this BSP/Tf₂O promoted one-pot synthesis was 42%.



Scheme 9. (a) BSP, Tf₂O, CH₂Cl₂, 4 Å MS, -70 °C to rt 42%; (b) (i) NH₂NH₂·H₂O, EtOH, reflux; (ii) Ac₂O, pyridine; (iii) NaOMe, MeOH; (iv) H₂, Pd-C, HOAc/THF/H₂O, 43%.

Global deprotection of **6** was performed in four steps⁷ (Scheme 9). The phthalimido functionality was removed with NH₂NH₂·H₂O in EtOH under reflux to release the amino group and then was acetylated with acetic anhydride in pyridine. The remaining benzoylate was cleaved by the treatment with NaOMe in methanol. The benzyl, benzylidene, and benzyl carbamate functionalities were deprotected by Pd-C catalyzed hydrogenolysis. The target pentasaccharide **3** (in the form of acetate) was obtained in 43% isolated yield from **6**. The characterization of **3** and the correct anomeric configuration of each glycosidic linkage were confirmed by its 1D ¹H NMR, ¹³C NMR and 2D correlations spectroscopy (HSQC, HMBC, TOCSY), and HRMS analysis.¹⁵

3. Conclusion

In summary, we have successfully synthesized the amino-propyl glycosides of two trisaccharides and a pentasaccharide which play an important role in the interaction with human anti-Gal antibodies. The protected oligosaccharides

were rapidly and efficiently synthesized by a one-pot sequential glycosylation strategy. This one-pot strategy is expected to be powerful in efficient synthesis of other α -Gal derivatives and oligosaccharides.

4. Experimental

4.1. General method

All chemicals were purchased as reagent grade and used without further purification. Dichloromethane and acetonitrile were distilled over CaH_2 . Benzene was distilled over sodium/benzophenone. Methanol was distilled from magnesium. DMF was stirred with CaH_2 and distilled under reduced pressure. Reactions were monitored with analytical thin-layer chromatography on silica gel 60 F254 plates, detected under UV (254 nm) and by staining with acidic ceric ammonium molybdate. Column chromatography was performed on silica gel (200–300 mesh). ^1H NMR and ^{13}C NMR spectra were recorded on 300 MHz Varian VXR and 500 MHz Varian INOVA spectrometer. Chemical shift (in ppm) was determined relative to tetramethylsilane in deuterated chloroform ($\delta=0$ ppm). Coupling constant are given in Hz. Mass spectra were recorded using a PE SCLEX QSTAR spectrometer. And elemental analysis data were recorded on PE-2400C elemental analyzer.

4.1.1. (3-Benzyl-3-benzyloxycarbonylamino)propyl 2,3,4,6-tetra-O-acetyl- β -D-glucopyranoside (16). Glucose pentaacetate (7.0 g, 0.018 mol) and benzyl *N*-(3-hydroxypropyl)-carbamate (4.5 g, 0.022 mol) were stirred in dry CH_2Cl_2 (100 mL) and $\text{BF}_3 \cdot \text{Et}_2\text{O}$ (15.3 mL, 15.3 g, 0.108 mol) was added. The reaction mixture was stirred at room temperature for 8 h and then diluted with CH_2Cl_2 (100 mL), washed sequentially with satd aq NaHCO_3 and brine, dried (Na_2SO_4), filtered, and concentrated. The residue was purified by column chromatography on silica gel (petroleum ether/EtOAc = 1:1). The product (3.9 g, 41%) was obtained as a yellow syrup. ^1H NMR (300 MHz, CDCl_3) δ : 7.20–7.29 (m, 5H, aromatic), 5.15–5.20 (m, 1H), 5.10 (t, $J=9.6$ Hz, 1H), 4.91–5.02 (m, 3H), 4.87 (dd, $J=8.1, 9.3$ Hz, 1H), 4.40 (d, $J=7.8$ Hz, 1H), 4.14 (dd, $J=4.5, 12.3$ Hz, 1H), 4.03 (dd, $J=2.4, 12.0$ Hz, 1H), 3.80 (dt, $J=9.9, 5.4$ Hz, 1H), 3.56–3.60 (m, 1H), 3.48 (dt, $J=9.3, 4.4$ Hz, 1H), 3.0–3.24 (m, 2H), 1.97 (s, 3H, COCH_3), 1.94 (s, 3H, COCH_3), 1.92 (s, 3H, COCH_3), 1.89 (s, 3H, COCH_3), 1.67–1.70 (m, 2H, $\text{OCH}_2\text{CH}_2\text{CH}_2\text{N}$); ^{13}C NMR (75 MHz, CDCl_3) δ : 170.5 (COCH_3), 170.0 (COCH_3), 169.2 (COCH_3), 156.3 (NCOO), 136.4, 128.2, 127.8, 127.8 (aromatics), 100.4 (C-1), 72.5, 71.5, 71.0, 68.1, 67.3, 66.2, 61.6, 37.9 ($\text{OCH}_2\text{CH}_2\text{CH}_2\text{N}$), 29.2 ($\text{OCH}_2\text{CH}_2\text{CH}_2\text{N}$), 20.4 (COCH_3), 20.4 (COCH_3), 20.4 (COCH_3); FAB-MS ($M+\text{H}$) $^+$ 540. Anal. Calcd for $\text{C}_{25}\text{H}_{33}\text{O}_{12}\text{N}$: C, 55.65; H, 6.16; N, 2.60. Found: C, 55.80; H, 6.19; N, 2.30.

4.1.2. (3-Benzyl-3-benzyloxycarbonylamino)propyl 4,6-O-benzylidene- β -D-glucopyranoside (17). To a stirred solution of **16** (3.0 g, 5.51 mmol) in methanol (50 mL), NaOMe (0.2 mL, 30% in MeOH , 0.55 mmol) was added. The reaction mixture was stirred at room temperature for 5 h and then neutralized with cation exchange resin (H^+). The resin was filtered off and the filtrate was concentrated. The residue

was suspended in dry CH_3CN (60 mL). Benzaldehyde dimethyl acetal (1.0 mL, 1.0 g, 6.61 mmol) and (\pm)-10-camphorsulfonic acid (0.1 g, 0.44 mmol) were added to the mixture. The reaction mixture was stirred for 5 h, then neutralized with triethylamine. The solvent was removed under reduced pressure. The residue was purified by column chromatography on silica gel (petroleum ether/EtOAc = 1:1), yielding a white glassy solid (1.7 g, 66%). ^1H NMR (500 MHz, $\text{DMSO}-d_6$) δ : 7.24–7.45 (m, 10H, aromatic), 5.57 (s, 1H, benzylidene-CH), 5.29 (dd, $J=5.0, 13.5$ Hz, 1H), 5.01 (br.m, 2H), 4.32 (d, $J=8.0$ Hz, 1H), 4.17 (dd, $J=3.5, 10.0$ Hz, 1H), 3.73 (dt, $J=10.0, 5.0$ Hz, 1H), 3.66–3.70 (m, 1H), 3.49 (dt, $J=9.0, 4.5$ Hz, 1H), 3.16–3.20 (m, 6H), 3.09–3.06 (m, 2H), 1.70–1.65 (m, 2H, $\text{OCH}_2\text{CH}_2\text{CH}_2\text{N}$); ^{13}C NMR (125 MHz, $\text{DMSO}-d_6$) δ : 156.1 (NCOO), 137.8, 137.2, 128.8, 128.4, 128.0, 127.8, 126.3 (aromatics), 103.4, 100.6, 80.6, 74.3, 72.8, 68.0, 66.8, 65.8, 65.2, 37.5 ($\text{OCH}_2\text{CH}_2\text{CH}_2\text{N}$), 29.6 ($\text{OCH}_2\text{CH}_2\text{CH}_2\text{N}$); FAB-MS ($M+\text{H}$) $^+$ 460. Anal. Calcd for $\text{C}_{24}\text{H}_{29}\text{O}_8\text{N}$: C, 62.73; H, 6.36; N, 3.05. Found: C, 62.55; H, 6.38; N, 2.83.

4.1.3. (3-Benzyl-3-benzyloxycarbonylamino)propyl 2,3-di-O-benzyl-4,6-O-benzylidene- β -D-glucopyranoside (18). Compound **17** (1.6 g, 3.53 mmol) and sodium hydride (0.36 mg, 14.12 mmol) were stirred in DMF (30 mL) at 0 °C for 10 min and benzyl bromide (1.7 mL, 2.4 g, 14.12 mmol) was added. The mixture was stirred at room temperature overnight and then poured into ice water (30 mL), which was extracted with EtOAc (3 × 30 mL), then dried (Na_2SO_4). The organic phase was concentrated for column chromatography on silica gel (petroleum ether/EtOAc = 4:1). Compound **18** (2.5 g, 97%) was obtained as a yellow syrup. ^1H NMR (500 MHz, $\text{DMSO}-d_6$) δ : 7.21–7.43 (m, 25H, aromatic), 5.66 (s, 1H, benzylidene-CH), 5.10 (br.s, 2H), 4.45–4.78 (m, 7H), 4.20 (m, 1H), 4.10 (q, $J=5.0$ Hz, 1H), 3.68–3.76 (m, 4H), 3.38–3.54 (m, 2H), 3.28 (m, 2H), 1.76 (m, 2H, $\text{OCH}_2\text{CH}_2\text{CH}_2\text{N}$); ^{13}C NMR (125 MHz, $\text{DMSO}-d_6$) δ : 155.8 (NCOO), 138.7, 138.4, 138.1, 137.6, 136.9, 128.7, 128.5, 128.4, 128.0, 127.8, 127.5, 127.4, 127.4, 127.3, 127.1, 127.0, 125.9 (aromatics), 102.9, 100.0, 81.6, 80.5, 80.1, 74.0, 73.7, 67.8, 67.0, 66.9, 66.4, 65.2, 50.0, 28.4 ($\text{OCH}_2\text{CH}_2\text{CH}_2\text{N}$); FAB-MS ($M+\text{H}$) $^+$ 730. Anal. Calcd for $\text{C}_{45}\text{H}_{47}\text{O}_8\text{N}$: C, 74.05; H, 6.49; N, 1.92. Found: C, 73.91; H, 6.49; N, 1.76.

4.1.4. (3-Benzyl-3-benzyloxycarbonylamino)propyl 2,3,6-tri-O-benzyl- β -D-glucopyranoside (9). To a mixture of compound **18** (2.4 g, 3.29 mmol), NaCNBH_3 (2.7 g, 0.041 mol), and 3 Å MS (2.5 g) in dry THF (50 mL), was added dropwise a solution of $\text{HCl-Et}_2\text{O}$ (66 mL, 1 M in Et_2O , 65.8 mmol) under N_2 at room temperature. The mixture was stirred for 10 min, then filtered off through Celite. The filtrate was washed sequentially with satd aq NaHCO_3 and brine, dried (Na_2SO_4), filtered, and concentrated. The residue was purified by column chromatography on silica gel (petroleum ether/EtOAc = 3:1). The product (2.1 g, 88%) was obtained as a yellow syrup. ^1H NMR (300 MHz, $\text{DMSO}-d_6$) δ : 7.23–7.32 (m, 25H, aromatic), 5.40 (d, $J=6.0$ Hz, 1H, H-1), 5.09 (br.s, 2H), 4.36–4.82 (m, 10H), 4.07–4.12 (m, 2H), 3.71–3.75 (m, 2H), 3.29–3.55 (m, 4H), 1.70–1.80 (m, 2H, $\text{OCH}_2\text{CH}_2\text{CH}_2\text{N}$); ^{13}C NMR (75 MHz, CDCl_3) δ : 156.6 (NCOO), 138.5, 138.3, 137.8, 137.7, 136.6, 129.6, 128.9, 128.5, 128.4, 128.3,

128.2, 127.9, 127.8, 127.8, 127.7, 127.6, 127.6, 127.2 (aromatics), 103.4 (C-1), 83.9, 81.6, 76.2, 75.2, 74.6, 74.0, 73.5, 71.4, 70.1, 67.1, 58.2, 50.6, 28.6 ($\text{OCH}_2\text{CH}_2\text{CH}_2\text{N}$); FAB-MS ($\text{M}+\text{H}$)⁺ 732. Anal. Calcd for $\text{C}_{45}\text{H}_{49}\text{O}_8\text{N}$: C, 73.85; H, 6.75; N, 1.91. Found: C, 74.12; H, 6.87; N, 1.72.

4.1.5. (3-Benzylloxycarbonylamino)propyl 3-O-benzyl-4,6-O-benzylidene-2-deoxy-2-phthalimido- β -D-glucopyranoside (20). To a mixture of compound **19**¹⁵ (100 mg, 0.17 mmol), benzyl *N*-(3-hydroxypropyl)-carbamate (48.6 mg, 0.22 mmol), and 4 Å MS (2.5 g) in dry CH_2Cl_2 (10 mL), were added NIS (39.5 mg, 0.18 mmol) and TfOH (69 μL , 0.5 M in Et_2O , 0.034 mmol) under N_2 at 0 °C. After stirred for 2 h, the mixture was neutralized with triethylamine, then filtered off through Celite. The filtrate was washed sequentially with satd aq NaHCO_3 and brine, dried (Na_2SO_4), filtered, and concentrated. The residue was purified by column chromatography on silica gel (petroleum ether/ EtOAc = 1:1). The product (56 mg, 49%) was obtained as a yellow solid. ¹H NMR (500 MHz, $\text{DMSO}-d_6$) δ : 7.71–7.92 (m, 4H, aromatic), 7.49 (d, J = 6.5 Hz, 2H, aromatic), 7.26–7.49 (m, 7H, aromatic), 7.07 (t, J = 5.0 Hz, 1H, aromatic), 6.97 (t, J = 7.0 Hz, 1H, aromatic), 6.87–6.92 (m, 4H, aromatic), 5.77 (s, 1H, benzylidene-CH), 5.14 (d, J = 8.5 Hz, 1H, H-1), 4.85 (br.s, 2H), 4.70 (d, J = 12.0 Hz, 1H), 4.40 (d, J = 12.5 Hz, 1H), 4.28–4.32 (m, 2H), 3.99 (dd, J = 8.5, 10.5 Hz, 1H), 3.98 (t, J = 9.5 Hz, 1H), 3.85 (t, J = 10.0 Hz, 1H), 3.67 (t, J = 10.0 Hz, 1H), 3.58 (dt, J = 4.5, 9.0 Hz, 1H), 3.34–3.42 (m, 2H), 3.12–3.20 (m, 1H), 2.76–2.80 (m, 2H), 1.40–1.49 (m, 2H); ¹³C NMR (125 MHz, $\text{DMSO}-d_6$) δ : 167.4 (Phth-CON), 155.9 (NCOO), 137.8, 137.6, 137.2, 134.7, 130.7, 128.9, 128.3, 128.2, 127.9, 127.7, 127.5, 127.4, 126.0, 123.4, 100.2, 98.3, 81.9, 74.6, 73.1, 67.8, 66.7, 65.7, 65.0, 55.4, 36.8, 29.4; FAB-MS ($\text{M}+\text{H}$)⁺ 679. Anal. Calcd for $\text{C}_{39}\text{H}_{38}\text{O}_9\text{N}_2$: C, 69.01; H, 5.64; N, 4.13. Found: C, 68.95; H, 5.64; N, 3.92.

4.1.6. (3-Benzylloxycarbonylamino)propyl 3,6-di-O-benzyl-2-deoxy-2-phthalimido- β -D-glucopyranoside (10). To a mixture of compound **20** (0.44 g, 0.66 mmol), NaCNBH_3 (0.55 g, 8.25 mmol), and 3 Å MS (2.5 g) in dry THF (50 mL), was added dropwise a solution of HCl – Et_2O (13.2 mL, 1 M in Et_2O 13.2 mmol) under N_2 at room temperature. The mixture was stirred for 30 min, then filtered off through Celite. The filtrate was washed sequentially with satd aq NaHCO_3 and brine, dried (Na_2SO_4), filtered, and concentrated. The residue was purified by column chromatography on silica gel (petroleum ether/ EtOAc = 3:1). The product (0.4 g, 91%) was obtained as a yellow syrup. ¹H NMR (300 MHz, $\text{DMSO}-d_6$) δ : 7.73–7.85 (m, 4H, aromatic), 7.28–7.37 (m, 9H, aromatic), 7.07 (t, J = 5.7 Hz, 1H, aromatic), 6.86–6.94 (m, 5H, aromatic), 5.65 (d, J = 6.6 Hz, 1H), 5.03 (d, J = 11.4 Hz, 1H), 4.89 (br.s, 2H), 4.76 (d, J = 12.0 Hz, 1H), 4.57 (br.s, 2H), 4.41 (d, J = 12.3 Hz, 1H), 4.02–4.14 (m, 2H), 3.35–3.86 (m, 7H), 2.81 (q, J = 6.3 Hz, 2H), 1.41–1.53 (m, 2H, $\text{OCH}_2\text{CH}_2\text{CH}_2\text{N}$); ¹³C NMR (75 MHz, $\text{DMSO}-d_6$) δ : 167.6 (Phth-CON), 167.4 (Phth-CON), 155.9 (NCOO), 138.6, 138.3, 137.2, 134.6, 130.8, 128.3, 128.2, 127.8, 127.7, 127.4, 127.3, 127.1, 123.2 (aromatics), 97.6 (C-1), 78.6, 75.7, 73.5, 72.3, 71.6, 69.1, 66.4, 65.0, 55.2, 37.0 ($\text{OCH}_2\text{CH}_2\text{CH}_2\text{N}$), 29.4 ($\text{OCH}_2\text{CH}_2\text{CH}_2\text{N}$); FAB-MS

($\text{M}+\text{H}$)⁺ 681. Anal. Calcd for $\text{C}_{39}\text{H}_{40}\text{O}_9\text{N}_2$: C, 68.81; H, 5.92; N, 4.12. Found: C, 68.80; H, 6.11; N, 3.76.

4.1.7. p-Methylphenyl 2-O-benzoyl-3-O-(2,3,4,6-tetra-O-benzyl- α -D-galactopyranosyl)-4,6-O-benzylidene-1-thio- β -D-galactopyranoside (11). Donor **7**^{9a} (44.6 mg, 0.069 mmol), BSP (12 mg, 0.063 mmol), and 4 Å MS (200 mg) were stirred in dry CH_2Cl_2 (2 mL) at room temperature for 0.5 h under N_2 . The mixture was cooled to –70 °C, followed by the addition of Tf_2O (11.9 μL , 19.5 mg, 0.069 mmol). After 10 min, a solution of acceptor **8**^{9a} (30 mg, 0.063 mmol) in dry CH_2Cl_2 (2 mL) was added to the reaction mixture, and the temperature was increased gradually to room temperature. After 2 h, the reaction was quenched with triethylamine (2 mL) and diluted with CH_2Cl_2 (10 mL). The reaction mixture was filtered and washed sequentially with satd aq NaHCO_3 and brine, dried (Na_2SO_4), filtered, and concentrated. The residue was purified by column chromatography on silica gel (petroleum ether/ EtOAc = 3:1). The product (56 mg, 90%) was obtained as a yellow syrup. ¹H NMR (500 MHz, CDCl_3) δ : 7.96 (d, J = 8.0 Hz, 2H, aromatic), 7.41–7.45 (m, 3H, aromatic), 7.34 (d, J = 7.5 Hz, 2H, aromatic), 7.02–7.27 (m, 23H, aromatic), 6.89 (d, J = 8.0 Hz, 2H, aromatic), 6.97 (d, J = 8.0 Hz, 2H, aromatic), 5.49 (t, J = 9.5 Hz, 1H, H-2), 5.32 (s, 1H, benzylidene-CH), 4.98 (d, J = 3.0 Hz, 1H, H-1'), 4.70 (d, J = 11.8 Hz, 1H), 4.65 (d, J = 9.5 Hz, 1H), 4.55 (d, J = 12.0 Hz, 1H), 4.49 (d, J = 11.5 Hz, 1H), 4.39 (d, J = 11.5 Hz, 1H), 4.35 (d, J = 12.0 Hz, 1H), 4.24–4.31 (m, 4H), 4.18 (d, J = 12.0 Hz, 1H), 3.84–3.94 (m, 3H), 3.74 (t, J = 6.0 Hz, 1H), 3.55 (d, J = 10.0 Hz, 1H), 3.34 (d, J = 13.0 Hz, 2H), 3.05–3.20 (m, 2H), 2.26 (s, 3H, SPhCH_3); ¹³C NMR (125 MHz, CDCl_3) δ : 164.6 (CO), 138.8, 138.7, 138.5, 138.3, 138.1, 137.7, 134.2, 132.9, 130.1, 129.8, 129.5, 128.9, 128.3, 128.2, 128.1, 128.1, 128.0, 127.8, 127.7, 127.6, 127.5, 127.4, 127.3, 127.2, 126.6 (aromatics), 101.0, 94.6, 85.4, 78.6, 75.8, 75.5, 74.9, 74.6, 74.2, 73.1, 72.2, 71.8, 69.9, 69.8, 69.3, 69.0, 68.7, 21.2 (SPhCH_3); TOF-MS ($\text{M}+\text{NH}_4$)⁺ 1018. Anal. Calcd for $\text{C}_{61}\text{H}_{60}\text{O}_{11}\text{S}$: C, 73.17; H, 6.04. Found: C, 72.84; H, 6.17.

4.1.8. p-Methylphenyl 4,6-O-p-methoxybenzylidene-2-deoxy-2-(2,2,2-trichloroethoxylcarbonyl-amino)-1-thio- β -D-glucopyranoside (21). To a stirred solution of *p*-methylphenyl 3,4,6-tri-O-acetyl-2-deoxy-2-(2,2,2-trichloroethoxylcarbonylamino)-1-thio- β -D-glucopyranoside^{9a} (1.100 g, 1.9 mmol) in methanol (40 mL), NaOMe (13 μL , 30% in MeOH, 0.37 mmol) was added. The reaction mixture was stirred at room temperature for 6 h and then neutralized with cation exchange resin (H^+). The resin was filtered off and the filtrate was concentrated. The residue (white solid) was suspended in dry CH_3CN (40 mL). *p*-Methoxybenzaldehyde dimethyl acetal (0.63 mL, 685 mg, 3.74 mmol) and (±)-10-camphorsulfonic acid (87 mg, 0.374 mmol) were added to the mixture. The reaction mixture was stirred for 5 h then neutralized with triethylamine. The solvent was removed by rotaevaporator. The residue was purified by column chromatography on silica gel (petroleum ether/ EtOAc = 1:2), yielding a white glassy solid (0.95 g, 90%). ¹H NMR (300 MHz, CDCl_3) δ : 7.37–7.40 (m, 4H, aromatic), 7.14 (d, J = 8.1 Hz, 2H, aromatic), 6.87 (d, J = 8.7 Hz, 2H, aromatic), 5.48 (s, 1H, *p*-methoxybenzylidene-CH), 5.28 (d, J = 6.0 Hz, 1H),

4.84 (d, $J=10.5$ Hz, 1H), 4.82 (d, $J=12.0$ Hz, 1H), 4.70 (d, $J=12.0$ Hz, 1H), 4.34 (dd, $J=4.2$, 10.2 Hz, 1H), 3.90–4.05 (m, 1H), 3.78 (s, 3H), 3.71–3.75 (m, 1H), 3.39–3.48 (m, 2H), 2.97 (br.s, 1H), 2.34 (s, 3H, SPhCH₃), 2.01 (d, $J=3.0$ Hz, 1H); ¹³C NMR (75 MHz, CDCl₃) δ : 160.3, 154.3, 138.7, 134.0, 133.5, 130.2, 129.9, 129.4, 127.7, 127.4, 113.8, 101.8, 86.7, 81.1, 74.7, 72.3, 70.3, 68.5, 55.3, 21.2; MALDI-TOF-MS (M+H)⁺ 578.

4.1.9. *p*-Methylphenyl 3-O-benzoyl-4,6-O-p-methoxybenzylidene-2-deoxy-2-(2,2,2-trichloroethoxylcarbonylamino)-1-thio-β-D-glucopyranoside (22). Compound **21** (1.03 g, 1.8 mmol) in pyridine (30.0 mL) was stirred at 0 °C and benzoyl chloride (1.0 mL, 1.00 g, 7.1 mmol) was added. After 5 h, pyridine was evaporated in vacuum and the residue was dissolved in CH₂Cl₂. The resulting pyridinium salt was filtered off, and the filtrate was concentrated. The residue was recrystallized with petroleum ether/EtOAc (1:2) to give a yellow crystal (1.02 g, 83%). ¹H NMR (300 MHz, CDCl₃) δ : 8.02 (d, $J=7.2$ Hz, 2H, aromatic), 7.54 (t, $J=7.5$ Hz, 1H, aromatic), 7.37–7.46 (m, 4H, aromatic), 7.27 (d, $J=8.7$ Hz, 2H, aromatic), 7.09 (d, $J=7.8$ Hz, 2H, aromatic), 6.73 (d, $J=9.0$ Hz, 2H, aromatic), 5.90 (d, $J=9.9$ Hz, 1H), 5.66 (t, $J=9.6$ Hz, 1H), 5.45 (s, 1H, p-methoxybenzylidene-CH), 4.80 (d, $J=10.5$ Hz, 1H), 4.58–4.71 (ABq, $J=12.3$ Hz, 2H), 4.23 (dd, $J=4.8$, 10.2 Hz, 1H), 4.05 (q, $J=10.2$ Hz, 1H), 3.80 (q, $J=9.3$ Hz, 2H), 3.72 (s, 3H), 3.60–3.65 (m, 1H), 2.32 (s, 3H, SPhCH₃); ¹³C NMR (75 MHz, CDCl₃) δ : 166.7, 160.0, 154.4, 138.4, 133.5, 133.3, 130.2, 130.0, 129.8, 129.3, 129.1, 128.5, 128.4, 127.3, 113.5, 101.2, 95.3, 88.4, 78.6, 74.4, 73.4, 70.7, 68.4, 55.2, 21.2; MALDI-TOF-MS (M+H)⁺ 682. Anal. Calcd for C₃₁H₃₀Cl₃NO₈S: C, 54.52; H, 4.43; N, 2.05. Found: C, 54.53; H, 4.52; N, 1.92.

4.1.10. *p*-Methylphenyl 3-O-benzoyl-6-O-p-methoxybenzyl-2-deoxy-2-(2,2,2-trichloroethoxyl carbonylamino)-1-thio-β-D-glucopyranoside (14). Compound **22** (0.70 g, 1.0 mmol), NaCNBH₃ (0.34 g, 5.2 mmol), and 4 Å MS (1.25 g) were stirred in dry DMF (10.0 mL) at room temperature for 0.5 h under N₂. Then the reaction mixture was cooled to 0 °C, a solution of trifluoroacetic acid (0.77 mL, 1.17 g, 10.3 mmol) in dry DMF (7.0 mL) was added dropwise. The reaction temperature was increased to room temperature in 1.5 h. After another 11 h of stirring, the reaction mixture was filtered and the filtrate was diluted with H₂O (100 mL), extracted with EtOAc (3×50 mL), then dried (Na₂SO₄). The organic phase was concentrated for column chromatography on silica gel (petroleum ether/EtOAc=2:1). Compound **14** (0.57 g, 80%) was obtained as a white solid. ¹H NMR (300 MHz, DMSO-d₆) δ : 8.03 (d, $J=9.6$ Hz, 1H, aromatic), 7.90 (d, $J=7.2$ Hz, 2H, aromatic), 7.63 (t, $J=7.2$ Hz, 1H, aromatic), 7.49 (t, $J=7.8$ Hz, 2H, aromatic), 7.36 (d, $J=8.1$ Hz, 2H, aromatic), 7.24 (d, $J=8.4$ Hz, 2H, aromatic), 7.07 (d, $J=8.4$ Hz, 2H, aromatic), 6.90 (d, $J=8.7$ Hz, 2H, aromatic), 5.61 (d, $J=5.4$ Hz, 1H), 5.20 (t, $J=9.3$ Hz, 1H), 4.91 (d, $J=10.5$ Hz, 1H), 4.80 (d, $J=12.6$ Hz, 1H), 4.58 (d, $J=12.9$ Hz, 1H), 4.35–4.47 (m, 2H), 3.26–3.70 (m, 8H), 2.26 (s, 3H, SPhCH₃); ¹³C NMR (75 MHz, DMSO-d₆) δ : 165.2, 158.7, 154.1, 136.8, 133.2, 131.2, 130.5, 129.8, 129.7, 129.6, 129.4, 129.1, 128.5, 113.6, 96.0, 85.4, 79.4, 77.4, 73.1, 72.0, 69.0, 68.1, 55.0, 54.7, 20.6; MALDI-TOF-MS (M+NH₄)⁺ 701. Anal. Calcd

for C₃₁H₃₂Cl₃NO₈S: C, 54.36; H, 4.71; N, 2.04. Found: C, 54.27; H, 4.82; N, 2.00.

4.1.11. *p*-Methylphenyl 3-O-benzoyl-2-deoxy-2-(2,2,2-trichloroethoxyl carbonylamino)-1-thio-β-D-glucopyranoside (23). Compound **22** (40.8 mg, 0.06 mmol) was stirred in acetic acid (80%, 2.0 mL) at room temperature overnight. After removal of the solvent, the residue was purified by column chromatography on silica gel (petroleum ether/EtOAc=1:1), yielding a colorless solid (29.7 mg, 91%). ¹H NMR (300 MHz, CDCl₃) δ : 7.95 (d, $J=7.2$ Hz, 2H, aromatic), 7.53 (t, $J=7.5$ Hz, 1H, aromatic), 7.33–7.38 (m, 4H, aromatic), 7.08 (d, $J=7.2$ Hz, 2H, aromatic), 5.61 (d, $J=9.3$ Hz, 1H), 5.34 (t, $J=9.3$ Hz, 1H), 4.79 (d, $J=10.5$ Hz, 1H), 4.69 (d, $J=12.0$ Hz, 1H), 4.53 (d, $J=12.3$ Hz, 1H), 3.53–3.96 (m, 4H), 3.49–3.52 (m, 1H), 2.67 (br, 2H), 2.31 (s, 3H, SPhCH₃); ¹³C NMR (75 MHz, CDCl₃) δ : 167.4, 154.3, 138.4, 133.7, 132.9, 130.0, 129.8, 128.9, 128.5, 95.3, 87.2, 79.4, 74.3, 69.3, 62.3, 55.0, 21.2.

4.1.12. *p*-Methylphenyl 3-O-benzoyl-6-O-tert-butylidiphenylsilyl-2-deoxy-2-(2,2,2-trichloroethoxyl carbonylamino)-1-thio-β-D-glucopyranoside (15). To a solution of **23** (1.60 g, 2.9 mmol) in DMF (10.0 mL), *tert*-butyldiphenylsilyl chloride (1.5 mL, 1.60 g, 5.7 mmol) and imidazole (0.50 g, 7.2 mmol) were added. The mixture was stirred overnight. After removal of the solvent, the residue was purified by column chromatography on silica gel (petroleum ether/EtOAc=3:1), yielding a yellow solid (1.90 g, 86%). ¹H NMR (300 MHz, CDCl₃) δ : 8.00 (d, $J=7.2$ Hz, 2H, aromatic) 7.66–7.71 (m, 4H, aromatic), 7.54 (t, $J=7.2$ Hz, 1H, aromatic), 7.24–7.42 (m, 10H, aromatic), 7.03 (d, $J=8.1$ Hz, 2H, aromatic), 5.32 (t, $J=9.0$ Hz, 2H), 4.73 (d, $J=10.5$ Hz, 1H), 4.71 (d, $J=12.0$ Hz, 1H), 4.53 (d, $J=12.3$ Hz, 1H), 3.83–3.97 (m, 5H), 3.51–3.56 (m, 1H), 2.30 (s, 3H, SPhCH₃), 1.05 (s, 9H, C(CH₃)₃); ¹³C NMR (75 MHz, CDCl₃) δ : 167.3, 154.1, 138.2, 135.7, 135.6, 133.6, 133.0, 132.8, 132.7, 130.1, 129.9, 129.7, 129.1, 128.4, 95.3, 87.3, 79.3, 74.4, 70.5, 64.3, 54.8, 26.8, 21.2, 19.2; MALDI-TOF-MS (M+H)⁺ 802.

4.1.13. (3-Benzyl-3-benzyloxycarbonylamino)propyl 2,3,6-tri-O-benzyl-4-O-[2-O-benzoyl-3-O-(2,3,4,6-tetra-O-benzyl-α-D-galactopyranosyl)-4,6-O-benzylidene-β-D-galactopyranosyl]-β-D-glucopyranoside (4). Building block **7** (0.16 g, 0.25 mmol), building block **8** (0.10 g, 0.21 mmol), and 4 Å MS (0.50 g) were stirred in dry CH₂Cl₂ (10.0 mL) at 0 °C under N₂, which was followed by the addition of NIS (0.13 g, 0.25 mmol) and TfOH (42 μ L, 0.5 M in Et₂O, 0.015 mmol). After stirred for 0.5 h, TLC (petroleum ether/acetone=3:2) showed complete consumption of building block **8**. Then building block **9** (0.23 g, 0.31 mmol), NIS (0.13 g, 0.25 mmol), and TfOH (42 μ L, 0.5 M in Et₂O, 0.015 mmol) were added to the reaction mixture. The reaction mixture was stirred for 3 h and quenched with triethylamine, then filtered off through Celite. The filtrate was washed sequentially with satd aq NaHCO₃ and brine, dried (Na₂SO₄), filtered, and concentrated. The residue was purified by column chromatography on silica gel (petroleum ether/acetone=4:1). The product (175 mg, 55%) was obtained as a yellow solid. ¹H NMR (500 MHz, DMSO-d₆) δ : 7.94 (d, $J=7.5$ Hz, 2H, aromatic), 7.61 (t, $J=7.5$ Hz, 1H, aromatic), 7.10–7.41 (m, 52H,

aromatic), 5.54 (s, 1H, benzylidene-CH), 5.34 (dd, $J=8.5$, 10.0 Hz, 1H), 5.29 (d, $J=3.0$ Hz, 1H, H-1''), 5.06 (br.s, 3H), 4.82 (d, $J=7.5$ Hz, 1H), 4.18–4.72 (m, 17H), 3.93–4.03 (m, 3H), 3.72–3.79 (m, 4H), 3.40–3.50 (m, 6H), 3.16–3.28 (m, 7H), 1.66–1.82 (m, 2H, OCH₂CH₂CH₂N); ¹³C NMR (125 MHz, DMSO-*d*₆) δ : 164.5, 139.1, 138.6, 138.5, 138.2, 138.1, 136.9, 133.6, 129.4, 129.0, 128.7, 128.4, 128.3, 128.23, 128.17, 128.1, 128.0, 127.8, 127.7, 127.5, 127.4, 127.3, 127.2, 127.1, 127.0, 126.2, 102.0, 100.3, 99.8, 93.1, 82.1, 81.2, 77.7, 77.2, 75.1, 74.4, 74.2, 74.0, 73.6, 73.4, 73.3, 72.4, 72.1, 71.9, 71.1, 70.7, 68.9, 68.2, 68.1, 66.3, 66.2, 49.9, 43.6, 39.0, 29.0; MALDI-TOF-MS (M+Na)⁺ 1630, (M+K)⁺ 1646. Anal. Calcd for C₉₉H₁₀₁O₁₉N: C, 73.90; H, 6.33; N, 0.87. Found: C, 73.66; H, 6.53; N, 0.56.

4.1.14. 3-Aminopropyl 4-*O*-[3-*O*-(α -D-galactopyranosyl)- β -D-galactopyranosyl]- β -D-glucopyranoside (1). Compound **4** (60.0 mg, 0.037 mmol) was dissolved in methanol (5.0 mL), and to this NaOMe (30% in MeOH, 10 μ L) was added. The mixture was stirred for 6 h and then neutralized with cation exchange resin (H⁺). The resin was filtered off and the filtrate was evaporated in vacuum. The residue was purified by silica gel column chromatography (petroleum ether/acetone = 4:1). A mixture of the purified residue, 10% Pd-C (15.0 mg) in HOAc (4 mL), THF (2 mL), H₂O (1 mL) was stirred under H₂ atmosphere for 24 h. The catalyst was then removed by filtration and the filtrate was concentrated. The residue was subjected to a C-18 reverse phase column chromatography (H₂O) to give **1** (14.6 mg, 70%) as a white solid after lyophilization. ¹H NMR (500 MHz, D₂O) δ : 5.13 (d, $J=3.5$ Hz, 1H, H-1''), 4.51 (d, $J=8.0$ Hz, 1H), 4.50 (d, $J=8.0$ Hz, 1H), 4.16–4.20 (m, 2H), 3.90–4.10 (m, 4H), 3.69–3.89 (m, 8H), 3.55–3.69 (m, 4H), 3.15 (t, $J=7.0$ Hz, 2H, OCH₂CH₂CH₂N), 1.98–2.05 (m, 2H, OCH₂CH₂CH₂N); ¹³C NMR (125 MHz, D₂O) δ : 182.1, 103.6, 102.8, 96.2 (C-1''), 79.4, 77.9, 75.8, 75.5, 75.2, 73.5, 71.6, 70.3, 70.0, 69.9, 68.9, 68.6, 65.5, 61.7, 61.6, 60.8, 38.3 (OCH₂CH₂CH₂N), 27.4 (OCH₂CH₂CH₂N), 23.9; HRMS (M+Na) calcd for C₂₁H₃₉O₁₆NNa 584.2167, found 584.2168.

4.1.15. (3-Benzylloxycarbonylamino)propyl 3,6-di-*O*-benzyl-4-*O*-[2-*O*-benzoyl-3-*O*-(2,3,4,6-tetra-*O*-benzyl- α -D-galactopyranosyl)-4,6-*O*-benzylidene- β -D-galactopyranosyl]-2-deoxy-2-phthalimido- β -D-glucopyranoside (5). Building block **7** (0.82 g, 1.25 mmol), building block **8** (0.50 g, 1.05 mmol), and 4 Å MS (1.00 g) were stirred in dry CH₂Cl₂ (30.0 mL) at 0 °C under N₂, which was followed by the addition of NIS (0.66 g, 1.25 mmol) and TfOH (0.21 mL, 0.5 M in Et₂O, 0.105 mmol). After stirred for 0.5 h, TLC (petroleum ether/acetone = 3:2) showed complete consumption of building block **8**. Then building block **10** (1.20 g, 1.58 mmol), NIS (0.66 g, 1.25 mmol), and TfOH (0.21 mL, 0.5 M in Et₂O, 0.105 mmol) were added to the reaction mixture. The reaction mixture was stirred for 3 h and quenched with triethylamine, then filtered off through Celite. The filtrate was washed sequentially with satd aq NaHCO₃ and brine, dried (Na₂SO₄), filtered, and concentrated. The residue was purified by column chromatography on silica gel (petroleum ether/acetone = 4:1). The product (814.0 mg, 55%) was obtained as a yellow solid. ¹H NMR (500 MHz, CDCl₃) δ : 8.00 (d, $J=7.5$ Hz, 2H, aromatic), 7.60–7.65 (m, 2H, aromatic), 7.51 (t, $J=7.5$ Hz, 1H,

aromatic), 7.10–7.38 (m, 39H, aromatic), 6.97 (dd, $J=2.0$, 7.5 Hz, 2H, aromatic), 6.72–6.80 (m, 3H, aromatic), 5.64 (dd, $J=8.5$, 10.0 Hz, 1H, H-2'), 5.31 (s, 1H, benzylidene-CH), 4.96–5.06 (m, 6H), 4.79 (d, $J=11.5$ Hz, 1H), 4.72 (d, $J=8.5$ Hz, 1H), 4.50–4.63 (m, 5H), 4.44 (d, $J=12.0$ Hz, 1H), 4.21–4.38 (m, 7H), 4.04–4.12 (m, 4H), 3.97 (dd, $J=3.5$, 10 Hz, 1H), 3.83–3.92 (m, 2H), 3.81 (dd, $J=3.5$, 10.0 Hz, 1H), 3.67–3.72 (m, 3H), 3.51–3.55 (m, 2H), 3.38–3.41 (m, 2H), 3.27 (dd, $J=7.0$, 9.0 Hz, 1H), 3.15–3.18 (m, 1H), 2.98–3.02 (m, 1H), 1.65–1.74 (m, 2H, OCH₂CH₂CH₂N); ¹³C NMR (125 MHz, CDCl₃) δ : 167.7, 164.7, 156.3, 138.7, 138.68, 138.6, 138.5, 138.3, 138.1, 137.8, 136.7, 133.6, 133.1, 131.6, 130.9, 129.8, 128.7, 128.44, 128.4, 128.3, 128.2, 128.14, 128.1, 128.0, 127.9, 127.8, 127.78, 127.7, 127.6, 127.5, 127.4, 127.3, 127.2, 126.8, 126.3, 123.2, 101.1, 100.8, 98.2, 95.8, 78.5, 78.2, 75.8, 75.3, 75.1, 74.9, 74.7, 74.6, 73.2, 73.2, 73.1, 72.3, 72.2, 71.3, 69.9, 68.9, 68.6, 67.8, 66.6, 66.4, 66.3, 65.5, 58.4, 55.6, 37.7, 29.1; TOF-MS (M+NH₄)⁺ 1574. Anal. Calcd for C₉₃H₉₂O₂₀N₂: C, 71.71; H, 5.95; N, 1.80. Found: C, 71.49; H, 5.89; N, 1.55.

4.1.16. 3-Aminopropyl 4-*O*-[3-*O*-(α -D-galactopyranosyl)- β -D-galactopyranosyl]-2-acetamido-2-deoxy- β -D-glucopyranoside (2). Compound **5** (44.0 mg, 0.028 mmol) was dissolved in EtOH (3.0 mL) and treated with NH₂NH₂·H₂O (1.0 mL). The mixture was heated under reflux for 24 h, it was then concentrated under reduced pressure and the residue was co-evaporated with toluene (3 × 5 mL). The crude product was dissolved in pyridine (3.0 mL) and acetic anhydride (1.0 mL). After stirring for 8 h, the solvent was removed in vacuum. The residue was dissolved in methanol (3.0 mL), and NaOMe (30% in MeOH, 10 μ L) was added. The mixture was stirred for 6 h and then neutralized with cation exchange resin (H⁺). The resin was filtered off and the filtrate was evaporated in vacuum. The residue was purified by silica gel column chromatography (petroleum ether/acetone = 4:1). A mixture of the purified residue, 10% Pd-C (15.0 mg) in HOAc (4.0 mL), THF (2.0 mL), H₂O (1.0 mL) was stirred under H₂ atmosphere for 24 h. The catalyst was then removed by filtration and the filtrate was concentrated. The residue was subjected to a C-18 reverse phase column chromatography (H₂O) to give **2** (12.0 mg, 70%) as a white solid after lyophilization. ¹H NMR (500 MHz, D₂O) δ : 5.14 (d, $J=3.0$ Hz, 1H, H-1''), 4.54 (d, $J=8.0$ Hz, 1H), 4.52 (d, $J=8.0$ Hz, 1H), 4.15–4.21 (m, 2H), 3.97–4.40 (m, 3H), 3.94 (dd, $J=3.0$, 10 Hz, 1H), 3.63–3.88 (m, 12H), 3.58–3.63 (m, 2H), 3.08 (t, $J=7.0$ Hz, 2H, OCH₂CH₂CH₂N), 2.04 (s, 3H, CH₃CON), 1.92–1.97 (m, 2H, OCH₂CH₂CH₂N); ¹³C NMR (125 MHz, D₂O) δ : 175.4 (CH₃CON), 103.6, 101.9, 96.2 (C-1''), 79.4, 77.9, 75.8, 75.4, 73.0, 71.6, 70.3, 70.0, 69.9, 68.9, 68.7, 65.5, 61.7, 61.6, 60.8, 55.8, 38.6 (OCH₂CH₂CH₂N), 27.4 (OCH₂CH₂CH₂N), 24.0, 22.9; HRMS (M+Na) calcd for C₂₃H₄₂O₁₆N₂Na 625.2432, found 625.2439.

4.1.17. (3-Benzyl-3-benzylloxycarbonylamino)propyl 2,3,6-tri-*O*-benzyl-4-*O*-(2,4,6-tri-*O*-benzyl-3-*O*-(3,6-di-*O*-benzyl-2-deoxy-2-phthalimido-4-*O*-[2-*O*-benzoyl-3-*O*-(2,3,4,6-tetra-*O*-benzyl- α -D-galactopyranosyl)-4,6-*O*-benzylidene- β -D-galactopyranosyl]- β -D-glucopyranosyl]- β -D-glucopyranosyl)- β -D-glucopyranoside (6). Building block **11** (30.0 mg, 0.030 mmol), building block

12¹⁵ (21.5 mg, 0.036 mmol), BSP (2.9 mg, 0.015 mmol), and 4 Å MS (0.20 g) were stirred in dry CH₂Cl₂ (2.0 mL) at room temperature for 0.5 h under N₂. The mixture was cooled to −70 °C, followed by the addition of Tf₂O (3.1 μL, 5.1 mg, 0.018 mmol), then warmed gradually to room temperature. After 3 h, the donor was consumed and the reaction temperature was cooled to −70 °C again, to add a solution of building block **13¹⁵** (45.0 mg, 0.039 mmol) and BSP (2.9 mg, 0.015 mmol) in dry CH₂Cl₂ (2.0 mL). Subsequently Tf₂O (3.1 μL, 5.1 mg, 0.018 mmol) was added to the reaction mixture which was then warmed gradually to room temperature. After 3 h, the reaction was quenched with triethylamine (2.0 mL) and diluted with CH₂Cl₂ (10.0 mL). The reaction mixture was filtered and washed sequentially with satd aq NaHCO₃ and brine, dried (Na₂SO₄), filtered, and concentrated. The residue was purified by column chromatography on silica gel (petroleum ether/EtOAc = 3:1). The product (31.4 mg, 42%) was obtained as a yellow syrup. Saccharide **6** was spectroscopically identical to an authentic sample prepared previously.¹⁵

Acknowledgements

This work was financially supported by the National Natural Science Foundation of China and Peking University. Q.Y. and J.W. are on study leave from Department of Basic Science, Huazhong Agricultural University, Wuhan, China.

References and notes

- (a) Fryer, J. P.; Leventhal, J. R.; Matas, A. J. *Transplant Immunol.* **1995**, *3*, 21–31. (b) Sandrin, M. S.; McKenzie, I. F.C. *Curr. Opin. Immunol.* **1999**, *11*, 527–531. (c) Mollnes, T. E.; Fiane, A. E. *Mol. Immunol.* **1999**, *36*, 269–276. (d) Cascalho, M.; Platt, J. L. *Nat. Rev. Immunol.* **2001**, *1*, 154–160.
- (a) Galili, U.; Rachmilewitz, E. A.; Peleg, A.; Flechner, I. *J. Exp. Med.* **1984**, *160*, 1519–1531. (b) Galili, U.; Clark, M. R.; Shohet, S. B.; Buehler, J.; Mancher, B. A. *Proc. Natl. Acad. Sci. U. S. A.* **1987**, *84*, 1369–1373. (c) Galili, U.; Shohet, S. B.; Kobrin, E.; Stults, C. L. M.; Mancher, B. A. *J. Biol. Chem.* **1988**, *263*, 17755–17762. (d) Galili, U.; Mandrell, R. E.; Hamadeh, R. M.; Shohet, S. B.; Griffis, J. M. *Infect. Immun.* **1988**, *56*, 1730–1737. (e) Platt, J. L.; Vercellotti, G. M.; Dalmasso, A. P. *Immunol. Today* **1990**, *11*, 456–457. (f) Robert, C.; Platt, J. L. *J. Hepatol.* **1996**, *25*, 248–258.
- (a) Galili, U.; Mancher, B. A.; Buehler, J.; Shohet, S. B. *J. Exp. Med.* **1985**, *162*, 573–582. (b) Cooper, D. K. *Clin. Transplant.* **1992**, *6*, 178–183. (c) Good, A. H.; Cooper, D. K.; Malcolm, A. J.; Ippolito, R. M.; Koren, E.; Neethling, F. A.; Ye, Y.; Zuhdi, N.; Lamontagne, L. R. *Transplant. Proc.* **1992**, *24*, 559–562. (d) Cooper, D. K.; Koren, E.; Oriol, R. *Immunol. Rev.* **1994**, *141*, 31–58. (e) Hallberg, E. C.; Strokan, V.; Cairns, T. D. H.; Breimer, M. E.; Samuelsson, B. E. *Xenotransplantation* **1998**, *5*, 246–256.
- (a) Li, S.; Neethling, F.; Taniguchi, S.; Yeh, J.-C.; Kobayashi, T.; Ye, Y.; Koren, E.; Cummings, R. D.; Cooper, D. K. *Transplantation* **1996**, *62*(9), 1324–1331. (b) Simon, P. M.; Neethling, F. A.; Taniguchi, S.; Goode, P. L.; Zopf, D.; Hancock, W. W.; Cooper, D. K. *Transplantation* **1998**, *65*(3), 346–353.
- (a) Chen, Y.; Zhang, W.; Chen, X.; Wang, J.; Wang, P. G. *J. Chem. Soc., Perkin Trans. 1* **2001**, 1716–1722. (b) Naicker, K. P.; Li, H.; Heredia, A.; Song, H.; Wang, L.-X. *Org. Biomol. Chem.* **2004**, *2*, 660–664.
- (a) Fang, J.; Li, J.; Chen, X.; Zhang, Y.; Wang, J.; Guo, Z.; Zhang, W.; Yu, L.; Brew, K.; Wang, P. G. *J. Am. Chem. Soc.* **1998**, *120*, 6635–6641. (b) Zhang, W.; Wang, J.; Li, J.; Yu, L. *J. Carbohydr. Res.* **1999**, *18*, 1009–1017. (c) Fang, J. W.; Chen, X.; Zhang, W.; Janczuk, A.; Wang, P. G. *Carbohydr. Res.* **2000**, *329*, 873–878.
- Zhu, T.; Boons, G. J. *J. Chem. Soc., Perkin Trans. 1* **1998**, 857–860.
- Gege, C.; Kinzy, W.; Schmidt, R. R. *Carbohydr. Res.* **2000**, *328*, 459–466.
- (a) Zhang, Z.; Ollmann, I. R.; Ye, X.-S.; Wischnat, R.; Baasov, T.; Wong, C.-H. *J. Am. Chem. Soc.* **1999**, *121*, 734–753. (b) Ye, X.-S.; Wong, C.-H. *J. Org. Chem.* **2000**, *65*, 2410–2431. (c) Koeller, K. M.; Wong, C.-H. *Chem. Rev.* **2000**, *100*, 4465–4493. (d) Ley, S. V.; Priebe, H. W. M. *Angew. Chem. Int. Ed. Engl.* **1994**, *33*, 2292–2294. (e) Douglas, N. L.; Ley, S. V.; Lucking, U.; Warriner, S. L. *J. Chem. Soc., Perkin Trans. 1* **1998**, 51–65. (f) Grice, P.; Ley, S. V.; Pietruszka, J.; Priebe, H. W. M. *Angew. Chem. Int. Ed.* **1996**, *35*, 197–200. (g) Raghavan, S.; Kahne, D. *J. Am. Chem. Soc.* **1993**, *115*, 1580–1581. (h) Yamada, H.; Harada, T.; Takahashi, T. *J. Am. Chem. Soc.* **1994**, *116*, 7919–7920. (i) Geurtsen, R.; Holmes, D. S.; Boons, G.-J. *J. Org. Chem.* **1997**, *62*, 8145–8154. (j) Lu, S.-F.; O'yang, Q.; Guo, Z.-W.; Yu, B.; Hui, Y.-Z. *J. Org. Chem.* **1997**, *62*, 8400–8405.
- (a) Wang, J.-Q.; Chen, X.; Zhang, W.; Zacharek, S.; Chen, Y.; Wang, P. G. *J. Am. Chem. Soc.* **1999**, *121*, 8174–8181. (b) Liaigre, J.; Dubreuil, D.; Pradere, J.-P.; Bouhours, J.-F. *Carbohydr. Res.* **2000**, *325*, 265–277. (c) Dubber, M.; Lindhorst, T. K. *J. Org. Chem.* **2000**, *65*, 5275–5281. (d) Liu, B.; Roy, R. *J. Chem. Soc., Perkin Trans. 1* **2001**, 773–779. (e) Byrne, G. W.; Schwarz, A.; Fesi, J. R.; Birch, P.; Nepomich, A.; Bakaj, I.; Velardo, M. A.; Jiang, C.; Manzi, A.; Dintzis, H.; Diamond, L. E.; Logan, J. S. *Bioconjugate Chem.* **2002**, *13*, 571–581.
- Fügedi, P.; Garegg, P. J. *Carbohydr. Res.* **1986**, *149*, c9–c12.
- Konradsson, P.; Udodong, U. E.; Fraser-Reid, B. *Tetrahedron Lett.* **1990**, *31*, 4313–4316.
- (a) Martichonok, V.; Whitesides, G. M. *J. Org. Chem.* **1996**, *61*, 1702–1706. (b) Crich, D.; Sun, S. *Tetrahedron* **1998**, *54*, 8321–8348.
- (a) Crich, D.; Smith, M. *J. Am. Chem. Soc.* **2001**, *123*, 9015–9020. (b) Mong, T. K.-K.; Lee, H.-K.; Duron, S. G.; Wong, C.-H. *Proc. Natl. Acad. Sci. U. S. A.* **2003**, *100*, 797–802. (c) Codee, J. D. C.; van den Bos, L. J.; Litjens, R. E. J. N.; Overkleef, H. S.; van Boeckel, C. A. A.; van Boom, J. H.; van der Marel, G. A. *Tetrahedron* **2004**, *60*, 1057–1064.
- Wang, Y.; Huang, X.; Zhang, L.-H.; Ye, X.-S. *Org. Lett.* **2004**, *6*, 4415–4417.



Pergamon

TETRAHEDRON

Tetrahedron 57 (2001) 3267–3280

Practical syntheses of B disaccharide and linear B type 2 trisaccharide—non-primate epitope markers recognized by human anti- α -Gal antibodies causing hyperacute rejection of xenotransplants

Stephen Hanessian,^{a,*} Oscar M. Saavedra,^a Vincent Mascitti,^a Wolfgang Marterer,^b Reinhold Oehrlein^c and Ching-Pong Mak^b

^aDepartment of Chemistry, Université de Montréal, P.O. Box 6128, Succursale Centre-ville, Montreal, Quebec, Canada H3C 3J7

^bNovartis Pharma AG, Chemical and Analytical Development, Basel CH-4002, Switzerland

^cCiba Specialty Chemicals, Basel CH-4002, Switzerland

Received 19 December 2000; accepted 12 February 2001

Abstract—Synthetic protocols are presented for the elaboration of Gal α 1→3GalOR and Gal α 1→3Gal β 1→4GlcNAcOR di- and trisaccharides that use a common Gal donor/acceptor unit, and are potentially adaptable to scale-up. © 2001 Elsevier Science Ltd. All rights reserved.

1. Introduction

The replacement of vital organs in humans (allograft transplantation) is arguably one of the most dramatic scientific accomplishments in the annals of medical history. Through enormous advances and heroic efforts in the field of transplantation, such procedures are quasi routine today for a number of organs that include the heart, kidney, and liver for example. In spite of these monumental successes, the continued practice of one of the noblest of human life-saving procedures is severely jeopardized by the limited availability of suitable donors.¹

A possible solution has been considered through xenotransplantation, where suitable animal donors would be used. Although phylogenetically close to man, non-human primates such as apes, monkeys and baboons are not suitable donors for various ethical and epidemiological reasons.² Pigs, however, appear to present a good alternative³ since they can be bred in large numbers, even with genetically engineered variants.⁴ Moreover, they are anatomically and physiologically similar to man with suitable heart sizes. In spite of this somewhat futuristic notion with obvious advantages if successfully implemented, the practice of xenotransplantation from pig to man is plagued by at least two major obstacles. Firstly, the phenomenon of rejection

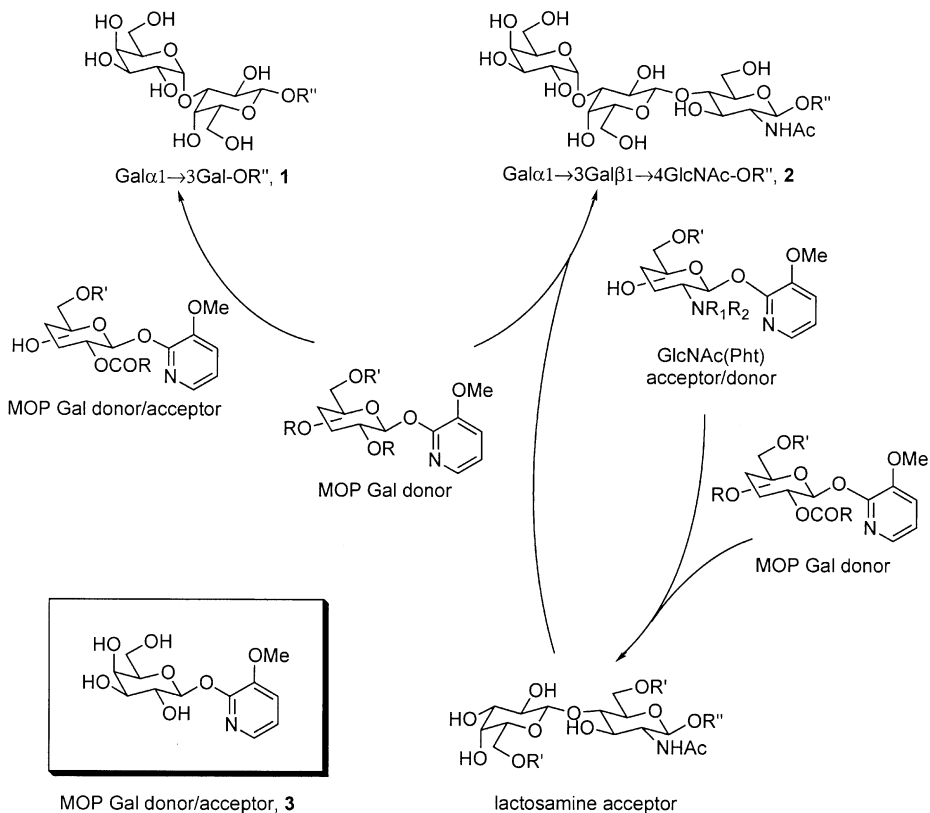
looms as a real threat, as discussed below.⁵ Secondly, in the advent of a successful transplant, extreme care must be exercised to avoid the transfer, either directly or through a dormant genetic mechanism, of the porcine endogenous retrovirus and other retroviruses to man.⁶ This socio-medical issue can, in principle, be resolved by breeding genetically modified pigs that do not encode for the virus, and its implications are outside the scope of this paper.

Of greater immediate concern, however, are the immunologic barriers to discordant xenotransplantation from pig to man.⁵ A major cause for hyperacute rejection of a xenograft would be the result of binding anti-pig antibodies to antigens expressed on the endothelium of the donated organ. α -Gal containing epitopes on pig tissues are abundantly expressed, and recognized by anti- α -Gal antibodies, which constitute approximately 1% of circulating antibodies (IgG, IgM and IgA) in humans.^{5,7} In fact, such antibodies bind to α -GalR containing oligosaccharide epitopes such as Gal α 1→3GalOR (B disaccharide antigen group) **1** and Gal α 1→3Gal β 1→4GlcNAcOR (linear B type 2 antigen group) **2** among others^{4,8} (Fig. 1).

Curiously, the Gal α 1→3Gal epitope is absent in all human tissue because α 1→3Gal transferase⁹ is not expressed except in certain malignancies.^{5,10} They do however produce large amounts of anti- α -Gal antibodies as part of a natural class of immunoglobulins, perhaps as a preventive measure toward bacteria and cells of other species.¹¹ It is clear then why the binding of human anti- α -Gal antibodies to α -GalOR containing epitopes of vascularized organ

Keywords: oligosaccharides; glycoside synthesis; new donors.

* Corresponding author. Tel.: +514-343-6738; fax: +514-343-5728; e-mail: hanessia@ere.umontreal.ca

**Figure 1.**

tissues results in hyperacute rejection. To achieve successful ‘accommodation’,¹² (adaptation, anergy) of the transplant, one must deplete the anti- α -Gal antibodies from the recipient before the new organ is placed.⁵ Although there are other barriers to successful xenotransplantation even if hyperacute rejection is minimized, such as acute vascular and cell-mediated phenomena, the notion of neutralizing anti- α -Gal natural antibodies with synthetic α -GalOR containing oligosaccharides prior to organ transplantation remains as an attractive protocol. It appears that once ‘removed’, the acquired acceptance (accommodation) can persist, even when the humoral antibodies are restored, as evidenced in allografts.¹³ Once the new organ is in place and antibody activity is curtailed, immunotherapy using immunosuppressant drugs can be initiated to ensure the patient’s well being and to maintain the new organ.

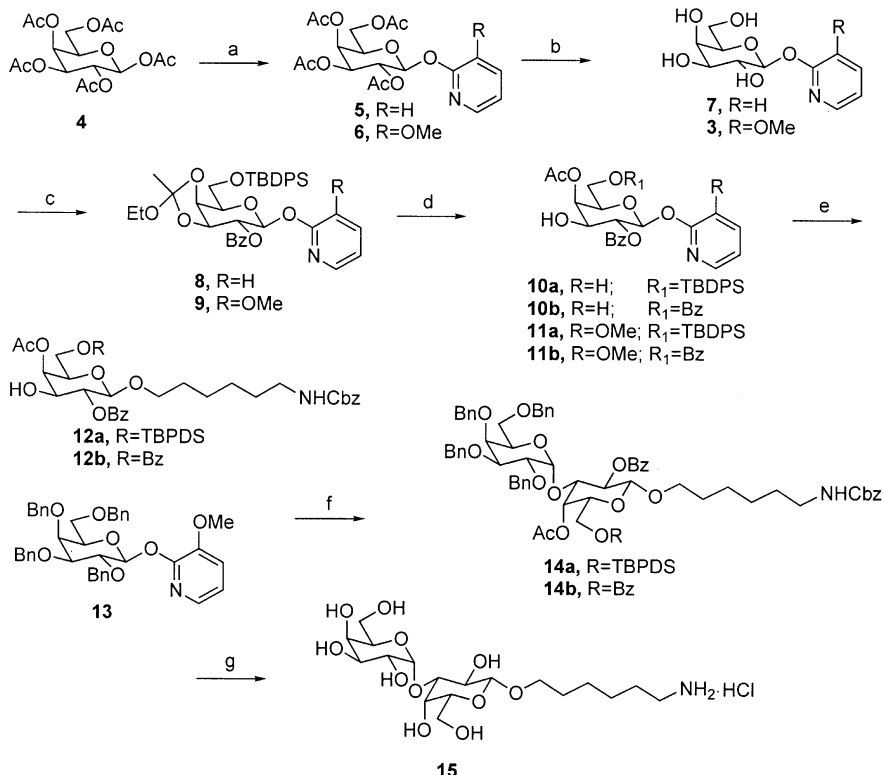
Extensive studies have shown that carbohydrate therapy in xenotransplantation with the aim of neutralizing anti- α -Gal antibodies is a viable experimental protocol. Although the clinical aspects of the procedure are not resolved, one extreme but successful protocol is the use of pretransplant extracorporeal immunoabsorption with columns containing pertinent α -GalOR epitope motifs that can entrap anti- α -Gal antibodies from the ‘patient’s’ blood that is perfused through the column.^{2b,8c} Transplantation could then be done when a low titer of the anti- α -Gal antibodies is reached. Another approach relies on specific intravenous α -GalOR therapy as demonstrated in baboon allografts.¹⁴

These and other studies directed at exploiting xenoreactive antigen–human antibody interactions¹⁵ has instigated a

need to devise practical syntheses of the Gal α 1-3GalOR (B disaccharide) **1** and Gal α 1-3Gal β 1-4GlcNAcOR (linear B type 2 trisaccharide) **2**.

Although several syntheses are known,^{16–22} we were particularly interested in devising synthetic protocols that avoided the use of thiol-based reagents, hydrolytically labile glycosyl donors, and potentially toxic reagents, with the prospects of adapting the protocol to potentially produce relatively large quantities of **1** and/or **2** in a process group environment. In order to explore practical methods to access the intended targets **1** and **2**, we chose a strategy that capitalizes on the ability of a common Gal unit to act as a donor and acceptor. We have previously shown that 2-pyridyl and 3-methoxy-2-pyridyl (MOP) glycosides are excellent anomeric activators under mild conditions.²³ Thus, unprotected MOP β -D-galactopyranoside **3** (Fig. 1) affords alkyl α -D-galactopyranosides (and oligosaccharides) upon treatment with a suitable alcohol or partially protected MOP glycoside.²⁴ Activation of the newly formed disaccharide, for example, and reaction with a suitably protected MOP glycoside allows for an iterative oligosaccharide synthesis. *O*-Protected MOP β -D-galactopyranosides can serve as glycosyl donors or acceptors depending on the nature of the *O*-protecting group.

Fig. 1 illustrates the common Gal donor/acceptor strategy in conjunction with the synthesis of **1** and **2**. It should be pointed out that MOP glycoside donors which contain participating groups at C-2 (ester) will lead to 1,2-*trans*-glycosides, while those with non-participating groups (ex. benzyl) will afford the 1,2-*cis*-glycosides as major products,²⁵ as in



Scheme 1. (a) i. HBr, Ac₂O, AcOH, 2 h rt. for **5** ii. silver 2-pyridoxide, toluene, reflux, 1 h, 71%; for **6** ii. silver 3-methoxy-2-pyridoxide, toluene, reflux, 1 h, 86%. (b) MeONa, MeOH, rt, 3–6 h, 94–95% (c) i. TBDPSCl, imidazole, DMF, 6 h, rt, 78–81% ii. MeC(OEt)₃, pyridinium triflate, DCM, 45–60 min, rt iii. BzCl, DMAP, DCM, 1 h 30 min, rt, (d) for R=H: i. 90% AcOH, 10 min, rt, 76%; for R=OMe: ii. AcOH, AcONa, H₂O pH=3–4, 1 h, 67%. (e) DCM, 1 h, rt, for **10a**: HBF₄-Et₂O, 80%; for **10b**: HBF₄-Et₂O, ~80%; for **11a**: HBF₄-Et₂O, 80% for TMStriflate, 78% or Cu(OTf)₂, 65%; for **11b**: HBF₄-Et₂O, 72%. (f) for **14a**: DCM, 2 h, rt, Yb(OTf)₃, 76% or toluene, 1 d, rt Cu(OTf)₂, 60%; for **14b**: toluene, 2d, 51%. (g) i. MeONa, MeOH, rt, 48 h. ii TBAF, THF, rt, 24 h. iii. 20% Pd(OH)₂/C, H₂, 60 psi, dioxane/water, 1 h, then HCl, H₂, 60 psi, rt, overnight.

well precedented examples using other anomeric activating groups.²⁶ Due to the much decreased reactivity of MOP glycosides that are only partially protected with ester groups,²⁷ they can also act as acceptors when allowed to react with other more reactive MOP glycosyl donors.

In order to test the feasibility of this strategy we considered the synthesis of the Gal α 1→3GalOR motif **1** in the form of its 6-aminohexyl β-D-glycoside as a representative hapten first (Scheme 1). Pyridyl²⁸ and MOP β-D-galactopyranosides were conveniently prepared from β-D-galactopyranose pentaacetate **4** in two steps to afford first the peracetates **5** and **6**, then the free glycosides **7** and **3**, respectively. Selective protection of the primary hydroxy group followed by treatment with trimethylorthoacetate led to the corresponding orthoesters, which were benzoylated to give **8** and **9**, respectively. Treatment with 90% acetic acid afforded the partially esterified MOP glycosides **10** and **11** in excellent yield. Previous work in our laboratory²⁹ had shown that compounds related to the corresponding orthoamide, easily prepared from **3** by selective protection then by treatment with *N,N*-dimethylacetamide dimethyl acetal, also afforded the diester **10**, but the cleavage was not as regioselective as in the case of the orthoesters **8** or **9**. As a parallel series, we also prepared the 2,6-dibenzoate analogs of **10** and **11**.

Perbenzylolation of MOP β-D-galactopyranoside under standard conditions gave the perbenzylated ether **13** which would act as the α-orienting Gal donor.²⁵ Having access

to pyridyl and MOP Gal acceptors **10** and **11**, with ether and ester C-6 substituents, we studied the coupling reaction with 6-N-benzyloxycarbonylamino 1-hexanol in the presence of a variety of activators. The Lewis acids TMS triflate, Yb(TfO)₃,³⁰ and Cu(TfO)₂,²⁵ and the protic acid HBF₄-Et₂O³¹ were effective activators, affording the alkyl β-D-galactopyranosides **12a** and **12b** in good yields. As expected, the glycosylation reaction was selective, favoring the acceptor alcohol (1.5 equiv.), with no trace of self-condensation products arising from **10a,b** or **11a,b**, acting as donor and acceptor to each other. It was important to use pre-dried Yb(TfO)₃ and Cu(TfO)₂ for efficient glycosylations. The reaction between the donor **13** and the acceptor **12a** was best achieved in the presence of dry Yb(TfO)₃ as activator, affording a 76% yield of the intended disaccharide **14a**. With Cu(TfO)₂, toluene was found to be better than dichloromethane as solvent, but conditions needed to be rigorously anhydrous. The yield of the glycosylation was found to be diminished when the dibenzoate **12b** was used as an acceptor. Sequential deprotection of **14a** afforded the intended disaccharide hapten **15**.

The above sequence demonstrated the successful utilization of a common Gal donor/acceptor to construct the Gal α 1→β GalOR disaccharide. For the synthesis of **2** we considered two approaches (Fig. 1). In the first, we envisaged the stepwise construction of the trisaccharide, utilizing a substituted MOP Galβ1→4 donor and an MOP GlcNAc(or NPh) acceptor, followed by coupling with MOP Gal α 1→3 donor

13. A more practical approach would capitalize on the ready availability of alkyl *N*-acetyl lactosaminides via chemoenzymatic routes as acceptor,³² and using **13** as a Gal α 1→3 donor.

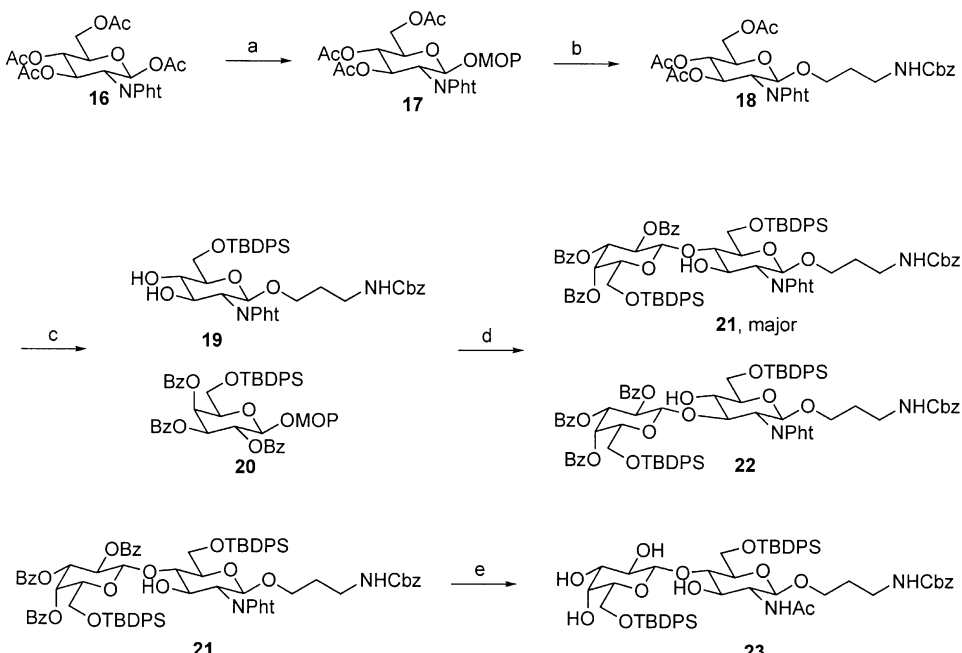
Scheme 2 illustrates the first approach in which 2-deoxy-2-phthalimido- β -D-glucopyranose pentaacetate **16** was converted to the corresponding MOP glycoside **17**. Treatment of **17** with 3-benzyloxycarbonylamino 1-propanol in the presence of HBF₄·Et₂O in dichloromethane led to the expected β -D-glycoside **18** in 65% yield. Deacetylation and selective protection of the primary hydroxy group afforded **19** in excellent yield. Glycosylation with 2,3,4-tri-*O*-benzoyl 6-*O*-*tert*-butyldiphenylsilyl MOP β -galactopyranoside **20** in the presence of Cu(TfO)₂²⁵ as activator gave the intended Gal β 1→4GlcNPh disaccharide **21** in 64% yield accompanied by the regioisomeric glycoside **22** as a minor product. Hydrolysis of the ester groups in the presence of sodium methoxide in methanol followed by hydrazinolysis and *N*-acetylation afforded **23**.

The alternative strategy utilizing a preformed 3-benzyloxycarbonylamino β -*N*-acetyl lactosaminide **24**,³² was next investigated (Scheme 3). Treatment with *tert*-butyldiphenylsilyl chloride afforded the selectively protected ether derivative **23** in excellent yield identical to the product obtained previously (Scheme 2). At this point we adapted the orthoester protocol to achieve selective esterification of the 3,4-diol in the terminal Gal unit, as was successfully implemented for the synthesis of **1** (Scheme 1). Thus, treatment of **23** with trimethyl orthoacetate in the presence of pyridinium triflate afforded the corresponding orthoester **25**, which was converted to the diacetate **26** upon treatment with acetic acid. We next studied the critical α 1→3 galactosylation reaction with **13** as donor and **26** as acceptor in the presence of two activators. Using Yb(TfO)₃ in dichloro-

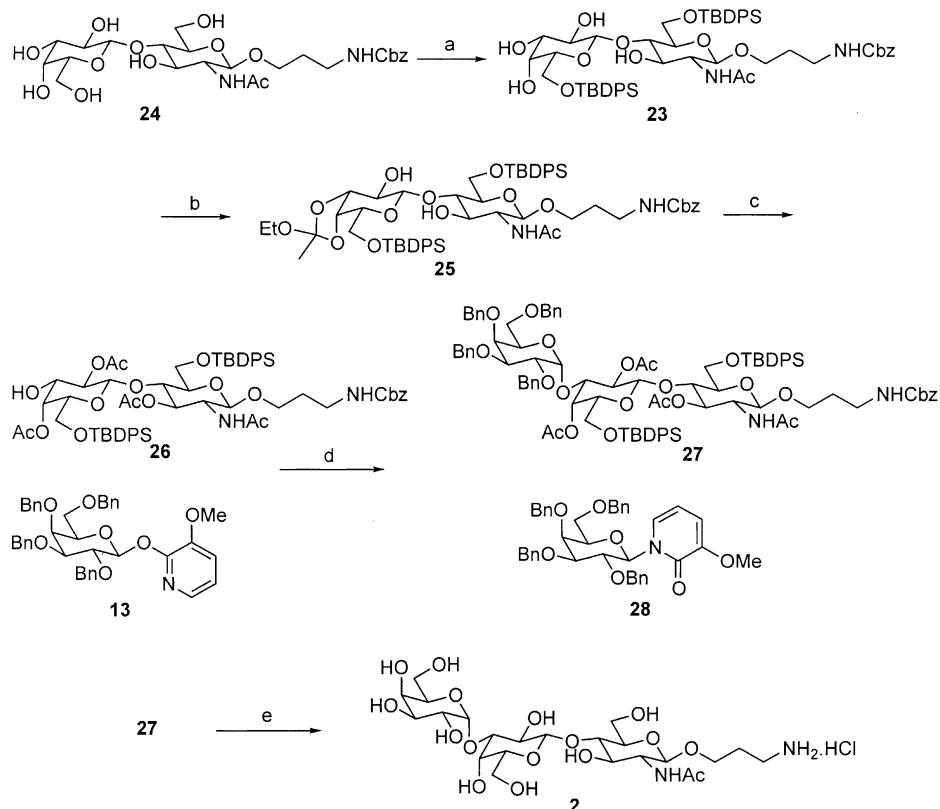
methane required 2 equiv. of donor **13**, affording 63% of the desired Gal α 1→3 trisaccharide **27**. Portionwise addition of 1 equiv. of **13** first and another equivalent after 4 h was found to give better results than addition in one portion. The reaction with **26** was slower in the presence of Cu(TfO)₂, but only 1 equiv. of donor **13** was required to give a 60% yield of **27**. Removal of traces of moisture by using previously dried activator was found to be highly beneficial. In both cases, a minor by-product was identified as the 2,3,4,6-tetra-*O*-benzyl β -D-galactopyranosyl *N*-3-methoxy-2-pyridone **28**. We have observed such *N*-glycosides in glycosylations of MOP donors with somewhat less reactive acceptors. They presumably result from the condensation of the 3-methoxy-2-pyridone formed in the reaction or cleaved due to adventitious moisture with the glycosyl cation.

There remained to deprotect **27** en route to the intended target **2**. Removal of the TBDPS protecting groups with fluoride ion was slow and afforded mixtures of esters, possibly resulting from ester migration. On the other hand, deesterification with sodium methoxide in methanol proceeded smoothly, after which the silyl ethers could be easily removed. Hydrogenolysis of the *N*-benzyloxycarbonyl and benzyl ether groups proved problematic, resulting in mixtures. However, using 20% palladium hydroxide on charcoal (Pearlman's catalyst) in aqueous dioxane proved successful, affording the desired trisaccharide **2** as a colorless powder.

We have reported on synthetic protocols for the elaboration of hapten-like motifs based on B disaccharide **1** and linear B type 2 trisaccharide **2**. A noteworthy feature in these protocols is the utilization of a common Gal unit as donor and acceptor having the same leaving group but differing in the *O*-substituents. The syntheses have elements of practicality and the potential for scale-up since they avoid the use



Scheme 2. (a) i. HBr, AcOH, Ac₂O, rt, 20 h. ii. silver 3-methoxy-2-pyridoxide, toluene, reflux 1 h, 50% two steps. (b) HBF₄·Et₂O, DCM, 12 h, rt, 65%. (c) i. MeONa, MeOH, overnight, rt, 91%. ii. TBDPSCl, imidazole, DMF, rt, overnight, 92%. (d) Cu(OTf)₂, DCM, rt, 6 h, 64%. (e) i. MeONa/MeOH, rt, overnight. ii. hydrazine hydrate, EtOH, reflux, 4 h. iii. Ac₂O, MeOH, 61%.



Scheme 3. (a) TBDPSCl , imidazole, DMF, 6 h, rt. (b) $\text{MeC}(\text{OEt})_3$, pyridinium triflate, DCM, 45–60 min, rt. (c) i. Ac_2O , DMAP, DCM, 1 h. ii. 90% AcOH , 10 min, rt, 86%. (d) $\text{Cu}(\text{OTf})_2$, toluene, 20 h, **27**, 60%; or 2 equiv. **13**, $\text{Yb}(\text{OTf})_3$, DCM, 8 h, **27**, 63%, **28** also isolated. (e) i. MeONa , MeOH , rt, 48 h. ii. TBAF , THF, rt, 24 h. iii. 20% $\text{Pd}(\text{OH})_2/\text{C}$, H_2 , 60 psi, dioxane/water, 1 h, then HCl , H_2 , 60 psi, rt, overnight, 65%.

of toxic heavy metal salts, thiol reagents, or unstable intermediates.

2. Experimental

2.1. General information

Solvents were distilled under positive pressure of dry nitrogen before use and dried by standard methods: THF and ether, from Na/benzophenone; and CH_2Cl_2 , from CaH_2 . All commercially available reagents were used without further purification. All reactions were performed under nitrogen atmosphere. NMR (^1H , ^{13}C) spectra were recorded on AMX-300 and ARX-400 spectrometers. The term $[(-)]$ in ^{13}C data refers to the sign of the corresponding peak in the DEPT 135 NMR experiment. Low- and high-resolution mass spectra were recorded on VG Micromass, Ael-MS902 or Kratos MS-50 spectrometers using fast atom bombardment (FAB) or electrospray techniques. Optical rotations were recorded on a Perkin–Elmer 241 polarimeter in a 1 dm cell at ambient temperature. Analytical thin-layer chromatography was performed on Merck 60F₂₅₄ pre-coated silica gel plates. Visualization was performed by ultraviolet light and/or by staining with ceric ammonium molybdate or ninhydrin. Flash column chromatography was performed using (40–60 μm) silica gel at increased pressure.

2.1.1. Silver 2-pyridoxide. 2-Hydroxypyridine (10 g, 105.14 mmol) was dissolved in a solution of sodium hydroxide (4.2 g, 1 equiv.) in H_2O (70 mL). This solution

was poured under heavy stirring into a solution of silver nitrate (17.8 g, 1 equiv.) in H_2O (70 mL). The mixture was stirred for 15 min, the slurry was filtered, washed with water (500 mL), MeOH (100 mL) and dried under vacuum overnight. The crusty material thus obtained was pulverized and the powder further dried overnight under vacuum to give silver 2-pyridoxide (20.5 g, 101.5 mmol, 97%) as an amorphous white solid.

2.1.2. 3-Methoxy-2-(1*H*)-pyridone. To a 1.4 M aqueous solution of sodium hydroxide at 0°C was added 2,3-dihydroxypyridine (100 g, 0.9 mol). After 15 min dimethylsulfate (85.2 mL, 1 equiv.) was added carefully at 0°C and the mixture was stirred at room temperature for 3 h. Neutralization with acetic acid till pH 7, extraction of the crude product with chloroform (10×1 L) and concentration of the organic layer gave the title compound, which was recrystallized in chloroform to provide pure 3-methoxy-2-(1*H*)-pyridone as cream-colored needles (85.1 g, 75.5%): mp 118°C. ^1H NMR (CDCl_3 , 400 MHz); δ : 7.04 (d, $J_{\text{ac}}=6.5$ Hz, 1H, H-C), 6.76 (d, $J_{\text{ab}}=7.4$ Hz, 1H, H-B), 6.23 (dd, $J_{\text{ab}}=7.4$ Hz, $J_{\text{ac}}=6.5$ Hz, 1H, H-A), 3.84 (s, 3H, OMe). ^{13}C NMR (CD_3OD , 100 MHz); δ : 160.3 (CO-pyridyl), 149.6 (CO-pyridyl), 125.3 (CH-pyridyl), 114.7 (CH-pyridyl), 106.5 (CH-pyridyl), 55.7 (OMe). HR-FABMS calcd for $\text{C}_6\text{H}_7\text{O}_2\text{N}$ m/z 125.0477; found 125.0479.

2.1.3. Silver 3-methoxy-2-pyridoxide. 3-Methoxy-2-(1*H*)-pyridone (6 g, 48 mmol) was dissolved in a solution of sodium hydroxide (1.92 g, 1 equiv.) in water (140 mL). This solution was poured under heavy stirring into a

solution of silver nitrate (8.15 g, 1 equiv.) in water (70 mL), the mixture was stirred for 30 min, the slurry was filtered, washed with water (500 mL), methanol (100 mL) and dried under vacuum overnight. The crusty material thus obtained was pulverized and the powder further dried overnight under vacuum to give silver 3-methoxy-2-pyridoxide as a purple powder (10.5 g, 45 mmol, 94%).

2.1.4. 2-Pyridyl 2,3,4,6-tetra-O-acetyl- β -D-galactopyranoside (5). To a suspension of 1,2,3,4,6-penta-O-acetyl- β -D-galactopyranose **4** (10 g, 25.63 mmol) in Ac₂O (1.25 mL) and AcOH (25 mL) was added HBr (30% in AcOH, 12.5 mL) dropwise. The reaction mixture was stirred for 2 h at room temperature, diluted with toluene (250 mL), washed with ice water (2×150 mL), cold saturated NaHCO₃ (100 mL), ice water (100 mL) and concentrated. The residue was redissolved in toluene, concentrated and the residue dried by codistillation with dry toluene (2×75 mL). The residue was redissolved in dry toluene (80 mL) and silver 2-pyridoxide (5.95 g, 15% excess) was added in one portion. The mixture was refluxed under vigorous stirring for 1 h, allowed to cool down to room temperature, filtered through Celite®, and the bed was washed with toluene (150 mL). The filtrate was washed with saturated NaHCO₃ (100 mL); the heterogeneous mixture was filtered through a Celite® pad, rinsed with toluene and both phases separated. The organic phase was washed with water (100 mL), dried (Na₂SO₄), concentrated and purified by flash chromatography (EtOAc/hexanes 1:1) giving **5** (7.73 g, 18.17 mmol, 71% yield) as a white foam: [α]_D=+27 (c 1.0, CHCl₃). ¹H NMR (CDCl₃, 400 MHz); δ ppm: 8.13 (1H), 7.61 (1H), 6.97 (1H) and 6.80 (1H) (4m, PyH), 6.17 (d, 1H, H-1, J_{1,2}=8.3 Hz), 5.49 (dd, 1H, H-2, J_{2,3}=10.4 Hz), 5.45 (dd, 1H, H-4, J_{4,3}=3.4 Hz, J_{4,5}=0.0 Hz), 5.15 (dd, 1H, H-3), 4.13 (m, 3H, H-5, H-6 and H-6A), 2.15 (s, 3H), 1.99 (s, 6H) and 1.95 (s, 3H), (COCH₃). ¹³C NMR (CDCl₃, 100 MHz); δ ppm: 170.2, 170.1, 169.9 and 169.4 (CO), 161.1 (PyC), 146.6, 139.2, 118.7, and 111.6 (4PyCH), 93.7 (C-1), 70.9, 70.9, 68.3, and 66.8 (C-2 to C-5), 60.8 [(-), C-6], 20.5, (2C), 20.4 and 20.4 (4COCH₃). HR-FABMS calcd for C₁₉H₂₄O₁₀N m/z 426.1400; found 426.1417.

2.1.5. 3-Methoxy-2-pyridyl 2,3,4,6-tetra-O-acetyl- β -D-galactopyranoside (6). Using the same procedure as above, a solution of **4** (4 g, 10.25 mmol), Ac₂O (0.5 mL) and AcOH (10 mL), and HBr (30% in AcOH, 5 mL) afforded the corresponding bromide which was dissolved in dry toluene (36 mL). Silver 3-methoxy-2-pyridoxide (2.8 g, 20% excess) was added in one portion, and the system was refluxed under vigorous stirring for 1 h. Work-up and purification (flash chromatography, EtOAc/hexanes 1:1) gave **6** (4.03 g, 8.85 mmol, 86% yield) as a white foam: [α]_D=+35.18 (c 1.1, CHCl₃). ¹H NMR (CDCl₃, 400 MHz); δ ppm: 7.70 (dd, 1H, J=1.3, 4.9 Hz, PyCH), 7.10 (dd, 1H, J=1.3, 7.9 Hz, PyCH), 6.94 (dd, 1H, J=4.9, 7.8 Hz, PyCH), 6.21 (d, 1H, H-1, J_{1,2}=8.3 Hz), 5.57 (dd, 1H, H-2, J_{2,3}=10.4 Hz), 5.45 (dd, 1H, H-4, J_{4,3}=3.3 Hz, J_{4,5}=0.0 Hz), 5.16 (dd, 1H, H-3), 4.13 (m, 3H, H-5, H-6 and H-6A), 3.82 (s, 3H, OCH₃), 2.15 (s, 3H), 1.99 (s, 6H), and 1.95 (s, 3H) (CH₃CO). ¹³C NMR (CDCl₃, 100 MHz); δ ppm: 170.3, 170.2, 170.1 and 169.3 (CO), 151.5, and 144.1 (PyC), 136.6, 119.1, and 118.9 (PyCH), 93.8 (C-1),

71.1, 71.0, 68.3, and 66.9 (C-2 to C-5), 61.0 [(-), C-6], 55.8 (OCH₃), 20.6, and 20.5 (COCH₃). HR-FABMS calcd for C₂₀H₂₆O₁₁N m/z 456.1505; found 456.1496.

2.1.6. 2-Pyridyl β -D-galactopyranoside (7). To a solution of **5** (10.99 g, 25.84 mmol) in MeOH (85 mL) was added sodium methoxide (0.5N in MeOH, 0.2 mL) and the reaction mixture was stirred for 6 h at room temperature. The solution was neutralized with Amberlite® IRC-50S (H⁺) ion-exchange resin, the resin filtered off, and washed with MeOH. The resulting solution was concentrated under vacuum giving 2-pyridyl β -D-galactopyranoside **7** (6.3 g, 24.5 mmol, 95%) as a white foam: [α]_D=−14 (c 1.0, CH₃OH). ¹H NMR (CD₃OD, 400 MHz); δ ppm: 8.16 (m, 1H, PyCH), 7.76 (m, 1H, PyCH), 7.06 (m, 1H, PyCH), 6.96 (m, 1H, PyCH), 5.63 (d, 1H, H-1, J_{1,2}=8.0 Hz), 3.94 (dd, 1H, H-4, J_{4,3}=3.3 Hz, J_{4,5}=0.0 Hz), 3.84 (dd, 1H, H-2, J_{2,3}=9.8 Hz), 3.73–3.76 (m, 3H, H-5, H-6 and H-6A) and 3.62 (dd, 1H, H-3). ¹³C NMR (CD₃OD, 100 MHz); δ ppm: 164.0 (PyC), 147.8, 141.1, 119.7, and 112.5 (PyCH), 98.9 (C-1), 77.0, 74.9, 71.9, 70.1 (C-2 to C-5), 62.3 [(-), C-6]. HR-FABMS calcd for C₁₁H₁₆O₆N m/z 258.0977; found 258.0967.

2.1.7. 3-Methoxy-2-pyridyl β -D-galactopyranoside (3). Using the same procedure **7** (4.01 g, 8.8 mmol) was dissolved in MeOH (30 mL) and sodium methoxide (0.5N in MeOH, 0.2 mL). Neutralization and concentration gave **3** (2.37 g, 8.25 mmol, 94%) as a white foam: [α]_D=+0.7 (c 0.7, CH₃OH). ¹H NMR (CD₃OD, 400 MHz); δ ppm: 7.68 (dd, 1H, J=1.3, 4.9 Hz), 7.10 (dd, 1H, J=1.3, 7.9 Hz), and 6.94 (dd, 1H, J=4.9, 7.8 Hz) (PyCH), 5.86 (d, 1H, H-1, J_{1,2}=8.1 Hz), 3.93 (dd, 1H, H-4, J_{4,3}=3.2 Hz, J_{4,5}=0.0 Hz), 3.90 (dd, 1H, H-2, J_{2,3}=9.5 Hz), 3.86 (m, 3H, H-5, H-6 and H-6A), 3.72 (s, 3H, OCH₃), 3.62 (dd, 1H, H-3). ¹³C NMR (CD₃OD, 100 MHz); δ ppm: 153.7 and 145.8 (PyC), 137.7, 120.5, and 119.7 (PyCH), 97.8 (C-1), 76.9, 75.0, 71.7, and 70.1 (C-2 to C-5), 62.2 [(-), C-6], 56.3 (OCH₃). HR-FABMS calcd for C₁₂H₁₈O₇N m/z 288.1083; found 288.1078.

2.1.8. 2-Pyridyl 4-O-acetyl-2-O-benzoyl-6-O-tert-butyl-diphenylsilyl- β -D-galactopyranoside (10a). (a) *Orthoester approach.* To a solution of **7** (1.42 g, 5.52 mmol) in dry DMF (20 mL) was added TBDPSCl (1.58 mL, 1.1 equiv.) dropwise and the reaction mixture stirred for 5 h at room temperature. The solution was diluted with EtOAc (150 mL), extracted with H₂O (2×100 mL), dried (Na₂SO₄) and concentrated. The residue was purified by flash chromatography (EtOAc/hexanes 1:2 then EtOAc) affording 2-pyridyl 6-O-tert-butyl-diphenylsilyl- β -D-galactopyranoside (2.21 g, 4.46 mmol, 81%) as a white foam: HR-FABMS calcd for C₂₇H₃₄O₆NSi m/z 496.2155; found 496.2126. A solution of the preceding compound (1.95 g, 3.93 mmol), triethyl orthoacetate (1.00 mL, 2 equiv.) and pyridinium triflate (2 mg) in CH₂Cl₂ (35 mL) was stirred at room temperature for 45 min. The reaction mixture was quenched with DMAP (0.96 g, 7.88 mmol), the solvent removed under vacuum, and the solid residue dried under high vacuum (20 min at 40°C bath temperature). The residue was redissolved in CH₂Cl₂ (17.5 mL), BzCl (0.55 mL, 20% excess) was added and the solution stirred for 1 h 30 min at room temperature. The excess BzCl was quenched

by stirring the reaction mixture for 15 min after addition of MeOH (0.5 mL). The solution was concentrated under vacuum and the residue consisting of **8** was redissolved in AcOH (90%, 20 mL). The solution was stirred for 15 min at room temperature, diluted with CH₂Cl₂ (150 mL), washed with ice water (100 mL), cold saturated NaHCO₃ solution (100 mL), ice H₂O (100 mL), dried (Na₂SO₄), filtered and concentrated. The crude product was purified by flash chromatography (EtOAc/hexanes 1:3) giving **10a** (1.92 g, 2.99 mmol, 76%) as white foam: $[\alpha]_D = -14.4$ (*c* 1.1, CHCl₃). ¹H NMR (CDCl₃, 300 MHz); δ ppm: 8.15 (1H), 6.92 (1H) and 6.74 (1H) (m, 3PyH), 7.98 (2H), 7.62–7.58 (4H), 7.58–7.48 (2H), 7.42–7.30 (8H), (m, 15PhCH and 1PyH), 6.36 (d, 1H, H-1, $J_{1,2} = 8.3$ Hz), 5.64 (dd, 1H, H-4, $J_{4,3} = 3.5$ Hz, $J_{4,5} = 0.7$ Hz), 5.54 (dd, 1H, H-2, $J_{2,3} = 10.0$ Hz), 4.20 (dd, 1H, H-3), 4.05 (ddd, 1H, H-5, $J_{5,6} = 6.0$ Hz, $J_{5,6A} = 7.6$ Hz), 3.78 (dd, 1H, H-6, $J_{6,6A} = 10.0$ Hz), 3.73 (dd, 1H, H-6A), 2.10 (s, 3H, COCH₃), 1.03 (s, 9H, SiC(CH₃)₃). ¹³C NMR (CDCl₃, 100 MHz); δ ppm: 171.1 and 166.7 (CO), 161.5 (PyC), 133.0, 132.9, and 129.4 (PhC), 135.6, 133.3, 129.9, 129.8, 129.7, 128.3, 127.7, and 127.7 (PhCH), 146.6, 139.3, 118.6, and 111.9 (PyCH), 93.7 (C-1), 74.1, 73.0, 72.0, and 69.8 (C-2 to C-5), 61.5 [(-), C-6], 20.8 (COCH₃), 26.7 and 19.1 (q) (SiC(CH₃)₃). FABMS (rel. intensity) 642.4 (29), [M+H]⁺. HR-FABMS calcd for C₃₆H₄₀O₈NSi *m/z* 642.2523; found 642.2513.

(b) *Orthoamide approach.* To a solution of **7** (317 mg, 0.632 mmol) in dry CH₂Cl₂ (9 mL) was added *N,N*-dimethylacetamide dimethyl acetal (0.11 mL, 20% excess) under nitrogen and the reaction mixture was stirred for 15 min at room temperature. The solvent was removed under vacuum and the residue concentrated under high vacuum (20 min, 40°C bath temperature). To a solution of the crude product in dry CH₂Cl₂ (6 mL) was added a solution of dry DMAP (154.4 mg, 2 equiv.) in CH₂Cl₂ (3 mL) via cannula followed by benzoyl chloride (0.077 mL, 5% excess). The reaction mixture was stirred under nitrogen for 2 h at room temperature, diluted with CH₂Cl₂ (30 mL), washed with water (20 mL), dried (Na₂SO₄), and concentrated. The crude product was dissolved in AcOH (90% aq., 5 mL) and stirred for 15 min at room temperature. The solution was diluted with CH₂Cl₂ (50 mL), washed with ice water (30 mL), cold saturated NaHCO₃ (30 mL), ice water (30 mL), dried (Na₂SO₄) and concentrated. The crude product was purified by flash chromatography (EtOAc/hexanes 1:3, two columns were necessary) affording pure **10a** (228 mg, 0.35 mmol, 55%) and the corresponding 3-acetate (68 mg, 0.11 mmol, 17%), both as white foams.

2.1.9. 3-Methoxy-2-pyridyl 4-O-acetyl-2-O-benzoyl-6-O-tert-butylidiphenylsilyl-β-D-galactopyranoside (11a). A solution of **3** (2 g, 6.69 mmol) and TBDPSCl (1.9 mL, 1.1 equiv.) in DMF (24 mL) was stirred at room temperature for 5 h to afford after work-up and purification 3-methoxy-2-pyridyl 6-O-tert-butylidiphenylsilyl-β-D-galactopyranoside (2.75 g, 5.23 mmol, 78%) as a white foam: HR-FABMS calcd for C₂₈H₃₆O₇NSi *m/z* 526.2261; found 526.2286. The preceding compound (142.5 mg, 0.271 mmol), triethyl orthoacetate (99 μmL) and pyridinium triflate (1 mg), in CH₂Cl₂ (2.5 mL), was stirred at room temperature for 1 h 15 min, and DMAP (66 mg,

2 equiv.) was added; the solid residue obtained after evaporation was dissolved in CH₂Cl₂ (1.3 mL) and the solution stirred for 1 h at room temperature after addition of BzCl (38 μL). The excess BzCl was quenched by addition of methanol and the crude product obtained after work-up consisting of **9** was treated with a solution of AcOH, AcONa and water (90% aq. AcOH+AcONa until pH ~4, 2 mL). The solution was stirred at room temperature until no more starting material was detected by TLC (~2 h). Work-up and purification (flash chromatography with pure EtOAc) afforded **11a** (122.9 mg, 0.183 mmol, 67%) as white foam: $[\alpha]_D = -7.9$ (*c* 1.1, CHCl₃). ¹H NMR (CDCl₃, 300 MHz); δ ppm: 7.98 (2H), 7.65 (4H), 7.52 (1H), and 7.46–7.32 (8H) (4m, 15H, 15PhCH), 7.72 (1H), 7.02 (1H), and 6.90 (1H) (3m, 3H, PyCH), 6.44 (d, 1H, H-1, $J_{1,2} = 8.2$ Hz), 5.66 (dd, 1H, H-4, $J_{4,3} = 3.4$ Hz, $J_{4,5} = 0.0$ Hz), 5.59 (dd, 1H, H-2, $J_{2,3} = 9.9$ Hz), 4.20 (ddd, 1H, $J_{3,OH} = 3.0$ Hz, H-3), 4.04 (ddd, 1H, H-5, $J_{5,6} = 4.1$ Hz, $J_{5,6A} = 6.4$ Hz), 3.88–3.72 (m, 2H, H-6, and H-6A), 3.70 (s, 3H, OCH₃), 3.06 (d, 1H, OH), 2.10 (s, 3H, COCH₃), 1.03 (s, 9H, SiC(CH₃)₃). ¹³C NMR (CDCl₃, 100 MHz); δ ppm: 171.0 and 166.6 (CO), 151.8 and 144.1 (PyC), 132.9, 129.4, and 128.4 (PhC), 136.5, 119.0, and 118.7 (PyCH), 135.5, 133.1, 129.8, 129.7, 129.6, 128.1, 127.6, and 127.5 (PhCH), 93.7 (C-1), 74.0, 73.3, 72.0, and 69.5 (C-2 to C-5), 61.2 [(-), C-6], 55.6 (OCH₃), 20.7 (COCH₃), 26.6 and 18.9 (q) (SiC(CH₃)₃). HR-FABMS calcd for C₃₇H₄₂O₉NSi *m/z* 672.2628; found 672.2623.

2.1.10. 2-Pyridyl 4-O-acetyl-2,6-di-O-benzoyl-6-O-tert-butylidiphenylsilyl-β-D-galactopyranoside (10b). A solution of **8** (1.50 g, 3.03 mmol), triethyl orthoacetate (0.73 mL, 1.3 equiv.) and pyridinium triflate (1 mg) in CH₂Cl₂ (30.3 mL) was stirred at room temperature for 45 min. After the addition of one drop of Et₃N and stirring the solution for 5 min at room temperature, the reaction mixture was concentrated to dryness under vacuum. The residue was dissolved in THF (3 mL), TBAF (3.3 mL, 1.1 equiv.) was added and the solution stirred for 2 h at room temperature. The reaction mixture was diluted with CH₂Cl₂ (100 mL), extracted with water, dried (Na₂SO₄) and concentrated. To the solution of the crude product in CH₂Cl₂ (15.2 mL), DMAP (3.3 g, 1.2 equiv.) and benzoyl chloride (0.772 mL, 1.1 equiv.) were added and the mixture was stirred for 1 h 30 min at room temperature. Excess BzCl was quenched by addition of MeOH (0.5 mL) and stirring for 15 min. The solution was concentrated under vacuum, the residue dissolved in AcOH (90%, 20 mL), and stirred for 15 min at room temperature. The reaction mixture was diluted with CH₂Cl₂ (150 mL), washed with ice water (100 mL), cold saturated NaHCO₃ (100 mL), ice water (100 mL), dried (Na₂SO₄), filtered and concentrated. The crude was purified by flash chromatography (EtOAc/hexanes 1:2) to give **10b** (0.84 g, 1.66 mmol, 55%) as a white foam: $[\alpha]_D = +18.6$ (*c* 1.1, CHCl₃). ¹H NMR (CDCl₃, 300 MHz); δ ppm: 8.10 (1H), 6.92 (1H), and 6.78 (1H) (3m, 3PyCH), 8.01 (4H), 7.55 (3H), and 7.44 (4H) (3m, 10PhCH and 1PyCH), 6.39 (d, 1H, H-1, $J_{1,2} = 8.3$ Hz), 5.64 (dd, 1H, H-2, $J_{2,3} = 10.0$ Hz), 5.61 (dd, 1H, H-4, $J_{4,3} = 3.4$ Hz, $J_{4,5} = 0.0$ Hz), 4.50 (dd, 1H, H-6, $J_{6,5} = 7.1$ Hz, $J_{6,6A} = 11.1$ Hz), 4.40 (dd, 1H, H-6A, $J_{6A,5} = 6.3$ Hz), 4.30 (dd, 1H, H-5), 4.21 (dd, 1H, H-3), 3.44 (br, 1H, OH), 2.24 (s, 3H, COCH₃). ¹³C NMR

(CDCl₃, 100 MHz); δ ppm: 170.8, 166.7 and 165.9 (CO), 161.3 (PyC), 129.4 and 129.1 (2PhC), 146.5, 139.1, 118.5, and 111.7 (4PyCH), 133.3, 133.0, 129.8, 129.6, 128.2 (2C) (PhCH), 93.6 (C-1), 72.8, 71.6, 71.4, and 69.7 (C-2 to C-5), 61.8 [(-), C-6], 20.7 (3COCH₃). HR-FABMS calcd for C₂₇H₂₆O₉N m/z 508.1607; found 508.1619.

2.1.11. 3-Methoxy-2-pyridyl 4-O-acetyl-2,6-di-O-benzoyl-6-O-tert-butyldiphenylsilyl-β-D-galactopyranoside (11b). A solution of **9** (1.90 g, 3.03 mmol), triethyl ortho-acetate (0.73 mL, 1.3 equiv.) and pyridinium triflate (1 mg) in CH₂Cl₂ (30.3 mL) was stirred for 45 min. The mixture was treated with Et₃N (1 drop) and worked-up as described above. The solid residue was redissolved in THF (2.1 mL), TBAF (2.09 mL, 1.1 equiv.) was added and the mixture was stirred for 2 h at room temperature and worked-up as usual. The crude product was treated with DMAP (0.557 g, 1.2 equiv.) and BzCl (485 mL, 1.1 equiv) in CH₂Cl₂ (9.5 mL) for 3 h at room temperature and the reaction mixture worked-up as before. The crude product was dissolved in 15 mL of buffered AcOH (90% AcOH+A-cONA, pH ~4, 10 mL) and stirred at room temperature until TLC indicated the completeness of the reaction, ~1 h. After the same work-up described for **10b**, the crude was purified by flash chromatography (EtOAc/hexanes 2:3) giving **11b** (0.61 g, 1.66 mmol, 60%) as white foam: $[\alpha]_D=+16.1$ (*c* 1.0, CHCl₃). ¹H NMR (CDCl₃, 300 MHz); δ ppm: 8.00 (4H), 7.55 (2H), and 7.41 (4H) (3m, 10H, PhCH), 7.70 (1H), 7.04 (1H), and 6.92 (1H) (3m, 3H, PyCH), 6.47 (d, 1H, H-1, J_{1,2}=8.2 Hz), 5.65 (dd, 1H, H-2, J_{2,3}=9.8 Hz), 5.60 (dd, 1H, H-4, J_{4,5}=3.2 Hz, J_{4,5}=0.0 Hz), 4.51 (dd, 1H, H-6, J_{6,5}=6.9 Hz, J_{6,6A}=11.2 Hz), 4.39 (dd, 1H, H-6A, J_{6A,5}=6.5 Hz), 4.29 (dd, 1H, 3H), 4.20 (ddd, 1H, H-3, J_{3,OH}=6.2 Hz), 3.71 (s, 3H, OCH₃), 3.25 (d, 1H, OH), 2.25 (s, 3H, COCH₃). ¹³C NMR (CDCl₃, 100 MHz); δ ppm: 170.9, 166.9 and 166.0 (CO), 151.7 and 144.2 (PyC), 129.5 and 129.3 (PhC), 136.6, 119.1, and 118.9 (PyCH), 133.3, 133.1, 129.9, 129.7, 128.3, and 128.3 (PhCH), 93.7 (C-1), 73.2, 72.0, 71.6, and 69.7 (C-2 to C-5), 62.0 [(-), C-6], 55.7 (OCH₃), 20.8 (COCH₃). HR-FABMS calcd for C₂₈H₂₈O₁₀N m/z 538.1713; found 538.1724.

2.1.12. 6-Benzoyloxycarbonylamino-1-hexanyl 4-O-acetyl-2-O-benzoyl-6-O-tert-butyldiphenylsilyl-β-D-galactopyranoside (12a). A. From 10a using HBF₄Et₂O as activator. To a solution of **10a** (0.96 g, 1.5 mmol) and 6-benzoyloxycarbonylamino-1-hexanol (0.45 g, 1.2 equiv.) in CH₂Cl₂ (21.4 mL) was added HBF₄Et₂O (58% in Et₂O, 184 μ L, 1.1 equiv.) in one portion and the mixture was stirred for 1 h at room temperature. The reaction mixture was diluted with CH₂Cl₂ (150 mL), washed with water (75 mL), 1N HCl (75 mL), water (75 mL), dried (Na₂SO₄) and concentrated. The crude product was purified by flash chromatography (EtOAc/hexanes 1:2) giving **12a** (0.96 g, 1.2 mmol, 80%) as a white foam.

B. From 11a. a. Using HBF₄Et₂O as activator: To a solution of **11a** (2.0 g, 2.98 mmol) and 6-benzoyloxycarbonylamino-1-hexanol (1.12 g, 1.2 equiv.) in CH₂Cl₂ (60 mL) was added HBF₄Et₂O (58% in Et₂O, 365 μ L, 1.1 equiv.) in one portion and the mixture stirred for 1 h at room temperature. The reaction mixture was diluted with CH₂Cl₂ (150 mL),

washed with water (75 mL), 1N HCl (75 mL), water (75 mL), dried (Na₂SO₄) and concentrated. The crude was purified by flash chromatography (EtOAc/hexanes 1:2) giving **12a** (1.95 g, 2.44 mmol, 82%) as a white foam.

b. Using TMS triflate as activator: To a solution of **11a** (1 g, 1.49 mmol) and 6-benzoyloxycarbonylamino-1-hexanol (411 mg, 1.1 equiv.) in CH₂Cl₂ (29.8 mL) was added TMSTf (285 μ L mg, 1.1 equiv.) in one portion and the mixture stirred for 1 h at room temperature. The reaction mixture was diluted with CH₂Cl₂ (150 mL), washed with water (50 mL), 1N HCl (50 mL), water (50 mL), dried (Na₂SO₄) and concentrated. The crude was purified by flash chromatography (EtOAc/hexanes 1:2) giving **12a** (0.94 mg, 1.17 mmol, 78%) as a white foam.

c. Using Cu(TfO)₂ as activator: To a solution of **11a** (55.0 mg, 0.082 mmol) and 6-benzoyloxycarbonylamino-1-hexanol (30.5 mg, 1.5 equiv.) in CH₂Cl₂ (2 mL) containing molecular sieves (20 mg) was added Cu(TfO)₂ (43.9 mg, 1.5 equiv.) in one portion and the mixture stirred for 6 h at room temperature. The reaction mixture was quenched with a drop of pyridine, diluted with CH₂Cl₂ (20 mL) and filtered through a Celite® pad. The solution was washed with water (15 mL), 1N HCl (15 mL), water (15 mL), dried (Na₂SO₄) and concentrated. The crude product was purified by flash chromatography (EtOAc/hexanes 1:2) giving **12a** (43 mg, 0.053 mmol, 65%) as a white foam: $[\alpha]_D=-28.5$ (*c* 1.1, CHCl₃). ¹H NMR (CDCl₃, 300 MHz); δ ppm: 8.06 (2H), 7.66 (4H), 7.56 (1H), 7.48–7.31 (13H), (4m, 20H, PhCH), 5.56 (dd, 1H, H-4, J_{4,3}=3.5 Hz, J_{4,5}=0.0 Hz), 5.24 (dd, 1H, H-2, J_{2,1}=7.9 Hz, J_{2,3}=10.0 Hz), 5.09 (s, 2H, CH₂Ph), 4.62 (m, 1H, NHCbz), 4.56 (d, 1H, H-1), 4.03 (dd, 1H, H-3), 3.87 (1H) and 3.43 (1H) (2 m, OCH₂R), 3.78 (m, 3H, H-5, H-6 and H-6A), 3.01 (m, 3H, 2NCH₂R), 2.78 (br, 1H, OH), 2.08 (s, 3H, COCH₃), 1.48 (2H) and 1.16 (6H) (2 m, -CH₂-), 1.08 (s, 9H, SiC(CH₃)₃). ¹³C NMR (CDCl₃, 100 MHz); δ ppm: 171.1 and 166.5 (CO), 133.1, 132.9, 128.0 and 129.7 (PhC), 135.6, 135.5, 133.2, 129.8, 129.8, 128.4, 128.3, 127.7, and 127.7 (PhCH), 101.1 (C-1), 73.6 (2C), 71.8 and 69.7 (C-2 to C-5), 69.8, 66.5, and 61.6 [(-), OCH₂R, CH₂Ph, and C-6], 40.8 [(-), NHCH₂R], 29.6, 29.2, 26.2, and 25.5 [(-), -CH₂-], 20.7 (COCH₃), 26.7 and 19.1 (q) (SiC(CH₃)₃). HR-FABMS calcd for C₄₅H₅₆O₁₀NSi m/z 798.3673; found 798.3689.

2.1.13. 6-Benzoyloxycarbonylamino-1-hexanyl 4-O-acetyl-2,6-di-O-benzoyl-β-D-galactopyranoside (12b) from 11b using HBF₄Et₂O as activator. Adopting the same procedure as described for **11a** but using **11b** (0.301 g, 0.56 mmol) and 6-benzoyloxycarbonylamino-hexanol (0.189 g, 1.2 equiv.) in CH₂Cl₂ (8 mL) and HBF₄Et₂O (58% in Et₂O, 54.4 μ L, 1.1 equiv.) afforded after flash chromatography (EtOAc/hexanes 1:1) **12b** (0.267 g, 0.40 mmol, 72%) as syrup: $[\alpha]_D=-12.0$ (*c* 1.1, CHCl₃). ¹H NMR (CDCl₃, 300 MHz); δ ppm: 8.04 (4H), 7.58 (2H), 7.46 (4H), 7.35 (5H), (4m, 15H, PhCH), 5.53 (dd, 1H, H-4, J_{3,4}=3.0 Hz, J_{4,5}=0.6 Hz), 5.31 (dd, 1H, H-2, J_{2,1}=7.9 Hz, J_{2,3}=10.0 Hz), 5.08 (s, 2H, CH₂Ph), 4.70 (m, 1H, NHCbz), 4.61 (d, 1H, H-1), 4.55 (dd, 1H, H-6, J_{6,5}=6.9 Hz, J_{6,6A}=11.3 Hz), 4.36 (dd, 1H, H-6A, J_{6A,5}=6.6 Hz), 4.01 (m, 2H, H-3, H-5), 3.90 (1H) and 3.47 (1H) (2m, 2H, 2OCH₂R), 3.18 (br, 1H, OH), 2.18 (m, 2H, NHCH₂R),

2.00 (s, 3H, COCH₃), 1.50 (1H) and 1.18 (1H) (m, 2H, 8 – CH₂–). ¹³C NMR (CDCl₃, 100 MHz); δ ppm: 171.0, 166.5, 166.1, and 156.3 (CO), 136.0 and 128.6 (2C) (3PhC), 133.3, 133.3, 129.8, 129.7, 129.5, 128.4, 128.4 and 128.0 (PhCH), 101.3 (C-1), 73.4, 71.3, 71.0 and 69.9 (C-2 to C-5), 70.1, 66.5 and 62.1 [(–), C-6, OCH₂R and CH₂Ph], 40.8 [(–), NHCH₂R], 29.6, 29.2, 26.2, and 25.4 [(–), 4 –CH₂–], 20.8 (COCH₃). HR-FABMS calcd for C₃₆H₄₂O₁₁N m/z 664.2757; found 664.2770.

2.1.14. 3-Methoxy-2-pyridyl 2,3,4,6-tetra-O-benzyl-β-D-galactopyranoside (13). To a solution of **3** (2 g, 6.97 mmol) in dry DMF (69.7 mL) was added NaH (1.4, 60% in mineral oil, washed with hexanes) at 0°C; the mixture was stirred until no more gas evolved, ~1 h. At the same temperature was added dropwise BnBr (4.01 mL, 1.25 equiv.) and the mixture stirred for 1 h. The reaction mixture was allowed to warm up to room temperature then stirred overnight. The excess BnBr was quenched by adding MeOH then diluted with EtOAc (250 mL), extracted with water (2×150 mL) and brine (50 mL), dried (Na₂SO₄), concentrated, and purified by flash chromatography (EtOAc/hexanes 1:3) giving **13** as a syrup: [α]_D=+29.9 (c 1.0, CHCl₃). ¹H NMR (CDCl₃, 300 MHz); δ ppm: 7.78 (1H), 7.12 (1H), and 6.96 (1H) (3m, PyH), 7.48–7.22 (m, 20PhCH), 6.13 (d, 1H, H-1, J_{1,2}=8.0 Hz), 5.05 and 4.83 (AB, 2H, J=11.6 Hz), 5.01 and 4.68 (AB, 2H, J=11.4 Hz), 4.83 (narrow AB, 2H), 4.52 and 4.45 (AB, 2H, J=11.7 Hz) (8CH₂Ph), 4.27 (dd, 1H, H-2, J_{2,3}=9.7 Hz), 4.07 (dd, 1H, H-4, J_{4,3}=2.9 Hz, J_{4,5}=0.0 Hz), 3.90 (ddd, 1H, H-5, J_{5,6}=5.8 Hz, J_{5,6A}=6.8 Hz), 3.85 (s, 3H, OCH₃), 3.79–3.66 (m, 3H, H-3, H-6 and H-6'). ¹³C NMR (CDCl₃, 100 MHz); δ ppm: 149.93 and 141.70 (PyC), 136.3, 136.2, 136.0, and 135.4 (PhC), 134.4, 115.4, and 115.7 (PyCH), 125.8, 125.6, 125.5, 125.5, 125.4, 125.2, 125.0, 124.9, 124.8, and 124.4 (PhCH), 94.1 (C-1), 79.7, 76.4, 71.3, and 71.1 (C-2 to C-5), 72.6, 72.1, 70.9 and 70.4 [(–), 4CH₂Ph], 62.7 [(–), C-6], 53.1 (OCH₃). HR-FABMS calcd for C₄₀H₄₂O₇N m/z 648.2961; found 648.2976.

2.1.15. 6-Benzoyloxycarbonylamino-1-hexanyl O-(2,3,4,6-tetra-O-benzyl-α-D-galactopyranosyl)-(1→3)-4-O-acetyl-2-O-benzoyl-6-O-tert-butyldiphenylsilyl-β-D-galactopyranoside (14a). (a) *Using Yb(TFO)₃ as activator.* A 10 mL round bottom flask containing a mixture of **12a** (150 mg, 0.188 mmol) and **13** (121 mg, 1.0 equiv.), and a magnetic stirrer were dried overnight under vacuum over P₂O₅. The mixture was dissolved in dry CH₂Cl₂ (2.7 mL) and Yb(TFO)₃ (117 mg, 1.0 equiv. dried at 200°C 2 h under vacuum just before use) was added quickly and the mixture stirred for 2 h at room temperature under argon. A second portion of **13** (24.3 mg, 0.2 equiv.) was added and the mixture stirred at room temperature for 2 h. The reaction mixture was diluted with CH₂Cl₂ (50 mL), washed with water (20 mL), 1N HCl (20 mL), water (20 mL), dried (Na₂SO₄) and concentrated. Purification (flash chromatography, EtOAc/hexanes 1:3) afforded pure **14a** (189 mg, 0.143 mmol, 76%) as a white foam.

(b) *Using Cu(TFO)₂ as activator.* A 10 mL round bottom flask containing a mixture of **12a** (423.9 mg, 0.531 mmol) and **13** (344 mg, 1.0 equiv.), and a magnetic stirrer was dried overnight under vacuum over P₂O₅. The mixture

was dissolved in dry toluene (7.6 mL) and Cu(TFO)₂ (192 mg, 1.0 equiv. dried at 200°C for 2 h under vacuum just before use) was added quickly and the mixture stirred for one day at room temperature under argon. The same work-up as described above afforded **14a** (424.3 g, 0.321 mmol, 60%) as a white foam: [α]_D=+34.5 (c 1.1, CHCl₃). ¹H NMR (CDCl₃, 300 MHz, assigned by COSY45); δ ppm: 8.03 (2H), 7.66 (4H), 7.5–7.20 (32H), and 7.15 (2H) (4m, 40H, PhH), 5.67 (dd, 1H, H-4, J_{4,3}=3.1 Hz, J_{4,5}=0.0 Hz), 5.48 (dd, 1H, H-2, J_{2,1}=8.0 Hz, J_{2,3}=10.2 Hz), 5.31 (d, 1H, H-1', J_{1',2'}=4.0 Hz), 4.43 (d, 1H, H-2), 5.1 (s, 2H), 4.79–4.54 (m, 6H) and 4.42–4.30 (m, 3H) (5CH₂Ph and NHCbz), 4.12 (dd, 1H, H-3), 3.95 (2H), 3.80–3.62 (3H), 3.62–3.48 (2H) and 3.28–3.20 (2H) (4m, 9H, H-5, H-6, H-6A, H-2', H-3', H-4', H-5', H-6' and H-6A'), 3.84 (1H) and 3.39 (1H) (2 m, OCH₂R), 2.98 (m, 2H, NCH₂R), 1.78 (s, 3H, COCH₃), 1.48 (2H) and 1.16 (6H) (2 m, –CH₂–), 1.08 (s, 9H, SiC(CH₃)₃). ¹³C NMR (CDCl₃, 100 MHz); δ ppm: 170.11, 164.8 and 156.3 (CO), 138.8 (3C), 138.4 (2C), 136.7, 133.2 and 133.1 (8PhC), 135.6, 135.6, 133.1, 129.8, 129.7, 128.5, 128.4, 128.3, 128.2, 128.0, 127.9, 127.7, 127.7, 127.9, 127.4, 127.3, and 127.2 (PhCH), 101.6 (C-1), 93.2 (C-1'), 78.8, 77.3, 75.8, 75.0, 71.6, 71.0, 73.9 and 64.7 (C-2 to C-5 and C-2' to C-5') 74.5, 73.4, 73.3, 73.1, 69.8 (2C), 66.5 and 61.8 [all (–), C-6, C-6', OCH₂R and 5CH₂Ph], 40.8 [(–), NHCH₂R], 29.6, 29.2, 26.2, and 25.5 [all (–), 4–CH₂–], 20.52 (COCH₃), 26.8 and 19.1 (q) (SiC(CH₃)₃). FABMS (rel. intensity) 1320.3 (2), [M]⁺. Anal. Calcd for C₇₉H₈₉NO₁₅Si: C, 71.85; H, 6.79; N, 1.06. Found: C, 71.82; H, 6.67; N, 1.1.

2.1.16. 6-Benzoyloxycarbonylamino-1-hexanyl O-(2,3,4,6-tetra-O-benzyl-α-D-galactopyranosyl)-(1→3)-4-O-acetyl-2,6-di-O-benzoyl-β-D-galactopyranoside (14b). Using Cu(TFO)₂ as activator applying the same procedure as described for **14a** but using: **12b** (150 mg, 0.226 mmol) and **13** (146 mg, 1.0 equiv.), and Cu(TFO)₂ (81.0 mg, 1.0 equiv.) in toluene (5.3 mL) and stirring the reaction mixture for two days at room temperature gave after flash chromatography (EtOAc/hexanes 1:2, two columns were necessary) **14b** (178 mg, 0.116 mmol, 51%) as a white foam: [α]_D=+36.2 (c 1.1, CHCl₃). ¹H NMR (CDCl₃, 300 MHz); δ ppm: 8.05 (4H), 7.60 (1H), 7.48 (3H), 7.40–7.18 (25H), and 7.15 (2H) (m, 35H, PhH), 5.66 (d, 1H, H-4, J_{4,3}=3.0 Hz, J_{4,5}=0.0 Hz), 5.54 (dd, 1H, H-2, J_{2,1}=8.0 Hz, J_{2,3}=10.2 Hz), 5.23 (d, 1H, H-1', J_{1',2'}=3.4 Hz), 5.1 (s, 2H), 4.77 (d, 1H, J=11.5 Hz), and 4.69–4.28 (m, 11H) (5CH₂Ph, H-1A, NHCbz, H-6, and H-6A), 4.14 (dd, 1H, H-3), 3.97–3.85 (m, 4H), 3.61 (dd, 1H, J=2.7, 10.1 Hz), 3.50–3.43 (m, 2H), and 3.27–3.19 (m, 2H) (4m, 9H, H-5, H-2', H-3', H-4', H-5', H-6', H-6A', and 2OCH₂R), 3.01–2.98 (m, 2H, NCH₂R), 1.90 (s, 3H, COCH₃), 1.48 (2H) and 1.16 (6H) (2 m, –CH₂–). ¹³C NMR (CDCl₃, 100 MHz); δ ppm: 170.4, 166.0, 164.7 and 156.3 (4CO), 138.6, 138.3, 133.2, 133.1, 129.7, 128.4, 128.3, 128.2, 128.1, 127.8, 127.5, 127.5, and 127.4 (PhC and PhCH), 101.7 (C-1), 98.5 (C-1'), 78.7, 75.6, 74.9, 71.5, 71.0, 70.7, 69.8, and 64.8, (C-2 to C-5 and C-2' to C-5'), 74.4, 73.3, 73.2, 70.0, 69.6, 66.5, and 62.1 [all (–), C-6, C-6', 2OCH₂R and 5CH₂Ph], 40.8 [(–), NHCH₂R], 29.6, 29.2, 26.2, and 25.4 [all (–), 4–CH₂–], 20.50 (COCH₃). FABMS (rel. intensity) 1186.7 (5), [M]⁺. Anal. Calcd for C₇₀H₇₅O₁₆N: C, 70.87; H, 6.37; N, 1.18. Found: C, 69.61; H, 6.46; N, 1.21.

2.1.17. 6-Amino-1-hexanyl *O*-(α -D-galactopyranosyl)- β -D-galactopyranoside hydrochloride (15). To a solution of **14a** (72.5 mg, 0.0549 mmol) in dry MeOH (2 mL) was added sodium methoxide (0.5 M in MeOH, 100 μ L) and the reaction mixture stirred for 48 h at room temperature. The solution was concentrated under vacuum, the residue dissolved in CH₂Cl₂ (30 mL), washed with water, dried and concentrated. To a solution of the crude product in THF (0.6 mL) was added in one portion TBAF (60 μ L, 1.1 equiv.). The solution was stirred for 6 h at room temperature, concentrated and purified by flash chromatography (CH₂Cl₂/MeOH 15:1) affording 6-benzyloxycarbonyl-amino-1-hexanyl 3-*O*-(2,3,4,6-tetra-*O*-benzyl- α -D-galactopyranosyl)- β -D-galactopyranoside (33 mg, 0.035 mmol, 65%) as a syrup: FABMS (rel intensity) 936.4 (1.0), [M]⁺. To a solution of the preceding compound in dioxane/water (2:1, 5 mL) was added 20% palladium-on-carbon (Pearlman's catalyst, ~20 mg). The mixture was stirred for 2 h under hydrogen (60 psi) at room temperature, the hydrogen pressure was relieved, HCl (1N in dioxane, ~1 equiv.) was added and the mixture stirred under hydrogen (60 psi) overnight. The suspension was filtered through a Celite® pad, and the pad rinsed with water (20 mL). The filtrate was concentrated under vacuum to about 5 mL, the solution was passed through an ion exchange resin column (Dowex® 1×8-50 in the chloride form), the column was rinsed with water and lyophilized to give pure **15** (17.3 mg, 0.039 mmol, 95%; overall yield from **14a**, 62%) as a white powder: $[\alpha]_D=+76.2$ (*c* 0.5, DMSO). ¹H NMR (D₂O, CH₃OD internal standard at δ =3.35 ppm, 300 MHz); δ ppm: 5.15 (d, 1H, H-1', $J_{1',2'}=3.7$ Hz), 4.46 (d, 1H, H-1, $J_{1,2}=7.9$ Hz), 4.02–3.60 (m, 12H, H-2 to H-6 and H-6A, H-1' to H-6' and H-6A', and 2OCH₂R), 3.00 (m, 2H, NCH₂R), 1.64 (4H) and 1.40 (4H) (2 m, 8H, -CH₂-). ¹³C NMR (D₂O, CH₃OD internal standard at δ =49.6 ppm, 100 MHz); δ ppm: 103.2 (C-1'), 95.9 (C-1), 78.0, 75.5, 71.5, 69.9 (2C), 69.8, 68.9, 65.5 (C-2 to C-5 and C-2' to C-5'), 71.0 and 61.6 (2C) [(-), C-6, C-6', and OCH₂R], 40.1 [(-), NHCH₂R], 29.1, 27.3, 26.0, and 25.2 [(-), 4 -CH₂-]. FABMS (rel. intensity) 442.2 (11), [M-Cl]⁺. HR-FABMS calcd for C₁₈H₃₆O₁₁N *m/z* 442.2288; found 442.2275.

2.1.18. 3-Methoxy-2-pyridyl 3,4,6-tri-*O*-acetyl-2-deoxy-2-phthalimido- β -D-glucopyranoside (17). A solution of tetra-*O*-acetyl-2-deoxy-2-phthalimido- β -D-glucopyranose **16** (2.77 g, 5.81 mmol) and Ac₂O (1.38 mL) in HBr (30% in AcOH, 90 mL) was stirred for 2 h at room temperature. The reaction mixture was diluted with toluene (250 mL), washed with ice water (2×150 mL), cold saturated NaHCO₃ (100 mL), ice water (100 mL) and concentrated. The residue was redissolved in toluene, concentrated and codistilled twice with dry toluene (2×75 mL). The residue was redissolved in dry toluene (110 mL) and silver 3-methoxy-2-pyridoxide (1.66 g, 1.3 equiv.) was added in one portion. The system was refluxed under vigorous stirring for 1 h, and allowed to cool down to room temperature. The mixture was filtered through Celite®, and the bed was washed with toluene (150 mL). The filtrate was treated with saturated NaHCO₃ (100 mL), the biphasic mixture was filtered through a Celite® pad, the pad rinsed with toluene and both phases separated. The organic phase was washed with water (100 mL), dried (Na₂SO₄), concentrated and purified by flash chromatography (EtOAc/hexanes 1:1)

giving **17** (1.58 g, 2.9 mmol) as a white foam: $[\alpha]_D=+73$ (*c* 1.0, CHCl₃). ¹H NMR (CDCl₃, 400 MHz, assigned by COSY45); δ ppm: 7.78 (2H) and 7.67 (2H) (2m, ArCH), 7.55 (dd, 1H, $J=1.5, 4.9$ Hz), 6.95 (dd, 1H, $J=1.5, 7.9$ Hz), and 6.79 (dd, 1H, $J=4.9, 7.8$ Hz) (PyCH), 6.91 (d, 1H, H-1, $J_{1,2}=8.8$ Hz), 5.96 (dd, 1H, H-3, $J_{3,2}=10.6$ Hz, $J_{3,4}=9.1$ Hz), 5.24 (dd, 1H, H-4, $J_{4,5}=10.0$ Hz), 4.68 (dd, 1H, H-2), 4.31 (dd, 1H, H-6, $J_{6,5}=4.4$ Hz, $J_{6,6A}=12.4$ Hz), 4.13 (dd, 1H, H-6A, $J_{6A,5}=2.2$ Hz), 4.08 (ddd, 1H, H-5), 3.62 (s, 3H, OCH₃), 2.08, 2.06, and 1.85 (s, 9H, COCH₃). ¹³C NMR (CDCl₃, 100 MHz); δ ppm: 170.7, 170.1, 169.5, and 167.5 (CO), 151.4 and 144.0 (PyC), 131.4 (ArC), 136.9, 119.1, and 119.0 (PyCH), 134.4, 134.1, 123.7, and 123.5 (ArCH), 91.8 (C-1), 72.1, 70.8, 78.74, 55.6, and 54.1 (C-2 to C-5, OCH₃), 61.8 [(-), C-6], 20.7, 20.6, and 20.4 (COCH₃). HR-FABMS calcd for C₂₆H₂₇O₁₁N₂ *m/z* 543.1615; found 543.1666.

2.1.19. 3-Benzylloxycarbonylamino-1-propyl 3,4,6-tri-*O*-acetyl-2-deoxy-2-phthalimido- β -D-glucopyranoside (18). To a solution of **17** (0.5 g, 0.92 mmol) and 3-benzyloxycarbonylamino-1-propanol (0.289 g, 1.5 equiv.) in CH₂Cl₂ (13.1 mL) was added HBF₄·Et₂O (58% in Et₂O, 90 μ L, 1.1 equiv.) in one portion and the mixture was stirred for 12 h at room temperature. The reaction mixture was diluted with CH₂Cl₂ (150 mL), washed with water (75 mL), 1N HCl (75 mL), water (75 mL), dried (Na₂SO₄) and concentrated. The crude product was purified by flash chromatography (EtOAc/hexanes 1:1) giving **18** (375.4 mg, 0.6 mmol, 65%) as a white foam: $[\alpha]_D=+18.1$ (*c* 1.1, CHCl₃). ¹H NMR (CDCl₃, 400 MHz, assigned by COSY45); δ ppm: 7.82 (2H) and 7.72 (2H) (m, ArCH), 7.34 (m, 5H, PhCH), 5.76 (dd, 1H, H-3, $J_{3,2}=10.6$ Hz, $J_{3,4}=9.2$ Hz), 5.38 (d, 1H, H-1, $J_{1,2}=8.5$ Hz), 5.16 (d, 1H, H-4, $J_{4,5}=9.9$ Hz), 4.99 (m, 3H, CH₂Ph and NHCbz), 4.29 (dd, 1H, H-6, $J_{6,5}=4.4$ Hz, $J_{6,6A}=12.3$ Hz), 4.31 (dd, 1H, H-2), 4.19 (dd, 1H, H-6A, $J_{6A,5}=1.9$ Hz), 3.85 (m, 2H, H-5, OCH₂R), 3.56 (m, 1H, OCH₂R), 3.10 (m, 2H, NCH₂R), 2.06, 2.02, and 1.86 (s, 9H, COCH₃), 1.68 (m, 2H, -CH₂-). ¹³C NMR (CDCl₃, 100 MHz); δ ppm: 170.7, 170.1, 169.4, and 156.2 (CO), 136.5 and 131.2 (PhC), 134.3, 128.4, 127.9, and 123.5 (PhCH), 98.0 (C-1), 71.8, 70.6, 68.8, and 54.4 (C-2 to C-5), 67.2, 66.3, and 61.8 [all (-), C-6, OCH₂R and CH₂Ph], 37.6 and 37.5 [(-), NHCH₂R], 29.2 [(-), -CH₂-], 20.6, 20.5, and 20.3 (3COCH₃). HR-FABMS calcd for C₃₁H₃₅O₁₂N₂ *m/z* 627.2189; found 627.2183.

2.1.20. 3-Benzylloxycarbonylamino-1-propyl 6-*O*-tert-butylidiphenylsilyl-2-deoxy-2-phthalimido- β -D-glucopyranoside (19). To a solution of **18** (303.6 mg, 0.485 mmol) in MeOH (9.7 mL) was added sodium methoxide (0.5N in MeOH, 0.1 mL) and the reaction mixture stirred for 6 h at room temperature. The solution was neutralized with Amberlite® IRC-50S (H⁺) ion-exchange resin, the resin filtered off, and washed with MeOH. The resulting solution was concentrated under vacuum giving 3-benzylloxycarbonylamino-1-propyl 2-deoxy-2-phthalimido- β -D-glucopyranoside (0.22 g, 0.41 mmol, 91%) as white foam: FABMS (rel. intensity) 501.1 (7), [M+H]⁺. HR-FABMS calcd for C₂₅H₂₉O₁₀N₂ *m/z* 501.18732; found 501.1859. To a solution of the preceding product (219.4 mg, 0.438 mmol) and imidazole (59.6 mg, 2 equiv.) in dry DMF (2.2 mL) was added TBDPSCl (180 μ L,

1.5 equiv.) dropwise and the reaction mixture stirred for 5 h at room temperature. The solution was diluted with EtOAc (50 mL), extracted with H₂O (2×25 mL), dried (Na₂SO₄) and concentrated. The residue was purified by flash chromatography (CH₂Cl₂/MeOH 20:1) affording **19** (300 mg, 0.406 mmol, 92%) as a white foam: [α]_D=+20.2 (c 1.0, CHCl₃). ¹H NMR (CDCl₃, 400 MHz, assigned by COSY45); δ ppm: 7.80–7.55 (m, 8H), 7.50–7.39 (m, 6H), and 7.30 (m, 5H) (PhCH), 5.20 (d, 1H, H-1, J_{1,2}=8.4 Hz), 5.00–4.92 (m, 3H, 2CH₂Ph and NHCbz), 4.33 (dd, 1H, H-3, J_{3,2}=10.8 Hz, J_{3,4}=8.6 Hz), 4.11 (dd, 1H, H-2B), 3.97 (m, 2H, H-6 and H-6A), 3.81 (m, 1H, OCH₂R), 3.66 (dd, 1H, H-4, J_{4,5}=9.3 Hz), 3.58 (ddd, 1H, H-5, J_{5,6}=J_{5,6A}=4.8 Hz), 3.47 (m, 1H, OCH₂R), 3.06 (m, 2H, NCH₂R), 1.62 (m, 2H, –CH₂–), 1.05 (s, 9H, SiC(CH₃)₃). ¹³C NMR (CDCl₃, 100 MHz); δ ppm: 168.3 and 156.2 (CO), 136.5, 132.8, 132.7, and 131.4 (PhC), 135.5, 135.4, 134.0, 129.8, 128.3, 127.8, 127.7, and 123.3 (PhCH), 98.0 (C-1), 74.8, 73.5, 71.6, and 56.2 (C-2 to C-5), 66.9, 66.2, and 64.5 [all (–), C-6, OCH₂R and CH₂Ph], 38.0 [(–), NHCH₂R], 29.2 [(–), –CH₂–], 26.6 and 19.2 (q) (SiC(CH₃)₃). HR-FABMS calcd for C₄₁H₄₇O₉N₂Si m/z 739.3051; found 739.3085.

2.1.21. 3-Methoxy-2-pyridyl 2,3,4-tri-O-benzoyl-6-O-tert-butylidiphenylsilyl-β-D-galactopyranoside (20). To a solution of 3-methoxy-2-pyridyl 6-O-tert-butylidiphenylsilyl-β-D-galactopyranoside²⁴ (2.31 g, 4.30 mmol) in pyridine (43.9 mL) was added BzCl (2.1 mL, ~4 equiv.) dropwise and the solution stirred overnight at room temperature. The excess BzCl was quenched with MeOH and the mixture concentrated under vacuum. The crude product was redissolved in CH₂Cl₂ (50 mL) and washed with aqueous dilute HCl (1N, 25 mL) and water (25 mL), dried (Na₂SO₄), concentrated, and purified by flash chromatography (EtOAc/hexanes 1:3) affording **20** (2.95 g, 3.52 mmol, 82%) as a white foam: [α]_D=+131 (c 1.0, CHCl₃). ¹H NMR (CDCl₃, 300 MHz); δ ppm: 8.08 (2H), 7.86 (4H), 7.72 (1H), 7.60 (3H), 7.50–7.21 (14H), 7.04 (3H), and 6.90 (1H) (8m, 28H, 3PyCH and 25PhCH), 6.53 (d, 1H, H-1, J_{1,2}=8.3 Hz), 6.17 (dd, 1H, H-4, J_{4,3}=3.4 Hz, J_{4,5}=1.0 Hz), 6.09 (dd, 1H, H-2, J_{2,3}=10.4 Hz), 5.79 (dd, 1H, H-3), 4.36 (ddd, 1H, H-5, J_{5,6}=J_{5,6A}=6.5 Hz), 3.86 (m, 2H, H-6 and H-6A), 3.70 (s, 3H, OCH₃), 0.98 (s, 9H, SiC(CH₃)₃). ¹³C NMR (CDCl₃, 100 MHz); δ ppm: 165.5, 165.4, and 165.0 (CO), 151.8 and 144.1 (2PyC), 132.6, 132.4, and 128.9 (PhC), 136.7, 119.1, and 118.8 (3PyCH), 135.5, 135.3, 133.1, 132.9, 132.8, 129.9, 129.7, 129.6, 129.4, 128.3, 128.1, 128.0, 127.5, and 127.3 (PhCH), 94.6 (C-1), 74.2, 72.2, 69.6, and 67.7 (C-2 to C-5), 61.0 [(–), C-6], 55.7 (OCH₃), 26.5 and 18.8 (q) (SiC(CH₃)₃). HR-FABMS calcd for C₄₉H₄₈O₁₀NSi m/z 838.3047; found 838.3067.

2.1.22. 3-Benzoyloxycarbonylamino-1-propyl O-(2,3,4-tri-O-benzoyl-6-O-tert-butylidiphenylsilyl-β-D-galactopyranosyl)-(1→4)-6-O-tert-butylidiphenylsilyl-2-deoxy-2-phthalimido-β-D-glucopyranoside (21). A 10 mL round bottom flask containing a mixture of **19** (191.3 mg, 0.259 mmol) and **20** (217 mg, 1.0 equiv.), and a magnetic stirrer was dried overnight under vacuum over P₂O₅. The mixture was dissolved in dry CH₂Cl₂ (3.7 mL) and Cu(TfO)₂ (112.4 mg, 1.2 equiv. dried at 200°C for 2 h

under vacuum just before use) was added quickly and the mixture was stirred under argon for 6 h at room temperature. The reaction mixture was quenched with a drop of pyridine, diluted with CH₂Cl₂ (50 mL) and filtered through a Celite® pad. The solution was washed with water (25 mL), 1N HCl (25 mL), water (25 mL), dried (Na₂SO₄) and concentrated. The crude product was purified by flash chromatography (gradient elution EtOAc/hexanes 1:3 to 1:2) affording **21** (240 mg, 0.165 mmol, 64%, white foam), **22** (39.1 mg, 0.027 mmol, 10%, syrup), and a by-product presumed to be the *N*-pyridone analog of **20** (38.7 mg, 0.046 mmol, syrup, 18%).

For **21**: [α]_D=+30.3 (c 1.4, CHCl₃). ¹H NMR (CDCl₃, 400 MHz, assigned by COSY45); δ ppm: 7.98 (m, 2H), 7.82–7.56 (m, 15H), and 7.50–7.05 (m, 26H) [3m, 44H, PhCH and ArCH], 5.98 (dd, 1H, H-4', J_{4',3'}=3.3 Hz, J_{4',5'}=0.0 Hz), 5.74 (dd, 1H, H-2', J_{2',1'}=8.0 Hz, J_{2',3'}=10.5 Hz), 5.58 (dd, 1H, H-3'), 5.14 (d, 1H, H-1, J_{1,2}=8.5 Hz), 5.05 (d, 1H, H-1'), 5.00 (m, 2H, CH₂Ph), 4.80 (t, 1H, J=6.3 Hz, NHCbz), 4.52 (dd, 1H, H-3, J_{3,2}=10.6 Hz, J_{3,4}=8.6 Hz), 4.18 (dd, 1H, H-2), 4.09–4.03 (m, 2H, H-4 and H-5'), 3.88–3.70 (m, 6H, H-6, H-6', H-6A', OH, and 1OCH₂R), 3.46–3.04 (m, 2H, H-5 and 1 OCH₂R), 3.20 (m, 2NHCH₂R), 1.64 (2m, 2H, –CH₂–), 1.10 and 0.92 (2 s, 18H, 2C(CH₃)₃). ¹³C NMR (CDCl₃, 100 MHz); δ ppm: 168.5, 165.5, 165.2, 165.0, and 156.2 (CO), 136.7, 133.7, 132.8, 132.4, 132.1, 131.7, 129.8, and 128.8 (PhC), 135.9, 135.5, 135.4, 134.0, 133.4, 133.2, 130.0, 129.8, 129.6, 128.6, 128.4, 128.2, 127.9, 127.8, 127.7, 123.6, and 123.1 (PhCH), 101.0 and 97.9 (C-1 and C-1'), 66.8, 66.3, 61.8, and 61.0 [all (–), C-6, C-6', OCH₂R and CH₂Ph], 79.6, 74.7, 74.2, 71.7, 69.9, 69.5, 67.6, and 56.1 (C-2 to C-5 and C-2' to C-5'), 38.3 [(–), NHCH₂R], 29.4 [(–), –CH₂–], 26.9, 26.6, 19.5 (q), and 18.8 (q) (SiC(CH₃)₃). FABMS (rel. intensity) 1473.9 (3.5), [M+Na]⁺. Anal. Calcd for C₈₄H₈₆N₂O₁₇Si₂: C, 69.50; H, 5.97; N, 1.93. Found: C, 70.09; H, 6.66; N, 1.83.

For **22**: [α]_D=+74.2 (c 1.2, CHCl₃). ¹H NMR (CDCl₃, 400 MHz, assigned by COSY45); δ ppm: 7.98 (m, 2H), 7.70–7.68 (m, 4H), 7.64–7.57 (m, 6H), 7.53–7.51 (m, 2H), 7.48–7.28 (m, 24H), 7.20–7.10 (m, 4H) and 7.05 (t, 2H, J=7.9 Hz) [7m, 44H, PhCH and ArCH], 5.82 (dd, 1H, H-4', J_{4',3'}=3.4 Hz, J_{4',5'}=0.0 Hz), 5.62 (dd, 1H, H-2', J_{2',1'}=8.0 Hz, J_{2',3'}=10.4 Hz), 5.45 (dd, 1H, H-3'), 5.00 (s, 2H, CH₂Ph), 4.97 (d, 1H, H-1, J_{1,2}=8.6 Hz), 4.78 (m, 2H, H-1' and NHCbz, J_{1,2'}=8.0 Hz), 4.60 (dd, 1H, H-3, J_{3,2}=10.9 Hz, J_{3,4}=8.3 Hz), 4.29–4.24 (m, H-2 and OH), 4.11 (t, 1H, H-5', J_{5',6'}=J_{5',6A'}=6.8 Hz), 4.06 (dd, 1H, H-6, J_{6,6A}=11.2 Hz, J_{6,5}=2 Hz), 3.90–3.77 (m, 3H, H-6A, H-6' and 1OCH₂R), 3.73–3.69 (m, 2H, H-4 and H-6A'), 3.53 (m, H-5), 2.98 (m, 2NHCH₂R), 1.64 (2m, 2H, –CH₂–), 1.05 and 0.97 (2 s, 18H, 2C(CH₃)₃). ¹³C NMR (CDCl₃, 100 MHz); δ ppm: 165.2, 165.1, 164.5 and 156.0 (CO), 136.5, 133.4 (2C), 132.2, 132.0, 130.6 (2C), and 128.4 (PhC), 135.5, 135.4, 135.3, 133.5, 133.3, 133.0, 132.5, 129.7, 129.4, 129.2, 128.4, 128.2, 127.9, 127.7, 127.6, 127.4, 123.2, and 122.6 (PhCH), 101.3 and 97.9 (C-1 and C-1'), 66.5, 66.1, 63.4, and 61.2 [all (–), C-6, C-6', OCH₂R and CH₂Ph], 82.3, 74.1, 71.4, 69.9 (2C), 69.7, 67.3, and 54.6 (C-2 to C-5 and C-2' to C-5'), 37.97 [(–), NHCH₂R], 29.3 [(–), –CH₂–], 26.6, 26.4, 19.1 (q), and 18.7 (q) (SiC(CH₃)₃). FABMS (rel.

intensity) 1474.5 (3.5), $[M+Na]^+$. Anal. Calcd for $C_{84}H_{86}N_2O_{17}Si_2$: C, 69.50; H, 5.97; N, 1.93. Found: C, 70.37; H, 6.78; N, 1.83.

2.1.23. 3-Benzylcarboxylamino-1-propyl O-(6-O-*tert*-butyldiphenylsilyl- β -D-galactopyranosyl)-(1 \rightarrow 4)-2-acetamido-6-O-*tert*-butyldiphenylsilyl-2-deoxy- β -D-glucopyranoside (23). From 24: To a solution of 24 (2.0 g, 0.438 mmol) and imidazole (1.07 g, 3 equiv.) in dry DMF (34.8 mL) was added TBDPSCl (2.9 mL, 3.0 equiv.) dropwise and the reaction mixture stirred for 6 h at room temperature. The excess TBDPSCl was quenched adding MeOH (5 mL) and the solution stirred for 30 min. The reaction mixture was concentrated under vacuum and the residue purified by flash chromatography ($CH_2Cl_2/MeOH$ 20:1) affording 23 (3.36 g, 2.95 mmol, 85%) as a white foam.

From 21: To a solution of 21 (112.3 mg, 77.35 μ mol) in MeOH (3.8 mL) was added sodium methoxide (~10 equiv.) and the reaction mixture was stirred overnight at room temperature. The solution was neutralized with Amberlite® IRC-50S (H^+) ion-exchange resin, the resin filtered off, and washed with MeOH, the filtrate concentrated, purified by flash chromatography (CH_3OH/CH_2Cl_2 1:20) and the product redissolved in EtOH (7.7 mL). To the refluxing mixture was added H_2NNH_2 hydrate portionwise (5 μ L at a time, every 15–20 min) until the reaction was completed. The solution was concentrated, the residue pumped overnight, and redissolved in MeOH (7.7 mL). To the solution was added Ac_2O (146 μ L, 20 equiv.) and the solution stirred at room temperature for 1 h. The mixture was concentrated and purified by flash chromatography ($CH_2Cl_2/MeOH$ 20:1) affording 23 (49.8 mg, 47.4 μ mol, 61%) as a white foam: $[\alpha]_D=-6.47$ (*c* 1.0, CH_3OH). 1H NMR (CD_3OD , 400 MHz, assigned by COSY45); δ ppm: 7.80–7.77 (m, 4H), 7.70–7.66 (m, 4H), 7.44–7.25 (m, 17H) (PhCH), 5.05 (s, 2H, CH_2Ph), 4.57 (d, 1H, $J=7.7$ Hz) and (d, 1H, $J=8.3$ Hz) (H-1 and H-1'), 4.22 (dd, 1H, $J=11.0$, 3.3 Hz), 3.98 (d, 1H, $J=11.0$ Hz), 3.89–3.83 (m, 5H), 3.77 (dd, 1H, $J=10.2$, 8.6 Hz), 3.67–3.58 (m, 3H), 3.49–3.43 (m, 3H), 3.27–3.13 (m, 2H, $NHCH_2R$), 1.95 (s, 18H, $SiC(CH_3)_3$). ^{13}C NMR (CD_3OD , 100 MHz); δ ppm: 173.5 and 158.8 (2CO), 138.4, 134.9, 134.3 (2C) and 134.2 (5CPh), 137.0, 136.8, 136.7, 130.9, 130.8, 129.4, 128.8 and 128.6 (CHPh), 104.8 and 102.5 (C-1 and C-1'), 79.6, 76.8, 76.5, 75.0, 73.9, 72.4, 69.7 and 56.8 (C-2 to C-5 and C-2' to C-5'), 67.6, 67.3, 63.6 and 63.4 [all (–), C-6, C-6', OCH_2R and CH_2Ph], 38.91 [(–), $NHCH_2R$], 30.8 [(–), $-CH_2-$], 23.0 (COCH₃), 27.4, 20.2 (q) and 19.9 (q) ($SiC(CH_3)_3$). FABMS (rel. intensity) 1073.5 (16), $[M+Na]^+$. Anal. Calcd for $C_{57}H_{74}N_2O_{13}Si_2$: C, 65.12; H, 7.09; N, 2.66. Found: C, 64.17; H, 6.88; N, 2.52.

2.1.24. 3-Benzylcarboxylamino-1-propyl O-(2,4-di-O-acetyl-6-O-*tert*-butyldiphenylsilyl- β -D-galactopyranosyl)-(1 \rightarrow 4)-3-O-acetyl-2-acetamido-6-O-*tert*-butyldiphenylsilyl-2-deoxy- β -D-glucopyranoside (26). A solution of 23 (2.90 g, 2.77 mmol), triethyl orthoacetate (0.66 mL, 1.3 equiv.) and pyridinium triflate (2 mg) in CH_2Cl_2 (27.7 mL) was stirred at room temperature for 1 h. The mixture was quenched with DMAP (1.1 g, 3 equiv.), the solvent removed under vacuum, and the solid residue dried under high vacuum (20 min at 40°C bath temperature)

to give the orthoester derivative 25 which was used in the next step. The residue was redissolved in CH_2Cl_2 (14 mL), Ac_2O (0.79 mL, 3 equiv.) was added and the solution stirred for 1 h at room temperature. The excess Ac_2O was quenched stirring the reaction mixture for 15 min after addition of MeOH (0.5 mL). The solution was concentrated under vacuum and the residue redissolved in AcOH (90%, 20 mL). The solution was stirred for 15 min at room temperature, then diluted with CH_2Cl_2 (150 mL), washed with ice water (100 mL), cold saturated $NaHCO_3$ solution (100 mL), cold water (100 mL), dried (Na_2SO_4), filtered and concentrated. The crude product was purified by flash chromatography (EtOAc/hexanes 1:4) giving 26 (2.80 g, 2.38 mmol, 86%) as a white foam: $[\alpha]_D=-7.8$ (*c* 1.0, $CHCl_3$). 1H NMR ($CDCl_3$, 300 MHz); δ ppm: 7.76–7.24 (m, 25 PhCH), 6.64 (d, 1H, $NHAc$, $J=8.6$ Hz), 5.44 (dd, 1H, H-4', $J_{3',4'}=3.3$ Hz, $J_{4',5'}=0.0$ Hz), 5.15–5.02 (m, 2H), 4.92 (dd, 1H, $J=9.5$, 9.5 Hz), 4.86 (dd, 1H, $J=9.6$, 8.4 Hz), 4.18–4.01 (m, 3H), 3.98–3.87 (m, 2H), 3.80–3.74 (m, 2H), 3.64–3.49 (m, 3H), and 3.36–3.40 (m, 3H) all other protons; 2.05 (s, 3H), 1.92 (s, 3H), 1.88 (s, 3H), and 1.80 (s, 3H) (4COCH₃), 1.62 (1H) and 1.00 (s, 19H) (2 m, 2 –CH₂–, and 2SiC(CH₃)₃). ^{13}C NMR ($CDCl_3$, 100 MHz); δ ppm: 171.1, 170.9, 170.7, 170.5, and 156.7 (5CO), 136.7, 133.5, 132.6 (2C), and 132.2 (5CPh), 135.9, 135.5, 135.4, 129.9, 128.5, 128.1, 128.0, 127.8, 127.7, and 127.6 (PhCH), 101.3 and 100.1 (C-1 and C-1'), 75.1, 74.1, 73.3, 73.0, 72.9, 71.7, 69.3, and 53.2 (C-2 to C-5 and C-2' to C-5'), 66.7, 66.0, 61.3, and 60.8 [all (–), C-6, C-6', OCH_2R and CH_2Ph], 37.4 [(-), $NHCH_2R$], 29.6 [(-), $-CH_2-$], 23.0, 20.8, and 20.7 (2C) (4 COCH₃), 26.7, 19.2 (q) and 19.0 (q) ($SiC(CH_3)_3$). FABMS (rel. intensity) 1177.81 (65, $[M+H]^+$). Anal. Calcd for $C_{63}H_{80}N_2O_{16}Si_2$: C, 64.26; H, 6.85; N, 2.38. Found: C, 64.11; H, 7.05; N, 2.34.

2.1.25. 3-Benzylcarboxylamino-1-propyl O-(2,3,4,6-tetra-O-benzyl- α -D-galactopyranosyl)-O-(1 \rightarrow 3)-(2,4-di-O-acetyl-6-O-*tert*-butyldiphenylsilyl- β -D-galactopyranosyl)-O-(1 \rightarrow 4)-3-O-acetyl-2-acetamido-6-O-*tert*-butyldiphenylsilyl-2-deoxy- β -D-glucopyranoside (27). (a) *Using Cu(TfO)₂ as activator.* A 25 mL round bottom flask containing a mixture of 26 (1.0 g, 0.849 mmol) and 13 (0.66 g, 1.2 equiv.), and a magnetic stirrer was dried overnight under vacuum over P_2O_5 . The mixture was dissolved in dry toluene (17.0 mL) and $Cu(TfO)_2$ (0.614 g, 2.0 equiv. dried at 200°C for 2 h under vacuum just before use) was added quickly and the mixture was stirred for 20 h at room temperature under argon. The reaction mixture was quenched with a few drops of pyridine, diluted with CH_2Cl_2 (100 mL) and filtered through a Celite® pad. The solution was washed with water (50 mL), 1N HCl (50 mL), water (50 mL), dried (Na_2SO_4) and concentrated. The crude was purified by flash chromatography (EtOAc/hexanes 1:1) giving 27 (67 mg, 0.039 mmol, 60%) as a white foam.

(b) *Using Yb(TfO)₃ as activator.* A 10 mL round bottom flask containing a mixture of 26 (90.6 mg, 0.077 mmol) and 13 (50 mg, 1.0 equiv.), and a magnetic stirrer was dried overnight under vacuum over Drierite®. The mixture was dissolved in dry CH_2Cl_2 (1.1 mL) and $Yb(TfO)_3$ (47.7 mg, 1.0 equiv. dried at 200°C for 2 h under vacuum just before use) was added quickly and the mixture stirred

for 4 h at room temperature under argon, a second portion of **13** (50 mg, 1.0 equiv.) was added and the system stirred for 4 h at room temperature. The reaction mixture was diluted with CH_2Cl_2 (50 mL), washed with water (20 mL), 1N HCl (20 mL), water (20 mL), dried (Na_2SO_4) and concentrated. After purification (flash chromatography, gradient elution $\text{CH}_2\text{Cl}_2/\text{MeOH}$ 30:1 to 20:1) the reaction afforded **27** (81.9 mg, 0.048 mmol, 63%) as a white foam and **28** (18.9 mg, 0.029 mmol, syrup).

For **27**: $[\alpha]_D = +18.2$ (*c* 1.1, CHCl_3). ^1H NMR (CDCl_3 , 300 MHz); δ ppm: 7.78–7.18 (m 45H, PhCH), 6.43 (d, 1H, NHAc, $J=7.9$ Hz), 5.73 (dd, 1H, H-4', $J_{4',3}=3.1$ Hz, $J_{4',5}=0.0$ Hz), 5.20 (d, 1H, H-1'', $J_{1'',2}=3.1$ Hz), 5.17 (d, 1H) and 5.06 (d, 1H) (AB, $J=12.0$ Hz), 4.97 (d, 1H) and 4.54 (d, 1H) (AB, $J=11.3$ Hz), 4.88 (d, 1H) and 4.75 (d, 1H) (AB, $J=11.8$ Hz), 4.78 (2, 2H) and 4.72 (d, 1H) (AB, $J=11.9$ Hz), 4.51 (d, 1H) and 4.39 (d, 1H) (AB, $J=11.8$ Hz) ($5\text{CH}_2\text{Ph}$), 5.1 (m, 2H, NHCbz and H-2'), 4.93 (dd, 1H, H-3, $J_{3,2}=J_{3,4}=8.7$ Hz), 4.63 (d, 1H, H-1', $J_{1',2}=8.0$ Hz), 4.15–3.98 (m, 4H), 3.98–3.82 (m, 6H), 3.80 (dd, 1H, $J=3.3$, 6.3 Hz), 3.73 (dd, 1H, $J=3.6$ Hz), 3.65 (dd, 1H, $J=8.6$, 8.3 Hz), and 3.58–3.45 (m, 18H) (H-1, H-2, H-4 to H-6A, H-3', H-5' to H-6A' and H-2'' to H-6A'', and OCH_2R), 3.32–3.11 (m, 3H, OCH_2R and $2\text{NHCH}_2\text{R}$), 1.94 (s, 3H), 1.82 (s, 6H), and 1.78 (s, 3H) (4COCH_3), 1.62 (m, 2H, $-\text{CH}_2-$), 1.00 (s 18H) (2 s, $\text{SiC}(\text{CH}_3)_3$). ^{13}C NMR (CDCl_3 , 100 MHz); δ ppm: 171.0, 170.8, 169.6, 169.1, and 156.9 (5CO), 139.0, 138.1, 136.9, 133.7, 133.1, 132.9, 132.7, and 128.5 (PhC), 136.0, 135.9, 135.7, 135.6, 130.0, 128.8, 128.3, 128.1, 128.0, 127.9, 127.8, 127.6, and 127.5 (PhCH), 101.7 and 100.4 (C-1 and C-1'), 95.9 (C-1''), 75.0, 73.7, 73.2 (2C), 68.4, 66.9, 66.3, and 61.2 (2C) [all (–), C-6, C-6', C-6'', OCH_2R and $5\text{CH}_2\text{Ph}$], 78.7, 76.2, 75.6, 75.5, 74.4, 73.5, 73.2 (2C), 71.6, 70.0, 65.3, and 53.2 (C-2 to C-5, C-2' to C-5', and C-2'' to C-5''), 37.6 [(–), NHCH_2R], 29.8 ($-\text{CH}_2-$), 23.3, 20.9, and 20.7 (2C) (4COCH_3), 27.1, 26.9, 19.5 (q) and 19.30 (q) ($2\text{SiC}(\text{CH}_3)_3$). FABMS (rel. intensity) 1700.8 (62), $[\text{M}+\text{H}]^+$, 1722.8 (50), $[\text{M}+\text{Na}]^+$. Anal. Calcd for $\text{C}_{97}\text{H}_{114}\text{N}_2\text{O}_{21}\text{Si}_2$: C, 68.53; H, 6.76; N, 1.65. Found: C, 68.04; H, 6.91; N, 1.67.

For **28**: $[\alpha]_D = +37.6$ (*c* 1.0, CHCl_3). ^1H NMR (CDCl_3 , 300 MHz); δ ppm: 7.44–7.08 (m, 20PhCH), 6.98 (dd, 1H, $J=1.5$, 7.1 Hz), 6.50 (dd, 1H, $J=1.5$, 7.4 Hz), 6.01 (dd, 1H, $J=7.1$, 7.4 Hz) (3PyCH), 6.27 (d, 1H, H-1, $J_{1,2}=9.0$ Hz), 5.0 (d, 1H, $J=11.4$ Hz), 4.75 (s, 2H), 4.64 (d, 2H, $J=11.4$ Hz), 4.63 (d, 1H, $J=11.3$ Hz), 4.46 (AB, 2H, $J=11.8$ Hz), and 4.35 (d, 1H, $J=11.3$ Hz) ($4\text{CH}_2\text{Ph}$), 4.06 (m, 2H), and 3.84 (m, 2H) (H-2, H-3, H-4 and H-5), 3.81 (s, 3H, OCH_3), 3.63 (dd, 1H, H-6, $J_{6,5}=7.8$ Hz, $J_{6,6A}=9.1$ Hz), 3.56 (dd, 1H, H-6A, $J_{6A,5}=5.6$ Hz). ^{13}C NMR (CDCl_3 , 100 MHz); δ ppm: 157.9 and 149.6 (PyC), 138.9, 138.2, 137.8, and 137.7 (4PhC), 128.4, 128.3, 128.2, 127.9, 127.8, 127.7, 127.6, and 127.4 (PhCH), 123.9 and 111.8 (2PyCH), 104.9 (C-1), 83.2, 81.3, 78.0, 75.7, and 73.8 (C-2, C-3, C-4, C-5, and CHPy), 74.7, 74.5, 73.5, and 74.8 [(–), $4\text{CH}_2\text{Ph}$], 68.0 [(–), C-6], 53.3 (OCH_3). HR-FABMS calcd for $\text{C}_{40}\text{H}_{42}\text{O}_7\text{N}$ *m/z* 648.2961; found 648.2976.

2.1.26. 3-Amino-1-propyl O - α -D-galactopyranosyl-(1 \rightarrow 3)- O - β -D-galactopyranosyl-(1 \rightarrow 4)- O -2-acetamido-2-deoxy-

β-D-glucopyranoside hydrochloride (2). To a solution of **27** (303.2 mg, 0.229 mmol) in dry MeOH (11 mL) was added sodium methoxide (~10 equiv.) and the reaction mixture stirred for 48 h at room temperature. The solution was concentrated under vacuum. To a solution of the crude product in THF (2.3 mL) was added in one portion TBAF (0.55 mL, 1.2 equiv.). The solution was stirred for 6 h at room temperature, concentrated and purified by flash chromatography ($\text{CH}_2\text{Cl}_2/\text{MeOH}$ 15:1) affording 3-benzyl-oxycarbonylamino-1-propyl 2,3,4,6-tetra-O-benzyl- α -D-galactopyranosyl-(1 \rightarrow 3)- O - β -D-galactopyranosyl-(1 \rightarrow 4)- O -2-acetamido-2-deoxy- β -D-glucopyranoside (172 mg, 0.156 mmol, 68%) as a glass: FABMS (rel. intensity) 1097.6 (13), $[\text{M}]^+$, also 1119.5 (69), $[\text{M}+\text{Na}]^+$. A portion of this product (64 mg, 0.058 mmol) was dissolved in dioxane (3.6 mL); water was added (18 mL) followed by 20% palladium-on-carbon (Pearlman's catalyst, ~20 mg). The mixture was stirred for 2 h under hydrogen (60 psi) at room temperature, the hydrogen pressure was relieved, HCl (1N in dioxane, ~1 equiv.) was added and the mixture stirred under hydrogen (60 psi) overnight. The suspension was filtered through a Celite® pad, and the pad rinsed with water (20 mL). The filtrate was concentrated under vacuum to about 5 mL passed through an ion exchange resin column (Dowex® 1×8-50 in the chloride form); the solution afforded after rinsing the column with water and lyophilizing the eluate pure **2** as the hydrochloride (35.8 mg, 0.056 mmol, 96% for the hydrogenation, 65% overall yield from **27**) as a white powder: $[\alpha]_D = +50$ (*c* 1.0, DMSO). ^1H NMR (D_2O , CH_3OD internal standard at $\delta=3.35$ ppm, 300 MHz); δ ppm: 5.15 (d, 1H, H-1'', $J_{1'',2}=3.7$ Hz), 4.51 (2 d, 2H, H-1 and H-1', $J_{1,2}=7.6$ Hz, $J_{1',2}=7.6$ Hz), 4.19–4.15 (m, 2H) and 4.00–3.50 (m, 18H) [H-2 to H-6 and H-6A, H-2' to H-6' and H-6A', H-2'' to H-6'' and H-6A'' and 2 OCH_2R], 3.00 (t, 2H, NCH_2R , $J_{\text{NCH}_2\text{R}-\text{CH}_2}=7$ Hz), 2.05 (s, 3H, COCH_3), 1.95 (m, 2H, $-\text{CH}_2-$). ^{13}C NMR (D_2O , CH_3OD internal standard at $\delta=49.6$ ppm, 100 MHz); δ ppm: 175.6 (CO), 104.0 and 102.4 (C-1 and C-1'), 96.7 (C-1''), 80, 78.5, 76.2, 75.9, 73.4, 72, 70.7, 70.5, 70.3, 69.4 and 66.0 (C-3 to C-5, C-2' to C-5', and C-2'' to C-5''), 69.1, 62.1 (2C), 61.2 [all (–), C-6, C-6', C-6'', OCH_2R], 56.1 (C-2), 38.9 [(–), NHCH_2R], 27.8 [(–), $-\text{CH}_2-$], 23.2 (COCH_3). HR-FABMS calcd for $\text{C}_{23}\text{H}_{44}\text{O}_{16}\text{N}_2$ *m/z* 603.2612; found 603.2603.

Acknowledgements

We thank NSERC of Canada for general financial assistance.

References

- Bühler, L.; Friedman, T.; Iacomini, J.; Cooper, D. K. C. Xenotransplantation—state of the art. *Front. Biosci.* **1999**, *4*, 416.
- (a) Butler, D. *Nature* **1999**, *398*, 549. (b) Cooper, D. K. C.; Good, A. H.; Koren, E.; Oriol, R.; Malcolm, A. J.; Ippolito, R. M.; Neethling, F. A.; Ye, Y.; Romano, E.; Zuhdi, N. *Transpl. Immunol.* **1993**, *1*, 198. (c) Sandrin, M. S.; McKenzie, I. F. C. *Immunol. Rev.* **1994**, 168.
- (a) Cooper, K. K. C.; Ye, Y.; Rolf, Jr., L. L.; Zuhdi, N. *Xenotransplantation*; Springer: Berlin, 1991; p. 481. (b) Niekrasz,

- M.; Ye, Y.; Rolf, Jr., L. L.; Zuhdi, N. *Transplant. Proc.* **1992**, *94*, 625.
4. (a) Onishi, A.; Iwamoto, M.; Akita, T.; Mikawa, S.; Takeda, K.; Awata, T.; Hanada, H.; Perry, A. C. F. *Science* **2000**, *289*, 1188. (b) Cooper, D. K. C.; Koren, E.; Oriol, R. *Lancet* **1993**, *342*, 682. (c) Galili, U. *Immunol. Today* **1993**, *14*, 480. (d) Sandrin, M. S.; Vaughan, H. A.; Dabkowski, P. L.; McKenzie, T. F. C. *Proc. Natl. Acad. Sci. USA* **1993**, *90*, 1139.
 5. (a) Galili, U., Avila, J. L., Eds.; α -Gal and Anti-Gal, Sub-cellular Biochemistry; Kluwer Academic/Plenum Publishers: New York, 1999; Vol. 32. (b) Lawson, J. H.; Platt, J. L. *Transplantation* **1996**, *62*, 303.
 6. (a) Weiss, R. A. *Nature* **1998**, *391*, 327. (b) Paradis, K.; Langford, G.; Loug, Z.; Heneire, W.; Sandstrom, P.; Switzer, W. M.; Chapman, L. E.; Lockey, C.; Onions, D.; Otto, E. The XEN 111 Group; *Science* **1999**, *285*, 1236.
 7. (a) Avila, J. L.; Rojas, M.; Galili, U. *J. Immunol.* **1989**, *142*, 2828. (b) Galili, U.; Rachmilewitz, E. A.; Peleg, A.; Fleckhner, I. *J. Exp. Med.* **1984**, *160*, 1519.
 8. (a) Galili, U.; Macher, B. A.; Buehler, J.; Shohet, S. B. *J. Exp. Med.* **1985**, *62*, 573. (b) Weislander, J.; Mannson, O.; Kallin, E.; Gabrielli, A.; Nowack, H.; Timpl, R. *Glyconjugate J.* **1990**, *7*, 85. (c) Cooper, D. K. C.; Koren, E.; Oriol, R. *Immunol. Rev.* **1994**, *31*.
 9. Galili, U.; Clarck, M. R.; Shohet, S. B.; Buehler, J.; Macher, B. A. *Proc. Natl. Acad. Sci. USA* **1987**, *84*, 1369.
 10. Castronoro, V.; Colin, C.; Parent, B.; Foidart, J.-M.; Lambotte, R.; Mahieu, P. *J. Natl. Cancer Inst.* **1989**, *81*, 212.
 11. Galili, U.; Mandrell, R. E.; Hamedeh, R. M.; Shohet, S. B.; Griffiths, J. M. C. L. *Immun. Infect.* **1988**, *56*, 1730.
 12. Bach, F. H.; Turman, M. A.; Vercellotti, G. M.; Platt, J. L.; Dalmasso, A. P. *Transplant. Proc.* **1991**, *23*, 205.
 13. Platt, J. L.; Fischel, R. J.; Matas, A. J.; Reif, S. A.; Bolman, R. M.; Bach, F. H. *Transplantation* **1991**, *52*, 214.
 14. Cooper, D. K. C.; Ye, Y.; Niekrasz, M.; Kehve, M.; Martin, M.; Neethling, F. A.; Kosanke, S.; DeBault, L. E.; Worsley, G.; Zuhdi, N.; Oriol, R.; Romano, E. *Transplantation* **1993**, *56*, 769.
 15. (a) Galili, U.; Matta, K. L. *Transplantation* **1996**, *62*, 256. (b) Parker, W.; Lateef, J.; Everett, M. L.; Platt, J. L. *Glycobiology* **1996**, *6*, 499. (c) Samuelsson, B. E.; Rydberg, L.; Breimer, M. E.; Bäcker, A.; Gustavsson, M.; Holgersson, J.; Karlsson, E.; Uyterwaal, A.-C.; Cairns, T.; Welsh, K. *Immunol. Rev.* **1994**, *151*. (d) Cairns, T.; Lee, J.; Goldberg, L.; Look, T.; Simpson, P.; Spackman, D.; Palmer, A.; Tanbe, D. *Transplantation* **1995**, *60*, 1202.
 16. Garegg, P.; Oscarson, S. *Carbohydr. Res.* **1985**, *136*, 207.
 17. Jacquinet, J.-C.; Duchet, D.; Milat, N.-L.; Sinaÿ, P. *J. Chem. Soc., Perkin Trans. I* **1981**, 326.
 18. Reddy, G. V.; Jain, R. K.; Bhatti, B. S.; Matta, K. L. *Carbohydr. Res.* **1994**, *263*, 67.
 19. Vic, G.; Tran, C. H.; Scigelova, M.; Crout, D. H. G. *Chem. Commun.* **1997**, 169.
 20. Schaubach, R.; Hemberger, J.; Kinzy, W. *Liebigs Ann. Chem.* **1991**, 607.
 21. Nilsson, K. G. I. *Tetrahedron Lett.* **1997**, *38*, 133.
 22. Fang, J.; Li, J.; Chen, X.; Zhang, X.; Wang, J.; Guo, Z.; Zhang, W.; Yu, L.; Brew, K.; Wang, P. G. *J. Am. Chem. Soc.* **1998**, *120*, 6635.
 23. Hanessian, S.; Lou, B. *Chem. Rev.* **2000**, *12*, 4443. Hanessian, S. In *Preparative Carbohydrate Chemistry*; Hanessian, S., Ed.; Marcel Dekker: New York, 1996 (Chapters 16–20). (c) Hanessian, S. US Patent 5,767,256, June 16, 1998.
 24. Lou, B.; Reddy, G. V.; Wang, H.; Hanessian, S. In *Preparative Carbohydrate Chemistry*; Hanessian, S., Ed.; Marcel Dekker: New York, 1996; p. 389.
 25. Lou, B.; Huynh, H.-K.; Hanessian, S. In *Preparative Carbohydrate Chemistry*; Hanessian, S., Ed.; Marcel Dekker: New York, 1996; p. 413.
 26. Lemieux, R. U.; Hendricks, K. B.; Stick, R. V.; James, K. *J. Am. Chem. Soc.* **1975**, *97*, 4056.
 27. (a) See for example: (a) Paulsen, H.; Richter, A.; Sinnwell, V.; Stenzel, W. *Carbohydr. Res.* **1974**, *64*, 339. (b) Mootoo, D. R.; Konradsson, P.; Udodong, U.; Fraser-Reid, B. *J. Am. Chem. Soc.* **1988**, *110*, 5583.
 28. For a previous study of glycoside synthesis using *O*-benzylated 2-pyridyloxy glycosyl donors in the presence of Lewis acids see: Nicolaev, A. V.; Kochetkov, N. K. Use of (2-pyridyl)-2,3,4,6-tetra-*O*-benzyl-(*D*-glucopyranoside in the synthesis of 1,2-*cis*-linked disaccharides. *Izv. Akad. Nauk SSSR. Ser. Khim.* **1986**, 2556.
 29. Hanessian, S.; Moralioglu, E. *Can. J. Chem.* **1972**, *50*, 233.
 30. For the use of lanthanides such as $\text{Yb}(\text{OTf})_3$ as catalysts in glycoside synthesis, see: (a) Yamanoi, T.; Iwai, Y.; Inazu, T. *J. Carbohydr. Chem.* **1998**, *17*, 819. (b) Kim, W.-S.; Sasai, H.; Shibasaki, M. *Tetrahedron Lett.* **1996**, *37*, 7797. (c) Hosono, S.; Kim, W.-S.; Sasai, H.; Shibasaki, M. *J. Org. Chem.* **1995**, *60*, 4. (d) Sanders, W.; Kiessling, L. *Tetrahedron Lett.* **1994**, *35*, 7335. (e) Inanaga, J.; Yokoyama, Y.; Hanemoto, T. *Tetrahedron Lett.* **1993**, *34*, 2791. (f) Kobayashi, S.; Hachiya, I.; Takahori, T.; Araki, M.; Ashitani, H. *Tetrahedron Lett.* **1992**, *33*, 6815.
 31. For the use of tetrafluoroboric acid as a catalyst in carbohydrate acetal protection and deprotection see: Albert, R.; Dan, K.; Pleschko, R.; Stutz, D. *Carbohydr. Res.* **1985**, *137*, 282.
 32. (a) Alkyl *N*-acetyl lactosaminides are prepared in a chemo-enzymatic process using β -1,4-galactosyltransferase from bovine milk (Fluka); Marterer, W. et al., unpublished results. (b) The experimental procedure is based on a protocol for structurally closely related compounds; see: Baish, G.; Oehrlein, R. *Bioorg. Med. Chem.* **1998**, *6*, 1673.



Virus-based nanoparticles as platform technologies for modern vaccines

Karin L. Lee,¹ Richard M. Twyman,² Steven Fiering³ and Nicole F. Steinmetz^{1,4,5,6,7*}

Nanoscale engineering is revolutionizing the development of vaccines and immunotherapies. Viruses have played a key role in this field because they can function as prefabricated nanoscaffolds with unique properties that are easy to modify. Viruses are immunogenic via multiple pathways, and antigens displayed naturally or by engineering on the surface can be used to create vaccines against the cognate virus, other pathogens, specific molecules or cellular targets such as tumors. This review focuses on the development of virus-based nanoparticle systems as vaccines indicated for the prevention or treatment of infectious diseases, chronic diseases, cancer, and addiction. © 2016 Wiley Periodicals, Inc.

How to cite this article:

WIREs Nanomed Nanobiotechnol 2016, 8:554–578. doi: 10.1002/wnan.1383

INTRODUCTION

Vaccines are designed to elicit a strong immune response and to provide long-lasting protective immunity by generating neutralizing antibodies, activating cellular immunity and inducing immune memory.^{1,2} The earliest reports of vaccination were subjects protected against smallpox by exposure to powders from infected scabs. However, Edward Jenner presented the first formal description of a vaccine in 1798, when he observed that milkmaids previously

infected with the less virulent *Cowpox virus* were no longer susceptible to smallpox. In 1967, the World Health Organization (WHO) oversaw a worldwide smallpox eradication program, which was completed by 1980.³ Since then, eradication programs have been established for other diseases such as polio, measles, mumps, rubella, and malaria.^{4,5} Vaccines have also been developed against other prevalent infectious diseases, such as hepatitis B, rabies, anthrax, and cholera.^{6–9} The development of vaccines has achieved an immense socioeconomic impact by reducing the burden of erstwhile pandemic diseases responsible for widespread morbidity and mortality. Even so, several major pathogens cannot yet be controlled by vaccines including *Human immunodeficiency virus* (HIV) and hemorrhagic fever viruses, such as those responsible for the recent Ebola outbreak affecting West African countries. More recently vaccines have also developed been against noninfectious diseases including cancer and chronic disorders.

*Correspondence to: nicole.steinmetz@case.edu

¹Department of Biomedical Engineering, Case Western Reserve University Schools of Engineering and Medicine, Cleveland, OH, USA

²TRM Ltd, York, UK

³Department of Microbiology and Immunology and Norris Cotton Cancer Center, The Geisel School of Medicine at Dartmouth, Lebanon, NH, USA

⁴Department of Radiology, Case Western Reserve University School of Medicine, Cleveland, OH, USA

⁵Department of Materials Science and Engineering, Case School of Engineering, Cleveland, OH, USA

⁶Department of Macromolecular Science and Engineering, Case School of Engineering, Cleveland, OH, USA

⁷Case Comprehensive Cancer Center, Case Western Reserve University School of Medicine, Cleveland, OH, 44106, USA

Conflict of interest: The authors have declared no conflicts of interest for this article.

VIRUS-BASED NANOPARTICLES AS PLATFORM TECHNOLOGIES

Nanoparticle-based vaccines have been developed using a diverse range of materials (Figure 1), including synthetic particles (e.g., gold, polymers or lipid micelles) and biological particles (e.g., nucleic acids

and proteins, including viruses).^{10,11} We consider two broad types of particles in the latter category: virus-based nanoparticles (VNPs) that feature a modified capsid encapsulating the virus genome, and virus-like nanoparticles (VLPs) that comprise protein components alone.

Virus-based materials have many beneficial properties. Their proteinaceous, highly-ordered, multivalent structures, when combined with an appropriate adjuvant, often elicit robust cellular and humoral immune responses.¹² They display antigens in a repetitive array (which promotes B cell crosslinking and subsequent activation) and pathogen-associated molecular patterns (PAMPs) that induce stronger and longer-lasting antigen-specific immune responses than soluble antigens.^{13–15} The single-stranded viral RNA (ssRNA) found in VNPs is also a PAMP, and this is a natural ligand for Toll-like receptors 7 and 8 that induce cytokine expression.^{16–19} The size range of virus particles (20–500 nm) means they are efficiently taken up by antigen presenting cells (APCs), including dendritic cells (DCs) and other phagocytes, thus stimulating T cells.^{20,21}

Viral vaccines can be divided into four categories (Figure 2): live-attenuated, inactivated, subunit vaccines, and native or recombinant VNP/VLP structures. The latter are considered safer because there is no risk of virulence, yet stronger than inactivated viruses or subunit vaccines because they induce a robust immune response without multiple doses.^{22,23} Native VLPs lack the viral genome but are otherwise identical to the infectious virus, making them highly immunogenic but unable to replicate. These are particularly suitable when the native virus replicates and causes disease in humans. VNPs retain the genome and are therefore easier to produce by relying on natural virus replication. This format is particularly suitable when the native virus does not replicate in humans, i.e., bacteriophage and plant viruses. Recombinant VLP/VNP formats add an important further layer of advantages because they can be engineered to present antigenic epitopes of a counterpart virus or any other disease-associated antigen. VLPs and VNPs can be manufactured in heterologous production systems, including plants, mammalian cells, yeast and bacteria.²⁴

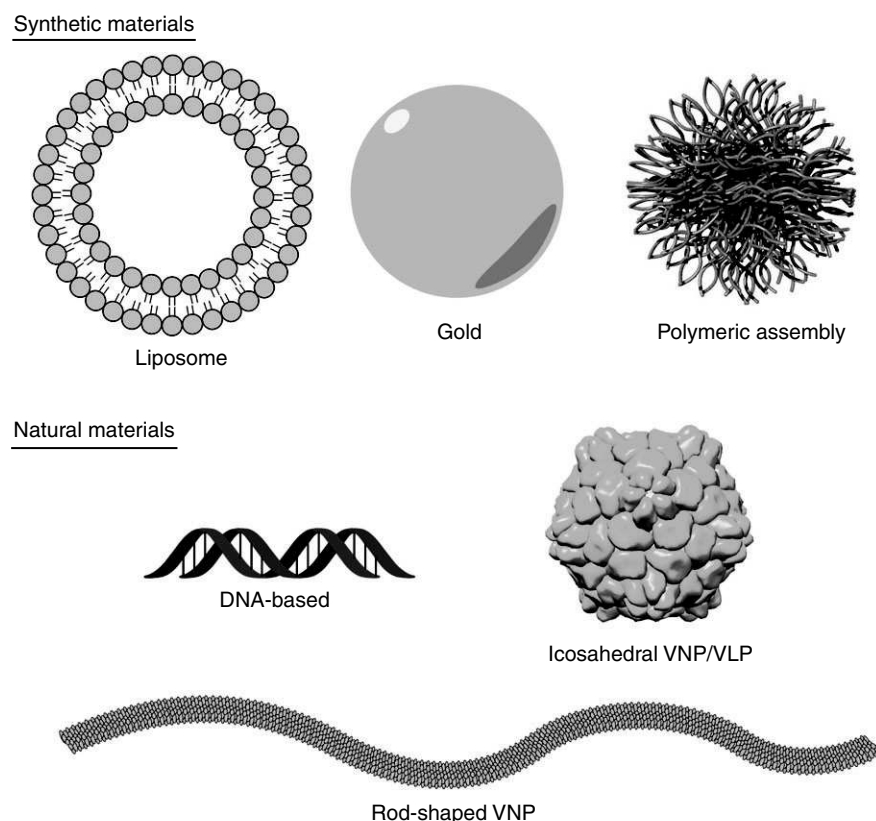


FIGURE 1 | Nanoparticles as vaccination platforms. (The polymeric assembly was provided by courtesy of Dr. Pokorski)

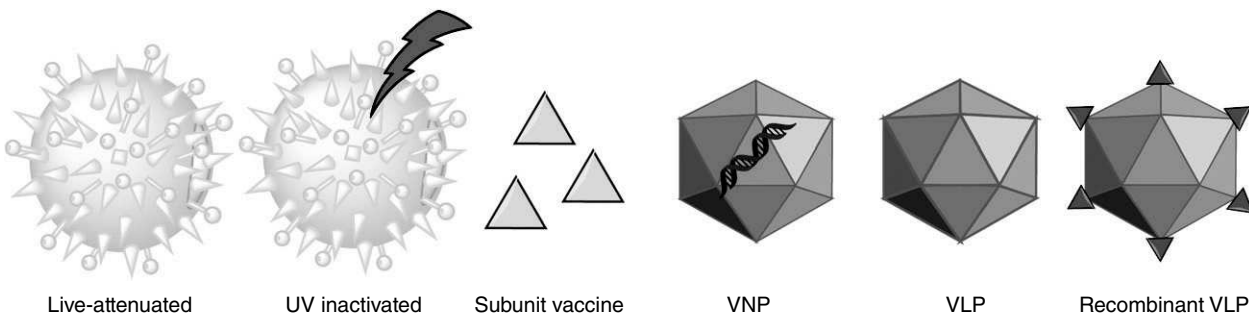


FIGURE 2 | Categories of viral vaccines; UV = ultraviolet; VNP = viral nanoparticle; VLP = virus-like particle.

CHEMICAL AND GENETIC ENGINEERING OF VIRUS-BASED SCAFFOLDS

Viruses comprise many identical copies of one or more coat proteins arranged in helical or icosahedral symmetry to form a capsid that encapsulates the genome. The structure of many virus capsids has been solved at atomic resolution, allowing site-specific modification and the multivalent display of antigenic epitopes on particular surface loops or the N/C-terminal region of the coat protein. Epitopes and/or other immunostimulatory molecules can be introduced by chemical engineering (bioconjugation) of particular residues (Figure 3) or genetic engineering of the coat protein sequence (Figure 4).

Chemical Conjugation Strategies

Antigenic peptide sequences can be added to a virus coat protein by chemical modification strategies that target 5 of the 20 naturally occurring amino acids: lysine (amine functional group), glutamic and aspartic acid (carboxylate functional group), cysteine (thiol functional group), and tyrosine (hydroxyl functional group). Lysine residues contain a highly nucleophilic amine that reacts with isothiocyanate or *N*-hydroxysuccinimide (NHS) esters. Amines can also be covalently attached to carboxylate groups through the formation of an amide (peptide) bond, facilitated by a carboxylate-selective coupling agent such as 1-ethyl-3-(3-dimethylaminopropyl)carbodiimide (EDC). Glutamic and aspartic acid residues contain carboxylate groups that can be modified using EDC to react with amine-functionalized peptides resulting in the formation of a stable amide bond, in the mirror image of the reaction described above. Cysteine residues contain thiol groups that can be reacted with haloacetyls or maleimides. Finally, tyrosine residues

contain a phenolic hydroxyl group, which can be modified using diazonium coupling strategies, although this is more complex than the other reactions listed above.

As well as these direct bioconjugation strategies, bifunctional linkers can be used to introduce additional functionalities that are not naturally found in virus coat proteins. Bio-orthogonal reactions, including ‘click chemistries’ such as Cu(I)-catalyzed azide-alkyne cycloaddition are particularly useful because the kinetics of the reaction are much more efficient than standard coupling. Ligation handles can be introduced via the biocoujugation of an azide or alkyne-NHS ester to a lysine side chain, or through the incorporation of non-natural amino acids *in vitro*. The diverse chemistries used to engineer viruses have been reviewed in detail.²⁵

Genetic Engineering Strategies

Unlike synthetic nanoparticles, VNPs can be modified not only chemically but also genetically, i.e., the nucleic acid sequence encoding the coat protein can be changed to exchange particular amino acids or introduce additional contiguous amino acids to form linear epitopes. Three major approaches are used to insert additional peptides into the virus coat protein, resulting in a coat protein fusion or chimera: direct fusion, linker fusion, and the ‘protein overcoat’ strategy. In the direct fusion approach, the foreign peptide is linked directly to the N-terminus^{26–28} or C-terminus^{28–31} of the coat protein or inserted into flexible surface loops presented on the capsid surface.^{29,32} Although the external surface is usually chosen for the presentation of native antigens recognized by B cells, the internal surface may be more suitable in some applications that involve the presentation of processed peptides.^{33,34} In contrast, linker fusion involves the inclusion of a short sequence of

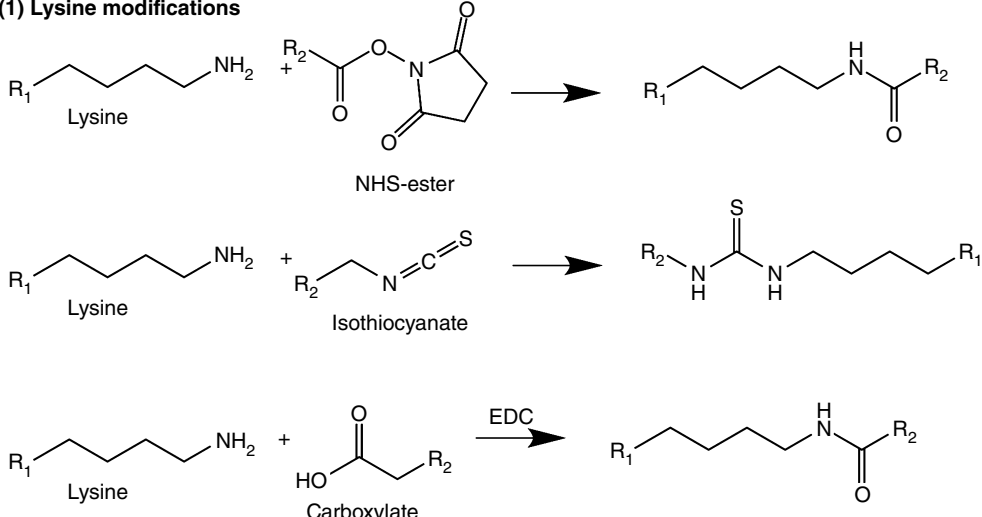
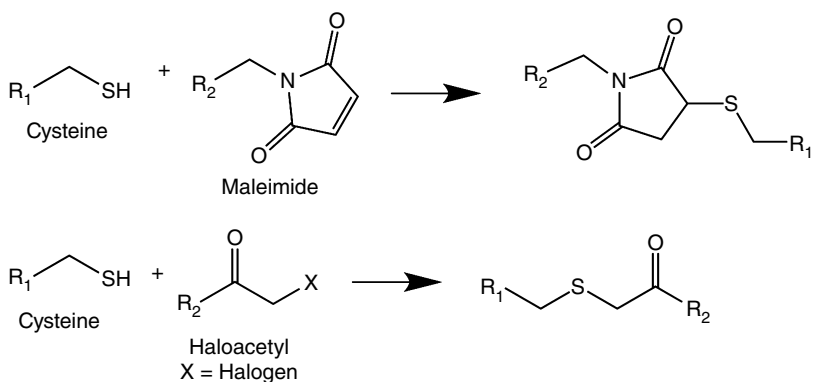
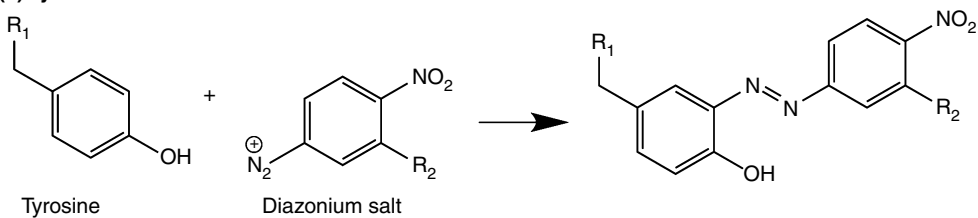
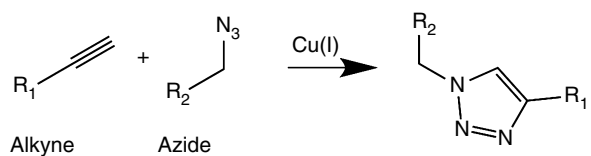
(1) Lysine modifications**(2) Cysteine modifications****(3) Tyrosine modifications****(4) "Click" chemistry**

FIGURE 3 | Chemical conjugation strategies (bioconjugation); NHS = N-hydroxysuccinimide; EDC = 1-Ethyl-3-(3-dimethylaminopropyl) carbodiimide.

amino acids (e.g., multiple glycine residues) between the foreign peptide and the end of the coat protein to allow flexibility. Finally, the ‘protein overcoat’ strategy places the *Foot and mouth disease virus* (FMDV)

2A sequence between the foreign peptide and coat protein sequences, causing an inconsistent ribosomal skip during translation. The outcome is a mixture of native coat proteins and fusion proteins, which is

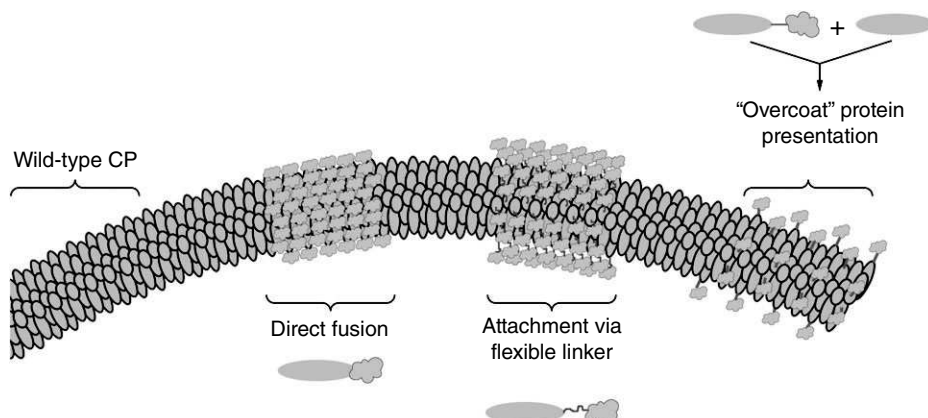


FIGURE 4 | Genetic engineering strategies for the display of epitopes on viral coat proteins.

useful if the inserted sequence is so large that its presence on every copy of the coat protein would prevent virus assembly.³⁵

VNP AND VLP VACCINES AND IMMUNOTHERAPIES

The first vaccines were developed against infectious diseases and likewise the first VLP and VNP vaccines were developed as strategies to contain the disease caused by the corresponding native form of the virus. However, as chemical and genetic engineering strategies have become more sophisticated, VLPs and VNPs have been adapted into platform technologies for the presentation of more diverse antigens, including abnormal self-proteins that can be used to treat chronic diseases and cancer. Several key vaccines based on VLPs or chimeric VNPs are summarized in Table 1.

Infectious Diseases

HIV

HIV (Figure 5) is unusual in that it primarily attacks the immune system and therefore destroys the very cells whose function is to neutralize it. By disabling the immune system, HIV not only achieves a successful infection but it also renders the body susceptible to other adventitious pathogens, i.e., acquired immunodeficiency syndrome (AIDS). There is no cure for HIV/AIDS. More than 35 million people are currently infected with HIV, two thirds of the infected population living in sub-Saharan Africa.⁹² The current best treatment option is highly active antiretroviral therapy, a cocktail of drugs consisting of a non-nucleoside reverse transcriptase inhibitor and two nucleoside analog reverse transcriptase inhibitors.⁹³

Early HIV vaccine candidates based on inactivated or attenuated viruses were ineffective or unsafe.^{94,95} More recent vaccine development strategies have focused on eliciting both humoral and cell-mediated responses targeting HIV envelope proteins.

Recombinant VLPs and VNPs displaying full-length HIV envelope proteins, individual glycoproteins, glycoprotein precursors or fragments thereof, include carriers such as *Flock House virus* (FHV),⁹⁶ *Hepatitis B virus* (HBV),⁹⁷ papillomaviruses,³⁷ bacteriophages Q β , AP205³⁶ and MS2,⁹⁸ and plant viruses such as *Tobacco mosaic virus* (TMV)^{99,100} and *Potato virus X* (PVX).²⁷ The membrane-proximal external region (MPER) of gp41 can be recognized and neutralized by monoclonal antibodies thus providing a good target for a vaccine candidate.³⁶ Accordingly, a set of gp41 peptides chemically conjugated to VLPs derived from phage AP205 elicited high-titer, peptide-specific antibodies in mice. Depending on the peptide, sera were able to neutralize a highly-sensitive laboratory strain of HIV-1 and a less-sensitive primary isolate, but not a clade C primary isolate. Some sera exhibited antibody-dependent cell-mediated cytotoxicity (ADCC) in infected cells, indicating that ADCC epitopes are most likely located in the distal region of gp41.³⁶ The highly conserved epitope of gp41 (ELDKWA) has been genetically fused to the N-terminus of PVX, among other platforms.^{27,101,102} Sera from mice immunized with these chimeric virus particles contained high IgG titers specific for HIV-1 MN gp160-derived synthetic peptide (H66), and were able to neutralize HIV-1. Additionally, human DCs pulsed with the vaccine triggered the proliferation of peripheral blood lymphocytes *in vivo*.²⁷ Multiple gp41 epitopes such as a trimeric recombinant gp41 (rgp41), which contains several conserved gp41 epitopes, were conjugated to influenza virosomes. Vaccinated

TABLE 1 | Key VLP/VNP-based Vaccines Approved or Under Development

Vaccine Target	Platform	Composition	Stage of Development	References
HIV	AP205	gp41 epitope	Animal studies	36
HIV	PVX	gp41 epitope	Animal studies	27
HIV	BPV-1	CCR5 peptide	Animal studies	37
HIV	Q β	CCR5 peptides	NHP studies	38
HIV	Canarypox	env, gag, pol genes + AIDSVAX (gp120)	Testing in humans	39–43
HIV/SIV	RABV	SIV envelope	Animal studies	44
HIV/SIV	Virosomes	gp41 epitopes	NHP studies	45
Ebola	Ebola	VP40 and GP	Animal studies	46,47
Ebola	Ebola	GP, NP, and VP40	NHP studies	48
Ebola	Ebola	EBOV Δ VP30	NHP studies	49
Ebola	rVSV	GP	Testing in humans	50
Ebola	RABV	GP	NHP Studies	51,52
Sudan virus and Marburg virus	RABV	GP	Animal studies	52
Influenza (pandemic)	Influenza	HA, NA, and M1 from H1N1	Animal studies	53
Influenza (pandemic)	Influenza	HA and NA from H7N9; M1 from H5N1	Animal studies	54
Influenza (pandemic)	Influenza	HA and NA from H1N1; M1 from H5N1	Testing in humans	55
Influenza (pandemic)	Influenza	H5 and H1	Testing in humans	56
Influenza (universal vaccine)	Influenza	HA, NA, and M1 from H5N1	Animal studies	57
Influenza (universal vaccine)	HBc	HA	Animal studies	58
Influenza (universal vaccine)	Dd	M1	Cell studies	59
Influenza (universal vaccine)	PapMV	M2e	Animal studies	60
Influenza (universal vaccine)	IBDV	HA and M2 from H1N1	Animal studies	61
Influenza (universal vaccine)	PapMV	NP	Animal studies	62
Influenza (universal vaccine)	PVX	NP	Animal studies	63
Influenza (universal vaccine)	P22	NP	Animal studies	34
Influenza (universal vaccine)	sHSP	n/a	Animal studies	64,65
Leukemia	TMV	TACA	Animal studies	66
Leukemia	Q β	TACA	Animal studies	67
Melanoma	TMV	p15e and Trp2	Animal studies	68
Lymphoma	PVX	Id	Animal studies	69
Ductal adenocarcinoma	BPV	MUC-1	Animal studies	70
HPV (prophylactic)	HPV-16, -18	L1	Clinically available	Cervarix®
HPV (prophylactic)	HPV-6, -11, -16, -18	L1	Clinically available	Gardasil®

TABLE 1 | Continued

Vaccine Target	Platform	Composition	Stage of Development	References
HPV (prophylactic)	MS2	L2 from HPV-16 and -31	Animal studies	71,72
HPV (prophylactic)	PP7	L2 from HPV-1, -16, and -18	Animal studies	72
HPV (prophylactic)	HPV-18 L1 VLP	L2 from HPV-18, -45, and -59	Animal studies	73
HPV (therapeutic)	HPV-16	E7	Testing in humans	74
HPV (therapeutic)	HPV-16 L1 VLP	E6 and E7	Animal studies	75
HBV (prophylactic)	HBV	HBsAg	Clinically available	Recombivax HB
HBV (therapeutic)	HBC	HBx-derived cytotoxic T lymphocyte epitopes and PADRE	Animal studies	76
HER-2 ⁺ breast cancer	IRIV	P4, P6, and P7	Testing in humans	77
HER-2 ⁺ breast cancer	Influenza	GPI-HER-2	Animal studies	78
HER-2 ⁺ breast cancer	MPyV	HER-2 _{1–683}	Animal studies	79
HER-2 ⁺ breast cancer	T7	p66	Animal studies	80
HER-2 ⁺ breast cancer	PVX	P4	Animal studies	81
Nicotine addiction	Qβ	Nicotine	Testing in humans	82
Nicotine addiction	dAd5	AM1	Animal studies	83
Cocaine addiction	dAd5	GNC	Animal studies	84
Cocaine addiction	dAd5	GNE	Animal studies	85
Hypertension	Qβ	Angiotensin II peptide (8 aa)	Testing in humans	28
Alzheimer's disease	HPV-16	Aβ peptides	Animal studies	86
Alzheimer's disease	Qβ	Aβ _{1–9}	Animal studies	86
Alzheimer's disease	Qβ	Aβ _{1–6}	Testing in humans	87,88
Alzheimer's disease	HBcΔ	Aβ _{1–15}	Animal studies	89
Alzheimer's disease	BPV1	Aβ _{1–9}	Animal studies	90

rhesus monkeys were challenged intravaginally 13 times with a heterologous simian HIV (SHIV). All subjects vaccinated through intramuscular or intranasal route were protected from challenge, whereas only 50% of the intramuscular-only group was protected.⁴⁵

Other HIV vaccine development approaches include the targeting of host cell receptors such as the C-C chemokine receptor CCR5 co-receptor used by macrophage strains of HIV-1.^{103–107} *Bovine papillomavirus* type 1 (BPV-1) VLPs were engineered to express CCR5 peptides. Vaccinated mice produced high antibody titers against CCR5, and functional studies demonstrated that sera displaced the native CCR5 ligand in a competition assay. Most importantly, sera from immunized mice neutralized HIV-1 in cells transfected with a human-mouse chimeric receptor of CCR5.³⁷ CCR5 peptides have also been conjugated to bacteriophage Qβ. Two peptides, representing the N-terminus (EC1) or second

extracellular loop (ECL2) of macaque CCR5 (mCCR5), were conjugated to Qβ and administered to rhesus macaques. Animals immunized with Qβ-EC1 and Qβ-ECL2 produced high titers of anti-CCR5 antibodies. When vaccinated animals were challenged with SIV, the viral load was lower than in nonvaccinated controls.³⁸

Another promising strategy is the combination of ALVAC-HIV, a vaccine based on *Canarypox virus* (vCP1521), and AIDSVAx (VaxGen), which consists of gp120 from two different HIV strains.^{39,43} Unlike the vaccines discussed above, the ALVAC *Canarypox virus* vector contains the HIV *env*, *gag*, and *pol* genes.⁴⁰ The two treatments were tested together in a clinical trial in Thailand (RV 144). Vaccinated subjects showed a 31% lower rate of HIV infection compared to the placebo group.⁴³ Despite this, ALVAC-HIV alone has shown promise as a pediatric HIV therapy involving infants born to HIV-positive mothers. Low levels of binding antibodies were

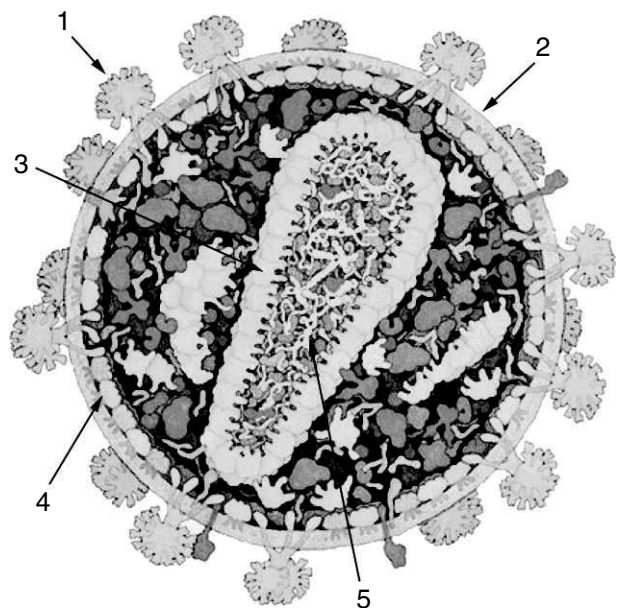


FIGURE 5 | Structure of HIV-1, with structural proteins in blue, viral enzymes in magenta, accessory proteins in green, and viral RNA in yellow. (1) Envelope glycoprotein spike, comprised of transmembrane glycoprotein gp41 and external envelope glycoprotein gp120; (2) lipid membrane; (3) capsid; (4) matrix; (5) viral RNA. (Adapted from Johnson GT, Goodsell DS, Autin L, Forli S, Sanner MF, Olson AJ. 3D molecular models for whole HIV-1 virions generated with cellPACK. Faraday Discuss 2014, 169:23-44 – Published by The Royal Society of Chemistry)

detected in one subject as expected because the subjects did not receive a gp120 boost.⁴⁰ The addition of recombinant glycoprotein subunit vaccine (rgp120) to ALVAC-HIV resulted in higher levels of HIV-specific serum antibodies in infants that were distinguishable from maternal antibodies. Additionally, 50% of subjects who received both ALVAC-HIV and rgp120 generated neutralizing antibodies against homologous strains of HIV.⁴¹

Ebola Virus Disease and Related Diseases

Ebola virus disease is caused by four different filoviruses of the genus *Ebolavirus*: *Bundibugyo ebolavirus*, *Sudan ebolavirus*, *Tai Forest ebolavirus*, and the eponymous *Ebola virus* (formerly *Zaire ebolavirus*) which is the most dangerous and prolific (Figure 6). The ease of infection^{108,109} and lack of clinically approved treatment produces mortality rates of up to 90%.¹¹⁰

VLP/VNP vaccines against *Ebola virus* are currently in the development pipeline, using either complete Ebola VLPs or specific components such as the viral matrix protein (VP40), nucleoprotein (NP), and

glycoprotein (GP) displayed on other viruses. Recombinant VLPs containing *Ebola virus* VP40 and GP were constructed using a baculovirus system. The VLPs yielded high levels of GP-specific antibodies in mice, particularly the IgG2a subtype which is needed to achieve protective immunity. Additionally, VLPs induced the secretion of IL-6, IL-10, IL-12, and TNF α from DCs, confirming their adjuvant and immunostimulatory properties. Serum from vaccinated mice was also able to block the infection of JC53 cells by a pseudotyped virus.⁴⁷ The immunization of rodents with VLPs comprising the viral envelope (including GP, NP, and VP40) has also conferred protection against Ebola challenge.⁴⁸ Furthermore, immunized cynomolgus macaques were completely protected when challenged with *Ebola virus*.⁴⁸ VLPs based on recombinant *Vesicular stomatitis virus* (rVSV) expressing *Ebola virus* glycoproteins were shown to protect mice and nonhuman primates against a lethal challenge with homologous *Ebola virus* after a single injection.^{111,112} Post-exposure protection was also conferred.¹¹³ The rVSV-EBOV vaccine showed a good safety profile in nonhuman primates and pigs^{114,115} and was able to prevent the disease when administered during an outbreak in a ring vaccination strategy.⁵⁰

Other examples include the application of an inactivated *Rabies virus* fused to *Ebola virus* GP (INAC-RV-GP) resulting in a strong, multivalent humoral response against both viruses in mice and nonhuman primates, protecting the animals against both diseases.^{51,116} The titer of neutralizing antibodies was increased further by the addition of an adjuvant and resulted in 100% protection from a lethal challenge.⁵² The inactivated *Rabies virus* platform has also been expanded to express the GP from other filoviruses, including *Sudan ebolavirus* and *Marburg virus*.⁵²

Influenzavirus

Seasonal influenza epidemics cause up to 500,000 deaths every year^{117–119} as well as regular pandemics, which can result in millions of deaths in a relatively short time span.^{118,120} Seasonal influenza epidemics are typically caused by human influenza viruses (Figure 7) that have acquired mutations, whereas pandemics occur when the influenza viruses cross species barriers.^{121,122} Seasonal vaccines are typically based on whole-inactivated viruses or live-attenuated viruses, both of which achieve good protection and significantly improve public health.¹²³ However, these vaccines are based on hemagglutinin (HA) and neuraminidase (NA), the major targets of the immune system.¹²³ Epitopes on both proteins are

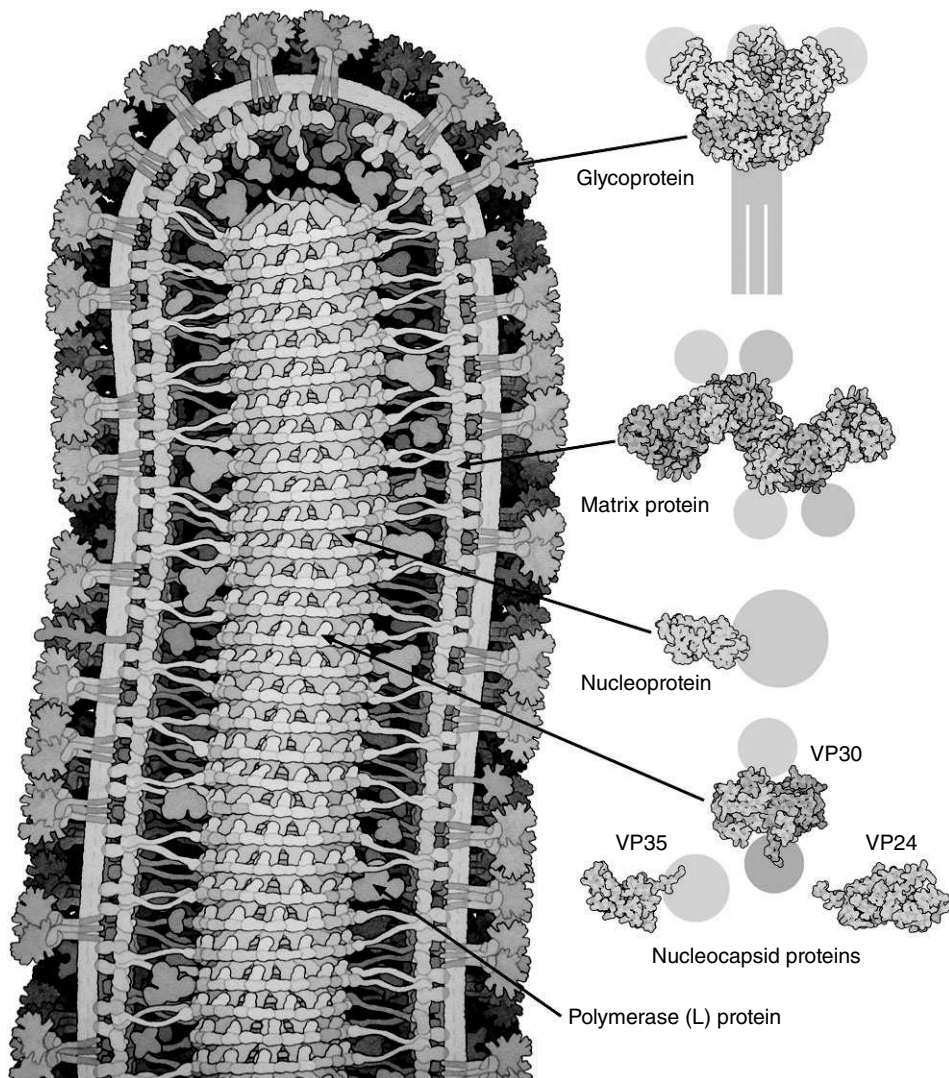


FIGURE 6 | Structure of *Ebola virus* (Courtesy of David S. Goodsell and RCSB PDB).

highly prone to genetic drift, leading to the rapid emergence of influenza strains that are not genetically similar to the strains covered by the vaccine.^{53,124–126} Seasonal vaccines must therefore be updated every year, and vaccines against pandemic strains must be developed in response to the pathogen, a reactive strategy that places millions of people at risk. Preclinical and clinical research has focused on the development of a proactive universal influenza vaccine based on more conserved epitopes such as the matrix proteins (M1 and M2) and NP.^{127,128} Other strategies include the development of multivalent VLPs with HA and/or NA epitopes from diverse strains, combined with immunostimulatory molecules.

Recombinant influenza virus VLPs based on HA, NA, and M1 have recently been used to develop

heterotypic vaccines.^{53–55,57} Studies in mice and ferrets indicate that H1N1 VLP vaccination protects against challenges with the homologous subtype (H1N1) as well as a heterologous subtype (H5N1), and intranasal administration elicited higher IgG and IgA titers than intramuscular vaccination.⁵³ These VLP vaccines were well-tolerated in a phase II study.⁵⁵ Other VLPs have been developed based on the highly pathogenic avian influenza (HPAI) H5N1 and avian-origin influenza A (H7N9).^{54,57} The H5N1 VLP was composed of HA, NA, and M1 from H5N1, whereas the H7N9 vaccine was composed of HA and NA from H7N9 and M1 from H5N1.^{54,57} Mice vaccinated with H5N1 VLPs were challenged with homologous or heterologous (H5N8) strains and all survived. Ferrets immunized with H7N9 VLPs plus adjuvant produced high titers of H7N9-

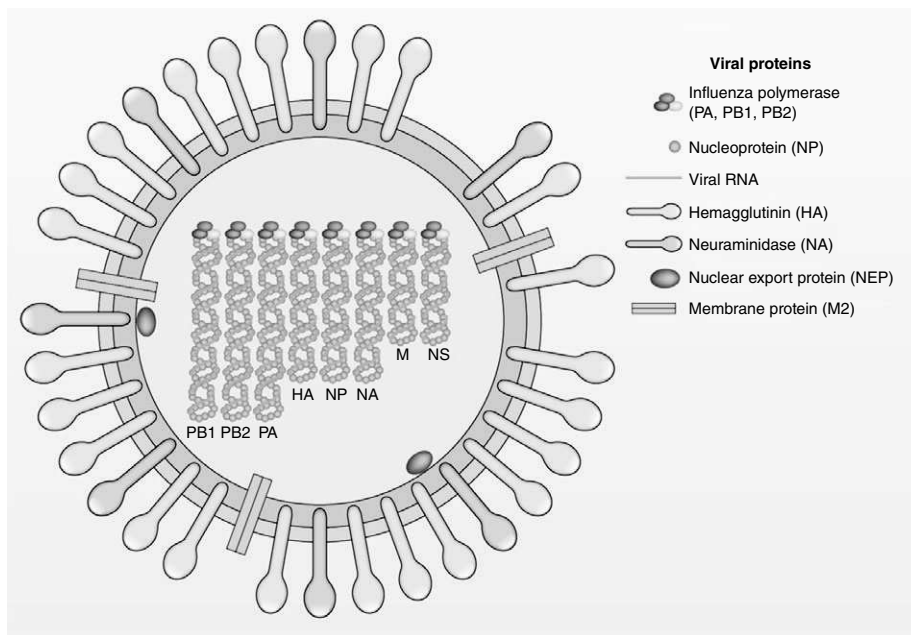


FIGURE 7 | Structure of influenza A virus. Three viral proteins are on the outer surface of virus particles: haemagglutinin (HA), neuraminidase (NA), and M2. Influenza virus matrix protein M1 associates inside the membrane, and the viral genome is packaged into the particle as a ribonucleoprotein in complex with nucleocapsid protein (NP) and viral polymerases (PA, PB1, PB2). (From Tao YJ, Zheng W. Visualizing the Influenza Genome. *Science* 2012; 338: 1545–1546. Reprinted with permission from AAAS.)

specific neutralizing antibodies, and viral loads in the lungs and viral shedding were both reduced compared to controls.⁵⁴

Influenzavirus epitopes have also been expressed on the surface of VLPs based on HPV core protein (HBc),⁵⁸ *Infectious bursal disease virus* (IBDV),⁶¹ PVX,⁶³ *Papaya mosaic virus* (PapMV),^{60,62} Adenovirus,⁵⁹ and *Simian virus 40* (SV40).¹²⁹ Several of these platforms were used to display HA, NA, and matrix proteins, similar to the influenza virus VLPs.

Influenza vaccines can also be developed to promote the formation of inducible bronchus-associated lymphoid tissue (iBALT), which plays a role in adaptive immunity in the lungs, similar to the role of the spleen in primary adaptive immunity.¹³⁰ Small heat shock protein (sHSP) cages are structurally similar to VLPs, and when administered to the lung they promote the formation of iBALT, which includes B cells, follicular DCs, and CD4⁺ and CD8⁺ T cells. Mice treated with sHSP cages were protected from primary influenza virus infection, as well as from a secondary infection from a different strain of the virus.⁶⁵ The sHSP cages also induced antibody class-switching when mice were challenged with influenza virus, increasing the amount of IgA and IgG present in the lung.⁶⁴

Seasonal influenza vaccines are usually produced in eggs, or in avian or mammalian cell cultures. However, pandemic strains that develop when viruses cross the species barrier (particularly the avian-to-human barrier) are more difficult to produce in avian cells and alternative production platforms are required. One particularly attractive option is to produce the influenza virus VLPs in plants. The H5 and H1 proteins have each been successfully expressed in *Nicotiana benthamiana* plants and can self-assemble into VLPs. The molecular farming of VLPs has several advantages: in planta production greatly reduces the risks associated with human viruses because plants do not support the replication of human viruses, and the process is highly scalable. For example, Figure 8 shows the Medicago production facility. Mice immunized with plant-derived H5-VLPs were protected from homologous and heterologous viral challenge.¹³¹ Furthermore, when the plant-derived VLPs were tested in a phase I clinical trial, none of the subjects developed allergy or hypersensitivity symptoms, and the IgG and IgE responses to plant-derived epitopes returned to baseline after 6 months. Additionally, there was no IgE response to the glycan motif MMXF, which is associated with allergenicity,⁵⁶ confirming the safety profile of the vaccine.



FIGURE 8 | Production facility at Medicago. The photograph was provided by courtesy of Medicago Inc.

Cancer

Cancer is one of the leading causes of death worldwide, with 14 million new cases diagnosed every year and over 8 million cancer-related deaths. Although cancer includes a diverse spectrum of diseases with different causes, sites of origin, and clinical outcomes, they are all defined by six hallmarks: sustained proliferative signaling, evasion of growth suppressors, promotion of invasion and metastasis, limitless replicative potential, induction of angiogenesis, and resistance to programmed cell death.¹³² Some cancers are caused by viral infections and can thus be prevented with vaccines. The first VLP vaccine offering protection against a cancer-causing virus (*Hepatitis B virus*, HBV) was approved in 1981 for infants. Two vaccines against *Human papillomavirus* (HPV) have been approved more recently for the prevention of cervical cancer, or oropharyngeal cancers. In addition to these FDA-approved vaccines, numerous VLP vaccine candidates are being investigated for the prevention or treatment of lymphoma, leukemia, melanoma, and breast cancer.

VLP-based cancer vaccines can also be developed to enhance the tumor-antigen-specific T-cell response and elicit antibodies against tumor-specific surface antigens. In addition to papillomaviruses,⁷⁰ such vaccines have been developed using bacteriophages⁶⁷ and plant viruses^{66,68,69} as delivery platforms because the native viruses do not infect or replicate in human cells so the virus genome can be left intact. The coat proteins of TMV and

bacteriophage Q β have been modified to present the tumor-associated carbohydrate antigen (TACA), which normally has low immunogenicity. TMV-TACA generated much higher titers of antigen-specific antibodies than the soluble form of the antigen, whereas Q β -TACA elicited a stronger humoral response to the TACA than the soluble form or TACA attached to other nanoparticles.⁶⁷ The resulting IgG antibodies also reacted strongly *in vitro* against cells expressing the antigen.⁶⁷

Tolerance against self-peptides with low immunogenicity can be broken using VLP/VNP-based immunotherapy platforms. For example, the immunogenicity of melanoma T-cell epitopes p15e and tyrosinase-related protein-2 (Trp2) can be increased by presenting them together on a single bivalent TMV particle, improving cellular immunity and conferring protection against tumor challenge.⁶⁸ PVX has been modified with the idiotypic (Id) immunoglobulin from B-cell lymphomas, a weak tumor antigen. When administered to mice, Id-PVX induced high titers of anti-Id antibodies, which prolonged survival after lymphoma challenge.⁶⁹

In addition to traditional vaccines using VLP/VNP-based platforms, recent work has investigated the use of *in situ* vaccination to manipulate identified tumors to counteract local immunosuppression, resulting in systemic anti-tumor immunity. We have shown that VLPs from the cowpea mosaic virus (CPMV) devoid of RNA, LPS, or any other recognized immune adjuvant, stimulate a potent immune-

mediated anti-tumor response when introduced into the tumor microenvironment after tumor establishment. Efficacy was demonstrated in the setting of primary tumors and metastatic disseminated disease using mouse models of melanoma, breast, ovarian, and colon cancer. Importantly, the resulting effect was systemic and durable, resulting in immune-memory that protected mice from re-challenge.¹³³

The FDA-approved vaccines for HPV are based on papillomavirus VLPs. However, these VLPs can also be modified to express other tumor antigens, such as human mucin-1 (MUC-1), which is a marker of ductal adenocarcinoma. BPV-1 particles modified with a MUC-1 epitope were administered to mice, which were later challenged with a MUC-1⁺ lymphoma cell line. T cells were strongly induced in the vaccinated mice and their tumors grew more slowly, resulting in a smaller tumor mass at the end of the study.⁷⁰ We will consider HPV vaccines and hepatocellular carcinoma vaccines in more detail in the following sections because commercial vaccines are already available. We will also discuss HER-2⁺ breast cancer vaccines.

Prophylactic Vaccines to Protect Against Cervical Cancer Caused by HPV

Cervical cancer is the fourth most common cancer in women and more than 500,000 new cases are diagnosed each year.^{134,135} HPV, usually sexually transmitted, is implicated in 90% of cervical cancers.^{136,137} Among more than 150 known strains of HPV, up to 20 are designated high-risk because they cause almost all cervical cancers.¹³⁸ The two highest-risk strains are HPV-16 and HPV-18, which are responsible for 70% of all cases.^{139,140} There are currently two FDA-approved prophylactic vaccines for HPV: a bivalent vaccine (Cervarix) that protects against strains 16 and 18, and a quadrivalent vaccine (Gardasil) that protects against strains 6, 11, 16, and 18. Both vaccines are based on VLPs composed of the HPV L1 coat protein (Figure 9)⁷¹ combined with adjuvants to further boost the immune system. Both vaccines have proven efficacious after a three-dose schedule. However, the L1 protein is not conserved across all serotypes, so these vaccines only offer protection against the specific serotypes within each formulation.^{141–143}

The development of VLPs based on the more conserved L2 coat protein would offer increased cross-protection against multiple serotypes, and the next generation of HPV vaccines is likely to be based on this principle.⁷² L2 is naturally shielded from the immune system¹⁴⁴ but vaccination with L2 can nevertheless protect against a range of HPV

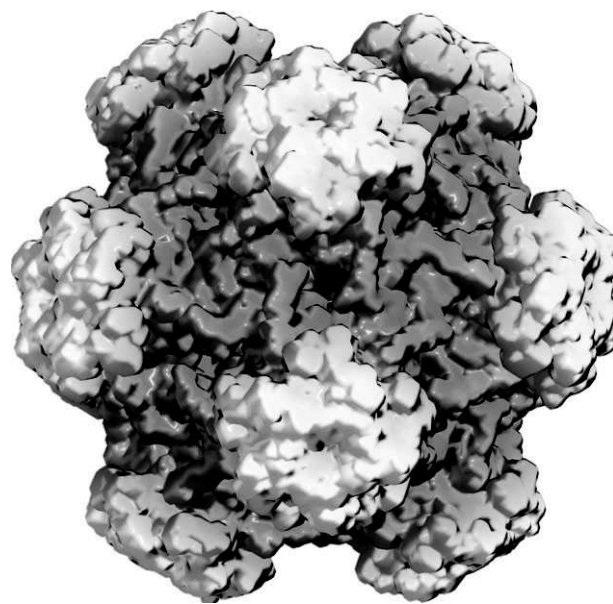


FIGURE 9 | Human papillomavirus 16L1 capsid (viperdb.scripps.edu).

serotypes.^{145–147} The first vaccines based on L2 were limited in efficacy by low antibody titers and the need to sufficiently protect against all high-risk serotypes^{148,149} so VLPs have been considered as a strategy to overcome these limitations.

Bacteriophage MS2 has been used to express L2 epitopes from HPV strains 16 and 31, individually or as a bivalent formulation. MS2-16 L2 was previously shown to confer protection against 11 HPV serotypes but not HPV31.⁷¹ Mice immunized with the individual constructs (MS2-16 L2 or MS2-31 L2) were protected against some strains, whereas the bivalent formulation (MS2-16/31 L2) elicited high antibody titers across a panel of HPV serotypes and strongly neutralized all HPV pseudoviruses.⁷² In a complementary approach, bacteriophage PP7 was modified to express L2 from HPV strains 16 and 18 (which are closely related) and 1 (which is more distant) individually and in pairwise combinations (PP7-18 L2, PP7-18/1 L2, and PP7-16/18 L2). Mice immunized with PP7-18/1 L2 only produced antibodies against HPV1 peptides, whereas PP7-18/16 L2 elicited antibodies that bound strongly to HPV16 and HPV18, as well as HPV1, HPV5, and HPV6. Only mice vaccinated with PP7-18/16 L2 were able to neutralize an HPV-6 pseudovirus, a heterologous serotype.⁷²

The high-risk HPV strains 18, 45, and 59 have been targeted by inserting a cross-neutralizing epitope from HPV45 L2 into a surface loop of HPV18 L1 and creating VLPs from the chimeric construct

(18 L1-45RG1). L2-specific antibodies from vaccinated rabbits reacted against HPV strains 39, 45, 68, and 70 (which are members of the same clade as HPV45 and HPV18). Additionally, when mice were passively immunized with immune sera from rabbits, they were protected against a challenge with HPV strains 18, 39, 45, and 68.⁷³

Vaccines to Treat Cancers Caused by HPV

Although prophylactic vaccines have been successful, they are unable to treat established tumors. The development of HPV therapeutic vaccines has focused on the E6 and E7 oncoproteins, which are necessary for tumor development and are expressed in all cervical cancer cells.¹⁵⁰ For example, HPV16L1 was genetically modified to express the HPV16 E7 protein. In mice, these recombinant VLPs induced L1-specific antibodies, as well as cytotoxic T cells that recognized L1 and E7.^{151–154} In a phase I trial, patients with proven ectocervical CIN 2/3 lesions who were also HPV16 mono-infected, were treated with HPV16L1E7 VLPs. Approximately 50% of vaccinated patients exhibited a 50% reduction in lesion size following the final vaccination.⁷⁴ Further improvements of this therapeutic strategy include the incorporation of T-cell epitopes from HPV16 E6 and E7. Preclinical studies in mice showed an 85% reduction in tumor size when immunized with such recombinant VLPs.⁷⁵

Vaccines Targeting Hepatocellular Carcinoma Caused by HBV

Liver cancer causes 600,000 deaths per year and there are 700,000 new cases, approximately 500,000 of whom are male, making it the fourth most common form of cancer in men.¹³⁴ Among these cases, 95% are classified as hepatocellular carcinoma,¹⁵⁵ which is associated with risk factors such as alcoholism, hepatitis B, hepatitis C, and liver cirrhosis.^{156,157} HBV (Figure 10) is responsible for about 50% of all primary hepatocellular carcinomas. A vaccine against HBV has been available since 1981, and is on the WHO's List of Essential Medicines. This vaccine is a VLP comprising the HBV surface antigen (HBsAg), which is administered as two or three injections within one year. The vaccine provides lasting immunity against HBV by producing anti-HBV antibodies.^{158,159}

The prophylactic HBV vaccine has greatly reduced the incidence of hepatocellular carcinoma but a therapeutic vaccine is needed to treat established disease. One of the key targets is the HBV X protein (HBx), a regulatory protein that promotes carcinogenesis and is expressed at high levels in

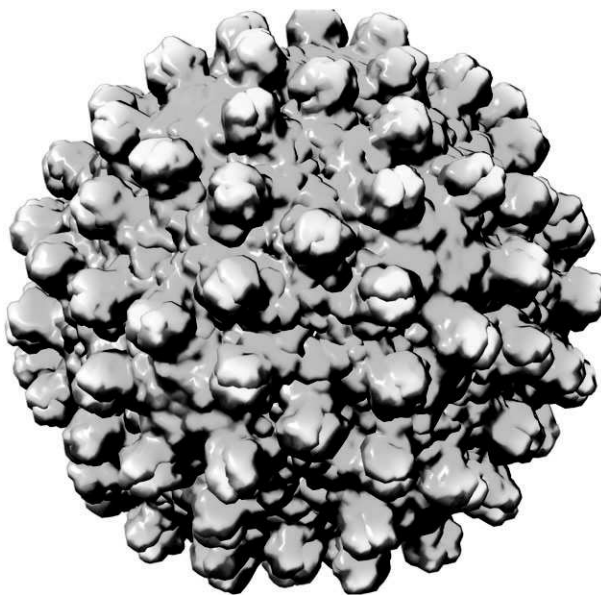


FIGURE 10 | Human *Hepatitis B* virus (viperdb.scripps.edu).

hepatocellular carcinoma.^{76,160} The HBc has therefore been genetically modified to express dominant HBx-derived cytotoxic T-cell epitopes, as well as the universal Th-cell epitope, pan-HLA DR-binding epitope (PADRE). These chimeric proteins self-assemble into VLPs, and mice vaccinated with this formulation inhibited tumor growth up to 30 days after tumor challenge, while also eliciting a strong T-cell response.⁷⁶

Vaccines Targeting HER-2⁺ Breast Cancer

Breast cancer is the most common form of cancer in women, as well as a minor form of cancer in men, with over one million cases diagnosed each year.¹³⁴ There are five molecular subtypes of breast cancer: normal-like, luminal A, luminal B, HER-2⁺, and triple negative.¹⁶¹ Each is defined by the expression of different receptors and the prognosis varies accordingly. HER-2⁺ tumors overexpress HER-2/neu/ERBb2. They do not express hormone receptors and they are associated with aggressive tumors, high rates of metastasis, and an overall poor prognosis.¹⁶² FDA-approved treatments include the HER2-specific antibodies trastuzumab and pertuzumab, which are used for passive immunotherapy and require repetitive administration.^{163,164} Passive immunization requires prolonged therapeutic delivery, cannot be developed as a prophylactic, and does not induce cellular immune responses.^{77,78} To overcome these challenges, HER-2⁺ breast cancer research is now focused on active immunotherapy that elicits long-lasting cellular and humoral responses.

VLPs that display full-length HER-2 or specific immunogenic epitopes have been tested in clinical trials.^{77–81} Peptides derived from the extracellular domain of HER-2 were incorporated into immunopotentiating reconstituted influenza virus virosomes (IRIVs).^{165–167} Three immunogenic peptides that are known to elicit B cell responses were tested: P4 (378–394), P6 (545–560), and P7 (610–623).¹⁶⁸ The clinical trial revealed that 80% of vaccinated patients produced peptide-specific antibodies, and HER-2-specific IgG was elicited in 70% of the patients after immunization. A cellular immune response was also observed following vaccination, involving the increased secretion of IL-2, TNF α , and IFN γ .⁷⁷ In a different approach, enveloped influenza virus VLPs were modified to incorporate glycosylphosphatidylinositol (GPI)-anchored HER-2 (GPI-HER-2-VLP). Preclinical studies showed strong anti-D2F2/E2 (HER-2 $^+$) serum IgG responses in mice, with comparable levels of IgG1, IgG2a, and IgG2b in the serum of vaccinated animals, indicating a balanced Th1 and Th2 response. In contrast, the vaccination of mice with soluble GPI-HER-2 predominantly elicited a Th2 response, whereas Th1-biased responses are needed to induce a potent anti-tumor reaction. When mice were challenged with HER-2 $^+$ cells, those vaccinated with GPI-HER-2 VLPs showed a slower tumor growth rate compared to those administered GPI-HER-2 alone. Sixty-seven percent of the mice vaccinated with GPI-HER-2 VLPs remained tumor free.⁷⁸

VLPs have also been genetically modified to express HER-2 peptides. The internal face of the murine polyomavirus (MPyV) major capsid protein (VP1) can bind to the minor capsid protein (VP2).¹⁶⁹ VP2 was genetically modified to express the N-terminal domain of HER-2, which contains the extracellular and transmembrane domains (VP2Her $_{2-683}$). VP1 and VP2Her $_{2-683}$ were produced in a baculovirus vector to obtain Her2 $_{1-683}$ PyVLPs. Immunized mice were challenged with HER-2 $^+$ D2F2/E2 cells, and 87% of the vaccinated mice did not develop tumors. Similar results were obtained using transgenic BALB-neuT mice, which overexpress the rat HER-2 oncogene. The mice did not produce HER-2-specific antibodies, but did induce HER-2-specific T cells.⁷⁹

A T7 bacteriophage was genetically modified to express a H-2k d -restricted cytotoxic T lymphocyte (CTL) epitope (p66) derived from rat HER-2 to investigate whether a CTL response is required for cancer immunotherapy. Preclinical studies showed that splenocytes from mice immunized with T7-p66 produced a higher IFN γ response than controls. Interestingly, splenocytes from mice vaccinated with

a mixture of unconjugated T7 and p66 did not yield a strong IFN γ response when challenged with p66, indicating that the CTL peptide must be attached to T7 in order to elicit the CTL response. Splenocytes from mice vaccinated with T7-p66 were also able to lyse target cells pulsed with p66-peptide *in vitro*. Healthy mice vaccinated with T7-p66 rejected HER-2 $^+$ TUBO cells, with five of the six mice remaining tumor-free 42 days after challenge. Furthermore, therapeutic vaccination with T7-p66 slowed the growth of pre-implanted tumors, eventually resulting in the full regression of HER-2 $^+$ tumors.⁸⁰

We have recently worked on the development of a HER-2 $^+$ breast cancer vaccine using the plant virus PVX. The chemical conjugation of PVX with the P4 B-cell epitope, which contains amino acids 387–394 from the extracellular domain of HER-2, elicited higher titers of HER-2-specific antibodies in mice than soluble P4 alone. These antibodies selectively recognized HER-2 $^+$ breast cancer cells.⁸¹

Addiction (cocaine and nicotine)

Addictive substances, such as nicotine and cocaine (Figure 11), affect the body by interacting with the nervous system. Nicotine and cocaine both modulate dopamine levels in the brain, thereby affecting the reward pathway. Vaccines against these addictive substances can help to reduce the severity of withdrawal symptoms and prevent relapse. However, small molecules tend to have low immunogenicity, so VLP platform technologies are required to elicit potent and long-lasting immune responses against the drugs.^{170–172} VLPs displaying nicotine or cocaine as multivalent arrays have been shown to elicit potent humoral responses, yielding drug-specific antibodies that prevent the substances from crossing the blood–brain barrier to exert their effects.^{173–175} Nicotine is the addictive component of tobacco, and tobacco use is the leading preventable cause of disease, disability, and death in the industrialized world.¹⁷³ Several vaccines against nicotine are currently undergoing clinical trials, including NicVaxTM, NIC002, SEL-068, Ta-NIC, and IP18-KLH, but

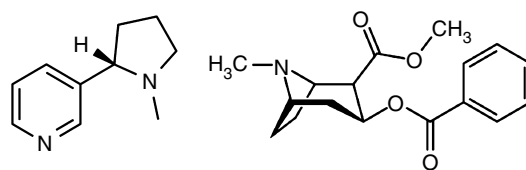


FIGURE 11 | Chemical structures of nicotine (left) and cocaine (right).

similar approaches are also under development for cocaine addiction.

NIC002 is a VLP vaccine in which bacteriophage Q β is chemically modified to display nicotine (NicQb).^{82,173,175} Preclinical studies in mice demonstrated the development of nicotine-specific antibodies.¹⁷³ Importantly, when challenged with nicotine, vaccinated mice showed a higher concentration of nicotine remaining in the blood and a corresponding reduction of nicotine levels in the brain, compared to nonvaccinated mice.¹⁷³ In phase I trials, NicQb was immunogenic, well tolerated and efficacious in patients with high antibody titers.⁸² In an alternative approach, a nicotine analog was chemically linked to disrupted serotype-5 adenovirus (dAd5). The dAd5 VLP lacks the E1 and E3 proteins, allowing the particle to circumvent any pre-existing Ad5 immunity, which is prevalent in the population.⁸³ Sera from vaccinated mice contained high titers of anti-nicotine antibodies for a prolonged duration, resulting in lower concentrations of nicotine in the brain than naïve mice, inversely related to the levels of nicotine in the serum.⁸³

The dAd5 VLP has also been conjugated with the cocaine analog. Vaccinated mice challenged with cocaine were found to have 41% less cocaine in the brain than naïve mice. Locomotor activity in vaccinated mice challenged with cocaine was the same as in nonchallenged mice treated with PBS, confirming that the vaccine reduced the cognitive impact of cocaine.⁸⁴ Similar strategies are being developed using alternative cocaine haptens.⁸⁵

Chronic Diseases

Chronic diseases are persistent or even life-long conditions that require regular therapeutic intervention as a form of disease management. The prevalence of chronic diseases is increasing globally due to the aging population and various dietary and lifestyle factors, which means that such diseases represent a significant and increasing public health burden in almost every country. Where chronic diseases are caused by malfunctioning self-proteins, vaccination can be used to induce the generation of autoantibodies. This approach has been tested in numerous disease models, including rheumatoid arthritis,^{176–181} osteoporosis,^{178,182} experimental autoimmune encephalitis,¹⁸⁰ myocarditis,¹⁸³ and obesity.¹⁸⁴ Many of these diseases are currently treated by passive immunotherapy, i.e., the regular administration of therapeutic antibodies targeting pathogenic self-proteins, which is expensive and restricts the patient. We will discuss hypertension and Alzheimer's disease as

case studies for the alternative active immunization approach. The reader is recommended to consult further review articles for information about the development of vaccines against other chronic diseases.^{185–187}

Hypertension

Hypertension (high blood pressure) is an underlying risk factor that promotes the development of cardiovascular disease, which can lead to life threatening events such as heart attack and stroke. Although hypertension can be regulated with drugs, many hypertensive individuals never receive a diagnosis and therapeutic compliance tends to be poor even in diagnosed hypertensive patients. Another risk factor is the so-called morning pressure surge, a steep increase in blood pressure prior to waking, before medication can be taken. Active immunotherapy could overcome many of these challenges by inducing long-lasting immune responses targeting key regulators of blood pressure.

Angiotensin I and II could be the first targets of hypertension immunotherapy. These are small, soluble regulatory peptides (10 and 8 amino acids in length, respectively) which do not elicit a strong immune response in their native state. As described above, the immunogenicity of small molecules can be increased by exploiting VLP technology. A vaccine candidate has therefore been developed in which angiotensin II is chemically coupled to bacteriophage Q β VLPs (AngQb). Preclinical studies in a rat model of hypertension showed that vaccination produced high titers of angiotensin II-specific IgGs and resulted in the normalization of blood pressure.¹⁸⁸ In clinical trials, the AngQb vaccine was well tolerated and no serious adverse effects were observed. The immunization of patients with mild to moderate hypertension reduced blood pressure during the daytime and especially in the early morning.¹⁸⁹

Alzheimer's Disease

Alzheimer's disease is a neurodegenerative disorder characterized by a decline in cognitive ability accompanied by neuropathological features such as the loss of neurons in the hippocampus and neocortex and the accumulation of intracellular and extracellular protein deposits.¹⁹⁰ Extracellular protein deposits (amyloid plaques) contain the amyloid- β (A β) peptide, which is 42 amino acids in length.^{191,192} Previous reports have shown that immunization with the A β peptide reduced the deposition of amyloid plaques in transgenic mouse models.¹⁹³ Furthermore, passive immunization with A β antibodies had a similar effect.¹⁹⁴ However, a clinical trial (AN1792)

using synthetic A β peptides for immunization showed minimal efficacy and was stopped after meningoencephalitis was reported in 6% of the subjects.¹⁹⁵ This unanticipated effect was attributed to a T-cell-mediated autoimmune response caused by the adjuvant QS21.^{195–197} The safety of A β -derived immunotherapies could therefore be improved by triggering a predominantly Th2-based immune response by delivering only B-cell epitopes, which are found on the N-terminus of the A β peptide.^{198,199} VLPs based on HPV, bacteriophage Q β , HBc, and BPV-1 have already been used to display A β peptides.^{86,89,90}

HPV-16 displaying A β peptides such as full-length A β (A $\beta_{1–40}$), N-terminal A β (A $\beta_{1–9}$ and A $\beta_{1–16}$), mid-domain A β (A $\beta_{12–28}$), and C-terminal A β (A $\beta_{17–40}$) have been tested as vaccines. HPV-A $\beta_{1–40}$ elicited IgG responses without the use of Freund's adjuvant in mice, whereas free A $\beta_{1–40}$ required Freund's adjuvant to achieve comparable titers. HPV conjugated to peptides from the N-terminal domain of A β elicited higher antibody titers than HPV conjugated to peptides from either the mid or C-terminal domains, indicating that N-terminal A β peptides are the most immunogenic when presented on HPV particles. Importantly, these antibodies were predominantly of subtype IgG1, indicating a Th2-biased immune response.⁸⁶

A β peptides have been directly conjugated to bacteriophage Q β . The N-terminal modified peptide (A $\beta_{1–9}$) with a C-terminal –GGC linker was conjugated to the bacteriophage using a bifunctional linker with both amine and sulfhydryl reactive arms (SMPH). Mice immunized with Q β -A $\beta_{1–9}$ VLPs without adjuvant produced higher titers of antibodies than those immunized with HPV-A $\beta_{1–9}$ and similar titers to those immunized with HPV-A β_{40} . The inclusion of incomplete Freund's adjuvant increased the IgG titers even further.⁸⁶

Bacteriophage Q β has also been conjugated with A $\beta_{1–6}$, which is shorter than the typical T-cell epitope. Mice were immunized three times with Q β -A $\beta_{1–6}$ and did not activate A β -specific T cells. Additionally, mice immunized with Q β -A $\beta_{1–6}$ produced high antibody titers against the A β peptide and formed fewer plaques than control mice.²⁰⁰ Q β -A $\beta_{1–6}$ was tested in a phase I trial (CAD106) and was deemed safe and tolerable in a double-blind, placebo-controlled, 52-week study. Importantly, no subjects recorded clinical or subclinical cases of meningoencephalitis, which halted the previous Alzheimer's disease immunotherapy clinical trial.⁸⁸ In a phase II trial, CAD106 was administered to 47 patients with Alzheimer's disease ($n = 11$ for placebo). The

patients received three subcutaneous or intramuscular doses of CAD106, followed by four additional subcutaneous or intramuscular injections. Long-term treatment induced prolonged high titers of A β -specific antibodies suggesting that CAD106, which recently entered phase III trials, could be developed into an effective immunotherapy for Alzheimer's disease.⁸⁷

A C-terminally truncated version of the HBc protein (HBc Δ) was genetically modified to include two copies of A $\beta_{1–15}$ in the MIR (A β -HBc).⁸⁹ The MIR was chosen because epitopes inserted there tend to be highly antigenic and immunogenic compared to other insertion sites.²⁰¹ Preclinical studies in mice showed that anti-A β antibodies, predominantly IgG1 and IgG2b subtypes (indicating a Th2-biased immune response) were generated. Free A β peptide with adjuvant also elicited high antibody titers, but was dominated by the IgG2a subtype. Sera from immunized mice also prevented the formation of A β fibrils and reduced the toxicity of the A β peptide toward PC12 cells.⁸⁹

In the final example based on BPV-1, the A $\beta_{1–9}$ peptide was fused with the L1 protein and the chimeric A β -VLPs self-assembled to form a structure resembling the native virus particle. Preclinical vaccination studies in rabbits indicated that sera from the treated rabbits recognized A $\beta_{1–9}$ and full-length A β , and that A β fibril formation was inhibited *in vitro*. Transgenic APP/PS1 mice, which spontaneously form A β plaques, were also immunized with A β -VLP without adjuvant eliciting high titers of A β -specific antibodies. Higher levels of circulating A β peptide were detected in these mice compared to naïve controls, corresponding to lower levels of A β peptide in the brain.⁹⁰

CONCLUSION

Vaccines based on viruses could be developed for the prevention and/or treatment of diverse diseases, including infectious diseases, cancer, addiction, and chronic disorders. One of the key advantages of viruses as a vaccine development platform is that they are naturally immunogenic, and are therefore ideal for the induction of immune responses even in the absence of an adjuvant. The success of prophylactic vaccines against HPV and HBV highlights the potential of this platform for the treatment of many other diseases. Many virus-based vaccines have shown promising results in nonhuman primates but a number of challenges remain to be overcome before such vaccines can be deployed in the clinic. The first

barrier is safety: the natural immunogenicity of virus-based particles makes them ideal for the display of antigenic epitopes but increases the risk of toxicity. Bacteriophage Q β vaccines for Alzheimer's disease and nicotine addiction have recently completed phase I safety tests, but other platforms remain to be

evaluated in clinical trials. Nevertheless, the phase I trials indicate that virus-based vaccines offer an alternative to other vaccine materials, and the promising results in primates indicate that this platform could be used to develop novel vaccines against a wide range of diseases.

ACKNOWLEDGMENTS

This work was supported in part by grants from the National Institute of Biomedical Imaging and Bioengineering of the National Institutes of Health (T32EB007509) to K.L.L., the National Science Foundation (CMMI NM 1333651 for VNP nanomanufacturing, and CMMI NM 1509232 for Ebola virus diagnostics), a Susan G. Komen grant (CCR14298962 for cancer vaccines); and Mt. Sinai Foundation and Case Western Reserve University startup funds to N.F.S.

REFERENCES

1. Clem AS. Fundamentals of vaccine immunology. *J Global Infect Dis* 2011; 3:73–78.
2. Pulendran B, Ahmed R. Immunological mechanisms of vaccination. *Nat Immunol* 2011; 12:509–517.
3. Riedel S. Edward Jenner and the history of smallpox and vaccination. *Proc (Bayl Univ Med Cent)* 2005; 18:21–25.
4. Miller M, Barrett S, Henderson DA. Control and eradication. In: Jamison DT, Breman JG, Measham AR, Alleyne G, Claeson M, Evans DB, Jha P, Mills A, Musgrove P, eds. *Disease Control Priorities in Developing Countries*. 2nd ed. Washington, DC: World Bank; 2006.
5. Knobler S, Lederberg J, Pray LA, eds. *Considerations for Viral Disease Eradication: Lessons Learned and Future Strategies: Workshop Summary*. Washington, DC: The National Academies Press; 2002.
6. Hicks DJ, Fooks AR, Johnson N. Developments in rabies vaccines. *Clin Exp Immunol* 2012; 169:199–204.
7. Geier MR, Geier DA, Zahalsky AC. A review of hepatitis B vaccination. *Expert Opin Drug Saf* 2003; 2:113–122.
8. Lopez AL, Gonzales ML, Aldaba JG, Nair GB. Killed oral cholera vaccines: history, development and implementation challenges. *Ther Adv Vaccines* 2014; 2:123–136.
9. Scorpio A, Blank TE, Day WA, Chabot DJ. Anthrax vaccines: Pasteur to the present. *Cell Mol Life Sci* 2006; 63:2237–2248.
10. Zhao L, Seth A, Wibowo N, Zhao CX, Mitter N, Yu C, Middelberg AP. Nanoparticle vaccines. *Vaccine* 2014; 32:327–337.
11. Gregory AE, Titball R, Williamson D. Vaccine delivery using nanoparticles. *Front Cell Infect Microbiol* 2013; 3:13.
12. Lua LH, Connors NK, Sainsbury F, Chuan YP, Wibowo N, Middelberg AP. Bioengineering virus-like particles as vaccines. *Biotechnol Bioeng* 2014; 111:425–440.
13. Jennings GT, Bachmann MF. The coming of age of virus-like particle vaccines. *Biol Chem* 2008; 389:521–536.
14. Peacey M, Wilson S, Baird MA, Ward VK. Versatile RHDV virus-like particles: incorporation of antigens by genetic modification and chemical conjugation. *Biotechnol Bioeng* 2007; 98:968–977.
15. Zhang W, Wang L, Liu Y, Chen X, Liu Q, Jia J, Yang T, Qiu S, Ma G. Immune responses to vaccines involving a combined antigen-nanoparticle mixture and nanoparticle-encapsulated antigen formulation. *Biomaterials* 2014; 35:6086–6097.
16. Heil F, Hemmi H, Hochrein H, Ampenberger F, Kirschning C, Akira S, Lipford G, Wagner H, Bauer S. Species-specific recognition of single-stranded RNA via toll-like receptor 7 and 8. *Science* 2004; 303:1526–1529.
17. Jegerlehner A, Maurer P, Bessa J, Hinton HJ, Kopf M, Bachmann MF. TLR9 signaling in B cells determines class switch recombination to IgG2a. *J Immunol* 2007; 178:2415–2420.
18. Bessa J, Jegerlehner A, Hinton HJ, Pumpens P, Saudan P, Schneider P, Bachmann MF. Alveolar macrophages and lung dendritic cells sense RNA and drive mucosal IgA responses. *J Immunol* 2009; 183:3788–3799.
19. Hou B, Saudan P, Ott G, Wheeler ML, Ji M, Kuzmich L, Lee LM, Coffman RL, Bachmann MF, DeFranco AL. Selective utilization of Toll-like receptor and MyD88 signaling in B cells for enhancement of the antiviral germinal center response. *Immunity* 2011; 34:375–384.

20. Cubas R, Zhang S, Kwon S, Sevick-Muraca EM, Li M, Chen C, Yao Q. Virus-like particle (VLP) lymphatic trafficking and immune response generation after immunization by different routes. *J Immunother* 2009, 32:118–128.
21. Manolova V, Flace A, Bauer M, Schwarz K, Saudan P, Bachmann MF. Nanoparticles target distinct dendritic cell populations according to their size. *Eur J Immunol* 2008, 38:1404–1413.
22. Vogel FR. Improving vaccine performance with adjuvants. *Clin Infect Dis* 2000, 30(Suppl 3):S266–S270.
23. Goldman MaL P-H. Immunological safety of vaccines: facts, hypotheses, and allegation. In: Kaufmann SHE, ed. *Novel Vaccination Strategies*. Germany: Wiley-VCH; 2004, 595–611.
24. Schneemann A, Young MJ. Viral assembly using heterologous expression systems and cell extracts. *Adv Protein Chem* 2003, 64:1–36.
25. Pokorski JK, Steinmetz NF. The art of engineering viral nanoparticles. *Mol Pharm* 2011, 8:29–43.
26. Shukla S, Dickmeis C, Nagarajan AS, Fischer R, Commandeur U, Steinmetz NF. Molecular farming of fluorescent virus-based nanoparticles for optical imaging in plants, human cells and mouse models. *Biomater Sci* 2014, 2:784–797.
27. Marusic C, Rizza P, Lattanzi L, Mancini C, Spada M, Belardelli F, Benvenuto E, Capone I. Chimeric plant virus particles as immunogens for inducing murine and human immune responses against human immunodeficiency virus type 1. *J Virol* 2001, 75:8434–8439.
28. Tissot AC, Renhofa R, Schmitz N, Cielens I, Meijerink E, Ose V, Jennings GT, Saudan P, Pumpens P, Bachmann MF. Versatile virus-like particle carrier for epitope based vaccines. *PLoS One* 2010, 5:e9809.
29. Turpen TH, Reinl SJ, Charoenvit Y, Hoffman SL, Fallarme V, Grill LK. Malarial epitopes expressed on the surface of recombinant tobacco mosaic virus. *BioTechnology (N Y)* 1995, 13:53–57.
30. Denis J, Majeau N, Acosta-Ramirez E, Savard C, Bedard MC, Simard S, Lecours K, Bolduc M, Pare C, Willems B, et al. Immunogenicity of papaya mosaic virus-like particles fused to a hepatitis C virus epitope: evidence for the critical function of multimerization. *Virology* 2007, 363:59–68.
31. Tremblay MH, Majeau N, Gagne ME, Lecours K, Morin H, Duvignaud JB, Bolduc M, Chouinard N, Pare C, Gagne S, et al. Effect of mutations K97A and E128A on RNA binding and self assembly of papaya mosaic potexvirus coat protein. *FEBS J* 2006, 273:14–25.
32. Phelps JP, Dang N, Rasochova L. Inactivation and purification of cowpea mosaic virus-like particles displaying peptide antigens from *Bacillus anthracis*. *J Virol Methods* 2007, 141:146–153.
33. O’Neil A, Prevelige PE, Basu G, Douglas T. Coconfinement of fluorescent proteins: spatially enforced communication of GFP and mCherry encapsulated within the P22 capsid. *Biomacromolecules* 2012, 13:3902–3907.
34. Patterson DP, Rynda-Apple A, Harmsen AL, Harmsen AG, Douglas T. Biomimetic antigenic nanoparticles elicit controlled protective immune response to influenza. *ACS Nano* 2013, 7:3036–3044.
35. Donnelly ML, Luke G, Mehrotra A, Li X, Hughes LE, Gani D, Ryan MD. Analysis of the aphthovirus 2A/2B polyprotein ‘cleavage’ mechanism indicates not a proteolytic reaction, but a novel translational effect: a putative ribosomal ‘skip’. *J Gen Virol* 2001, 82:1013–1025.
36. Pastori C, Tudor D, Diomede L, Drillet AS, Jegerlehner A, Rohn TA, Bomsel M, Lopalco L. Virus like particle based strategy to elicit HIV-protective antibodies to the α -helical regions of gp41. *Virology* 2012, 431:1–11.
37. Chackerian B, Lowy DR, Schiller JT. Induction of autoantibodies to mouse CCR5 with recombinant papillomavirus particles. *Proc Natl Acad Sci USA* 1999, 96:2373–2378.
38. Van Rompay KK, Hunter Z, Jayashankar K, Peabody J, Montefiori D, LaBranche CC, Keele BF, Jensen K, Abel K, Chackerian B. A vaccine against CCR5 protects a subset of macaques upon intravaginal challenge with simian immunodeficiency virus SIVmac251. *J Virol* 2014, 88:2011–2024.
39. Adis International L. HIV gp120 vaccine - VaxGen: AIDSVAX, AIDSVAX B/B, AIDSVAX B/E, HIV gp120 vaccine - Genentech, HIV gp120 vaccine AIDSVAX - VaxGen, HIV vaccine AIDSVAX - VaxGen. *Drugs R D* 2003, 4:249–253.
40. Kaleebu P, Njai HF, Wang L, Jones N, Ssewanyana I, Richardson P, Kintu K, Emel L, Musoke P, Fowler MG, et al. Immunogenicity of ALVAC-HIV vCP1521 in infants of HIV-1-infected women in Uganda (HPTN 027): the first pediatric HIV vaccine trial in Africa. *J Acquir Immune Defic Syndr* 2014, 65:268–277.
41. McFarland EJ, Johnson DC, Muresan P, Fenton T, Tomaras GD, McNamara J, Read JS, Douglas SD, Deville J, Gurwith M, et al. HIV-1 vaccine induced immune responses in newborns of HIV-1 infected mothers. *AIDS* 2006, 20:1481–1489.
42. Pitisuttithum P, Rerks-Ngarm S, Bussaratid V, Dhivatavat J, Maekanantawat W, Pungpak S, Suntharasamai P, Vanijanonta S, Nitayapan S, Kaewkungwal J, et al. Safety and reactogenicity of canarypox ALVAC-HIV (vCP1521) and HIV-1 gp120 AIDSVAX B/E vaccination in an efficacy trial in Thailand. *PLoS One* 2011, 6:e27837.
43. Rerks-Ngarm S, Pitisuttithum P, Nitayaphan S, Kaewkungwal J, Chiu J, Paris R, Premruek N,

- Namwat C, de Souza M, Adams E, et al. Vaccination with ALVAC and AIDSVAX to prevent HIV-1 infection in Thailand. *N Engl J Med* 2009, 361:2209–2220.
44. Dunkel A, Shen S, LaBranche CC, Montefiori D, McGettigan JP. A bivalent, chimeric Rabies virus expressing simian immunodeficiency virus envelope induces multifunctional antibody responses. *AIDS Res Hum Retroviruses* 2015, 31:1126–1138.
45. Bomsel M, Tudor D, Drillet AS, Alfsen A, Ganor Y, Roger MG, Mouz N, Amacker M, Chalifour A, Diomede L, et al. Immunization with HIV-1 gp41 subunit virosomes induces mucosal antibodies protecting nonhuman primates against vaginal SHIV challenges. *Immunity* 2011, 34:269–280.
46. Martins KA, Steffens JT, van Tongeren SA, Wells JB, Bergeron AA, Dickson SP, Dye JM, Salazar AM, Bavari S. Toll-like receptor agonist augments virus-like particle-mediated protection from Ebola virus with transient immune activation. *PLoS One* 2014, 9: e89735.
47. Ye L, Lin J, Sun Y, Bennouna S, Lo M, Wu Q, Bu Z, Pulendran B, Compans RW, Yang C. Ebola virus-like particles produced in insect cells exhibit dendritic cell stimulating activity and induce neutralizing antibodies. *Virology* 2006, 351:260–270.
48. Warfield KL, Swenson DL, Olinger GG, Kalina WV, Aman MJ, Bavari S. Ebola virus-like particle-based vaccine protects nonhuman primates against lethal Ebola virus challenge. *J Infect Dis* 2007, 196(Suppl 2):S430–S437.
49. Marzi A, Halfmann P, Hill-Batorski L, Feldmann F, Shupert WL, Neumann G, Feldmann H, Kawaoka Y. Vaccines. An Ebola whole-virus vaccine is protective in nonhuman primates. *Science* 2015, 348:439–442.
50. Henao-Restrepo AM, Longini IM, Egger M, Dean NE, Edmunds WJ, Camacho A, Carroll MW, Doumbia M, Draguez B, Duraffour S, et al. Efficacy and effectiveness of an rVSV-vectored vaccine expressing Ebola surface glycoprotein: interim results from the Guinea ring vaccination cluster-randomised trial. *Lancet* 2015, 386:857–866.
51. Blaney JE, Wirblich C, Papaneri AB, Johnson RF, Myers CJ, Juelich TL, Holbrook MR, Freiberg AN, Bernbaum JG, Jahrling PB, et al. Inactivated or live-attenuated bivalent vaccines that confer protection against rabies and Ebola viruses. *J Virol* 2011, 85:10605–10616.
52. Willet M, Kurup D, Papaneri A, Wirblich C, Hooper JW, Kwiila SA, Keshwara R, Hudacek A, Beilfuss S, Rudolph G, et al. Preclinical development of inactivated rabies virus-based polyvalent vaccine against rabies and filoviruses. *J Infect Dis* 2015, 212: S414–S424.
53. Perrone LA, Ahmad A, Veguilla V, Lu X, Smith G, Katz JM, Pushko P, Tumpey TM. Intranasal vaccination with 1918 influenza virus-like particles protects mice and ferrets from lethal 1918 and H5N1 influenza virus challenge. *J Virol* 2009, 83:5726–5734.
54. Liu YV, Massare MJ, Pearce MB, Sun X, Belser JA, Maines TR, Creager HM, Glenn GM, Pushko P, Smith GE, et al. Recombinant virus-like particles elicit protective immunity against avian influenza A(H7N9) virus infection in ferrets. *Vaccine* 2015, 33:2152–2158.
55. Lopez-Macias C, Ferat-Osorio E, Tenorio-Calvo A, Isibasi A, Talavera J, Arteaga-Ruiz O, Arriaga-Pizano L, Hickman SP, Allende M, Lenhard K, et al. Safety and immunogenicity of a virus-like particle pandemic influenza A (H1N1) 2009 vaccine in a blinded, randomized, placebo-controlled trial of adults in Mexico. *Vaccine* 2011, 29:7826–7834.
56. Ward BJ, Landry N, Trepanier S, Mercier G, Dargis M, Couture M, D'Aoust MA, Vezina LP. Human antibody response to N-glycans present on plant-made influenza virus-like particle (VLP) vaccines. *Vaccine* 2014, 32:6098–6106.
57. Ren Z, Ji X, Meng L, Wei Y, Wang T, Feng N, Zheng X, Wang H, Li N, Gao X, et al. H5N1 influenza virus-like particle vaccine protects mice from heterologous virus challenge better than whole inactivated virus. *Virus Res* 2015, 200:9–18.
58. Chen S, Zheng D, Li C, Zhang W, Xu W, Liu X, Fang F, Chen Z. Protection against multiple subtypes of influenza viruses by virus-like particle vaccines based on a hemagglutinin conserved epitope. *Biomed Res Int* 2015, 2015:901817.
59. Naskalska A, Szolajkska E, Chaperot L, Angel J, Plumas J, Chroboczek J. Influenza recombinant vaccine: matrix protein M1 on the platform of the adenovirus dodecahedron. *Vaccine* 2009, 27:7385–7393.
60. Denis J, Acosta-Ramirez E, Zhao Y, Hamelin ME, Koukavica I, Baz M, Abed Y, Savard C, Pare C, Lopez Macias C, et al. Development of a universal influenza A vaccine based on the M2e peptide fused to the papaya mosaic virus (PapMV) vaccine platform. *Vaccine* 2008, 26:3395–3403.
61. Pascual E, Mata CP, Gomez-Blanco J, Moreno N, Barcena J, Blanco E, Rodriguez-Frandsen A, Nieto A, Carrascosa JL, Caston JR. Structural basis for the development of avian virus capsids that display influenza virus proteins and induce protective immunity. *J Virol* 2015, 89:2563–2574.
62. Babin C, Majeau N, Leclerc D. Engineering of papaya mosaic virus (PapMV) nanoparticles with a CTL epitope derived from influenza NP. *J Nanobiotechnol* 2013, 11:10.
63. Lico C, Mancini C, Italiani P, Betti C, Boraschi D, Benvenuto E, Baschieri S. Plant-produced potato virus X chimeric particles displaying an influenza virus-

- derived peptide activate specific CD8+ T cells in mice. *Vaccine* 2009, 27:5069–5076.
64. Richert LE, Servid AE, Harmsen AL, Rynda-Apple A, Han S, Wiley JA, Douglas T, Harmsen AG. A virus-like particle vaccine platform elicits heightened and hastened local lung mucosal antibody production after a single dose. *Vaccine* 2012, 30:3653–3665.
65. Wiley JA, Richert LE, Swain SD, Harmsen A, Barnard DL, Randall TD, Jutila M, Douglas T, Broomell C, Young M, et al. Inducible bronchus-associated lymphoid tissue elicited by a protein cage nanoparticle enhances protection in mice against diverse respiratory viruses. *PLoS One* 2009, 4:e7142.
66. Yin Z, Nguyen HG, Chowdhury S, Bentley P, Bruckman MA, Miermont A, Gildersleeve JC, Wang Q, Huang X. Tobacco mosaic virus as a new carrier for tumor associated carbohydrate antigens. *Bioconjug Chem* 2012, 23:1694–1703.
67. Yin Z, Comellas-Aragones M, Chowdhury S, Bentley P, Kaczanowska K, Benmohamed L, Gildersleeve JC, Finn MG, Huang X. Boosting immunity to small tumor-associated carbohydrates with bacteriophage qβ capsids. *ACS Chem Biol* 2013, 8:1253–1262.
68. McCormick AA, Corbo TA, Wykoff-Clary S, Palmer KE, Pogue GP. Chemical conjugate TMV-peptide bivalent fusion vaccines improve cellular immunity and tumor protection. *Bioconjug Chem* 2006, 17:1330–1338.
69. Jobsri J, Allen A, Rajagopal D, Shipton M, Kanyuka K, Lomonossoff GP, Ottensmeier C, Diebold SS, Stevenson FK, Savelyeva N. Plant virus particles carrying tumour antigen activate TLR7 and induce high levels of protective antibody. *PLoS One* 2015, 10:e0118096.
70. Pejawar-Gaddy S, Rajawat Y, Hilioti Z, Xue J, Gaddy DF, Finn OJ, Viscidi RP, Bossis I. Generation of a tumor vaccine candidate based on conjugation of a MUC1 peptide to polyionic papillomavirus virus-like particles. *Cancer Immunol Immunother* 2010, 59:1685–1696.
71. Tumban E, Peabody J, Tyler M, Peabody DS, Chackerian B. VLPs displaying a single L2 epitope induce broadly cross-neutralizing antibodies against human papillomavirus. *PLoS One* 2012, 7:e49751.
72. Tyler M, Tumban E, Peabody DS, Chackerian B. The use of hybrid virus-like particles to enhance the immunogenicity of a broadly protective HPV vaccine. *Biotechnol Bioeng* 2014, 111:2398–2406.
73. Huber B, Schellenbacher C, Jindra C, Fink D, Shafti-Keramat S, Kirnbauer R. A chimeric 18L1-45RG1 virus-like particle vaccine cross-protects against oncogenic α-7 human papillomavirus types. *PLoS One* 2015, 10:e0120152.
74. Kaufmann AM, Nieland JD, Jochmus I, Baur S, Friese K, Gabelsberger J, Giesecking F, Gissmann L, Glasschroder B, Grubert T, et al. Vaccination trial with HPV16 L1E7 chimeric virus-like particles in women suffering from high grade cervical intraepithelial neoplasia (CIN 2/3). *Int J Cancer* 2007, 121:2794–2800.
75. Monroy-Garcia A, Gomez-Lim MA, Weiss-Steider B, Hernandez-Montes J, Huerta-Yepez S, Rangel-Santiago JF, Santiago-Osorio E, Mora Garcia Mde L. Immunization with an HPV-16L1-based chimeric virus-like particle containing HPV-16 E6 and E7 epitopes elicits long-lasting prophylactic and therapeutic efficacy in an HPV-16 tumor mice model. *Arch Virol* 2014, 159:291–305.
76. Ding FX, Wang F, Lu YM, Li K, Wang KH, He XW, Sun SH. Multiepitope peptide-loaded virus-like particles as a vaccine against hepatitis B virus-related hepatocellular carcinoma. *Hepatology* 2009, 49:1492–1502.
77. Wiedermann U, Wiltschke C, Jasinska J, Kundi M, Zurbriggen R, Garner-Spitzer E, Bartsch R, Steger G, Pehamberger H, Scheiner O, et al. A virosomal formulated Her-2/neu multi-peptide vaccine induces Her-2/neu-specific immune responses in patients with metastatic breast cancer: a phase I study. *Breast Cancer Res Treat* 2010, 119:673–683.
78. Patel JM, Kim MC, Vartabedian VF, Lee YN, He S, Song JM, Choi HJ, Yamanaka S, Amaram N, Lukacher A, et al. Protein transfer-mediated surface engineering to adjuvantate virus-like nanoparticles for enhanced anti-viral immune responses. *Nanomedicine* 2015, 11:1097–1107.
79. Tegerstedt K, Lindencrona JA, Curcio C, Andreasson K, Tullus C, Forni G, Dalianis T, Kiessling R, Ramqvist T. A single vaccination with polyomavirus VP1/VP2Her2 virus-like particles prevents outgrowth of HER-2/neu-expressing tumors. *Cancer Res* 2005, 65:5953–5957.
80. Pouyanfar S, Bamdad T, Hashemi H, Bandehpour M, Kazemi B. Induction of protective anti-CTL epitope responses against HER-2-positive breast cancer based on multivalent T7 phage nanoparticles. *PLoS One* 2012, 7:e49539.
81. Shukla S, Wen AM, Commandeur U, Steinmetz NF. Presentation of HER2 epitopes using a filamentous plant virus-based vaccination platform. *J Mater Chem B* 2014, 2:6249–6258.
82. Montoya ID. Biologics (vaccines, antibodies, enzymes) to treat drug addictions. In: Nady el-Guebaly GC, Galanter M, eds. *Textbook of Addiction Treatment: International Perspectives*. New York: Springer; 2015, 683–692.
83. De BP, Pagovich OE, Hicks MJ, Rosenberg JB, Moreno AY, Janda KD, Koob GF, Worgall S, Kaminsky SM, Sondhi D, et al. Disrupted adenovirus-based vaccines against small addictive molecules

- circumvent antiadenovirus immunity. *Hum Gene Ther* 2013, 24:58–66.
84. Hicks MJ, De BP, Rosenberg JB, Davidson JT, Moreno AY, Janda KD, Wee S, Koob GF, Hackett NR, Kaminsky SM, et al. Cocaine analog coupled to disrupted adenovirus: a vaccine strategy to evoke high-titer immunity against addictive drugs. *Mol Ther* 2011, 19:612–619.
85. Wee S, Hicks MJ, De BP, Rosenberg JB, Moreno AY, Kaminsky SM, Janda KD, Crystal RG, Koob GF. Novel cocaine vaccine linked to a disrupted adenovirus gene transfer vector blocks cocaine psychostimulant and reinforcing effects. *Neuropharmacology* 2012, 37:1083–1091.
86. Chackerman B, Rangel M, Hunter Z, Peabody DS. Virus and virus-like particle-based immunogens for Alzheimer's disease induce antibody responses against amyloid- β without concomitant T cell responses. *Vaccine* 2006, 24:6321–6331.
87. Farlow MR, Andreasen N, Riviere ME, Vostiar I, Vitaliti A, Sovago J, Caputo A, Winblad B, Graf A. Long-term treatment with active A β immunotherapy with CAD106 in mild Alzheimer's disease. *Alzheimers Res Ther* 2015, 7:23.
88. Winblad B, Andreasen N, Minthon L, Floesser A, Imbert G, Dumortier T, Maguire RP, Blennow K, Lundmark J, Staufenbiel M, et al. Safety, tolerability, and antibody response of active A β immunotherapy with CAD106 in patients with Alzheimer's disease: randomised, double-blind, placebo-controlled, first-in-human study. *Lancet Neurol* 2012, 11:597–604.
89. Feng G, Wang W, Qian Y, Jin H. Anti-A β antibodies induced by A β -HBc virus-like particles prevent A β aggregation and protect PC12 cells against toxicity of A β 1-40. *J Neurosci Methods* 2013, 218:48–54.
90. Zamora E, Handisurya A, Shafti-Keramat S, Borchelt D, Rudow G, Conant K, Cox C, Troncoso JC, Kirnbauer R. Papillomavirus-like particles are an effective platform for amyloid- β immunization in rabbits and transgenic mice. *J Immunol* 2006, 177:2662–2670.
91. Karlsson Hedestam GB, Fouchier RA, Phogat S, Burton DR, Sodroski J, Wyatt RT. The challenges of eliciting neutralizing antibodies to HIV-1 and to influenza virus. *Nat Rev Microbiol* 2008, 6:143–155.
92. Maartens G, Celum C, Lewin SR. HIV infection: epidemiology, pathogenesis, treatment, and prevention. *Lancet* 2014, 384:258–271.
93. Brecht JR, Breitbart W, Galietta M, Krivo S, Rosenfeld B. The use of highly active antiretroviral therapy (HAART) in patients with advanced HIV infection: impact on medical, palliative care, and quality of life outcomes. *J Pain Symptom Manage* 2001, 21:41–51.
94. Esparza J. A brief history of the global effort to develop a preventive HIV vaccine. *Vaccine* 2013, 31:3502–3518.
95. Dowdle W. The search for an AIDS vaccine. *Public Health Rep* 1986, 101:232–233.
96. Buratti E, Tismenetzky SG, Scodeller ES, Baralle FE. Conformational display of two neutralizing epitopes of HIV-1 gp41 on the Flock House virus capsid protein. *J Immunol Methods* 1996, 197:7–18.
97. Berkower I, Raymond M, Muller J, Spadaccini A, Aberdeen A. Assembly, structure, and antigenic properties of virus-like particles rich in HIV-1 envelope gp120. *Virology* 2004, 321:75–86.
98. Sun S, Li W, Sun Y, Pan Y, Li J. A new RNA vaccine platform based on MS2 virus-like particles produced in *Saccharomyces cerevisiae*. *Biochem Biophys Res Commun* 2011, 407:124–128.
99. Yusibov V, Modelska A, Steplewski K, Agadjanyan M, Weiner D, Hooper DC, Koprowski H. Antigens produced in plants by infection with chimeric plant viruses immunize against rabies virus and HIV-1. *Proc Natl Acad Sci USA* 1997, 94:5784–5788.
100. Sugiyama Y, Hamamoto H, Takemoto S, Watanabe Y, Okada Y. Systemic production of foreign peptides on the particle surface of tobacco mosaic virus. *FEBS Lett* 1995, 359:247–250.
101. Lu Y, Xiao Y, Ding J, Dierich M, Chen YH. Immunogenicity of neutralizing epitopes on multiple-epitope vaccines against HIV-1. *Int Arch Allergy Immunol* 2000, 121:80–84.
102. Arnold GF, Velasco PK, Holmes AK, Wrin T, Geisler SC, Phung P, Tian Y, Resnick DA, Ma X, Mariano TM, et al. Broad neutralization of human immunodeficiency virus type 1 (HIV-1) elicited from human rhinoviruses that display the HIV-1 gp41 ELDKWA epitope. *J Virol* 2009, 83:5087–5100.
103. Alkhatib G, Combadiere C, Broder CC, Feng Y, Kennedy PE, Murphy PM, Berger EA. CC CKR5: a RANTES, MIP-1 α , MIP-1 β receptor as a fusion cofactor for macrophage-tropic HIV-1. *Science* 1996, 272:1955–1958.
104. Choe H, Farzan M, Sun Y, Sullivan N, Rollins B, Ponath PD, Wu L, Mackay CR, LaRosa G, Newman W, et al. The β -chemokine receptors CCR3 and CCR5 facilitate infection by primary HIV-1 isolates. *Cell* 1996, 85:1135–1148.
105. Deng H, Liu R, Ellmeier W, Choe S, Unutmaz D, Burkhardt M, Di Marzio P, Marmon S, Sutton RE, Hill CM, et al. Identification of a major co-receptor for primary isolates of HIV-1. *Nature* 1996, 381:661–666.
106. Doranz BJ, Rucker J, Yi Y, Smyth RJ, Samson M, Peiper SC, Parmentier M, Collman RG, Doms RW. A dual-tropic primary HIV-1 isolate that uses fusin and

- the β -chemokine receptors CKR-5, CKR-3, and CKR-2b as fusion cofactors. *Cell* 1996, 85:1149–1158.
107. Dragic T, Litwin V, Allaway GP, Martin SR, Huang Y, Nagashima KA, Cayanan C, Madden PJ, Koup RA, Moore JP, et al. HIV-1 entry into CD4+ cells is mediated by the chemokine receptor CC-CKR-5. *Nature* 1996, 381:667–673.
 108. Park DJ, Dudas G, Wohl S, Goba A, Whitmer SL, Andersen KG, Sealfon RS, Ladner JT, Kugelman JR, Matranga CB, et al. Ebola virus epidemiology, transmission, and evolution during seven months in sierra leone. *Cell* 2015, 161:1516–1526.
 109. Goeijenbier M, van Kampen JJ, Reusken CB, Koopmans MP, van Gorp EC. Ebola virus disease: a review on epidemiology, symptoms, treatment and pathogenesis. *Neth J Med* 2014, 72:442–448.
 110. Baize S, Pannetier D, Oestereich L, Rieger T, Koivogui L, Magassouba N, Soropogui B, Sow MS, Keita S, De Clerck H, et al. Emergence of Zaire Ebola virus disease in Guinea. *N Engl J Med* 2014, 371:1418–1425.
 111. Matassov D, Marzi A, Latham T, Xu R, Ota-Setlik A, Feldmann F, Geisbert JB, Mire CE, Hamm S, Nowak B, et al. Vaccination with a highly attenuated recombinant vesicular stomatitis virus vector protects against challenge with a lethal dose of Ebola virus. *J Infect Dis* 2015, 212:S443–S451.
 112. Jones SM, Stroher U, Fernando L, Qiu X, Alimonti J, Melito P, Bray M, Klenk HD, Feldmann H. Assessment of a vesicular stomatitis virus-based vaccine by use of the mouse model of Ebola virus hemorrhagic fever. *J Infect Dis* 2007, 196(Suppl 2):S404–S412.
 113. Feldmann H, Jones SM, Daddario-DiCaprio KM, Geisbert JB, Stroher U, Grolla A, Bray M, Fritz EA, Fernando L, Feldmann F, et al. Effective post-exposure treatment of Ebola infection. *PLoS Pathog* 2007, 3:e2.
 114. Geisbert TW, Feldmann H. Recombinant vesicular stomatitis virus-based vaccines against Ebola and Marburg virus infections. *J Infect Dis* 2011, 204(Suppl 3):S1075–S1081.
 115. de Wit E, Marzi A, Bushmaker T, Brining D, Scott D, Richt JA, Geisbert TW, Feldmann H. Safety of recombinant VSV-Ebola virus vaccine vector in pigs. *Emerg Infect Dis* 2015, 21:702–704.
 116. Papaneri AB, Wirblich C, Cooper K, Jahrling PB, Schnell MJ, Blaney JE. Further characterization of the immune response in mice to inactivated and live rabies vaccines expressing Ebola virus glycoprotein. *Vaccine* 2012, 30:6136–6141.
 117. World Health Organization. Influenza (Seasonal) Fact Sheet. Available at: <http://www.who.int/mediacentre/factsheets/fs211/en/>.
 118. Lambert LC, Fauci AS. Influenza vaccines for the future. *N Engl J Med* 2010, 363:2036–2044.
 119. Krammer F. Emerging influenza viruses and the prospect of a universal influenza virus vaccine. *Biotechnol J* 2015, 10:690–701.
 120. Taubenberger JK, Morens DM. Influenza: the once and future pandemic. *Public Health Rep* 2010, 125(Suppl 3):16–26.
 121. World Health Organization Global Influenza Program Surveillance N. Evolution of H5N1 avian influenza viruses in Asia. *Emerg Infect Dis* 2005, 11:1515–1521.
 122. Riedel S. Crossing the species barrier: the threat of an avian influenza pandemic. *Proc (Bayl Univ Med Cent)* 2006, 19:16–20.
 123. Fiore AE, Bridges CB, Cox NJ. Seasonal influenza vaccines. *Curr Top Microbiol Immunol* 2009, 333:43–82.
 124. Krammer F, Palese P. Influenza virus hemagglutinin stalk-based antibodies and vaccines. *Curr Opin Virol* 2013, 3:521–530.
 125. de Jong JC, Beyer WE, Palache AM, Rimmelzwaan GF, Osterhaus AD. Mismatch between the 1997/1998 influenza vaccine and the major epidemic A(H3N2) virus strain as the cause of an inadequate vaccine-induced antibody response to this strain in the elderly. *J Med Virol* 2000, 61:94–99.
 126. Tricco AC, Chit A, Soobiah C, Hallett D, Meier G, Chen MH, Tashkandi M, Bauch CT, Loeb M. Comparing influenza vaccine efficacy against mismatched and matched strains: a systematic review and meta-analysis. *BMC Med* 2013, 11:153.
 127. Ito T, Gorman OT, Kawaoka Y, Bean WJ, Webster RG. Evolutionary analysis of the influenza A virus M gene with comparison of the M1 and M2 proteins. *J Virol* 1991, 65:5491–5498.
 128. Epstein SL, Kong WP, Misplon JA, Lo CY, Tumpey TM, Xu L, Nabel GJ. Protection against multiple influenza A subtypes by vaccination with highly conserved nucleoprotein. *Vaccine* 2005, 23:5404–5410.
 129. Kawano M, Morikawa K, Suda T, Ohno N, Matsushita S, Akatsuka T, Handa H, Matsui M. Chimeric SV40 virus-like particles induce specific cytotoxicity and protective immunity against influenza A virus without the need of adjuvants. *Virology* 2014, 448:159–167.
 130. Moyron-Quiroz JE, Rangel-Moreno J, Hartson L, Kusser K, Tighe MP, Klonowski KD, Lefrancois L, Cauley LS, Harmsen AG, Lund FE, et al. Persistence and responsiveness of immunologic memory in the absence of secondary lymphoid organs. *Immunity* 2006, 25:643–654.
 131. D'Aoust MA, Lavoie PO, Couture MM, Trepanier S, Guay JM, Dargis M, Mongrand S, Landry N, Ward BJ, Vezina LP. Influenza virus-like particles produced by transient expression in Nicotiana benthamiana induce a protective immune response

- against a lethal viral challenge in mice. *Plant Biotechnol J* 2008, 6:930–940.
132. Hanahan D, Weinberg RA. The hallmarks of cancer. *Cell* 2000, 100:57–70.
133. Lizotte PH, Wen AM, Sheen MR, Fields J, Rojanasopondist P, Steinmetz NF, Fiering S. In situ vaccination with cowpea mosaic virus nanoparticles suppresses metastatic cancer. *Nat Nanotechnol* 2015. doi: 10.1038/nnano.2015.292
134. American Cancer Society. *Global Cancer Facts & Figures*. 3rd ed. Atlanta, GA: American Cancer Society, Inc.; 2015.
135. Castellsague X, Bosch FX. Advances in cervical cancer prevention: HPV vaccines. *Fam Hosp* 2007, 31:261–263.
136. Bosch FX, de Sanjose S. The epidemiology of human papillomavirus infection and cervical cancer. *Dis Markers* 2007, 23:213–227.
137. Clifford GM, Gallus S, Herrero R, Munoz N, Snijders PJ, Vaccarella S, Anh PT, Ferreccio C, Hieu NT, Matos E, et al. Worldwide distribution of human papillomavirus types in cytologically normal women in the International Agency for Research on Cancer HPV prevalence surveys: a pooled analysis. *Lancet* 2005, 366:991–998.
138. Stanley M. Pathology and epidemiology of HPV infection in females. *Gynecol Oncol* 2010, 117: S5–S10.
139. Lehtinen M, Paavonen J, Wheeler CM, Jaisamrarn U, Garland SM, Castellsague X, Skinner SR, Apter D, Naud P, Salmeron J, et al. Overall efficacy of HPV-16/18 AS04-adjuvanted vaccine against grade 3 or greater cervical intraepithelial neoplasia: 4-year end-of-study analysis of the randomised, double-blind PATRICIA trial. *Lancet Oncol* 2012, 13:89–99.
140. Munoz N, Kjaer SK, Sigurdsson K, Iversen OE, Hernandez-Avila M, Wheeler CM, Perez G, Brown DR, Koutsy LA, Tay EH, et al. Impact of human papillomavirus (HPV)-6/11/16/18 vaccine on all HPV-associated genital diseases in young women. *J Natl Cancer Inst* 2010, 102:325–339.
141. Brown DR, Kjaer SK, Sigurdsson K, Iversen OE, Hernandez-Avila M, Wheeler CM, Perez G, Koutsy LA, Tay EH, Garcia P, et al. The impact of quadrivalent human papillomavirus (HPV; types 6, 11, 16, and 18) L1 virus-like particle vaccine on infection and disease due to oncogenic nonvaccine HPV types in generally HPV-naive women aged 16–26 years. *J Infect Dis* 2009, 199:926–935.
142. Wheeler CM, Kjaer SK, Sigurdsson K, Iversen OE, Hernandez-Avila M, Perez G, Brown DR, Koutsy LA, Tay EH, Garcia P, et al. The impact of quadrivalent human papillomavirus (HPV; types 6, 11, 16, and 18) L1 virus-like particle vaccine on infection and disease due to oncogenic nonvaccine HPV types in sexually active women aged 16–26 years. *J Infect Dis* 2009, 199:936–944.
143. Smith JF, Brownlow M, Brown M, Kowalski R, Esser MT, Ruiz W, Barr E, Brown DR, Bryan JT. Antibodies from women immunized with Gardasil cross-neutralize HPV 45 pseudovirions. *Hum Vaccin* 2007, 3:109–115.
144. Roden RB, Yutzy WH, Fallon R, Inglis S, Lowy DR, Schiller JT. Minor capsid protein of human genital papillomaviruses contains subdominant, cross-neutralizing epitopes. *Virology* 2000, 270:254–257.
145. Gambhira R, Karanam B, Jagu S, Roberts JN, Buck CB, Bossis I, Alphs H, Culp T, Christensen ND, Roden RB. A protective and broadly cross-neutralizing epitope of human papillomavirus L2. *J Virol* 2007, 81:13927–13931.
146. Pastrana DV, Gambhira R, Buck CB, Pang YY, Thompson CD, Culp TD, Christensen ND, Lowy DR, Schiller JT, Roden RB. Cross-neutralization of cutaneous and mucosal Papillomavirus types with anti-sera to the amino terminus of L2. *Virology* 2005, 337:365–372.
147. Schellenbacher C, Kwak K, Fink D, Shafti-Keramat S, Huber B, Jindra C, Faust H, Dillner J, Roden RB, Kirnbauer R. Efficacy of RG1-VLP vaccination against infections with genital and cutaneous human papillomaviruses. *J Invest Dermatol* 2013, 133:2706–2713.
148. Karanam B, Jagu S, Huh WK, Roden RB. Developing vaccines against minor capsid antigen L2 to prevent papillomavirus infection. *Immunol Cell Biol* 2009, 87:287–299.
149. Tumban E, Peabody J, Peabody DS, Chackerian B. A pan-HPV vaccine based on bacteriophage PP7 VLPs displaying broadly cross-neutralizing epitopes from the HPV minor capsid protein, L2. *PLoS One* 2011, 6:e23310.
150. zur Hausen H. Papillomaviruses causing cancer: evasion from host-cell control in early events in carcinogenesis. *J Natl Cancer Inst* 2000, 92:690–698.
151. Muller M, Zhou J, Reed TD, Rittmuller C, Burger A, Gabelsberger J, Braspenning J, Gissmann L. Chimeric papillomavirus-like particles. *Virology* 1997, 234:93–111.
152. Schafer K, Muller M, Faath S, Henn A, Osen W, Zentgraf H, Benner A, Gissmann L, Jochmus I. Immune response to human papillomavirus 16 L1E7 chimeric virus-like particles: induction of cytotoxic T cells and specific tumor protection. *Int J Cancer* 1999, 81:881–888.
153. Kaufmann AM, Nieland J, Schinz M, Nonn M, Gabelsberger J, Meissner H, Muller RT, Jochmus I, Gissmann L, Schneider A, et al. HPV16 L1E7 chimeric virus-like particles induce specific HLA-restricted T cells in humans after in vitro vaccination. *Int J Cancer* 2001, 92:285–293.

154. Ohlschlager P, Osen W, Dell K, Faath S, Garcea RL, Jochmus I, Muller M, Pawlita M, Schafer K, Sehr P, et al. Human papillomavirus type 16L1 capsomeres induce L1-specific cytotoxic T lymphocytes and tumor regression in C57BL/6 mice. *J Virol* 2003, 77:4635–4645.
155. London WT, McGlynn KA. Liver cancer. In: Schottenfeld DFJJ, Fraumeni JFJ, eds. *Cancer Epidemiology and Prevention*. 3rd ed. New York: Oxford University Press; 2006, 763–786.
156. Mittal S, El-Serag HB. Epidemiology of hepatocellular carcinoma: consider the population. *J Clin Gastroenterol* 2013, 47(Suppl):S2–S6.
157. El-Serag HB. Hepatocellular carcinoma. *N Engl J Med* 2011, 365:1118–1127.
158. McAleer WJ, Buynak EB, Maigetter RZ, Wampler DE, Miller WJ, Hilleman MR. Human hepatitis B vaccine from recombinant yeast. *Nature* 1984, 307:178–180.
159. Andre FE, Safary A. Summary of clinical findings on Engerix-B, a genetically engineered yeast derived hepatitis B vaccine. *Postgrad Med J* 1987, 63(Suppl 2):169–177.
160. Su F, Schneider RJ. Hepatitis B virus HBx protein sensitizes cells to apoptotic killing by tumor necrosis factor α . *Proc Natl Acad Sci USA* 1997, 94:8744–8749.
161. Sorlie T, Perou CM, Tibshirani R, Aas T, Geisler S, Johnsen H, Hastie T, Eisen MB, van de Rijn M, Jeffrey SS, et al. Gene expression patterns of breast carcinomas distinguish tumor subclasses with clinical implications. *Proc Natl Acad Sci USA* 2001, 98:10869–10874.
162. Ross JS, Slodkowska EA, Symmans WF, Pusztai L, Ravdin PM, Hortobagyi GN. The HER-2 receptor and breast cancer: ten years of targeted anti-HER-2 therapy and personalized medicine. *Oncologist* 2009, 14:320–368.
163. Jhaveri K, Esteva FJ. Pertuzumab in the treatment of HER2+ breast cancer. *J Natl Compr Canc Netw* 2014, 12:591–598.
164. Hortobagyi GN. Trastuzumab in the treatment of breast cancer. *N Engl J Med* 2005, 353:1734–1736.
165. Zurbriggen R. Immunostimulating reconstituted influenza virosomes. *Vaccine* 2003, 21:921–924.
166. Bovier PA. Epaxal: a virosomal vaccine to prevent hepatitis A infection. *Expert Rev Vaccines* 2008, 7:1141–1150.
167. Thompson FM, Porter DW, Okitsu SL, Westerfeld N, Vogel D, Todryk S, Poulton I, Correa S, Hutchings C, Berthoud T, et al. Evidence of blood stage efficacy with a virosomal malaria vaccine in a phase IIa clinical trial. *PLoS One* 2008, 3:e1493.
168. Wagner S, Jasinska J, Breiteneder H, Kundi M, Pehamberger H, Scheiner O, Zielinski CC, Wiedermann U. Delayed tumor onset and reduced tumor growth progression after immunization with a Her-2/neu multi-peptide vaccine and IL-12 in c-neu transgenic mice. *Breast Cancer Res Treat* 2007, 106:29–38.
169. Chen XS, Stehle T, Harrison SC. Interaction of polyomavirus internal protein VP2 with the major capsid protein VP1 and implications for participation of VP2 in viral entry. *EMBO J* 1998, 17:3233–3240.
170. Carrera MR, Ashley JA, Parsons LH, Wirsching P, Koob GF, Janda KD. Suppression of psychoactive effects of cocaine by active immunization. *Nature* 1995, 378:727–730.
171. Fox BS, Kantak KM, Edwards MA, Black KM, Bollinger BK, Botka AJ, French TL, Thompson TL, Schad VC, Greenstein JL, et al. Efficacy of a therapeutic cocaine vaccine in rodent models. *Nat Med* 1996, 2:1129–1132.
172. Kinsey BM, Jackson DC, Orson FM. Anti-drug vaccines to treat substance abuse. *Immunol Cell Biol* 2009, 87:309–314.
173. Maurer P, Jennings GT, Willers J, Rohner F, Lindman Y, Roubicek K, Renner WA, Muller P, Bachmann MF. A therapeutic vaccine for nicotine dependence: preclinical efficacy, and Phase I safety and immunogenicity. *Eur J Immunol* 2005, 35:2031–2040.
174. Maoz A, Hicks MJ, Vallabhjosa S, Synan M, Kothari PJ, Dyke JP, Ballon DJ, Kaminsky SM, De BP, Rosenberg JB, et al. Adenovirus capsid-based anti-cocaine vaccine prevents cocaine from binding to the nonhuman primate CNS dopamine transporter. *Neuropharmacology* 2013, 38:2170–2178.
175. Bachmann MF, Jennings GT. Therapeutic vaccines for chronic diseases: successes and technical challenges. *Philos Trans R Soc Lond B Biol Sci* 2011, 366:2815–2822.
176. Chackerian B, Lowy DR, Schiller JT. Conjugation of a self-antigen to papillomavirus-like particles allows for efficient induction of protective autoantibodies. *J Clin Invest* 2001, 108:415–423.
177. Spohn G, Keller I, Beck M, Grest P, Jennings GT, Bachmann MF. Active immunization with IL-1 displayed on virus-like particles protects from autoimmune arthritis. *Eur J Immunol* 2008, 38:877–887.
178. Spohn G, Bachmann MF. Targeting osteoporosis and rheumatoid arthritis by active vaccination against RANKL. *Adv Exp Med Biol* 2007, 602:135–142.
179. Spohn G, Guler R, Johansen P, Keller I, Jacobs M, Beck M, Rohner F, Bauer M, Dietmeier K, Kundig TM, et al. A virus-like particle-based vaccine selectively targeting soluble TNF- α protects from arthritis without inducing reactivation of latent tuberculosis. *J Immunol* 2007, 178:7450–7457.
180. Rohn TA, Jennings GT, Hernandez M, Grest P, Beck M, Zou Y, Kopf M, Bachmann MF.

- Vaccination against IL-17 suppresses autoimmune arthritis and encephalomyelitis. *Eur J Immunol* 2006, 36:2857–2867.
181. Nakajima A, Seroogy CM, Sandora MR, Tarner IH, Costa GL, Taylor-Edwards C, Bachmann MF, Contag CH, Fathman CG. Antigen-specific T cell-mediated gene therapy in collagen-induced arthritis. *J Clin Invest* 2001, 107:1293–1301.
182. Spohn G, Schwarz K, Maurer P, Illges H, Rajasekaran N, Choi Y, Jennings GT, Bachmann MF. Protection against osteoporosis by active immunization with TRANCE/RANKL displayed on virus-like particles. *J Immunol* 2005, 175:6211–6218.
183. Sondergaard I, Rohn TA, Kurrer MO, Iezzi G, Zou Y, Kastelein RA, Bachmann MF, Kopf M. Neutralization of IL-17 by active vaccination inhibits IL-23-dependent autoimmune myocarditis. *Eur J Immunol* 2006, 36:2849–2856.
184. Fulurija A, Lutz TA, Sladko K, Ostro M, Wielinga PY, Bachmann MF, Saadan P. Vaccination against GIP for the treatment of obesity. *PLoS One* 2008, 3:e3163.
185. Chackerian B. Virus-like particles: flexible platforms for vaccine development. *Expert Rev Vaccines* 2007, 6:381–390.
186. Bachmann MF, Whitehead P. Active immunotherapy for chronic diseases. *Vaccine* 2013, 31:1777–1784.
187. Jennings GT, Bachmann MF. Immunodrugs: therapeutic VLP-based vaccines for chronic diseases. *Annu Rev Pharmacol Toxicol* 2009, 49:303–326.
188. Ambühl PM, Tissot AC, Fulurija A, Maurer P, Nussberger J, Sabat R, Nief V, Schellekens C, Sladko K, Roubicek K, et al. A vaccine for hypertension based on virus-like particles: preclinical efficacy and phase I safety and immunogenicity. *J Hypertens* 2007, 25:63–72.
189. Tissot AC, Maurer P, Nussberger J, Sabat R, Pfister T, Ignatenko S, Volk HD, Stocker H, Müller P, Jennings GT, et al. Effect of immunisation against angiotensin II with CYT006-AngQb on ambulatory blood pressure: a double-blind, randomised, placebo-controlled phase IIa study. *Lancet* 2008, 371:821–827.
190. Liebscher S, Meyer-Luehmann M. A peephole into the brain: neuropathological features of Alzheimer's disease revealed by in vivo two-photon imaging. *Front Psychiatry* 2012, 3:26.
191. Hardy JA, Higgins GA. Alzheimer's disease: the amyloid cascade hypothesis. *Science* 1992, 256:184–185.
192. Haass C, Selkoe DJ. Cellular processing of β -amyloid precursor protein and the genesis of amyloid β -peptide. *Cell* 1993, 75:1039–1042.
193. Schenk D, Barbour R, Dunn W, Gordon G, Grajeda H, Guido T, Hu K, Huang J, Johnson-Wood K, Khan K, et al. Immunization with amyloid- β attenuates Alzheimer-disease-like pathology in the PDAPP mouse. *Nature* 1999, 400:173–177.
194. Bard F, Cannon C, Barbour R, Burke RL, Games D, Grajeda H, Guido T, Hu K, Huang J, Johnson-Wood K, et al. Peripherally administered antibodies against amyloid β -peptide enter the central nervous system and reduce pathology in a mouse model of Alzheimer disease. *Nat Med* 2000, 6:916–919.
195. Orgogozo JM, Gilman S, Dartigues JF, Laurent B, Puel M, Kirby LC, Jouanny P, Dubois B, Eisner L, Flitman S, et al. Subacute meningoencephalitis in a subset of patients with AD after A β 42 immunization. *Neurology* 2003, 61:46–54.
196. Nicoll JA, Wilkinson D, Holmes C, Steart P, Markham H, Weller RO. Neuropathology of human Alzheimer disease after immunization with amyloid- β peptide: a case report. *Nat Med* 2003, 9:448–452.
197. Ferrer I, Boada Rovira M, Sanchez Guerra ML, Rey MJ, Costa-Jussa F. Neuropathology and pathogenesis of encephalitis following amyloid- β immunization in Alzheimer's disease. *Brain Pathol* 2004, 14:11–20.
198. Bard F, Barbour R, Cannon C, Carretero R, Fox M, Games D, Guido T, Hoenow K, Hu K, Johnson-Wood K, et al. Epitope and isotype specificities of antibodies to β -amyloid peptide for protection against Alzheimer's disease-like neuropathology. *Proc Natl Acad Sci USA* 2003, 100:2023–2028.
199. Seabrook TJ, Bloom JK, Iglesias M, Spooner ET, Walsh DM, Lemere CA. Species-specific immune response to immunization with human versus rodent A β peptide. *Neurobiol Aging* 2004, 25:1141–1151.
200. Wiessner C, Wiederhold KH, Tissot AC, Frey P, Danner S, Jacobson LH, Jennings GT, Luond R, Ortmann R, Reichwald J, et al. The second-generation active A β immunotherapy CAD106 reduces amyloid accumulation in APP transgenic mice while minimizing potential side effects. *J Neurosci* 2011, 31:9323–9331.
201. Karpenko LI, Ivanisenko VA, Pika IA, Chikaev NA, Eroshkin AM, Veremeiko TA, Ilyichev AA. Insertion of foreign epitopes in HBCAg: how to make the chimeric particle assemble. *Amino Acids* 2000, 18:329–337.